Facoltà di Scienze Matematiche, Fisiche e Naturali

Dipartimento di Chimica

Shotgun proteomic analytical approach for characterizing “protein coronas” of different liposome nanovectors suitable for gene delivery

Anna Laura Capriotti

Tutor: Prof. Aldo Laganà

Doctoral thesis in "Chimica analitica e dei sistemi reali"

(XXV Ciclo)

2012

Se vuoi convertire i tuoi sogni in realtà,
dovrai imparare a conoscere te stessa.
Quanto più ti conoscerai, tanto più ti
avvicinerai a ciò che desideri ottenere.
Quanto più ti conoscerai, più ti amerai.
E solo nel momento in cui ti amerai
davvero, potrai condividere il tuo amore
con gli altri.

A tutti quelli che me lo hanno insegnato in questi anni.

LIST OF PUBLICATIONS

1) DNA affects the composition of lipoplex protein corona: A proteomics approach. Capriotti, A.L., Caracciolo, G., Caruso, G., Foglia, P., Pozzi, D., Samperi, R., Laganà, A. **Proteomics 2011** 11 (16), pp. 3349-3358.

2) Shotgun proteomic analytical approach for studying proteins adsorbed onto liposome surface. Capriotti, A.L., Caracciolo, G., Cavaliere, C., Crescenzi, C., Pozzi, D., Laganà, A. **Analytical and Bioanalytical Chemistry 2011** 401 (4), pp. 1195-1202.

3) Do plasma proteins distinguish between liposomes of varying charge density? Capriotti A.L., Caracciolo, G., Cavaliere, C., Foglia, P., Pozzi, D., Samperi, R., Laganà, A. **Journal of Proteomics 2012** 75 (6), pp. 1924-1932.

4) Evolution of the protein corona of lipid gene vectors as a function of plasma concentration. Caracciolo, G., Pozzi, D., Capriotti A.L., Cavaliere, C., Foglia, P., Amenitsch H., Laganà A. **Langmuir 2011** 27 (24), pp. 15048-15053.

5) Factors determining the superior performance of lipid/DNA/ protammine nanoparticles over lipoplexes. Caracciolo, G., Pozzi, D., Capriotti, A.L., Marianecci, C., Carafa, M., Marchini, C., Montani, M., Amici, A., Amenitsch, H., Digman, M. A., Gratton, E., Sanchez, S.S., Laganà, A. **Journal of Medicinal Chemistry 2011** 54 (12), pp. 4160-4171.

6) Differential analysis of "protein corona" profile adsorbed onto different nonviral gene delivery systems. Capriotti, A.L., Caracciolo, G., Caruso, G., Foglia, P., Pozzi, D., Samperi, R., Laganà, A. **Analytical Biochemistry 2011** 419 (2), pp. 180-189.

7) Label-free quantitative analysis for studying the interactions between nanoparticles and plasma proteins. Capriotti, A.L., Caracciolo, G., Caruso, G., Cavaliere, C., Pozzi, D., Samperi, R., Laganà, A. **Analytical and Bioanalytical Chemistry 2012.** Article in press DOI 10.1007/s00216-011-5691-y.

Other papers dealing with nanoparticle proteomic characterization but not included in this thesis:

8) Effect of membrane charge density on the protein corona of cationic liposomes: Interplay between cationic charge and surface area. Caracciolo, G., Pozzi, D., Candeloro De Sanctis, S., Capriotti, A.L., Caruso, G., Samperi, R., Laganà, A. **Applied Physics Letters 2011** 99 (3), art. no. 033702.

9) Analysis of plasma protein adsorption onto DC-Chol-DOPE cationic liposomes by HPLC-CHIP coupled to a Q-TOF mass spectrometer. Capriotti, A.L., Caracciolo, G., Caruso, G., Cavaliere, C., Pozzi, D., Samperi, R., Laganà, A. **Analytical and Bioanalytical Chemistry 2010** 398 (7-8), pp. 2895-2903.

10) Surface adsorption of protein corona controls the cell uptake mechanism in efficient cationic liposome/DNA complexes in serum. Pozzi, D., Caracciolo, G., Marchini, C., Montani,1 M., Amici, A., Callipo, L., Capriotti, A.L., Cavaliere C., Laganà, A. **Journal of controlled release: official journal of the Controlled Release Society 2010** 148 (1), pp. e94-95.

11) Cancer cell targeting of lipid gene vectors by protein corona. Caracciolo, G., Pozzi, D., Capriotti, A.L., Cavaliere, C., Cardarelli, F., Bifone, A., Bardi, G., Salomone F., Laganà, A. Technical Proceedings of the 2012 NSTI Nanotechnology Conference and Expo, NSTI-Nanotech 2012, pp. 354-357.

Papers not included in this thesis:

12) Multiclass screening method based on solvent extraction and liquid chromatography-tandem mass spectrometry for the determination of antimicrobials and mycotoxins in egg. Capriotti, A.L., Cavaliere, C., Piovesana, S., Samperi, R., Laganà, A. **Journal of Chromatography A 2012.** Article in press http://dx.doi.org/10.1016/j.chroma.2012.10.040.

13) Polyphenol content in white table grape (Vitis Vinifera) berries of cultivar Italia: Interactive effect of irrigation, delayed harvest and storage. Capriotti, A.L., Caruso, G., Cavaliere, C., Foglia, P., Laganà, A., Samperi, R. **Natural Product Research 2012** 26 (19), pp. 1787-1795.

14) Comparison of three different enrichment strategies for serum low molecular weight protein identification using shotgun proteomics approach. Capriotti, A.L., Caruso, G., Cavaliere, C., Piovesana, S., Samperi, R., Laganà, A. **Analytica Chimica Acta 2012** 740, pp. 58-65.

15) Multiclass mycotoxin analysis in food, environmental and biological matrices with chromatography/mass spectrometry. Capriotti, A.L., Caruso, G., Cavaliere, C., Foglia, P., Samperi, R., Laganà, A. **Mass Spectrometry Reviews 2012** 31 (4), pp. 466-503.

16) Intact protein separation by chromatographic and/or electrophoretic techniques for top-down proteomics. Capriotti, A.L., Cavaliere, C., Foglia, P., Samperi, R., Laganà, A. **Journal of Chromatography A 2011** 1218 (49), pp. 8760-8776.

17) Extending the applicability of pressurized hot water extraction to compounds exhibiting limited water solubility by pH control: Curcumin from the turmeric rhizome. Euterpio, M.A., Cavaliere, C., Capriotti, A.L., Crescenzi, C. **Analytical and Bioanalytical Chemistry 2011** 401 (9), pp. 2977-2985.

18) Nanostructured functional co-polymers bioconjugate integrin inhibitors. Laganà, A., Venditti, I., Fratoddi, I., Capriotti, A.L., Caruso, G., Battocchio, C., Polzonetti, G., Accomcia, F., Marino M., Russo, M.V. **Journal of Colloid and Interface Science 2011** 361 (2), pp. 465-471.

19) Rapid resolution liquid chromatography/high resolution tandem mass spectrometry to characterize metabolic changes in subjects involved in MARS500 project. Capriotti, A.L., Caruso, G., Cavaliere, C., Foglia, P., Bizzarri, M., Laganà, A. **Chromatographia 2011** 73 (SUPPL. 1), pp. S45-S53.

20) Evaluation of different two-dimensional chromatographic techniques for proteomic analysis of mouse cardiac tissue. Callipo, L., Capriotti, A.L., Cavaliere, C., Gubbiotti, R., Samperi, R., Laganà, A. **Biomedical Chromatography 2011** 25 (5), pp. 594-599.

21) Development and validation of a liquid chromatography/ atmospheric pressure photoionization-tandem mass spectrometric method for the analysis of mycotoxins subjected to commission regulation (EC) No. 1881/2006 In cereals. Capriotti, A.L., Foglia, P., Gubbiotti, R., Roccia, C., Samperi, R., Laganà, A. **Journal of Chromatography A 2010** 1217 (39), pp. 6044-6051.

22) Recent developments in matrix solid-phase dispersion extraction. Capriotti, A.L., Cavaliere, C., Giansanti, P., Gubbiotti, R., Samperi, R., Laganà, A. **Journal of Chromatography A 2010** 1217 (16), pp. 2521-2532.

LIST OF ABBREVIATIONS

DC-Chol	(3-[N-(N,N-dimethylaminoethane)-carbamoyl])-cholesterol
DOTAP	1,2-dioleoyl-3-trimethylammonium propane
AUC	area under curve
CT	calf thymus
CL	Cationic liposome
CHO	Chinese hamster ovary cells
CAT	chloramphenicol acetyltransferase
CID	collision-induced dissociation
CB	competitive binding
DOPE	dioleoylphosphatidylethanolamine
ESI	electrospray ionization
FDR	false discovery rate
HPLC	High performance liquid chromatography
HEK293	human embryonic kidney cells
HAS	human serum albumin
R_H	hydrodynamic radius
LTQ	Linear Tap Quadrupole
LPD	lipid/protamine/DNA
LA	low affinity
MS	mass spectrometry
MS	mass spectrometry
MS/MS	mass/mass
MALDI	matrix-assisted laser desorption ionization
MW	molecular weight

NIH 3T3	mouse embryonal cells
A17	murine cancer cells
NSI	nanospray ionisation
NSC	normalized spectrum count
Pdi	polydispersity index
P/DNA	protamine/DNA
RT	room temperature
SAXS	small-angle X-ray scattering
SDS-PAGE	sodium dodecyl sulfate polyacrylamide gel electrophoresis
SC	spectral count/counting
TPP	Trans Proteomic Pipeline
TE	transfection efficiency
TFA	trifluoracetic acid
USC	unweighted spectrum count
ζ_p	zeta-potential

ABSTRACT

This PhD thesis is a part of the study concerning non-viral nanocarriers for gene therapy. In modern molecular medicine, gene therapy is a very promising research. One issue with gene therapy is the efficient delivery of the genetic material into the cell. Naked DNA cannot pass freely the cell membrane because it is made up of very large molecules with a hydrophilic nature provided by the negatively charged phosphate groups; moreover it can be easily degraded by nucleases. For these reasons the development of suitable vectors for an efficient transfection is fundamental in order to facilitate and optimize gene transfer to targeted cells without degradation. One of the most important requirements in gene therapy is the development of safe and efficient gene delivery systems. In the past two decades viral vectors, such as adenovirus and retrovirus, were the most used in several clinical trials. Today non-viral vectors have attracted a growing interest in the scientific community, thanks to their preparation reproducibility, lack of immunogenicity and almost no size limit to the piece of DNA carried into cells.

The aim of this PhD thesis was to identify and compare plasma proteins bound to different kind of non-viral nanovetcors commonly employed for gene therapy studies. The knowledge about the interaction between plasma proteins and nanocarriers is fundamental to understand the *in vivo* biodistribution, thus the transfection efficiency (TE).

Protein adsorption onto nanoparticle surface (protein corona) is strongly affected by vector surface characteristics. In general, the primary interaction is thought to be electrostatic, thus surface charge of carriers is supposed to

play a central role in protein adsorption. Because protein corona composition can be critical in modifying the interactive surface that is recognized by cells, an insight into its formation onto lipid particles may serve as a fundamental predictive model for the *in vivo* efficiency of a lipid vector.

A shotgun analytical proteomics approach was employed in all studies to compare human plasma protein binding capability to cationic liposomes (CLs), lipoplexes and protamine/DNA (P/DNA) complexes. This approach exploited a centrifugation-based protocol for the separation of the nanoparticle-protein complexes, followed by "in solution" proteolytic digestion of the whole protein mixtures and determination of the resulting peptides by nano-high performance liquid chromatography (nanoHPLC) coupled to a high-resolution linear trap quadrupole (LTQ) Orbitrap XL mass spectrometer.

Paper I described and compared the adsorption of human plasma proteins bound to cationic liposomes, made of (3-[N-(N,N-dimethylaminoethane)-carbamoyl])-cholesterol (DC-Chol) and the zwitterionic lipid dioleoylphosphatidylethanolamine (DOPE), and their relative DNA cationic lipoplexes. A shotgun proteomics approach based on HPLC coupled to high resolution mass spectrometry (MS) was used for an efficient identification of proteins adsorbed onto liposome and lipoplex surfaces. The distinct pattern of proteins adsorbed helped to better understand the DNA compaction process. The experimental evidence lead us to hypothesize that polyanionic DNA is associated to the lipoplex surface and can interact with basic plasma proteins. Such a finding is in agreement with recent results showing that lipoplexes are multilamellar DNA/lipid domains partially

decorated with DNA at their surface. Proteomics experiments showed that the lipoplex corona is rich of biologically relevant proteins such as fibronectin, histones and complement proteins. Our results provided novel insights to understand how lipoplexes activate the immune system and why they are rapidly cleared from the bloodstream. The differences in the protein adsorption data detected in the presented experiments could be the basis for the establishment of a correlation between protein adsorption pattern and the *in vivo* fate of intravenously administered nanoparticles, and will require some consideration in the future.

Paper II and **III** investigated the liposomes made of the cationic lipid DC-Chol DOPE and the possible effect of membrane charge density on the formation of the protein corona. The membrane charge density is the average charge per unit area of the membrane and it is controlled by the ratio of neutral to cationic lipid in the liposome formulation. To vary it, the neutral/total lipid molar ratio was changed, "diluting" the cationic lipid in the membrane with the neutral helper lipid. In **paper II** the proteomic study was carried out in order to portrait the protein corona composition from a qualitative point of view. This initial study was performed validating Mascot search results with the Trans-Proteomic Pipeline (TPP) platform. In **paper III** the experiment was repeated to add a label-free quantitation based on spectral count (SC) by Scaffold. Fibrinogen displayed higher association with CLs having a higher membrane charge density, while apolipoproteins and C4b-binding protein with CLs having a lower membrane charge density. These results are discussed in terms of the different lipid compositions of CLs and may have a deep biological impact for *in vivo* applications. Surface charge of nanoparticles is emerging as a relevant

factor determining the corona composition after interaction with plasma proteins. Remarkably, it was also shown that the charge of the protein corona formed around CLs is strongly related to their membrane charge density.

In **paper IV** we investigated the compositional evolution of the protein corona of 1,2-dioleoyl-3-trimethylammonium propane (DOTAP) CLs and DOTAP/DNA lipoplexes over a wide range of plasma concentrations (2.5-80%). The composition of the hard corona of lipoplexes was quite stable, differently from that of CLs, which did evolve considerably, instead. We showed that the protein corona of CLs was made of both low-affinity and competitive-binding proteins, the relative abundance of which revealed to be dependent on the plasma concentration to which they were exposed.

In **paper V** we examined the advantages of exploiting a P/DNA complex coated with a lipid envelope made of the cationic lipid DOTAP, for transfecting CHO (Chinese hamster ovary cells), HEK293 (human embryonic kidney cells), NIH 3T3 (mouse embryonal cells), and A17 (murine cancer cells) cells. Recent studies, in fact, showed superiority of LPD-mediated gene transfer over conventional liposomes for delivering a gene to the liver. To demonstrate this evidence, we investigated complex formation, DNA protection ability, surface properties, nanostructure, ability to release DNA upon interaction with cellular lipids, and intracellular trafficking.

In **papers VI** and **VII,** after investigating the physical-chemical properties of LDP complexes, we employed a shotgun proteomics approach to discuss the protein coronas of DOTAP, DOTAP/DNA and LPD complexes. In **paper VI** we carried out a qualitative study, whereas in **paper VII** we also

added a label-free quantification performed by two distinct methods: the spectral counting (SC), in which the number of spectra matched to peptides from a protein was used as a surrogate measure of protein abundance, and the area under the curve (AUC) or signal intensity measurement, in which protein abundance was derived from the extracted ion chromatograms.

Our results could help in designing gene delivery systems, because some proteins could be more selectively bound than others, thus affecting the biodistribution of liposome nanovectors and provide a more efficient *in vivo* delivery in gene therapy applications.

1. INTRODUCTION AND LITERATURE REVIEW

Gene therapy

Gene therapy is a technique used to introduce new genetic materials to hosts; in recent years it has attracted a growing interest because it provides a tool to study gene function and its regulation, in order to explore potential therapeutic applications (1). Gene therapy was first conceptualized in 1947 as "a therapeutic technique" for "correction of hereditary diseases" (2), long before the discovery of specific genes causing a disease and years prior to the elucidation of the DNA structure by Watson and Crick (3).

In the most exploited form of gene therapy, a DNA sequence that encodes a functional, therapeutic gene is introduced into a target cell in order to replace a mutated gene. Alternatively, it is possible to use the genetic material to correct a mutation or induce the expression of a therapeutic protein drug, rather than a natural human gene.

In gene therapy, two different approaches are possible: the somatic and the germ line gene therapy. In the first one, which currently represents the main line of basic and clinical research, the therapeutic genes are transferred into the somatic cells of a patient to treat a disease in a single individual. Any modification is not inherited by later generations. On the contrary, in the second one**,** germ cells (sperm or eggs) are modified by the introduction of specific genes which are integrated into their genomes. This allows the therapy to be heritable and passed on to later generations (4). Somatic gene therapy can be carried out on cells which are collected from the patient, modified outside the body and then transplanted back in again to the target tissue (*ex vivo* approach). Alternatively, DNA can directly be delivered into

the resident cells of the target tissue which is easily accessible (*in vivo* approach) (5).

One issue with gene therapy is the efficient delivery of the genetic material into the cell. Naked DNA cannot freely pass the cell membrane, because it is made up of very large molecules with a hydrophilic nature provided by the negatively charged phosphate groups; moreover it can be easily degraded by nucleases. For these reasons the development of suitable vectors for an efficient transfection is fundamental in order to facilitate and optimize gene transfer to target cells without degradation (1).

Vectors should have peculiar features: they should be stable, biocompatible, non-toxic, cost effective, but most of all, they should specifically reach target cells avoiding surrounding cells, integrate and then express the therapeutic gene (transgene) at effective levels and for extended time periods (5). Generally employed gene vectors can be classified into two main groups: viral and non-viral vectors.

Viruses have been the first vectors employed for gene therapy, because they are the simplest biological agents evolved to deliver genetic information to cells. The efficiency in gene transfer is due to innate properties of viruses. In fact, viral particles (virions) posses a structure able to carry and protect the genetic material (DNA and RNA) during transport across the human body. Determinants on the surface of the virion guide the viral particle to specific cells minimizing immunostimulatory potential within the host. After infection of the cell, signals in the genetic material control gene expression from the virus, and in some cases viruses also have mechanisms of replication that allow them to be propagated in cell culture (6). For this reason, recombinant viruses (retrovirus, lentivirus, adenovirus, adeno-

associated virus and herpes simplex virus) have been widely exploited as vectors for gene transfer (1). However, apart from these advantages, viral vectors also have several intrinsic drawbacks and risks: the difficulty in manufacture, limited opportunity for repeated administrations due to acute inflammatory response, limitations in transgene size, as well as the potential to be pathogenic or cause insertional mutagenesis. In viral vector development the goal is to minimize the potential risks by using only components of the virus necessary for transduction and expression of the transgene (6).

These difficulties with viral vectors prompted the development of alternative gene delivery systems. The non-viral approaches comprise the direct injection of plasmids, a simple and reliable method because plasmids can be easily produced and are stable for long time spans. However TE is low and limited to the injection area. On the other hand, non-viral vectors are a valuable alternative to viruses; they are made of synthetic or natural compounds, which are generally less toxic and immunogenic than the viral counterparts, and cell or tissue specificity is achieved by binding cell-specific functionalities on the vectors. The practical advantages of these systems are that they can be easily and reproducibly prepared and can be repeatedly administrated because of their lack immunogenicity. Moreover non-viral vectors can be manufactured choosing different features, such as charge, morphology and composition, but especially size, allowing the introduction and transport of large genomic fragments, including complex transcriptional control elements. However they are generally less efficacious than the viral carriers, and in several cases, the gene expression is short-lived (**paper I**).

Liposomes

Liposomes are self-assembled fluid supramolecular assemblies formed via the accumulation of lipids interacting with one another. Their main feature is that they are able to separate hydrophobic or hydrophilic molecules from the solution. These vesicles are lacking in immunogenic response, have a low cost, can be found in many shapes and sizes, depending on lipid composition, and provide differential release characteristics; for these reasons they have been employed to envelope and protect several types of therapeutic biomolecules, including DNA (7).

Liposomes are generally formed by the self assembly of lipid molecules having hydrophobic tails facing each other to form a lipid bilayer and a hydrophilic head group facing outwards to the aqueous solution. Vesicle sizes fall into the nanometer to micrometer range. Liposomes can have two main structures. Unilamellar liposomes have a single bilayer membrane with an internal aqueous solution, thus separating it from the external medium (8). They can be small (0.02-0.2 μm), large (0.2-1 μm), or giant unilamellar vesicles (>1 μm). If the vesicle is quite large, other structures can be observed, such as the oligolamellar one, when there are only two concentric bilayers, and the multilamellar one, when multiple concentric bilayers are present (Figure 1); this latter type of liposomes is frequently used in pharmaceutical and cosmetic applications. Multivesicular vesicles are giant vesicles encapsulating smaller liposomes and have been employed in nanoreactor assemblies and drug delivery. Apart from multilamellar vesicles, the other morphologies are difficult to obtain (7).

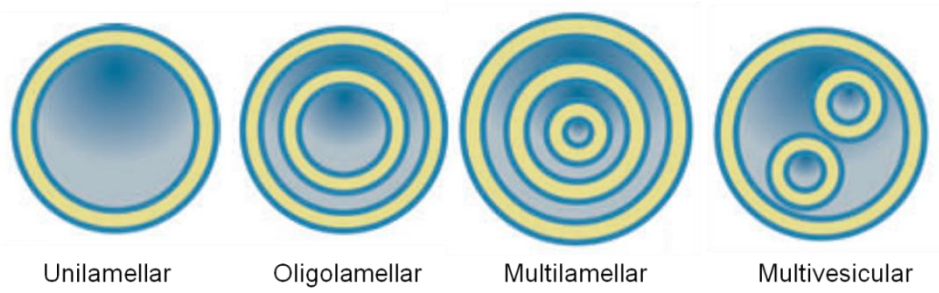

Figure 1 Representation of liposome possible structures

Liposome have an amphiphilic nature that allowed them to be extensively exploited for encapsulation and delivery of drugs. The main advantage of liposomal drug delivery systems is their ability to transport both hydrophilic molecules, which migrate to the inner watery core of the liposome, and hydrophobic ones, which are trapped within the phospholipid bilayer. In this way drugs are transported through a hydrophilic medium to target cells; here, the lipid bilayer of the liposome fuses with the cell membrane releasing the drug into the cell.

Liposomes for gene delivery are usually formulated adding specific lipids, both cationic or neutral. The lipids employed all share a common structure, a positively charged hydrophilic head and hydrophobic tail(s) connected via a linker, which controls the relative position of hydrophobic groups and thus the conformational flexibility, the stability and the biodegradability of the resulting liposome. The positively charged head groups are generally amines or quaternary ammonium salts, and are able to interact and stabilize DNA (or other anionic biomolecules) (1). The resulting lipoplexes protect DNA from degradation and have an overall positive charge that allows them to bind more efficiently to the negatively charged cell membranes compared to naked DNA, with a increased cellular uptake (9; 10). In this case the

resulting structure is the product of different energetic interactions, such as van der Waals and electrostatic forces. By adding a zwitterionic lipid in the bilayer, the overall membrane charge density can be varied. The lipid composition of the liposome determines the properties of the vector (shape, dimension, surface charge density) and can be optimized for a better transfection (11). The most exploited cationic lipids for liposome production are DOTAP and DC-Chol (Figure 2). DOPE is a zwitterionic lipid usually added to destabilize the membrane at low pH values, a phenomenon which promotes endosomal escape. Lipids usually have 8-18 carbon atoms in their tails, which may be saturated or with a single double bond. The two tails are usually symmetric, but it has been shown that asymmetric lipid mixtures with both short saturated and long unsaturated carbon chains lead to relatively high TEs as compared to mixed formulations of symmetric cationic lipids (7).

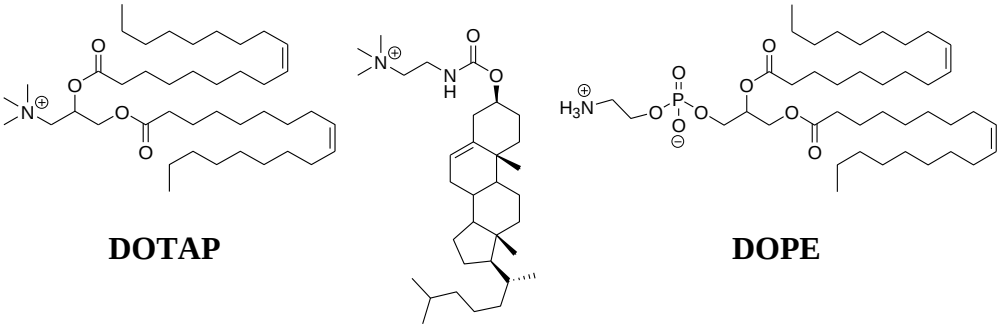

Figure 2 Structures of the cationic lipids DOTAP and DC-Chol and of the neutral helper lipid DOPE

DOTAP has a quaternary amine head group and a glycerol backbone with two oleoyl chains. The ester bonds, which are hydrolyzable, were added to make it biodegradable and reduce cytotoxicity. DOTAP is completely

protonated at pH 7.4 and liposomes completely made of DOTAP were discovered to be unsuitable for gene delivery, because the high density of positive charges on the surface results in a very high energy required to separate the DNA from the lipoplex. On the contrary, more efficient liposomes can be produced combining DOTAP with a neutral helper lipid, as seems to be the case for most cationic lipid formulations (7).

DC-Chol contains a dimethylethylenediamine group attached to cholesterol moiety by an ester bond. As previously, the cholesterol group has been introduced to enhance the biocompatibility and the stability of lipid membranes in the resulting liposomes. Most importantly, the chloramphenicol acetyltransferase expression (CAT) assay showed a better transfection activity with a significant reduction in cytotoxicity. In contrast to cationic liposomes containing fully charged quaternary amines like DOTAP, DC-Chol, in a 1:1 lipid ratio with DOPE, contains a tertiary amine groups charged on 50% of the liposome surface at pH 7.4, which reduces liposome aggregation and enhances a higher transgene expression and DNA dissociation (7).

DOPE is one of the most employed neutral helper lipids in liposome formulations. It is added to improve transfection efficiencies in many cell types changing liposome structure from lamellar, in which there are repeated layers of DNA/lipids, to an inverted hexagonal packing structure at low pH values, where DNA is placed inside the tubes and stabilized by electrostatic interactions. The hexagonal conformation is thought to facilitate the exit of complexed DNA from endosomal vesicles by destabilizing the vesicle membrane (7).

Lipoplexes

Cationic lipids for transfection have been selected to encapsulate DNA so that the interactions with the cellular membrane are favorable and endocytosis more efficient. The lipoplexes used in gene therapy are positively charged complexes of liposomes (formed by cationic lipids often in presence of a neutral helper) and DNA. Evidences showed that cationic liposomes have several advantages over viral vectors for gene therapy because there is no size limit for plasmid DNA transport, which is compacted inside the liposome and introduced into the cell by endocytosis, thanks to the interaction of the positively charged lipids with the negatively charged biological membranes (12). By choosing the lipid mixture and composition, lipoplexes can be made for cell-specific uptake through the addition of specific ligands (7).

The mechanisms of lipoplex formation is a matter still being under investigation; lipoplexes are considered the product of electrostatic interactions between cationic charge from lipids and anionic charges from DNA and the elasticity forces driven by the lipid hydrophobic moiety. In fact, lipoplex formation is a highly dynamic event, in which cationic lipid/DNA complex formation is also favoured by an increase of entropy associated with the release of counterions from DNA and the lipid bilayers.

Lipoplexes formation is considered determinant for the morphology and TE. A general two-step mechanisms has been proposed for lipoplex formation, in which the first step is the electrostatic binding of DNA to the liposome surface, and the second one is fusion and rearrangement of the liposomes, with the formation of short rod-like structures in which condensed DNA molecules are encapsulated within a lipid bilayer. The resulting complex can

further form string-like colloidal aggregates with ordered multilamellar structures (LC α), when the complexes are neutrally charged. Two models have been proposed for the description of cationic lipoplex structures, an "external" model, in which DNA is electrostatically adsorbed onto the surface of cationic liposomes, and an "internal" model, in which the DNA is surrounded by a lipid envelope. The type of structure depends on the lipid/DNA ratio: at low ratios, DNA is trapped into aggregated multilamellar structures; an excess of cationic surfactant leads to entrapment of the DNA molecules between the lamellas in clusters of aggregated multilamellar structures.

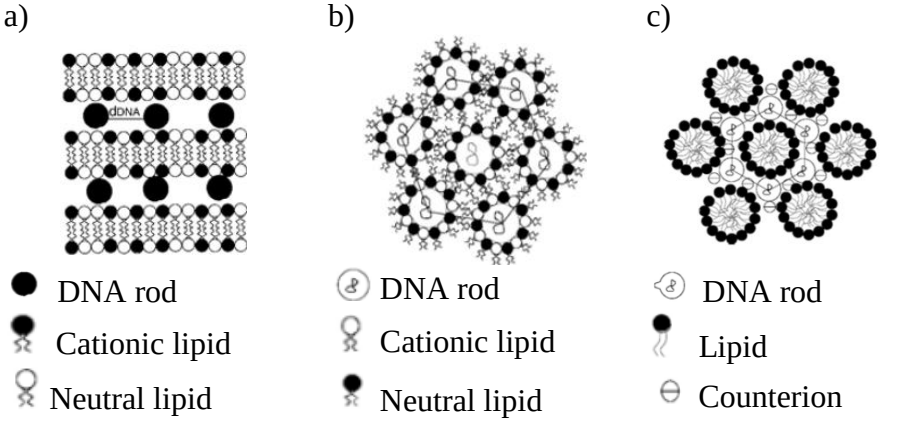

Figure 3 a) the lamellar structure (LCα) of cationic lipid/DNA lipoplexes, where the DNA rods are located between the lipid bilayers;

b) the inverted hexagonal structure (HCII), where DNA rods are coated by a lipid monolayer; the different units are arranged on a hexagonal lattice;

c) the intercalated hexagonal structure (HI), where DNA rods are covered by three lipid micelles arranged on a honeycombs-like hexagonal lattice

For cationic lipoplexes three are the most observed structures: multilamellar structure LC α (Figure 3a) and hexagonal structures containing inverted hexagonal HC II (Figure 3b) and hexagonal HI (Figure 3c).

Lipoplex structure can vary during transfection: in fact, it has been observed that lamellar structure present during the condensation and transport of the DNA changes to inverted hexagonal upon cell membrane contact (13).

Lipid-polycation-DNA complexes

LPD complexes represent a further improvement of lipoplex formulation. Cationic liposomes used to carry DNA form periodic multilayer structures with DNA chains adsorbed between lipid membranes. Once inside the cell, these structures protect DNA from degradation, but also often hinder adequate DNA release from the endosomal compartments. If this is the case, the lipoplex is shuttled to the lysosomes and DNA degraded by the abundant nucleases therein present. LPD complexes were designed to overcome this drawback: plasmid DNA is condensed with a polycation like protammine (small nuclear proteins that allow a denser DNA packaging than histones and are involved in spermatogenesis) and encapsulated by the lipid envelope. Experimental results evidenced that LPD-mediated gene transfer is improved with respect to conventional liposomes in the liver (14; 15).

Protein corona, biodistribution and targeting

Cationic lipoplexes showed to be effective in *in vitro* studies for transfection but when employed *in vivo* several drawbacks have emerged. Gene delivery vectors are usually administrated via parenteral injection, and once in the bloodstream they are immediately covered by plasma proteins which form a "protein corona" (16). The identification of those proteins with the highest affinity for nanoparticles with different surface composition or properties has become a critical aspect to investigate, in order to elucidate how protein

binding affects the biodistribution of the nanoparticles. Plasma proteins have a pivotal role in the identification of foreign bodies in the bloodstream. Unprotected nanoparticles are removed by macrophages within seconds after intravenous administration (17); the binding of proteins like opsonins (fibrinogen, IgG, complement factor, etc.) is recognized to enhance phagocytosis together with large particle sizes (>200 nm) (18; 19). On the contrary the binding of dysopsonins (human serum albumin HSA, apolipoproteins, etc.) and small sizes promote prolonged circulation time in blood (20). Moreover plasma proteins such as HSA, lipoproteins, fibrinogen and heparin can bind to lipid membranes and greatly alter lipoplex structure, inducing aggregation, consequently enhancing clearance or deterioration by nucleases and lowering the efficacy of intravenously administered cationic lipoplexes. Finally in the case of systemic administration, highly vascularized organs (heart, lung, liver, spleen) exhibit significantly higher expression of the transfected molecule, which is, as a consequence, cleared from the system (21).

In this context the nanoparticle-protein interactions are important for understanding the *in vivo* fate of the administrated gene delivery vector, because this phenomenon governs the circulation, clearance rates, blood half-life, stability, immunogenicity, and organ biodistribution of the nanoparticle.

The protein corona composition depends on the concentrations of plasma proteins and the kinetic and equilibrium binding constants of each protein, which in turn are a function of the vector features (particle size, shape, and surface characteristics, Figure 4). However, more recent findings have

revealed that the average composition of the protein corona does not reflect the relative abundance of proteins in human plasma (22).

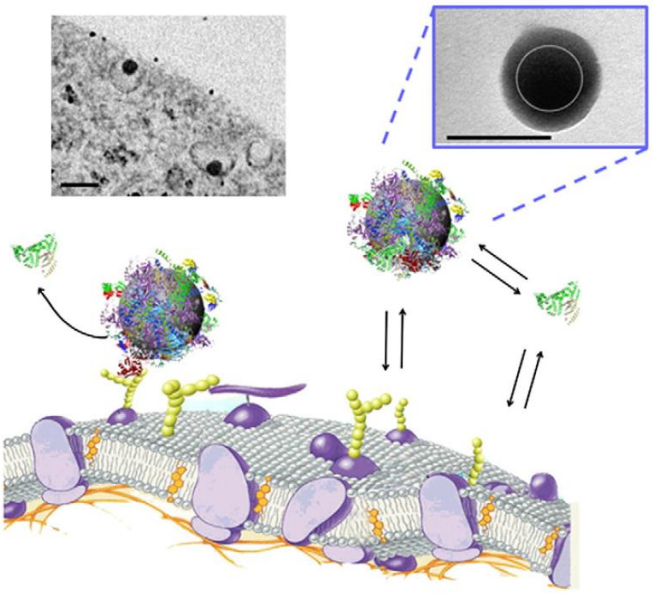

Figure 4 Picture displaying the equilibria between free proteins in solution, the protein corona and proteins on the cell membrane. In the upper part, image of silica nanoparticles entering a cell and polystyrene nanoparticle covered by a plasma protein corona (25)

Proteins present with high concentrations and/or with high association rate constants initially bind to the lipoplex surface, but over the time they may be displaced by proteins with a lower concentration, lower exchange rate, but higher affinity, resulting in the formation of a so called "hard corona" (23). This corona may contain only a few proteins in a relatively immobile layer, with a more loosely bound layer that is less well understood. In this context the most abundantly associated proteins do not necessarily have the most profound effect, because a less abundant protein with higher affinity and specificity for a particular receptor may be extremely important (**paper VII**). The protein corona envelopes the particle and it is what living cells

actually recognize. The composition of the hard corona varies according to protein concentration and during distribution, from one organ to another one or between cellular compartments (24). However, the primary nanoparticle-protein interaction is electrostatic, thus the surface charge of carrier is supposed to play a central role in protein adsorption (**paper II**). Understanding how and why plasma proteins are adsorbed to lipid particles would be important to elucidate delivery and uptake mechanisms. It may serve as a fundamental predictive model for the *in vivo* efficiency of the vector, as well as a starting point for the development of targeting strategies, in view of future clinical applications, but knowledge in this field is still limited.

Nanoparticles covered by plasma proteins interact with the cell surface and are internalized by nonspecific and/or highly specific pathways, such as receptor-ligand interactions. The principal entering for lipoplexes is believed to be endocytosis, although a fusion mechanism has also been proposed. Here, an exchange mechanism between lipoplexes and plasma membranes would cause the destabilization of the lipoplex structure with subsequent DNA release into the cytoplasm (23). There are two main approaches to target nanoparticles: in one approach the surface is engineered so that the specific recognition/targeting molecule is displayed, whereas all other undesired interactions with the surrounding environment are reduced to a minimum (adsorption-proof nanoparticle). The other approach exploits the formation of the protein corona for targeting, once the correct proteins for location delivery have been chosen (25). Both approaches have been applied with success: assessed that apolipoprotein E could target a drug to the brain, in one case the poly(alkyl cyanoacrylate) nanoparticle was

covered by a surfactant that enabled to spontaneously bind that protein from the medium (26) in the other one it was chemically bound to the nanoparticle itself (27). Adsorbed proteins play a fundamental role not only in the second approach, but also in the first one, because the efficiency of the targeting molecule does depend on the effect of the biomolecules that they interact with on-route to the target site, thus determining for both approaches nanoparticle uptake, transport and sub-cellular localization.

Shotgun proteomics approach

In the 2000s genomics succeeded in elucidating the genome of several organisms; this prompted the development of other "omics" disciplines, in particular proteomics, the next logical step that allowed to study proteins, the product of genes. Proteomics gives access to the functional aspects of cells but for this reason proteomic studies are complicated, because, if compared to the genome, the proteome of an organism is much more dynamic, and changes in response to cellular or environmental factors are frequent. The proteome is orders of magnitude more complex than the genome due to processes such as splicing, post-translational modifications, protein degradation, drug perturbations and disease, which deeply change protein structure (28).

Two are the possible approaches for proteomic studies, top-down approaches, which focus on the analysis at whole protein level, and bottom-up approaches, which focus on the peptide level. The shotgun methods are bottom-up approaches and currently represent the most commonly used strategy for protein analysis. Typically in shotgun proteomics experiments, a complex protein sample is digested by a protease, usually trypsin, and

turned into a peptide mixture. The advantage with respect to intact protein analysis is that peptides are more efficiently chromatographically separated and sequenced by mass spectrometry with a higher sensitivity. The resulting peptide mixture is separated by reverse phase liquid chromatography (RP-LC) prior to mass spectrometric analysis. Here a mass/mass (MS/MS) experiment is carried out, with eluting peptides fragmented by collision-induced dissociation (CID) into characteristic ion series. The number of acquired MS/MS spectra is very large and assignment is performed by specific software solutions, which searching a protein sequences database, give protein identifications. For this reason shotgun proteomics allows the global description of complex proteome profiles, as well as the ability to systematically analyze dynamic proteomes (29).

SDS-PAGE separation

Polyacrylamide gel electrophoresis has been employed to identify and characterize different kinds of biological macromolecules. This technique is relatively simple, rapid and highly sensitive for the study of proteins. The principle upon which it is based is that charged molecules migrate with different rates when subjected to an electric field. Proteins are supported by a matrix, usually agarose or polyacrylamide gels. The most common electrophoretic technique for protein separation is sodium dodecyl sulfate (SDS)-polyacrylamide gel electrophoresis (SDS-PAGE), which was originally described by Laemmli (30). Here a denatured protein mixture is separated in presence of SDS which, independently of the protein mixture, forms negatively charged complexes in which 1 g protein binds to 1.4 g SDS. These complexes are rod-shaped, have a similar charge density and

their length is proportional to the molecular weight (MW) of the protein, thus proteins are separated on the basis of their size only.

Nano-HPLC

The most employed separation technique for proteomic analyses is HPLC, because it can be easily coupled with electrospray and nanoelectrospray ionization (ESI and nanoESI) sources, thus ensuring a high degree of automation and throughput. In particular, in the recent years nano-HPLC has attracted much attention mainly because of the higher sensitivity when compared to conventional HPLC methods, allowing to analyse small amounts of sample with none or very low dilution. Column diameters and stationary-phase particle size are significantly reduced and pressures increased, drastically improving the performance of LC and leading to the development of ultrahigh pressure liquid chromatography. All system components have been downscaled, including flow rate, connecting tubing, detection and injection volumes. Pumping systems have been developed for providing flow rates in the nl/min range, suitable for very small amounts of sample. HPLC system may be with and without flow splitting. In apparatus with flow splitting, a high pump flow rate (200-300 µl/min) is divided into the column flow rate (100-300 nl/min) and the rest, which is directed into the waste. This configuration is the most common for proteomic analyses. Systems without flow splitting use syringe pumps to deliver the mobile phase to the column. Analytical columns for proteomics research usually use conventional C18 stationary phase. However, the need for higher selectivity, sensitivity and specificity has led to three main recent developments. RP stationary phases were modified to operate with very low

or no trifluoroacetic acid (TFA), as for PepMap® columns, thus making mobile phases more suitable for mass spectrometric acquisitions. New monolithic columns have been developed, where the stationary phase consists of a continuous, rigid polymeric rod with a porous structure that enables faster separations. Finally, columns have been miniaturized and reduced to a chip format. In the work discussed in this thesis, RP in-house manufactured 15 cm fritless silica microcolumns with a 75 µm i.d were used.

HPLC configurations also comprise trap columns or precolumns. Usually employed in column-switching modes, they enable injections of high volumes and highly diluted samples. They are shorter and larger than analytical columns (1-5 mm length and 300 µm i.d. *vs* 75 µm) and are used to load and desalt samples. They should have a high load capacity and low void volumes (31).

Mass spectrometry

Instruments should meet the increasing demand for better performance providing high resolution, mass accuracy, dynamic range, and tandem mass spectrometry capabilities coupled to automation of sample analysis. Mass spectrometry (MS) has become a leading technique for shotgun proteomics analyses because it is the most comprehensive and versatile tool currently available for large-scale proteomics. Here, the two main ionization techniques employed are the ESI and the matrix-assisted laser desorption ionization (MALDI).

In the work described in this thesis a LTQ Orbitrap XL mass spectrometer has been employed. The LTQ Orbitrap XL is a hybrid mass spectrometer

that combines the orbitrap detector with an external mass analyzer, a linear ion trap. This allows to perform multiple levels of fragmentation (MS^n). This mass spectrometer is equipped with a NSI source. It represents a miniaturization of the conventional ESI source, where flow rate and emitter tip diameter are reduced. This makes it ideal for dilute samples, with an increased tolerance to aqueous solvents and salts. The advantage of ESI source over other types of ionization techniques is that multiply-charged analyte ions are produced, thus high MW compounds can be observed at relatively low *m/z* values.

After ionization, ions pass through the ion transfer tube and pressure is gradually reduced from atmospheric values to void (1 Torr). Ion leaving the ion transfer tube are focused and the pressure is further decreased (10^{-5} Torr) before entering the LTQ, the linear ion trap (Figure 5).

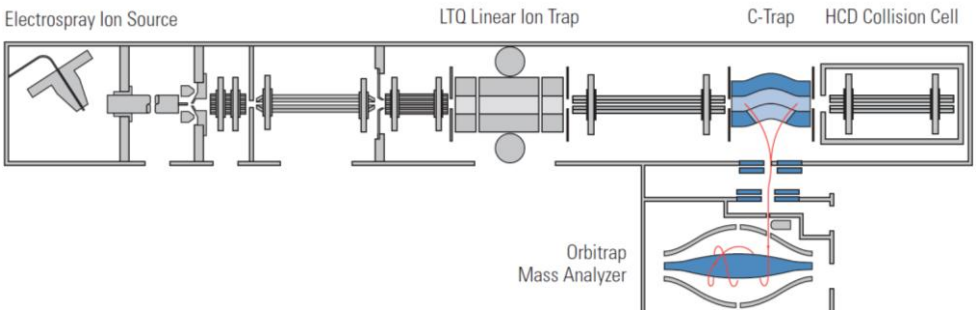

Figure 5 Schematic representation of a LTQ Orbitrap XL mass spectrometer

Ion optics use a combination of DC and RF voltage together with a vacuum gradient to guide ions towards the ion trap. The LTQ is a linear ion trap made up of two pairs of X and Y rods, as in a normal quadrupole system. In all scan events, the LTQ performs ion collection, regardless of mass (injection). After trapping, ions are ejected mass-selectively from the trap, ether all together (full scan mode) or after selection of specific *m*/*z* values of

interest (single ion monitoring and MS/MS modes). After the isolation process, the selected ions can be ejected and analyzed or subjected to fragmentation to yield product ions then ejected and analyzed.

For detection in the orbitrap analyzer, ions coming from the LTQ are trapped in the C-trap, which is used to store, collisionally cool and pack ions before injection into the orbital trap. Here ions are electrostatically trapped and begin to rotate around the central electrode inducing an image current in the outer halves of the orbitrap. A transient is acquired and then converted into frequencies and *m*/*z* values by use of the Fourier transformation. The orbitrap is employed as a high resolution and high mass accuracy detector.

The advantage of a hybrid LTQ orbitrap instrument is the possibility to work in the parallel acquisition mode. Parent ions can be analyzed in the orbitrap whereas the corresponding tandem mass spectra are obtained in the LTQ, which provides high speed and sensitivity. Fragment ions can also be analyzed in the orbitrap. This is a quite important aspect in shotgun studies, because uncertain or incorrect ion determination can lead to incorrect identifications (32). Moreover, the development of high-resolution and accurate mass spectrometry is essential for providing not only a qualitative description, but also a quantitative one, without compromising the quality of either strategy (33).

Protein and peptide validation

Non-targeted shotgun proteomics experiments produce a huge amount of raw data that need to be processed by suitable bioinformatic software for database searches and biostatistical analysis, in order to extract essential data, such as precursor ion charge state, calculation of fragment ion masses,

charge state deconvolution and deisotoping of fragment ions and general noise reduction (34). Multiple bioinformatic platforms are available. If the proteome of the organism being studied is known, databases of proteins sequences are available and downloadable in the FASTA format and are used for database searching. Commercial or open-source database searching algorithms for sequence identification of MS/MS data are available, such as Mascot (35), Sequest (36) and X! Tandem (37). These software match MS/MS spectra and precursor mass to protein sequences and include theoretical peptide masses *in silico* generated; a corresponding ion score, based on the percentage of sequence matched and the number of matching peptides, is also generated as a measure of how well the experimental spectra match the theoretical ones. Search engines also allow a second search, this time performed against a false database created by reversing or random scrambling the amino acid sequence of the original database (38). This approach is based on the assumption that decoy sequences are not biologically expressed and identifications are false. Identifications in the reverse/random database are used for calculation of a false discovery rate (FDR). Decoy search is an estimate of the empirical error rate, easy to be applied but one must take into account that the computer time is doubled with respect to a simple search and some reversed sequences might be homologous to true peptides (29). Database search for the works presented in this thesis have been performed using the Mascot search engine. It uses a FASTA file to perform three types of searches: peptide mass fingerprint (looks for peptide MWs expected from enzymatic digestion of a protein), sequence query (combination of mass data with amino acid sequences or physicochemical data which infer sequence or composition), MS/MS ion

search. The program reports peptide and protein identifications with the corresponding probability-based scores (35).

After sequence data base search, protein identification can be further refined applying filters, such as the minimum number of unique peptides for protein identification and probability thresholds for protein and peptide identification. As for database search, protein validation can be performed with suitable software in order to statistically validate search results and ensure confidence in the protein identification. Peptides with a probability of correct identification below the selected error threshold are rejected. When results come from a decoy database searches, Bayesian statistics or both methods are employed for protein validation.

The software solutions employed for validation in this work are Proteome Discoverer, the TPP and Scaffold.

Proteome Discoverer is a software suit developed and commercialized by the mass spectrometer vendor Thermo Scientific. It comprises a series of tools that allow to process Thermo Scientific instrument raw data integrating all the different steps in a quantitative proteomics experiment (i.e. MS/MS spectrum extraction, peptide identification, quantification) into user-configurable, automated workflows. Among other possible choices, it integrates the Mascot search engine for protein and peptide identifications and it has been employed for protein validation and subsequent quantitation with another Thermo Scientific software, SIEVE (37).

TPP and Scaffold are suits of software tools in which database search results are validated assigning peptide and protein probabilities by means of the Peptide (40) and ProteinProphet (41) algorithms. PeptideProphet employs search scores and additional information to distinguish between correctly

and incorrectly assigned peptides, calculating for each peptide assignment to an MS/MS spectrum a probability of being correct (40). Since MS/MS spectra are acquired from peptides and not proteins, a statistical model for validation of the identifications at the protein level is required. ProteinProphets uses PeptideProphet s results to calculate the probabilities for each protein of being in the sample. This probability takes into account if more peptides are assigned to the same protein and this grouping information is used to adjust the individual peptide probabilities. On the contrary, if peptides are shared among more proteins, a protein group is formed although only a subset of the proteins in a group is usually needed to explain the presence of all the peptides in the group (41). The TTP can also provide FDRs using Mayu (42). The Scaffold software does also calculate FDR, but in two different ways depending on whether the data has been searched against a decoy database or not. If a standard forward database has been employed for search, Scaffold uses a probabilistic method to infer FDR; on the contrary, if a decoy database has been employed, Scaffold uses an empirical method that considers the number of decoy matches (43). Moreover with respect to the TPP, the Scaffold software can also perform an additional search using the X! Tandem search engine and allows to perform label-free quantitation based on SCs (44).

Label-free quantification

LC-MS based shotgun proteomics has provided powerful tools for studying large scale protein expression and characterization of complex biological systems. The development of high resolution and high accuracy mass spectrometers enabled the quantitative analysis of biological samples. The

quantitative methods initially developed were based on stable isotope labelling, thus the incorporation of isotopic tags in proteins *in vivo* (such as metabolic stable isotope labelling with amino acids in cell culture, SILAC and 15N labelling), or *in vitro*, (such as isotope-coded affinity tags, ICAT, isobaric tag for relative and absolute quantification, iTRAQ, and 18O labelling). They are isotopically labelled internal standards having chromatographic and ionization characteristics which are highly similar to those of the target peptide, thus reducing variability due to ionization efficiency and suppression (29). However, they have potential limitations due to complex sample preparation, expensive reagents, the requirement for high sample concentration and incomplete labelling and chromatographic shifts that may complicate the quantification (45). Moreover this quantitative approach displayed a uniform distribution of percent error among all proteins except for very low concentrated proteins (46), but it is not suitable for complex, large studies, because the number of available tags is limited and does not allow for simultaneous quantification of several proteins. An alternative approach developed later performs a relative label-free quantitation by measuring the AUC in the chromatogram or the number of spectra acquired for each peptide. These approaches do not show the above mentioned limitations and do not require any special sample preparation (46). Label-free methods are characterized by a higher dynamic range of quantification than stable isotope labelling methods, advantageous for screening of large and global protein changes (29).

Relative label-free quantitation can be performed exploiting two different principles. One approach relies on the measurement of the AUC or signal intensity, in which protein abundance is derived from the extracted ion

chromatograms. The use of this method for relative quantitation in complex biological protein samples may have practical constraints: differences in peak intensities can be observed from run to run of the same sample and are caused by experimental variations, such as differences in sample preparation and injection. Moreover highly reproducible retention times among technical replicates are required because unaligned peaks lead to inaccuracy in quantitation but may be observed when multiple injections are performed onto the same column. Data collected during LC-MS/MS analysis of complex protein mixtures requires specific computer software to automatically compare the peak intensity between LC-MS. These software solutions detect peaks from background noise, then assign isotope patterns by deconvolution and align chromatograms to match retention times between LC-MS/MS runs (peak matching). Finally chromatographic peak intensities (peak area or height) are calculated and normalized, to assess for experimental differences in peptide analyses, and statistical significance of protein abundances changes are retrieved. For this thesis work the SIEVE software was employed. It implements the ChromAlign algorithm for chromatographic alignment and calculates a p-value for the expression ratio of each differential peak (45).

SC is the other approach available for relative quantitation. Here the number of assigned peptide spectra for a protein is used to infer protein abundance. This method is based on the assumption that an increase in protein abundance typically results in an increase in the number of its proteolytic peptides and, as a consequence, of sequence coverage, number of identified unique peptides and identified total MS/MS spectra (SC) for each protein (48). Liu et al. demonstrated that among all the these factors of

identification, only SC displayed a strong linear correlation with relative protein abundance over a dynamic range of 2 orders of magnitude (49). The advantage of the SC approach over the chromatographic peak intensity approach is that no peak alignment is necessary, and only normalization and statistical analysis of SC datasets are necessary.

2. BACKGROUND AND AIMS

Gene therapy represents a future perspective for treating disease. However, several drawbacks are still present, in particular, security, efficiency, target-specificity of the different gene vectors. Viral vectors are efficient, but their extensive use is hindered by their intrinsic risks and the limited capacity to transport large DNA pieces. For this reason alternative non-viral vectors gradually acquired increasing attention, with a particular interest in liposome gene vectors. However, once these foreign bodies are employed in *in vivo* applications, the organisms builds up a response. Gene vectors are usually administrated via parenteral injection and upon contact with biological fluids, in particular blood, proteins begin to cover the nanoparticle surface forming the so called "protein corona", the composition of which is highly variable but of extreme importance, because it is what living cells actually see and determines the biodistribution of the nanoparticle. In fact, proteins adsorbed onto the surface are responsible for clearance from the bloodstream, immunologic response, cell uptake and targeting. Given the high interest in the development and characterization of liposome gene vectors, and the importance of their modification once introduced into a biological medium, the aim of this thesis was to study different types of liposome systems suitable for application in gene therapy. At the beginning, the DC-Chol DOPE CLs and DNA lipoplexes were studied. The two liposome composition have the same lipid formulation and differences present in their protein corona were possibly due to DNA presence and could help to understand if specific DNA-binding proteins could be found on the lipoplex surface, in order to elucidate lipoplex

structure, compare it with data already available in the literature and infer what the fate of the lipoplex would be *in vivo*. In the next study, the effect of surface charge on the nanoparticle was also investigated, in order to understand if this physical property of the nanovector could have a significant impact in the protein binding and corona composition. Apart from the surface charge, another aspect was considered, the effect of plasma protein concentration on the type and amount of protein bound on the surface, this time choosing DOTAP CLs and lipoplexes as a model. The following studies focused also on another system that showed to be successful in recent studies, LPD complexes. A comparison of TE was carried out for four cell lines using DOTAP/DNA/protamine complexes as a model. Then the shotgun proteomic approach was employed to understand the differences among these LPD complexes and the corresponding CLs and lipoplexes, both from the qualitative protein profile and the quantitave analysis; two different software solutions were compared for protein quantitation, based on two complete different principles for retrieving protein abundances, the number of SCs and the measurement of the AUC in the chromatogram.

For these studies the protein-nanoparticle complexes were isolated by a centrifugation protocol and then the isolated pellets were analyzed both qualitatively and quantitatively. For the qualitative studies SDS-PAGE separation and evaluation of the protein profile was employed; protein identification was also performed by means of a shotgun proteomic approach on the isolated nanoparticle coronas, choosing an in-solution tryptic digestion, a nanoHPLC separation and peptide sequencing by high resolution MS spectrometry with a LTQ orbitrap XL. In the quantitative

studies, MS/MS data were further analyzed to retrieve relative label-free quantitation information, in order to give not only protein identifications, but also their amount differences in the original protein coronas.

This information represents additional characterization of these liposome nanovectors and may be useful for developing future gene therapy applications, providing the basis for understanding the clearance, biodistribution and cell targeting in real biological systems.

3. MATERIAL AND METHODS

Human plasma collection, preparation and storage

Human whole blood plasma was obtained from the Department of Experimental Medicine (Sapienza University of Rome), according to institutional bioethics approval, by venipuncture of ten healthy 20-40 year-old volunteers, by means of BD^{TM} P100 Blood Collection System (Franklin Lakes, NJ, USA) with K_2EDTA anticoagulant and protease inhibitors cocktail. Human plasma was prepared as follows: after clot formation, the samples were centrifuged at 1000 x *g* for 5 min to pellet the blood cells, and the supernatant plasma was removed. After checking the absence of haemolysis, the plasma collected from each donor was pooled, split into 200 µL aliquots, and stored at −80 °C in labelled Protein LoBind tubes, until further use. For analysis, the aliquots were thawed at 4 °C and then allowed to warm at room temperature (RT).

Procedure for preparation for all kinds of nanopaticles

DC-Chol DOPE cationic liposomes

DC-Chol and DOPE were purchased from Avanti Polar Lipids (Alabaster, AL) and used without further purifications. The liposome solutions were prepared dissolving appropriate amounts of DC-Chol and DOPE in $CHCl_3$ at three different molar ratios of neutral lipid in the bilayer Φ (neutral lipid/total lipid, mol/mol) = 0.3, 0.5, and 0.7, keeping constant the moles of the cationic lipid (i.e., the overall charge). The solvent was evaporated under vacuum for 12 h, and the obtained lipid film was hydrated with a buffer 10 mmol L^{-1} Tris-HCl (pH 7.4), 150 mmol L^{-1} NaCl, 1 mmol L^{-1} EDTA.

Small unilamellar vesicles were prepared by sonication and allowed to stay at 30 °C for 24 h to achieve full hydration.

DC-Chol DOPE/DNA cationic lipoplexes

For the preparation of lipoplexes calf thymus (CT) Na-DNA was employed. CT Na-DNA was solubilized in Tris-HCl buffer (1 mg mL^{-1}). Sonication for 5 min resulted in DNA fragmentation (length distribution between 500 and 1000 base pair, as determined by gel electrophoresis). Self-assembled DC-Chol-DOPE/DNA lipoplexes were obtained by mixing 24 mL DNA solution to 200 mL liposome dispersion and incubating at RT for 20 min.

DOTAP cationic liposomes

DOTAP was purchased from Avanti Polar Lipids (Alabaster, AL) and used without further purification. DOTAP CLs were thus prepared. In brief, a proper amount of DOTAP was dissolved in $CHCl_3$ and the solvent was evaporated under vacuum for at least 24 h. The obtained lipid films were hydrated with the appropriate amount of Tris-HCl buffer solution (10^{-2} mol L^{-1}, pH 7.4) to achieve the desired final concentration (1 mg mL^{-1}).

DOTAP/DNA lipoplexes

When adequate amounts of the DNA solution were mixed with suitable volumes of DOTAP liposomes dispersions, self-assembled DOTAP/DNA lipoplexes, at single lipid/DNA volume ratio (Rv = DOTAP/DNA = 1, v/v), were obtained. At this volume ratio, lipoplexes exhibited the lowest colloidal dimensions (about 200 nm), and were positively charged (about 50 mV).

LPD complexes

Negatively charged P/DNA microspheres were prepared at a protamine/DNA weight ratio (Rw) of 0.5. LPD complexes were prepared by mixing P/DNA microspheres with DOTAP small unilamellar vesicles at a single lipid/DNA volume ratio (Rv = DOTAP/DNA= 1, v/v). At this volume ratio, LPD systems exhibited the lowest colloidal dimensions (about 200 nm), and were positively charged (about 45 mV).

The characterization of the resulting vesicle dispersions and samples was made by means of size and zeta potential (ζ_p) measurements, respectively.

Size and zeta potential measurements

All sizing and zeta potential measurements were made on a Zetasizer Nano ZS90 (Malvern, UK) at 25°C with a scattering angle of 90.0°. Sizing measurements were made on the neat vesicle dispersions, whereas the samples were diluted 1/10 with distilled water for ζ_p measurements.

Table 1 Zeta-potential and hydrodynamic radius for the different nannoparticles under investigation

Type of nanoparticle	Zeta-potential (ζp) mV	Hydrodynamic radius (R_H) nm
DC-Chol DOPE (Φ = 0.3)	~ 60.1 ± 1.2	102 ± 4
DC-Chol DOPE (Φ = 0.5)	~ 56.3 ± 1.3	109 ± 2
DC-Chol DOPE (Φ = 0.7)	~ 55.7 ± 1.3	105 ± 1
DC-Chol DOPE/DNA (Φ = 0.5)	~ 48.1 ± 1.4	120 ± 3
DOTAP	~ 55.1 ± 1.2	61.2 ± 2.5
DOTAP/DNA	~ 42.3 ± 1.1	125.5 ±4.5
LPD complexes	~ 47.5 ± 1.3	200 ± 1.5

Table 1 shows the resulting mean values for ζ_p and size (reported as hydrodynamic radius, R_H) obtained across the experiments described in **papers I-VII** for all the nanoparticles studied.

Incubation of CLs, lipoplexes and LPD complexes

For all experiments performed plasma protein binding to nanoparticles was studied by incubating each type of the nanoparticles considered (1 mg mL^{-1}) in 10 mmol L^{-1} Tris-HCl (pH 7.4), 150 mmol L^{-1} NaCl and 1 mmol L^{-1} EDTA with 1:1 v/v amount of plasma in an ice bath for 1 h. Thereafter, the incubation was carried on at 25 °C for 1 h to promote aggregation. The sample was centrifuged at 15000 x *g* for 10 min to pellet the liposome-protein complexes. The pellet was washed with 250 μL 10 mmol L^{-1} Tris-HCl (pH 7.4), 150 mmol L^{-1} NaCl and 1 mmol L^{-1} EDTA, using a vortex mixer, transferred into a new Protein LoBind tube, and centrifuged again to pellet the liposome-protein complexes; this procedure was repeated twice. The tubes were changed after each washing step to minimize contamination of plasma proteins bound to the tubes. A plasma aliquot not incubated with nanoparticles was subjected to the same procedure as control to verify the absence of protein precipitation.

Centrifugation was chosen for the separation of the nanoparticle-protein complexes because this method does not destroy the complex nor induce the binding of additional proteins, since we were working on protein strongly adsorbed onto the nanoparticles, the so-called “hard corona”, whose biological macromolecules have a high affinity for the nanoparticle surface. To achieve this we used stringent washing conditions after centrifuging the plasma incubated with nanoparticles to obtain the pellet of the

nanoparticle/protein complex. We also used a short centrifugation time, just 2 min, to avoid sedimentation of large proteins, formation of protein aggregates, and co-precipitation. This procedure was chosen according to previous studies showing that under controlled conditions, washing and centrifugation, the nanoparticle/protein complexes are not destroyed nor any binding of additional proteins is induced (**paper IX**).

One-dimensional polyacrylamide gel electrophoresis

For separation by SDS-PAGE, proteins were eluted from the particles by adding SDS-PAGE sample buffer to the pellet and boiling the solution. A 12% polyacrylamide gel was employed to separate the proteins as reported elsewhere (**paper IX**). Coomassie PhastGel Blue R-350 was used to stain the gels with gentle agitation, in accordance with the manufacturer's manual (GE Healthcare, Milan, Italy). All experiments were conducted four times to ensure the reproducibility of the particle/protein complex pellet sizes, general pattern, and band intensities on the 1D gels. To determine the MWs of proteins after an electrophoretic run, protein MW markers were used. The MWs were finally obtained by means of Kodak dedicated software (Rochester, NY).

Proteomics experiments

In-solution trypsin digestion

A shotgun proteomics approach was used to analyze and compare human plasma protein binding capability with two different kinds of cationic liposomes, two types of lipoplexes and LPD complexes. The nanoparticle/protein complexes were resuspended in 8 mol L^{-1} urea solution

in 50 mmol L^{-1} NH_4HCO_3 and incubated with 200 mmol L^{-1} DTT at 37 °C for 1 h, under slight agitation, to denature proteins adsorbed onto liposomes, lipoplexes and LPD complexes. Afterwards, 200 mmol L^{-1} IAA were added to the samples and incubated at RT for 1 h in the dark. Subsequently, 200 mmol L^{-1} DTT were added and incubated at 37°C for 1 h, under slight agitation, to consume any leftover alkylating agent and to avoid trypsin alkylation. The sample solutions were then diluted with 50 mmol L^{-1} NH_4HCO_3 to obtain a final 1 mol L^{-1} urea concentration. Reconstituted trypsin solution (20 mg mL^{-1} in 50 mmol L^{-1} NH_4HCO_3) was added to ensure a minimum enzyme-to-substrate ratio of 1:20. Digestion of the protein samples was performed rotating overnight at 37°C and quenched the next day by adding formic acid. Digested samples were desalted by using a SPE C18 column (Bond Elut 1cc LRC-C18, VARIAN, Palo Alto, CA, USA) conditioned with ACN and rinsed with 0.1% TFA. Peptides were eluted from the SPE column with ACN:H_2O (50:50, v/v) containing 0.05% TFA and were dried in a Speed-Vac SC 250 Express (Thermo Savant, Holbrook, NY, USA). Each sample was re-constituted with a suitable volume of a 0.1% formic acid solution. Digested samples were stored at −80°C until analysis.

NanoHPLC-MS analysis

NanoHPLC was performed using a Dionex Ultimate 3000 instruments (Dionex, Sunnyvale, CA, USA) consisting of a nanopump with degasser, and a loading pump connected to a thermostatted microwell-plate autosampler. Sample was on-line enriched on a 300 μm i.d. × 5 mm Acclaim PepMap 100 C18 (5 μm particle size, 100 Å pore size) μ-precolumn (Dionex), employing a premixed mobile phase H_2O:ACN 98:2

(v/v; phase C) containing 0.1% (v/v) HCOOH at a flow rate of 10 μL min^{-1}. Peptides injected were separated on a Biobasic 18 (5 μm particle size, 300Å pore size) 75 μm i.d. × 100 mm, 15 μm tip picofrit column (Thermo Scientific, Bellefonte, PA, USA) operated at a flow rate of 250 nL min^{-1}. Phase A was H_2O and phase B was ACN, both containing 0.1% (v/v) HCOOH. A 120-min gradient was used: after an isocratic step at 5% B for 5 min, B was linearly increased to 30% within 75 min; afterwards, B was increased to 80% within 5 min, and to 95% within the following 10 min to rinse the column. Finally, B was reduced to 5% over 1 min and the column re-equilibrated for 24 min.

The nanoHPLC system was coupled to an LTQ-Orbitrap XL hybrid mass spectrometer (Thermo Fisher Scientific, Bremen, Germany) via a nanoESI ion source, operated in positive ionization mode, with spray and capillary voltage set at 2.90 kV and 42 V, respectively, and capillary temperature set at 180 °C. Full MS spectra were acquired in profile mode in the *m*/*z* range 350-1800 in the orbitrap with resolution set at 60000, whereas data-dependent MS/MS scan of the five most intense monoisotopic peaks in the spectra (top five strategy) was operated with CID activation at low resolution in the LTQ. Rejection of +1 and unassigned charge states was enabled. All MS/MS spectra were collected using a 35% normalized collision energy and an isolation window of 2*m*/*z*. Ion trap and orbitrap maximum ion injection times were set to 1000 and 200 ms, respectively. Automatic gain control was used to prevent overfilling of the ion traps and was set to 5×10^5 for full FTMS scan, and 1×10^4 ions in MS^n mode for the LTQ. To minimize redundant spectral acquisitions, dynamic exclusion was enabled with a repeat count of 1 and a repeat duration of 30 s. The whole

LC/MS system was managed by the Xcalibur software (v.2.07, ThermoFisher Scientific). Five technical replicates per sample were performed.

Data processing and statistical validation

For all experiments carried out on the various types of nanoparticles, thermo RAW data files were submitted to Mascot Deamon (v2.2.04, Matrix Science, London, UK) using the Thermo-Finnigan LCQ/DECA RAW file data import filter to perform database searches against the non-redundant Swiss-Prot database (v57.15; Homo sapiens taxonomy restriction, 20266 sequences, **papers I-VI**) and IPI human database (version 3.79, **paper VII**). For the database search, trypsin was specified as the proteolytic enzyme with a maximum of two missed cleavages. Carbamidomethylation was set as fixed modification of cysteine, whereas oxidation of methionine was chosen as variable modification. The monoisotopic mass tolerance for precursor ions and fragmentation ions were set to 10 ppm and 0.8 Da, respectively. Charge states of +2, or +3 were selected as precursor ions.

Regarding statistical data analysis for validation of peptide and protein, in **papers I**, **II**, **VI** we used a recently developed statistical open source software, the TPP. Peptide identification and protein assignment were statistically validated submitting the Mascot result files (.dat files) in the open source TPP software (Seattle Proteome Center, SPC, Proteomics Tools: http://tools.proteomecenter.org/software.php). After conversion of the output Mascot files in the .pepXML format, the PeptideProphet and ProteinProphet tools (40; 41; 50), included in TPP, were employed.

In **paper III**, in order to validate protein identifications derived from MS/MS sequencing results, the Mascot output files were submitted to the

commercial software Scaffold (v3.1.2, Proteome Software, Portland, Oregon, USA; http://www.proteomesoftware. com/) (44), which also employs a independent implementation of the Bayesian statistical algorithms developed by the Institute for Systems Biology, i.e. PeptideProphet and ProteinProphet (40; 41; 50). Scaffold tool to integrate Mascot identification results with X! Tandem search engine results (performed in automatic with the same parameters set for Mascot) was used.
In **paper VII** we used two different software solutions for label-free comparative analysis: SIEVE and Scaffold. In the case of the analysis with SIEVE, Proteome Discoverer software (version 1.3.0.339; Thermo Fisher Scientific) was used to validate identification of Mascot results. Proteins containing at least two identified peptides were accepted. SIEVE software (version 1.3; Thermo Fisher Scientific) was used to execute differential quantitative analysis on validated proteins. Alignment and framing (peak detection) were performed as follows: data were processed in the interval 13-80 min of the chromatographic separation (also processed for peptide identification), frames from MS/MS scans were used, a maximum of 200000 frames was set together with 105 as signal threshold, and peptides with MZStart 400 and MZStop 1800, MZWidth 0.01, and RTWidth 2.5 were used.
Scaffold (version 3.1.2; Proteome Software, Portland, OR, USA) was also used to validate MS/MS based peptide identifications that could be established at greater than 95% probability as specified by the PeptideProphet algorithm. Protein identifications were accepted if they could be established at greater than 99.0% probability by the ProteinProphet algorithm and contained at least two unique peptides. Proteins that

contained shared peptides and could not be differentiated on the basis of MS/MS analysis alone were grouped to satisfy the principles of parsimony. FDR was found to be 0.1% for proteins and 0.5% for peptides. Unweighted spectrum counts (USC) were used to assess the consistency of experimental replicates in quantitative analysis, and normalized spectrum counts (NSC) was used to retrieve protein abundance. The SC normalization is an option available in Scaffold by means of which SCs are multiplied by a fractional amount across samples, so that the total number of spectra are the same within each category and then across all categories. Fisher's exact test was used to identify significant differences and to calculate p-values. Ratios between NSCs were used to perform differential quantitative analysis.

4. RESULTS AND DISCUSSIONS

The results discussed in this section were initially reported in **papers I-VII**.

In **papers I**, **II** and **III** we investigated the binding of human plasma proteins to the surface of liposomes composed by the cationic lipid DC-Chol and the zwitterionic lipid (neutral helper lipid) DOPE. At the beginning, the features of this liposome formulation were analyzed and compared to those of the corresponding lipoplex system, then the attention was focused on the effect of membrane charge density on the binding of plasma proteins for liposomes with different neutral lipid/total lipid ratios, in order to have liposomes with three different membrane charge densities (Φ = 0.3, 0.5, 0.7). The resulting protein coronas have been characterized both qualitatively and quantitatively. The analysis of the observable protein patterns was interesting because this type of knowledge could help to better understand the DNA compaction process. Moreover this study might open up the way to understand molecular phenomena occurring upon lipoplex-protein interactions *in vivo*. Evidences in a recent study (22; 51) showed that clusters of multilamellar lipoplexes connected by DNA can coexist with DNA adsorbed onto unbroken vesicles. The interaction between nanoparticles and plasma proteins is mainly electrostatic, however several other factors influence the detailed nature of the protein corona. Among them, size, shape and surface hydrophilicity/hydrophobicity are fundamental features which determine the composition of the corona.

In the first study (**paper I**) two systems were initially compared, i.e. DC-Chol DOPE CLs (Φ = 0.5) and its DOPE/DNA lipoplex counterpart, in order to evaluate the effect of DNA presence. With this respect, our ζ_p

results (Table 1) showed that DC-Chol DOPE CLs and DC-Chol DOPE/DNA lipoplexes did not exhibit remarkable differences. These data were not enough to describe the exact structure. For this purpose, the two coronas were compared, because if the lipoplex structure were only multilamellar, the resulting protein profile would be the same for the liposome and the lipoplex. In fact in this type of structure, DNA molecules are enveloped by the lipid bilayer; on the contrary, in a cluster-like structure the two coronas would be different because DNA is also exposed on the surface and available for protein binding. A shotgun proteomics strategy was employed for the characterization of the two types of corona. Peptide and protein identifications were statistically validated submitting the Mascot result files to the TPP software. Here the peptide and protein probability thresholds were set at 0.7 and 0.9, respectively, for both liposomes and lipoplexes data sets. The related values for the error rate and sensitivity were 0.6, 84.4% for liposomes and 0.8, 83.0% for lipoplexes. Protein identifications were accepted if at least two unique tryptic peptides were present. Applying these conditions, 110 and 125 proteins were identified as adsorbed onto liposome and lipoplex surface, respectively, with 99 proteins being in common (Figure 6).

As Table 2 shows, individual proteins or protein classes, among which HSA, various Igs, apolipoproteins, fibrinogen, proteins of the complement pathways and other proteins, were identified. The most abundant protein in plasma, HSA, was found to be associated both with DC-Chol-DOPE CLs and DC-Chol-DOPE/DNA lipoplexes (**paper IX**).

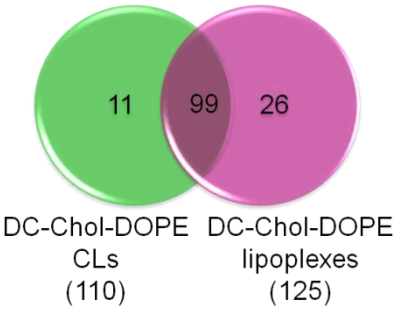

Figure 6 Venn diagram showing the distribution of TPP validated proteins for DC-Chol-DOPE CLs and lipoplexes

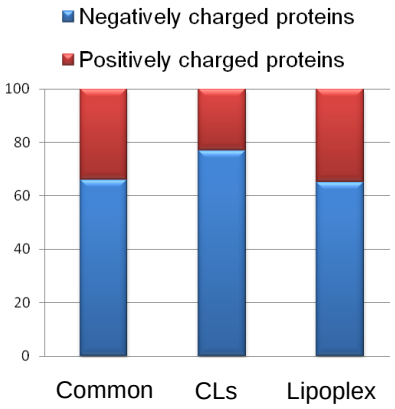

Figure 7 Charge calculated at pH 7 for the proteins identified in the protein corona of DC-Chol-DOPE LCs and DNA lipoplexes. ■ positively charged proteins; ■ negatively charged proteins

Concerning Igs, they were identified as part of the protein corona found around different nanoparticles and are involved in several biological processes (e.g. allergic reaction, immunity response and anaphylactic shock). IgG is also involved in transport across the placenta as well as in the opsonization process (52). Apolipoproteins represent the main constituents of the protein corona of particles with hydrophobic surface (23; 53). Furthermore, they are involved in the lipid and cholesterol transport throughout bloodstream (54) and, as such, are expected to greatly influence the intracellular trafficking, fate and transport of nanoparticles inside cells and body. The fibrinogen, a glycoprotein that is converted by thrombin into fibrin during blood coagulation, interacts with foreign surfaces and induces attachment of immune cells such as monocytes, macrophages and neutrophils. As a result, apoptosis is delayed and antibody-dependent cell cytotoxicity and phagocytosis are increased (55; 56).

Table 2 Proteins identified exclusively on the surface of CLs and lipoplexes, including their probability, sequence coverage, unique peptides and charge calculated at pH 7

Protein ID	Protein name	Protein probability	Coverage %	Unique peptides	Charge at pH 7
Liposomes					
	Protein transport protein Sec16A	0.9234	0.6	3	−51.3
	CD5 antigen-like	0.9846	18.7	4	−11.3
	Apolipoprotein M	0.9873	9	2	−3.8
	Angiotensinogen	0.9999	8.9	2	−5.8
	Ig k chain V-II region TEW	0.9904	32.7	2	−0.9
	Coagulation factor V	0.9623	1.1	2	−40.6
	CD9 antigen	0.9889	15.4	2	0.4
	Ubiquitin-conjugating enzyme E2 H	0.908	15.3	2	−13.3
	Apolipoprotein F	1	8.8	3	−6.7
	Collectin-11	1	29.2	6	−6.3
	Protein Z-dependent protease inhibitor	0.9995	7.9	2	4.1
Lipoplexes					
	Ras-related protein Rab-27B	0.9248	10.1	2	−2.9
	Putative nucleoside diphosphate kinase	0.9983	19	2	3.8
	Histone H2B type 1-K	1	34.9	4	18.6
	Serum deprivation-response protein	0.9913	12.5	4	−18.3
	Plasminogen	0.9308	3.7	2	3.4
	Complement C5	1	4.8	6	−9.8
	Kininogen-1	1	25.6	14	6.8
	Band 3 anion transport protein	0.9934	3.6	2	−27.7
	Fibronectin	1	4.4	7	−45.3
	Complement component C8 a chain	0.9991	7.9	2	−3.7
	Complement component C8 g chain	0.9953	16.3	2	3.1
	Histone H1.4	1	16.9	4	58.9
	Complement component C7	0.9797	3.8	2	−6.6
	Heat shock cognate 71 kDa protein	1	23.1	8	−11.4

	Solute carrier family 2, facilitated glucose transporter member 3	0.9999	8.1	3	0.4
	Keratin, type I cytoskeletal 10	1	25.7	8	−14.2
	Lipopolysaccharide binding prot	0.9573	6	2	−1.7
	Myosin regulatory light polypeptide 9	1	55.8	8	−11.1
	Peroxiredoxin 6	0.9869	16.1	2	−1.4
	Protein disulfide-isomerase A3	0.9963	18.2	3	−4.0
	Coronin-1A	0.9984	13.4	3	−1.9
	F Actin capping prot. Sub. a	0.9832	14	3	−7.2
	Nucleosome assembly prot 1 like 1	0.9207	14.3	3	−52.6
	Clathrin heavy chain	0.9036	1.6	2	−33.2
	Adenylyl cyclase-associated protein 1	1	29.5	6	5.8
	Latent transforming G.F. b bind	0.9328	3.1	3	−36.8

The nanoparticles studied were lipid nanovectors and for these systems the main interaction with plasma proteins was electrostatic; so this finding was striking because it was an evidence that lipoplex surface was different from that of pure CLs. The condensation of DNA on the lipid surface was a possible explanation for this phenomenon and was in agreement with the measures of ζ_p.

In order to elucidate the correlation between the nanoparticle surface charge and protein corona compositions, the charges at pH 7 for all the identified proteins was calculated using a specific software (http://www.scripps.edu/~cdputnam/protcalc.html, values are listed in Table 1). Figure 7 shows the fraction of negatively (blue) and positively (red) charged proteins in the overlap of the two protein coronas. As evident, the proteins common to both

coronas are principally negative (66%), an expected result because both DC-Chol-DOPE CLs and DC-Chol-DOPE/DNA lipoplexes are positively charged nanoparticles. The same consideration performed taking into account the unique proteins (i.e. those that are not common) gives a different result: in this case, the percentage of negatively charged proteins was found to be about 77% and 65% for liposomes and lipoplexes, respectively. On the other hand, the average charge of the proteins found in the coronas was -11 for DC-Chol-DOPE CLs and -6 for DC-Chol-DOPE/DNA lipoplexes. On average, the presence of more positively charged proteins in the lipoplex corona indicated that their surface was, at least locally, negatively charged. All these data showed that polyanionic DNA was associated with the lipoplex surface and could interact with positively charged plasma proteins. The evaluation of the lipoplex corona showed that it was rich of histones and complement proteins, which are DNA-binding protein, the presence of which further supported that a part of DNA was bound to the lipid surface. In particular, histones H1 and H2B type 1-K were identified exclusively in the lipoplex corona, suggesting that DNA was adsorbed at the lipoplex membrane and recognized by specific DNA-binding proteins as these. Complement proteins make up the complement system, a part of the immune system that contributes to clear pathogens from an organism (57). Their presence on the DNA-rich surface of lipoplexes was in very good agreement with the existence of a domain with DNA-binding activity in these proteins (58) and explains why lipoplexes are often rapidly cleared from the bloodstream and delivered to the Kupffer cells in the liver: indeed they form transmembrane channels on the surface of intruding pathogenic cells and cause lysis. Finally, another

protein found only on the lipoplex corona was fibronectin, which also has a DNA-binding domain. This is interesting because fibronectin can bind top cellular components known to promote the lipoplex-cell interaction and thus facilitate cell adhesion and internalization. This is supported by a work in which fibronectin was added to the surface or in solution with the lipoplexes and could enhance the substrate-mediated gene transfer efficiency (59).

After a qualitative characterization of the protein corona of DC-Chol-DOPE CLs and lipoplexes, the next step was to evaluate the effect of charge density on the nanoparticle surface (**papers II** and **III**), which is one of the known features affecting transfection, in order to evaluate if any difference could be established in the protein corona, both qualitatively and quantitatively. The membrane charge density is the average charge per unit area of the membrane and can be varied changing the ratio between the neutral and the cationic lipid employed in the liposome preparation (in this case, DOPE and DC-Chol, respectively). Three different molar ratios were chosen, Φ = 0.3, 0.5, and 0.7, keeping constant the moles of cationic lipid (i.e., the overall charge). In these studies the issue concerning biological and technical variability was analyzed. The reproducibility of MS analysis in proteomics depends upon variations in sample preparation, proteolytic digestion, on-line separation of peptides and MS data acquisition, analysis and interpretation (60). To minimize biological variability and consider only the variables due to the analytical protocol and methodology, a pool of plasma has been employed, because blood composition may change significantly from one person to another one, resulting in different interactions with the nanoparticles (23). This was adopted for all the experiments of this study. Moreover, for these experiments, three

experimental replicates, with five technical replicates each, were performed for each sample, in order to assess the experimental reproducibility, resulting in 15 data files for each CL formulation. The proteolytic digestion was controlled using a freeware, RawMeat, that allowed to visualize different information, such as the charge distribution in the full MS spectra of precursor ions. What could be established was that mass charge varied from +2 to +6, with +2 and +3 charge precursors being about 85% of the total, and +4 charge precursors representing another 10%; the absence of higher charge states indicated a satisfactory digestion for the all the samples analyzed. RawMeat also allowed to evaluate the retention time reproducibility among technical replicates by checking the alignment overlaying the total ion current of all the samples belonging to the same CL formulation. Good reproducibility was also obtained comparing retention times of some selected peaks for samples belonging to different CL formulations, if the same chromatographic column was used. The qualitative study of the nanoparticle corona was performed validating Mascot search results with the TPP platform, setting the peptide and protein probability thresholds at 0.7 and 0.9, respectively. The related FDR values and sensitivity were, respectively, 0.5% and 86.9% for CLs with $\Phi = 0.3$; 0.6% and 89.0% for CLs with $\Phi = 0.5$; and 0.6% and 90.7% for CLs with $\Phi = 0.7$. Protein identifications were accepted if at least two unique tryptic peptides were present. With these criteria, the proteins identified in the corona of CLs with $\Phi = 0.3$, 0.5, and 0.7 were, respectively, 133, 128, and 143, with a total of 169 proteins, 106 of which being in common (Figure 8a).

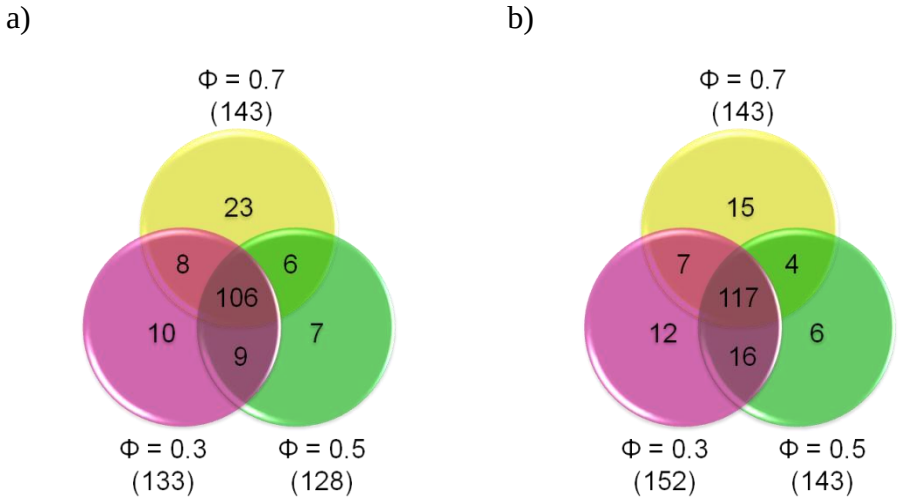

Figure 8 Venn diagrams for the three CLs formulations showing the distribution of all identified proteins in: a) the qualitative (**paper II**) and b) quantitative (**paper III**) experiment

As in the previous study, the majority of the 106 proteins were common to the three CL formulations and were involved in the immune or inflammatory processes (acute phase), blood coagulation, including platelet activation and degranulation, or in lipid transport functions (e.g., apolipoproteins).

The CLs with Φ = 0.7 were able to bind more proteins and, as a consequence, were also the nanoparticles having the highest percentage of proteins exclusively adsorbed onto their surface (16% *vs* 7.5% and 5.4% of CLs with Φ, respectively, 0.3 and 0.5). This result was likely due to the different CL characteristics because the moles of cationic lipids were fixed, whereas the moles of neutral lipids was varied to obtain the different Φ values, and CLs with higher Φ possess a larger surface area. On the other hand, to a higher Φ corresponds a smaller σ_M that, differently from our

initial hypothesis, seemed to have not a determinant role in protein adsorption.

After the study of the analytical reproducibility and qualitative analysis of the plasma proteins adsorbed onto the three different CLs, the experiment was repeated to add a label-free quantitative analysis based on SC (**paper III**). In this case, the validation of protein identifications was performed using the Scaffold software, also exploiting the X! Tandem search engine to increase confidence. Minimum peptide identification probability was set at 95% (the highest available value), whereas protein identification probability was set at 99%, with each identification accepted if at least two unique peptides were present. The original Mascot search was made against a standard forward database so, applying the just mentioned filters, a FDR < 0.1% was calculated, and a total of 177 proteins were identified; in particular, 152 proteins were identified for $\Phi = 0.3$ CLs and 143 for both $\Phi = 0.5$ and $\Phi = 0.7$ CLs, with 117 proteins being in common (Figure 8b). These results were slightly different from the ones obtained from the first experiment, but this difference could be assigned to subtle modifications in the validation algorithms implemented by the two software programs, as well as the additional X! Tandem second search. The aim of this work was to quantify both major and minor proteins forming the corona because such a knowledge could help in developing future predicting models for nanoparticle surface chemistry interactions and biodistribution. For protein quantitative analysis, the Scaffold software normalization of the SCs and various statistical tests, to identify significant abundance differences in two or more categories, were employed. Quantitative data showed that CLs with $\Phi = 0.3$ and $\Phi = 0.5$ had a similar protein abundance for almost all the

identified proteins, leading to the conclusion that the composition of these two CL formulations was roughly the same. More difference emerged from the comparison between the coronas of Φ = 0.3 CLs and Φ = 0.7 CLs, and for such a reason the following discussion of protein differences will be restricted to the comparison of these two CL fromulations only. In order to evaluate the actual contribution of each protein to the hard corona composition, another correction was adopted over the mean values of the NSCs for the three experimental replicates (61). This correction expressed a relative protein quantity and represented a normalization that considered the mass of each protein, and was calculated as follows (Equation 1).

$$MWNSC_k = \left(\frac{(NSC/MW)_k}{\sum_{i=1}^{n}(NSC/MW)_i}\right) \times 100 \qquad (1)$$

The $MWNSC_k$ is the percentage MW-normalized NSC for protein k (i.e. the relative protein abundance in the 'hard corona') (61), and MW is the MW in kDa for protein k. The quantitative analysis of the identified protein was performed, however it should be noted that the protein abundance did not necessarily reflect the biological impact of the nanoparticle. In fact, less abundant proteins bound to the nanoparticle surface can have a significant effect and can take part to several biological processes. However proteins, the relative abundance of which is extremely low, were not expected to be a determining factor for the fate and impact of the nanoparticle (61-63). In order to simplify data interpretation and evaluate only proteins with larger relative abundances, the attention was restricted to proteins with a $MWNSC_k \geq 1$. Relative abundances of protein satisfying such criterion is reported in Figure 9. The results appeared dependent upon the lipid composition, which was the main difference, since size and the ζ_p of CLs

with Φ = 0.3 and 0.7 were quite similar (Table 1). To better decipher data, we calculated the relative protein abundance ratio, R, defined as the ratio between the $MWNSC_k$ of Φ = 0.3 CLs and Φ = 0.7 CLs, considering significant only R > 2 and R < 0.5. This highlighted that fibrinogen was more associated with Φ = 0.3 CLs (R > 2) than all other identified proteins. On the other side, apolipoproteins and C4b-binding protein alpha chain are most abundantly associated with Φ = 0.7 CLs (R < 0.5, Figure 10). Considering that Φ = 0.7 CLs were richer in DOPE that Φ = 0.3 CLs, phospholipid-lipoprotein binding represented a general feature of lipid-based nanoparticles in physiological conditions. In fact, the results showed that apolipoproteins had hydrophilic phospholipids that could better interact with the phospholid moiety of DOPE rather than with the less hydrophilic head group of DC-Chol. Significant quantities of opsonins (in particular fibrinogen, which was abundant in Φ = 0.3 CLs, but also IgG, and complement factors), were detected and were supposed to promote rapid clearance from the bloodstream; on the contrary the binding of dysopsonins (in particular apolipoproteins were found abundant in Φ = 0.7 CLs corona) promotes prolonged circulation time in blood (61-63). The presence of apolipoproteins on CL surfaces was also associated with a enhanced interaction with low-density lipoprotein receptors, which facilitates the transport across the blood-brain barrier. The presence of C4b-binding protein, prevalent in Φ = 0.7 CLs, was not in contradiction with this suggestion because it has as inhibitory role in the complement system. This specific adsorption on CLs with different Φ was also confirmed by the lists of unique proteins for the two systems.

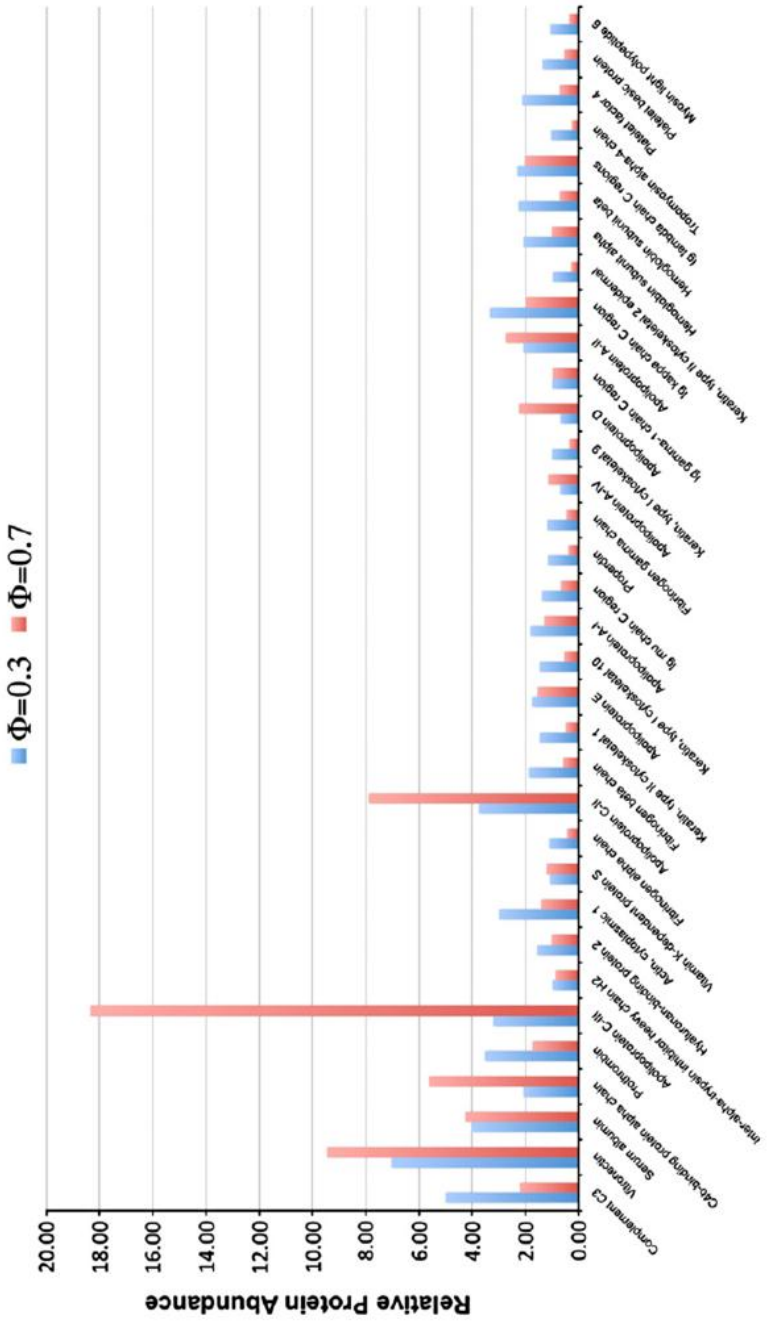

Figure 9 Picture displaying the relative protein abundance normalized to the MW (MWNSC) ≥ 1 for Φ = 0.3 (blue) and Φ= 0.7 (red) CLs

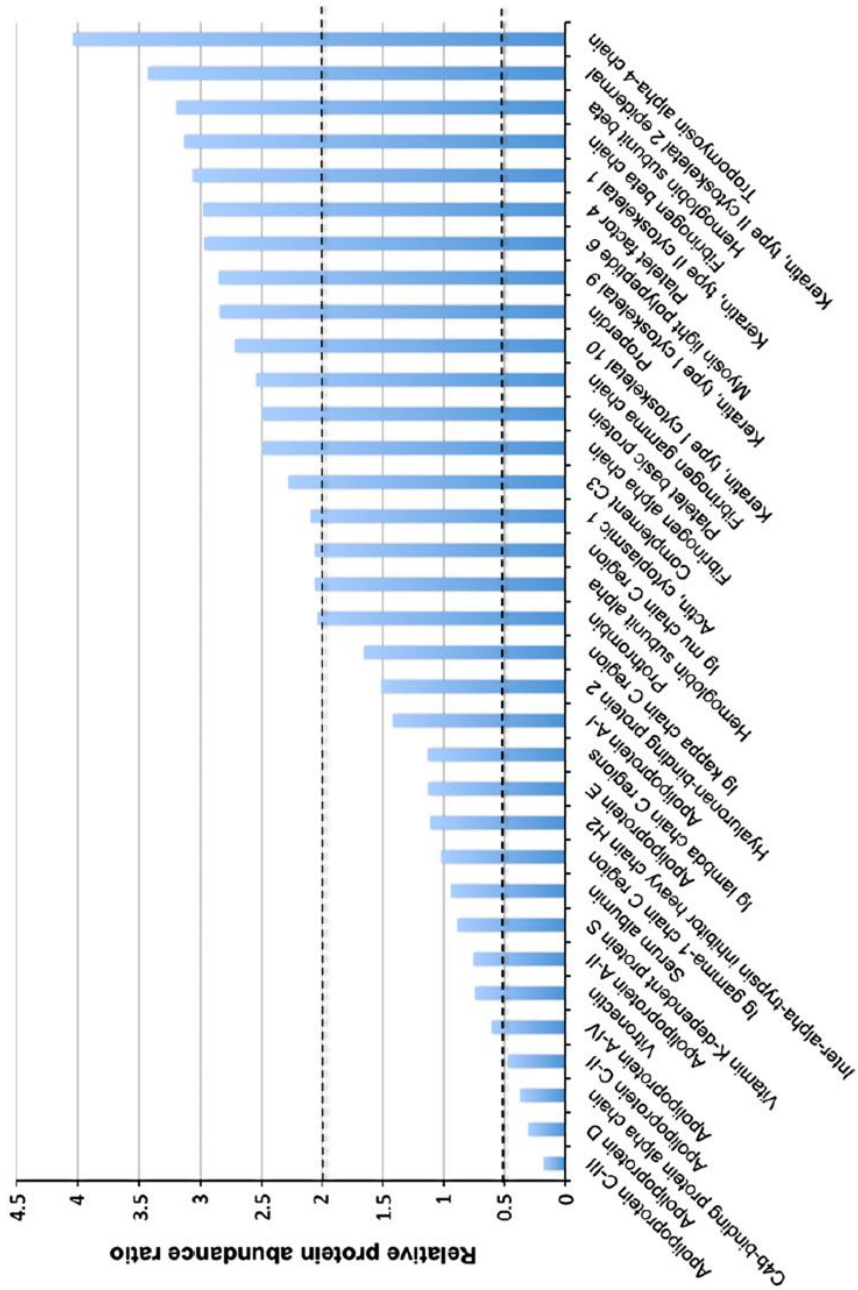

Figure 10 Picture displaying the relative protein abundance ratio R

Proteins bound to CLs with Φ = 0.7 (the most lipophilic nanopartciles characterized) were associated with the liver (a lipid-rich organ) and involved in blood coagulation process and complement pathway. On the contrary, the proteins that were found only in the Φ = 0.3 CL coronas have binding functions and are localized mostly in cytoplasm. However, the relative protein abundance of such "exclusive proteins" was lower than 1% in both the coronas. In this case, too, the charges at pH 7.4 of those proteins with $MWNSC_k \geq 1$ either in the corona of CLs with Φ = 0.3 or in that of CLs with Φ = 0.7 were calculated (http://www.scripps.edu/~cdputnam/protcalc.html). The relative charge, a measure of the relative amount of the charge on the protein corona, was calculated by multiplying the total charge on the protein k, q_k, for its relative protein abundance, $MWNSC_k$ (Equation 2).

$$Q(\phi) = \sum_{k=1}^{n} q_k \times MWNSC_k(\phi) \quad (2)$$

The relative charge of both the coronas was negative; with Q (Φ = 0.3) < Q (Φ = 0.7): it confirmed that the cationic surface interacted prevalently with negatively charged proteins. Moreover, considering that Φ = 0.3 CLs were more positively charged than Φ = 0.7 CLs, it could be established that the charge of the protein corona and the membrane charge density of cationic lipid membranes were strongly related to each other. Φ = 0.7 CLs had a larger amount of DOPE with a resulting electrostatic repulsion barrier that was low enough to be overcome by basic proteins; short-range attractive van der Waals forces could thus prevail over electrostatic repulsion, thereby inducing membrane aggregation and nanoparticle clustering, as also has been experimentally observed.

Once established that the amount of DOPE in the CL formulations could deeply influence the surface properties and the membrane charge density of cationic membranes, the effect of plasma concentration on the resulting protein corona was investigated, this time for DOTAP CLs and lipoplexes (**paper IV**). In fact, recent studies demonstrated that the actual composition of the hard corona of silica nanoparticles varied significantly with protein concentration (61). The choice of DOTAP CLs was made because they represented an excellent model systems of lipid nanoparticles in which a DNA/polycation core is coated with a lipid envelope (64-66). This aspect is quite interesting because it allowed to investigate the differences observed when nanovectors are used in *in vivo* studies instead of in *in vitro* studies, highlighting the effect of a real biological environment, with important consequences useful in future application of lipid-based gene vectors. Both CLs and lipoplex suspensions were incubated with different plasma concentrations (2.5, 5, 10, 20, 50, and 80%). In order to evaluate the differences in protein bound to the corona, a separation by SDS-PAGE was performed, to which a shotgun protein identification and quantitation was also added. Initially, a preliminary physical-chemical characterization of both DOTAP CLs and DOTAP/DNA lipoplexes was carried out. Sizing and ζ_p measurements showed that DOTAP CLs were small, positively charged vesicles (R_H = 61.2 nm; ζ_P potential = 55.1 ± 1.2 mV). DOTAP/DNA lipoplexes were larger, instead, (R_H = 125.5 nm), with a lower surface charge (ζ_p = 40.0 ± 1.1 mV). Synchrotron small-angle X-ray scattering (SAXS) intensity was used to investigate the structure, and indicated that CLs were simple unilamellar vesicles, whereas DOTAP/DNA lipoplexes were multilamellar onion-like structures, where DNA rods were densely

packed within more than 30 lipid bilayer/DNA monolayer aggregates, in agreement with the accepted model of the DNA-induced restructuring of CLs upon lipoplex formation (67). Data also confirmed the recent suggestion that lipoplexes are hybrid structures in which DNA chains could also be exposed on the surface (68), a fact which was expected to influence the nature of the protein corona. From the SDS-PAGE analysis it was evident that the increase in plasma concentration affected the pattern of proteins adsorbed onto the corona, in particular for DOTAP CLs (Figure 11a), whereas for lipoplexes the intensity of the protein bands seemed directly proportional to the increase of plasma concentration (Figure 11b). The differences among different gel runs were evaluated calculating the total band intensities of proteins recovered from DOTAP CLs (61) (Figure 11c) and DOTAP/DNA lipoplexes (Figure 11d).

For DOTAP CLs the total amount of protein was maximum at ~20% plasma and decreased at lower and higher plasma concentrations, a trend explained taking into account that the most abundant proteins (i.e., those binding at lower plasma concentrations) were progressively displaced by those with a higher affinity (16; 24; 61; 63; 69; 70). Aggregation of CLs was another possible explanation (24). The trend of total band intensity for DOTAP/DNA lipoplexes was quite different and increased with plasma concentration (Figure 11d), probably because more proteins of the same type bound at higher concentrations. DNA molecules affected the protein corona even at low plasma concentration because being partially exposed allowed them to be available for protein adsorption.

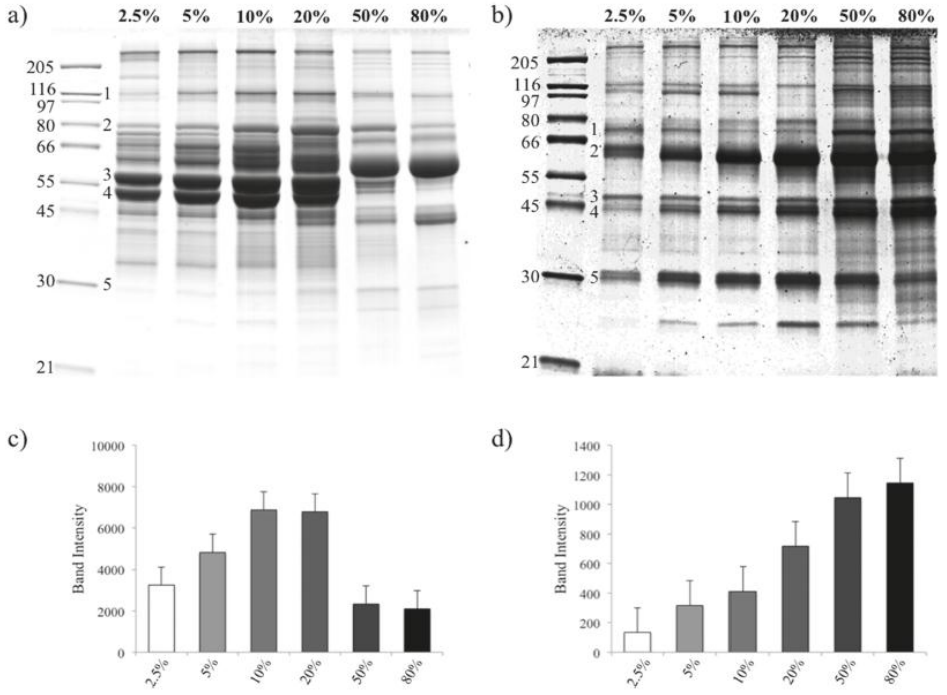

Figure 11 For 2.5 - 80% plasma concentrations, SDS-PAGE gels of proteins found in the corona of: a) DOTAP CLs, and b) DOTAP/DNA lipoplexes. Most abundant proteins are marked with numbers. At the bottom the histograms for the corresponding total band intensity are reported for: c) DOTAP CLs, and d) DOTAP/DNA lipoplexes.

The comparison among the gel band total intensities for a certain plasma concentration between the two systems highlighted that the intensity was higher for CLs than for lipoplexes, which meant that the lipid membrane area of CLs that was available for binding was larger than that of the lipoplexes, in agreement with the results of the preliminary physical-chemical characterization of lipoplexes as a multilamellar structure. Indeed, multilamellarity (71-73), is a factor known to reduce the fraction of the lipid available on the outer surface for binding. To further support this observation, the total intensity of each lane at a fixed plasma concentration from the gel reported in Figure 11b was divided by the total intensity of the

corresponding lane from the gel reported in Figure 11d. The calculated ratio, R_I, is reported in Figure 12.

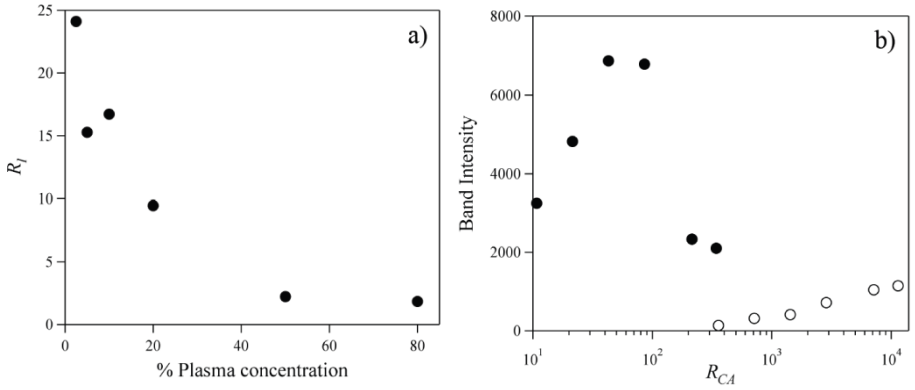

Figure 12 Plots showing a) R_I ratio as a funtion of plasma concentration, and b) total intensity from Figure11b *vs* R_{CA}

At the lowest plasma concentration (2.5%), R_I was found to be ~25, in agreement with the ratio of the exposed surface area for DOTAP CLs to that of the DOTAP/DNA lipoplexes. This ratio was kept constant in the experiment, nevertheless R_I decreased with the increase of plasma concentration. Moreover, although the ratio of the plasma concentration to the total particle surface (R_{CA}, area mL^{-1}) was not constant throughout the experiment, the two investigated regions were practically contiguous, and plotting the total intensity of each lane from the gels reported in Figure 11a,b against R_{CA} did not show any clear trend. (Figure 12b).

The interpretation of the data reported in Figure 12a was complicated by the fact that the exposed surface area of CLs is 30-fold larger than that of lipoplexes and the effective area per protein decreased with increasing protein concentration; other determining factors complicating data interpretation were the particle size, different for CLs and lipoplexes, and the nature of the surfaces, which for CLs were completely lipid, whereas for

lipoplexes DNA molecules were also present. All these aspects deeply affected the composition of the resulting protein corona in the different conditions for the two systems, and a quantitative comparison was not easy. In particular, a semiquantitative densitometry analysis was performed and the relative densitometry results as portrayed in Figure 13a for DOTAP CLs and Figure 13b for the corresponding lipoplexes. For the five major bands of Figure 11a, b, the intensity of each protein band was divided by the total intensity of the lane, and the same process was also carried out as a function of the plasma concentration during incubation (Figure 13a). From this analysis two groups of proteins could be found, low-affinity (LA) proteins, the relative amount of which showed a decreasing trend in the corona, and competitive-binding (CB) proteins, the relative amount of which had an increasing trend in the corona with increasing plasma concentration. For this reason, the formation of the corona for DOTAP CLs did not appear to be stable, with its composition probably affected by a cooperative phenomenon (61). However, for DOTAP/DNA lipoplexes, the relative intensities of all bands did not change significantly increasing from 2.5 to 80% plasma concentration, and the protein composition remained largely unchanged. The shotgun proteomics part of the experiments provided the identification of the proteins found in selected bands, which were cut from the gels and sequenced. As in previously described studies, the most abundant plasma proteins (albumin, fibrinogen, complement C5, apolipoprotein A-I, transferrin, vitronectin, and fibronectin) were identified for both systems.

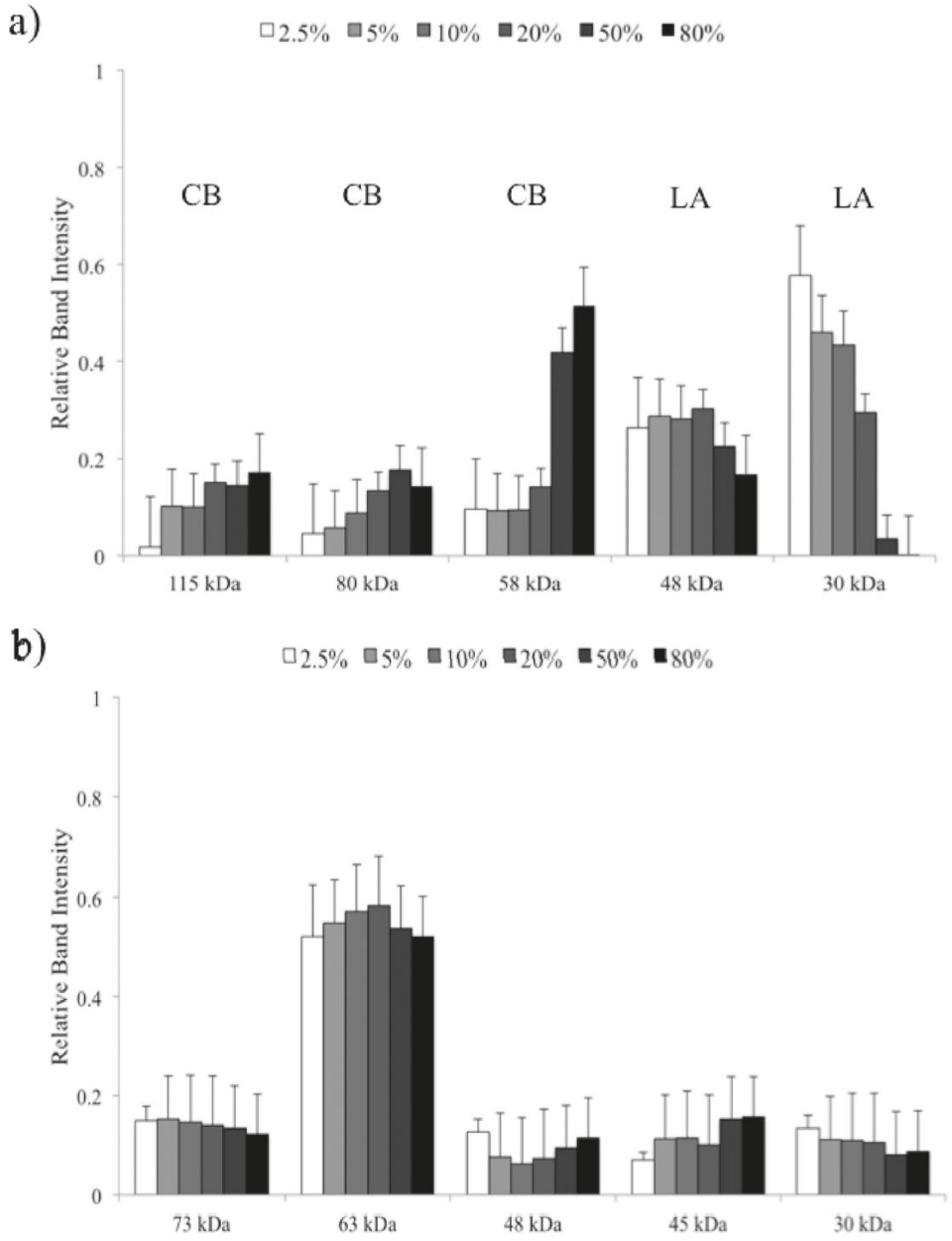

Figure 13 For the different plasma concentrations, after 1 h incubation, plots showing the relative amounts of proteins marked in Figure 11a, b for: a) DOTAP CLs, and b) DNA lipoplexes. The proteins for which the relative amount decreased with increasing plasma concentration were labeled low-affinity (LA) proteins; the proteins for which the relative amount increased with plasma concentration are labeled competitive-binding (CB) proteins

However, in the corona of DOTAP/DNA lipoplexes a larger amount of immunoglobulins was detected. They are mainly basic proteins and their presence revealed that the surface charge of lipoplexes could locally be negatively charged, probably due to DNA on the surface, as also supported by sizing, ζ_p and SAXS measurements. Histones were also unique of the lipoplex corona.

One common issue with liposome nanovectors is that the multilamellar structure of lipoplexes provides protection during transport, but also often hinders an adequate DNA release when inside the cell, with DNA trapped in the endosome and then degraded in the lysosomes (9; 74; 75). In order to increase transfection, lipoplexes were modified, condensing plasmid DNA with a polycation and forming lipid/DNA/polycation (LDP) complexes (76), which had successful results in delivering a gene to the liver with respect to more traditional liposome gene vectors (15).

The next studies carried out were set in this context, and demonstrated that the TE of P/DNAcomplexes coated with a lipid envelope made of DOTAP is 3-20 times higher than that of DOTAP/DNA lipoplexes, which were considered as a comparison model, and evaluated for transfection CHO, HEK293, NIH 3T3, and A17 cells (**paper V**, Figure 14).

Moreover, the encapsulation of precondensed DNA in the lipid envelope would have been a mean by which the interaction between DNA and basic serum proteins would be reduced (15; 65-66; 75-78). In order to elucidate this enhanced TE, several aspects were studied. The stabilization of these complexes was one issue to consider, and required the understanding of the factors that govern amphiphile-DNA interactions and subsequent complex formation.

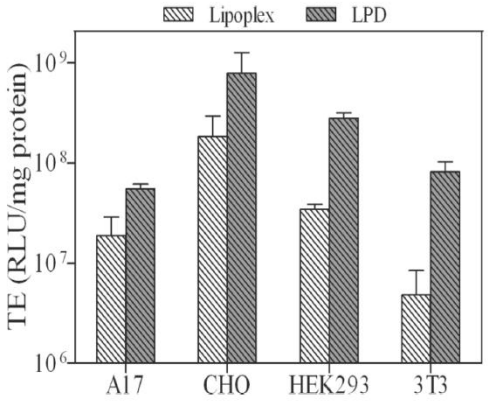

Figure 14 TE of lipoplexes and LPD complexes at lipid/DNA ratio 2. Luciferase activity is reported as relative light units mg^{-1} protein in cell lysate.

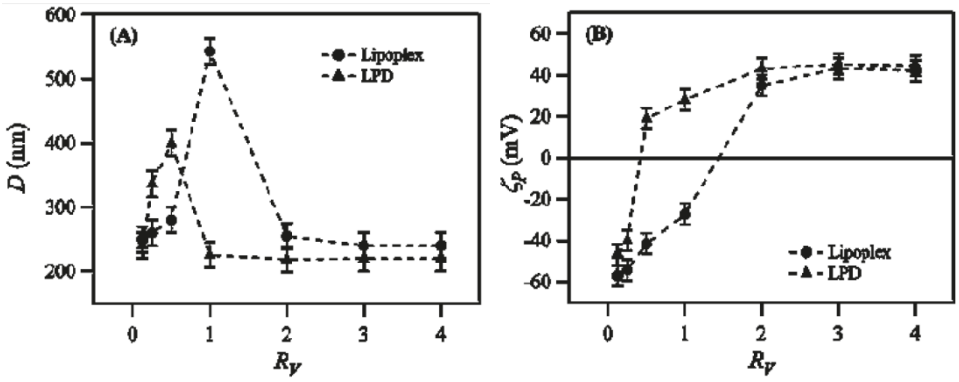

Figure 15 Plots showing the diameter (a) and zeta-potential (b) for lipoplexes (circles) and LPD complexes (triangles) as a function of lipid/DNA volume ratio Rv.

When the complex is formed, reentrant condensation and charge inversion (73; 79), occurred for both systems (Figure 15), but in the case of LPD complexes charge and size saturation occurred at R_V values smaller than those observed for lipoplexes; this meant that the complete encapsulation of P/DNAcore by a lipid envelope required a lower amount of cationic lipid than that for the formation of a similar lipoplex with the same amount of DNA. For this reason LPD complexes have an advantage over conventional

lipoplexes because they are potentially less toxic than for *in vivo* applications.

The enhanced TE of LPD complexes was also influenced by the capability of the nanovector to overcome a series of biological barriers (membrane, cytoplasmic compartment, nucleus) (80). This capability depends upon the physical-chemical properties of the vector, such as size (81-84), ζp (85; 86), nanostructure (71, 87), propensity to be disintegrated by anionic lipids (73, 79, 87-91) and ability to release DNA both in the cytosol and in the nucleus. However, no significant difference was observed for the ζp of LPD complexes and lipoplexes (ζp = 47.5 and 44.4 mV, respectively) or for their size, which could influence the uptake mechanisms (80), because both systems were larger than 200 nm and were supposed to enter via caveolae-mediated pathways.

More differences were expected in the fuse mechanisms with the cell membrane. Here, when the nanovector reaches the membrane, anionic cellular lipids begin to laterally diffuse into the complex neutralizing cationic lipids (92). Cationic/anionic mixed bilayers form and weaken the electrostatic attraction between cationic lipids and DNA, and when the positive lipoplex charge is neutralized, DNA can be released (92). SAXS measurements showed that DNA was not located in the lipid envelope of LPD complexes, but trapped inside the nanoparticle core. For this reason anionic cellular lipids could interact with LPD cationic lipids without competition with DNA, resulting in a more efficient DNA cytoplasmic release than normal lipoplexes, as observed by confocal microscopy experiments (Figure 16).

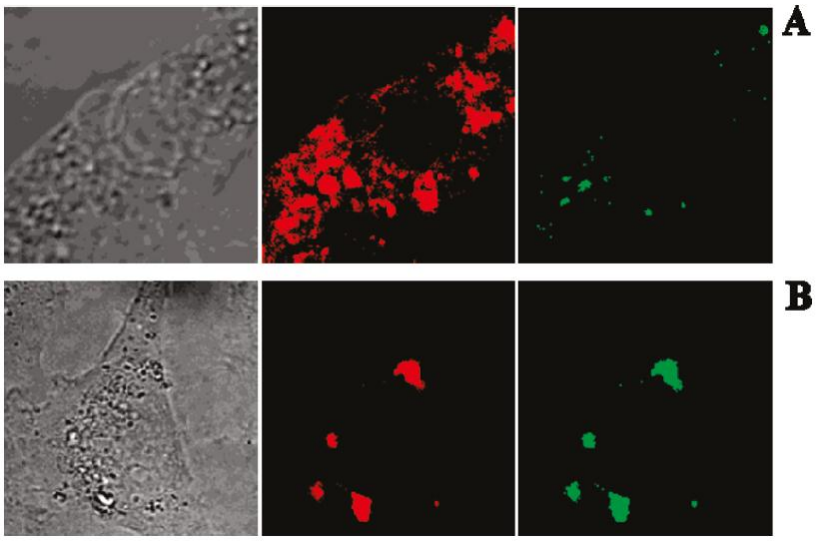

Figure 16 Confocal microscopy images of CHO-K1 cells 4 h after treatment with: a) LPD complexes , and b) lipoplexes; in the case of LPD complexes, the green-fluorescent NBD-DOTAP and red-fluorescent DNA have different localizations, with DNA spread into the cytoplasm; on the contrary, in the case of liposomes, a colocalization was observed, suggesting that lipoplexes remained intact

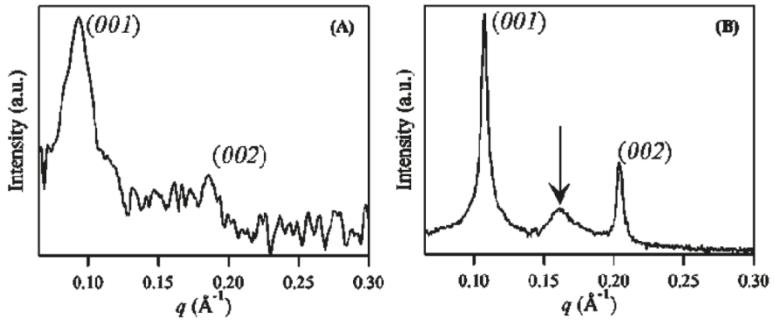

Figure 17 SAXS patterns for: a) LPD complexes, and b) lipoplexes, at DNA volume ratio $R_v = 2$; Sharp periodical peaks represented alternating lipid bilayers DNA/monolayer; the arrow-marked peak indicated the one-dimensional ordering of DNA placed between the lipid bilayers

Moreover, SAXS measurements have highlighted that LPD complexes were made of about 10 lipid layers in a highly swollen state, while lipoplexes were more ordered multilamellar structures in which 30 alternating lipid/

DNA layers were present (Figure 17). This could help the fusion process for LPD complexes because the number of lipid layers to be peeled off is inferior.

LPD complexes, as well as several other nanovectors used in gene delivery, are usually administrated intravenously; for this reason, after their preliminary physical-chemical characterization, LPD complexes were compared to simple DOTAP CLs and their corresponding lipoplexes, this time focusing the attention on the effect of their exposure to plasma. In fact the type of protein corona which is formed is essential for an adequate distribution *in vivo*. The proteomic study was initially qualitative: with Mascot search results submitted to the TPP for protein identification validation (**paper VI**). In this work the experimental and analytical reproducibility of the method described for the isolation and analysis of proteins adsorbed onto these systems was evaluated. In fact in proteomic studies it is frequent that the analysis of the same sample under the same experimental conditions can lead to the identification of a different protein set for each experiment (93-95). Usually it is very rare to observe a 100% overlap between two chromatographic runs even for the same sample, especially for very complex samples, where the degree of overlap can reach only about 20%. For this reason, the presence (or absence) of a protein in a sample can be a consequence of incomplete determination and may not reflect real biological difference between samples. To tackle this issue, three experimental replicates were performed, with five technical replicates each. Chosen a peptide and protein probability threshold for validation, in the best case (experimental replicate 1 of CLs), the false-positive rate is very low (error rate of 0.3%), with an extremely high percentage of correct

identifications (95.4%) (Table 3). On the other hand, in the worst instance (experimental replicate 2 of LPD complexes), the false-positive rate is also quite low 0.7%, with a percentage of correct identifications which was still good (81.0%). The agreement between experimental and technical replicates showed that the experiment had a high degree of reproducibility, with very similar sensitivities and error rates (Table 3).

Table 3 Protein identification sensitivity and error rates as calculated on the 5 technical replicates by the TPP, setting peptide probability ≥ 0.75 and protein probability ≥ 0.90

Experimental replicate	Sensitivity	Error rate
CLs		
1	95.4%	0.3%
2	92.5%	0.5%
3	93.7%	0.4%
Lipoplexes		
1	88.8%	0.6%
2	91.2%	0.6%
3	94.2%	0.7%
LPD complexes		
1	87.5%	0.8%
2	81.0%	0.7%
3	86.2%	0.7%

The percentage of overlap among the experimental replicates was also calculated and is reported in Table 4. Identified proteins for the three lipid vectors were classified for each experimental replicate, reporting the corresponding percentage of the total, number of proteins that did or did not overlap among the experimental replicates and the number of proteins uniquely identified in a single replicate. This classification showed that the number of proteins overlapping among the three systems in the three experimental replicates was very high, certainly because protein samples were not too complex and the number of chromatographic runs was quite high. Another aspect emerged from this comparison: the variation of protein

identifications was significantly larger for LPD complexes, indicating that the type of proteins adsorbed onto the surface of LPD complexes changed slightly between experimental replicates, probably because the presence of protamine could make the nanoparticles dynamically unstable. On the contrary the percentages of overlap among the three experimental replicates were very close to each other in the case of CLs and lipoplexes, because they were more stable systems (Table 4).

Table 4 Proteins overlapping among the three systems under investigation as validated from five technical replicates (the percentage of the total of proteins which were identified in each experimental replicate is also reported in brackets)

	Exp. replicate			Combined	Overlap		Only exp. replicate		
	1	**2**	**3**		**Yes**	**No**	**1**	**2**	**3**
CLs	90 (85.7%)	95 (90.5%)	94 (89.5%)	105	82	13	1	5	7
Lipoplexes	176 (84.6%)	186 (89.4%)	168 (80.8%)	208	140	26	9	10	7
LPD complexes	135 (85.4%)	110 (69.6%)	116 (73.4%)	158	92	47	26	6	15

The number of proteins identified for the three lipid vectors is depicted in Figure 18. Lipoplexes bound the largest number of proteins, 208, whereas only 105 were identified on the corona of CLs and 158 in the corona of LPD complexes. This could be a consequence of lipoplex structure and partial exposure of DNA on the surface, which made it available for binding of proteins, such as DNA-binding proteins and/or basic proteins that otherwise would not interact with simple cationic lipid membranes. The number of proteins bound to the surface of the LPD complexes was intermediate between those of CLs and lipoplexes. A possible explanation of this observation could be that, although in LPD complexes plasmid DNA was condensed with protamine and encapsulated within the lipid envelope, a

fraction of precondensed DNA used for preparation might be subtracted by cationic lipids, resulting in some intermediate structure in which DNA was still available to protein binding. This suggestion was also supported by a large percentage of overlap between lipoplexes and LPD complexes.

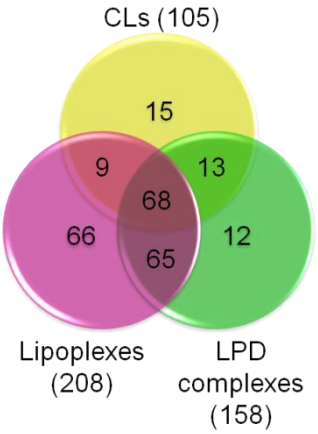

Figure 18 Venn diagram showing identified proteins for DOPE CLs, lipoplexes and LPD complexes

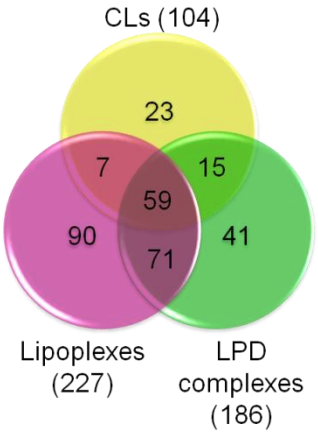

Figure 19 Venn diagrams showing the proteins validated by Proteome Discoverer

Established that the experimental conditions were suitable for differential proteomic analysis, the analysis of the protein corona of the three systems was possible. The experiment was repeated, this time with the aim of exploiting label-free quantitation approaches to add a quantitative description of the differences in protein forming the corona of the three nanovectors under investigation (**paper VII**). By means of Proteome Discoverer, 306 proteins were validated, in particular 104 for CLs, 227 for lipoplexes, which resulted to have the richest protein corona, and 186 for LPD complexes (Figure 19).

Lipoplexes had nearly twice as much protein identifications as CLs but only approximately 20% more proteins than the corresponding value for LPD

complexes. CLs and LPD complexes had nearly the same number of identifications, with that of LPD complexes being only 1.8 times that of CLs. The Venn diagram highlighted another aspect: only 59 proteins were shared among all samples; 71 proteins were common to lipoplexes and LPD complexes, a number which was 10 times and approximately 5 times the protein overlap for lipoplexes and CLs, and for LPD complexes and CLs, respectively. Comparisons for relative quantitative analysis were performed on two samples at a time considering the shared proteins only. For SIEVE analysis the change in abundance was expressed as the ratio of protein signal intensity measured for two samples. Changes were considered significant if the coefficient of variance was lower than 10%, the p-value was lower than 0.001, Mascot score was higher than 25, and peptides had unique protein assignment. Moreover, signal intensity (abundance) ratios had to be higher than 2 or lower than 0.5 with a CV lower than 0.33. This reduced the number of proteins found to satisfy the above conditions in the analysis to 9 for lipoplexes *vs* CLs, 2 for LPD complexes *vs* CLs, and 17 for lipoplexes *vs* LPD complexes. Results are shown in Table 5.

Table 5 Results of SIEVE quantitative analysis showing signal intensity ratios with CV < 10%, p-value < 0.001, Mascot score > 25, peptides unique assignment, and abundance ratio higher than 2 or lower than 0.5 with a CV < 0.33.

Protein name	**Abundance ratio**		
	Lipoplexes/Cls	**LPD complexes/ CLs**	**LPD complexes/ lipoplexes**
HSPA5 protein			0.20±0.04
Serum amyloid A-4 protein			0.16±0.04
Prothrombin (Fragment)	0.010±0.003		
PLG Plasminogen		4.5±1.5	0.44±0.09
C4b-binding protein alpha chain	0.04±0.01		
Apolipoprotein E		(1.3±0.2)	0.29±0.03

Apolipoprotein A-II			0.33±0.06
Apolipoprotein C-II			0.7±0.1
Apolipoprotein B-100	2.7±0.1	(0.59±0.07)	0.29±0.02
Complement C1q subcomponent subunit C			0.003±0.001
Complement C9	(1.8±0.3)[a]		0.28±0.04
Platelet factor 4	(1.6±0.4)[a]		0.07±0.01
Apolipoprotein(a)	2.2±0.2		0.49±0.06
Complement C5			(2.6±1.0)
Lipopolysaccharide-binding protein	3.0±0.6		0.20±0.06
Profilin-1	13±4		0.18±0.05
Serum paraoxonase/arylesterase 1	(2.0±1.6)[a]	0.010±0.003	
Thrombospondin-1			0.12±0.02
Vitronectin	(1.5±0.1)[a]		0.15±0.01
Talin-1	2.1±0.3		0.09±0.01
Histone H4			0.33±0.07
Complement C3 (Fragment)	2.1±0.4	(0.9±0.2)	
Complement component 6 precursor	0.45±0.06		

[a] Proteins that do not satisfy SIEVE's criteria but do for Scaffold's

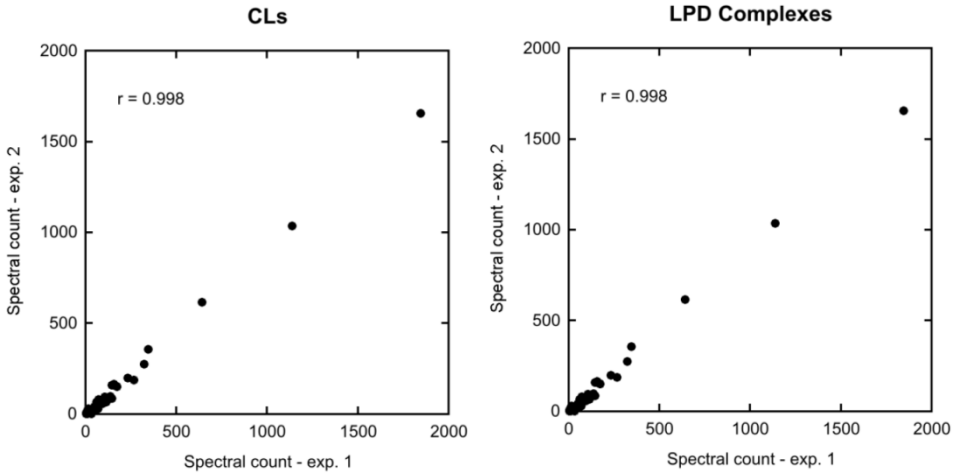

Figure 20 Correlation plots for DOTAP CLs and LPD complexes

For Scaffold analysis the experimental replicate were analyzed independently, combining all technical replicates in one analysis using

Scaffold's MuDPIT option. The reproducibility among replicate experiments was checked comparing the USC for each protein and Pearson's product was calculated showing that the experimental replicates were highly reproducible (Figure 20). For validation the chosen probability parameters were at least 95% for peptide and 99% for protein identifications, with each protein identification accepted if at least two unique peptides were present. Grouping proteins that could not be distinguished, a total of 268 proteins were validated with 0.1% protein FDR and 0.5% peptide FDR. USC were used to assess the consistency of experimental replicates in quantitative analysis, and NSC were used to retrieve protein abundances. Scaffold normalization consists in multiplying by a fractional amount across samples, so that the total number of spectra are the same within each category and then across all categories. To establish if any difference was statistically significant the Fisher's exact test was used to calculate p-values. Results obtained with this validation approach were consistent with the former obtained by Proteome Discoverer: again, the lipoplex protein corona was the richest in qualitative composition, whereas that of the CLs was the poorest; protein number ratios for one sample to another were also very close to those found in Proteome Discoverer analysis. 82 proteins are common among all the samples, as well as proteins shared between lipoplexes and LPD complexes, which was approximately 20 times and 7 times protein overlap between lipoplexes and CLs, and between LPD complexes and CLs, respectively (Figure 21).

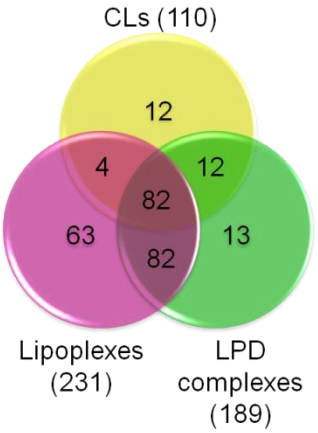

Figure 21 Venn diagram showing the proteins validated by Scaffold

From the NSCs, for each protein the mean value (with the corresponding standard deviation) was calculated and used for comparing two samples at a time, each time taking into account shared proteins only. Differences were considered significant if the Fisher's p-value was smaller than 0.001 and the NSC ratio higher than 2 or lower than 0.5, with a coefficient of variance lower than 0.33. In this way 22 proteins were found to be quantitatively different for lipoplexes *vs* CLs, 17 for LPD complexes *vs* CLs and 12 lipoplexes *vs* LPD complexes (Table 6).

Table 6 Results of Scaffold quantitative analysis showing NSC ratios for proteins having a p-value < 0.001, abundance ratio higher than 2 or lower than 0.5 and a CV < 0.33.

Protein name	**Abundance ratio**		
	Lipoplexes/ Cls	**LPD complexes/ CLs**	**LPD complexes/ lipoplexes**
Complement component C8 gamma chain		3.8±0.6	2.1±0.6
Prothrombin (Fragment)	(0.01±0.004)[b]		
Plasminogen			(1.6±0.5)[b]
cDNA FLJ55673, highly similar to Complem. fact. B		2.1±0.3	2.5±0.3
Properdin			2.39±0.23
C4b-binding protein alpha chain	0.09±0.01		
Apolipoprotein A-I	2.3±0.5	5.1±0.7	2.3±0.3

Apolipoprotein E	3.0±0.6	3.4±0.6	(1.1±0.3)[b]
Apolipoprotein C-III		2.9±0.4	2.2±0.3
Isoform 1 of Fibrinogen alpha chain	0.13±0.03	0.26±0.02	2.0±0.4
Apolipoprotein B-100	2.8±0.3	3.0±0.5	(1.6±0.5)[b]
Complement C1q subcomponent subunit A			0.03±0.01
Complement C1q subcomponent subunit C			0.06±0.02
Complement component C9	2.8±0.6	3.6±0.8	(1.3±0.3)[b]
Protein AMBP	0.13±0.02		
Platelet basic protein	4.8±0.5		
Platelet factor 4	4.2±0.8		
Apolipoprotein(a)	2.4±0.2	4.0±0.4	(1.7±0.1)[b]
Complement C5			2.7±0.8
Lipopolysaccharide-binding protein	3.3±0.9	2.42±0.56	
Isoform HMW of Kininogen-1		0.14±0.03	
PFN1 Profilin_1			(0.4±0.1)[b]
Isoform 2 of Phospholipid transfer protein			0.48±0.06
Serum paraoxonase/arylesterase 1	0.09±0.02	0.08±0.02	
Isoform 1 of Vinculin	3.1±0.1		
Isoform 1 of Clusterin	0.38±0.06	0.5±0.1	
Inter-alpha-trypsin inhibitor heavy chain H1	0.17±0.02	0.34±0.08	
Inter-alpha-trypsin inhibitor heavy chain H1			2.0±0.6
Vitamin K-dependent protein S		0.15±0.04	
Isoform 1 of Integrin alpha-IIb	2.5±0.5		
Fibrinogen beta chain	0.10±0.02	0.19±0.03	
Thrombospondin-1	2.4±0.4		
Vitronectin	2.5±0.3		(0.5±0.1)[b]
Talin-1	3.9±0.7		(0.08±0.05)[b]
Isoform 2 of Filamin-A	10±2		0.18±0.06
Hyaluronan-binding protein 2	2.2±0.4		
Complement C3 (Fragment)	(1.27±0.06)	2.4±0.1	

[a] Number of isoforms with shared peptides that could not be differentiated and were grouped together

[b] These proteins do not satisfy Scaffold's criteria but do for SIEVEs's

Both NSC Scaffold and AUC SIEVE analyses revealed that the quantitative differences among the tree coronas were approximately 10% of the validated proteins. Assuming the two methods of quantitation to be complementary, the relative amount (signal intensity and abundance ratio) of validated proteins for which at least one method has identified a

significant difference are compared in Figure 22. A good correlation for LPD complexes *vs* CLs and LPD complexes *vs* lipoplexes was observed, whereas a lower correlation was found for lipoplexes *vs* CLs.

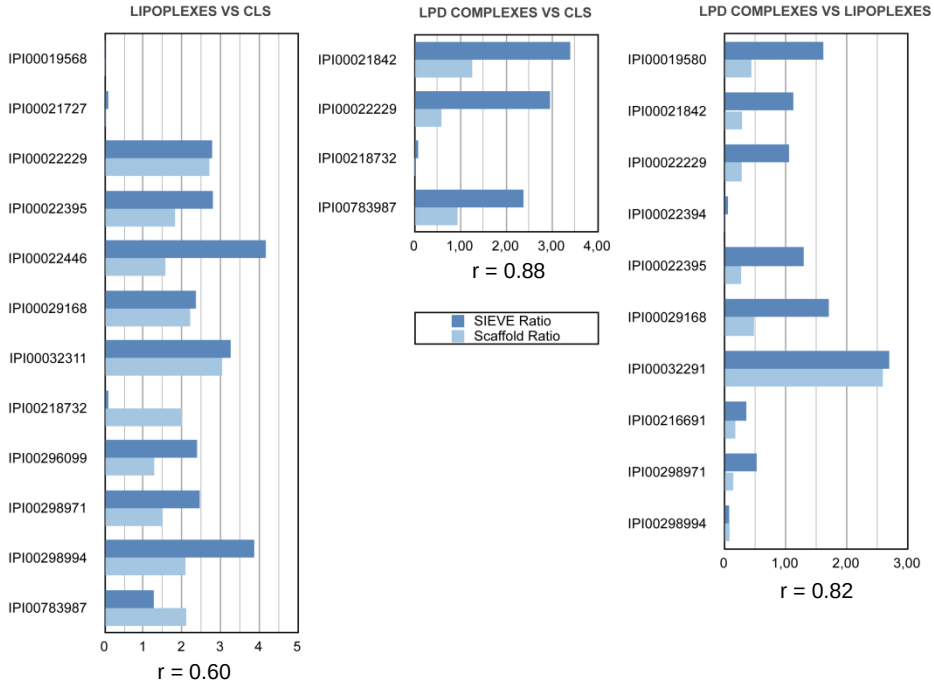

Figure 22 Graphs comparing relative protein abundance ratios as calculated by SIEVE or Scaffold; only proteins present in significant different amounts by either of the two programs are shown; Pearson's product are also reported

However, the correlation was substantially increased limiting the attention to only those proteins identified by both methods with a significant difference, irrespective of the CV (Figure 23).

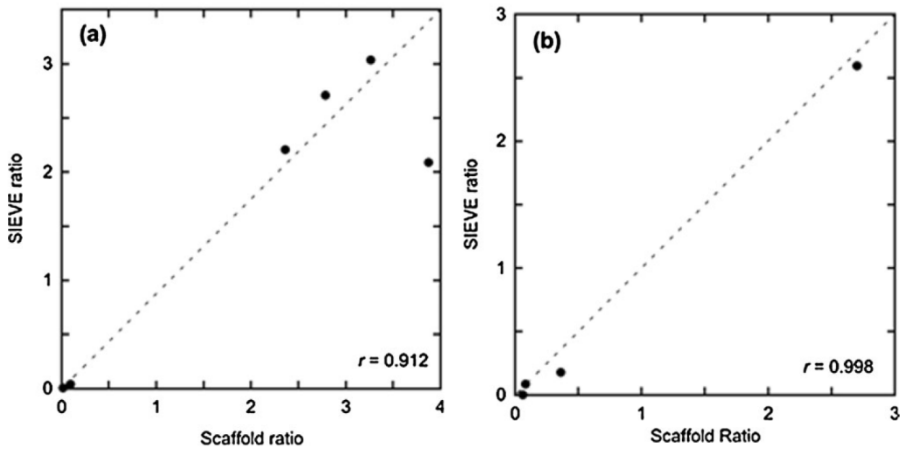

Figure 23 Plots comparing the significant relative abundance ratios of SIEVE *vs* Scaffold for lipoplexes *vs* CLs (a) and LPD complexes *vs* lipoplexes (b)

5. CONCLUSIONS

Because nanoparticle interactions with plasma proteins strongly affect the biodistribution of the vectors in the body, a deep understanding of these interactions could be useful in developing nanocarriers with surface, size and shape able to drive them to target organs.

Thanks to the study carried out in **paper I** it was possible to understand the DNA compaction process in the lipoplexes. The distinct pattern of protein adsorbed onto liposome and lipoplex surfaces showed the existence of hybrid structures in which the polyanionic DNA is associated with the lipoplex surface and could interact with positively charged plasma proteins. Our results suggested that lipoplexes were multilamellar onion-like system with DNA sandwiched between opposing lipid bilayers, but coexisted with other multilamellar complexes or with intact vesicles stuck together by DNA.This result was supported by the type of proteins adsorbed onto lipoplexes, such as histones and complement proteins, which are DNA-binding proteins.

Subsequently in **papers II** and **III** we studied the effect of membrane charge density and demonstrated a preferential adsorption for some classes of proteins. Our results showed that lipid composition did control the surface properties of nanoparticles and could entirely change the nature of the biologically active proteins in the corona, with subsequent possibly relevant biological impacts.

Once established that the amount of DOPE in the CL formulations could deeply influence the surface properties and the membrane charge density of cationic membranes, the effect of plasma concentration on the resulting

protein corona was investigated, this time for DOTAP CLs and lipoplexes (**paper IV**). We showed that the protein corona of CLs was made of both low-affinity and competitive binding proteins, the relative abundance of which changes with the plasma concentration. Such effects might be so striking because the biological response to lipid gene vectors with DNA cargo confined in their interior space may change dramatically as the amount of protein in the environment changes. The protein corona of lipoplexes changed in abundance but not in composition. We concluded that the evolution of protein corona passing from *in vitro* to *in vivo* conditions could be affected by the presence of DNA. This aspect should be carefully considered for the rational design of lipid gene vectors.

The next study (**paper V**) showed that LPD complexes were more efficient in transfecting cells if compared to the corresponding lipoplexes, probably because of the different packaging when complexes with DNA were formed. In the LPD complexes DNA was condensed with a polycation and encapsulated by a lipid envelope. This kind of structure represented an ideal strategy to shield the mutual interactions between DNA and basic serum proteins for *in vivo* applications but, most importantly, LPD complexes showed a enhanced capacity to release their DNA payload, while lipoplexes remained largely intact and accumulated at the cell nucleus.

The last two studies (**papers VI** and **VII**) compared the protein coronas adsorbed onto DOTAP, DOTAP/DNA lipoplexes and LPD complexes. The protein coronas resulted to be different in terms of qualitative composition. These studies confirmed that the protein coronas of lipoplexes and LPD complexes were more variable than those of CLs, whereas small differences were detected between those of lipoplexes and LPD complexes.

All results could help in designing gene delivery systems, because some proteins could be more selectively bound than others, and their presence could be exploited for the biodistribution of the nanoparticles *in vivo*, in order to target to specific cells or tissues and provide a more efficient and effective gene therapy.

6. REFERENCES

1) Al-Dosari MS, Gao X. Nonviral Gene Delivery: Principle, Limitations, and Recent Progress. AAPS J 2009; 11: 671-681.
2) Keeler CE. Gene therapy. J Hered 1947; 38: 294-298.
3) Limberis MP. Phoenix rising: gene therapy makes a comeback. Acta Biochim Biophys Sin 2012; 44: 632-640.
4) Strachnan T, Read A. Human Molecular Genetics, 3rd Edition. Garland Publishing; 2004, p. 616.
5) Selkirk SM. Gene therapy in clinical medicine. Postgrad Med J 2004; 80:560-570.
6) Lentz TB, Gray SJ, Samulski RJ. Viral vectors for gene delivery to the central nervous system. Neurobiol Dis 2012; 48:179-188.
7) Balazs DA, Godbey WT. Liposomes for Use in Gene Delivery**.** J Drug Deliv. 2011;2011:326497. doi: 10.1155/2011/326497. Epub 2010 Dec 15.
8) Jesorka A, Owe O. Liposomes: Technologies and analytical applications. Annu Rev Anal Chem 2008; 1:801-832.
9) Elouahabi A, Ruysschaert J45M. Formation and intracellular trafficking of lipoplexes and polyplexes. Mol Ther 2005; 11:336-347.
10) Pires P, Simões S, Nir S, Gaspar R, Düzgünes N, Pedroso de Lima MC. Interaction of cationic liposomes and their DNA complexes with monocytic leukemia cells. Biochim Biophys Acta 1999; 1418:71-84.

11) Caracciolo G, Amenitsch H. Cationic liposome/DNA complexes: from structure to interactions with cellular membranes. Eur Biophys J 2012; 41:815-829.
12) Tros de Ilarduya C, Arangoa MA,. Moreno-Aliaga MJ, Düzgünes N. Enhanced gene delivery in vitro and in vivo by improved transferrin-lipoplexes. Biochim Biophys Acta 2002; 1561:209-221.
13) Ma B, Zhang S, Jiang H, Zhao B, Lv H. Lipoplex morphologies and their influences on transfection efficiency in gene delivery. J Controlled Release 2007; 123:184-194.
14) Kogure K, Moriguchi R, Sasaki K, Ueno M, Futaki S, Harashima H. Development of a non-viral multifunctional envelope-type nano device by a novel lipid film hydration method. J Controlled Release 2004; 98:317-323.
15) Yamauchi J, Hayashi Y, Kajimoto K, Akita H, Harashima H. Comparison between a multifunctional envelope-type nano device and lipoplex for delivery to the liver. Biol Pharm Bull 2010; 33:926-929.
16) Cedervall T, Lynch I, Lindman S, Berggard T, Thulin E, Nilsson H, Dawson KA, Linse S. Understanding the nanoparticle-protein corona using methods to quantify exchange rates and affinities of proteins for nanoparticles. Proc Natl Acad Sci USA 2007; 104:2050-2055.
17) Gref R, Minamitake Y, Peracchia MT, Trubetskoy V, Torchilin V, Langer R. Biodegradable long-circulating polymeric nanospheres. Science 1994; 263:1600-1603.

18) Ishida T, Harashima H, Kiwada H. Interactions of liposomes with cells in vitro and in vivo: opsonins and receptors. Curr Drug Metab 2001; 2:397-409.

19) Camner P, Lundborg M, Lastbom L, Gerde P, Gross N, Jarstrand C. Experimental and calculated parameters on particle phagocytosis by alveolar macrophages. J Appl Physiol 2002; 92:2608-2616.

20) Ogawara K, Furumoto K, Nagayama S, Minato K, Higaki K, Kai T, Kimura T. Pre-coating with serum albumin reduces receptor-mediated hepatic disposition of polystyrene nanosphere: implications for rational design of nanoparticles. J Controlled Release 2004; 100:451-455.

21) Resina S, Prevot P, Thierry AR. Physico-Chemical Characteristics of Lipoplexes Influence Cell Uptake Mechanisms and Transfection Efficacy. PLoS ONE 2009; 4:e6058.

22) Caracciolo G, Callipo L, Candeloro De Sanctis S, Cavaliere C, Pozzi D, Laganà A. Surface adsorption of protein corona controls the cell internalization mechanism of DC-Chol-DOPE/DNA lipoplexes in serum. Biochim Biophys Acta 2010; 1798:536-543.

23) Cedervall T, Lynch I, Foy M, Berggård T, Donnelly SC, Cagney G, Linse S, Dawson KA. Detailed identification of plasma proteins adsorbed on copolymer nanoparticles. Angew Chem Int Ed 2007; 46: 5754-5756.

24) Lundqvist M, Stigler J, Cedervall T, Berggård T, Flanagan MB, Lynch I, Elia G, Dawson K. The evolution of the protein corona around nanoparticles: a test study. ACS Nano 2011; 5:7503-7509.

25) Mahon E, Salvati A, Baldelli Bombelli F, Lynch I, Dawson KA. Designing the nanoparticle-biomolecule interface for "targeting and therapeutic delivery". J Controlled Release 2012; 161:164-174.

26) Kreuter J. Influence of the surface properties on nanoparticle-mediated transport of drugs to the brain. J Nanosci Nanotechnol 2004;4:484-488.

27) Kreuter J, Shamenkov D, Petrov V, Ramge P, Cychutek K, Koch-Brandt C, Alyautdin R. Apolipoprotein-mediated transport of nanoparticle-bound drugs across the blood-brain barrier. J Drug Target 2002; 10:317-325.

28) Gilmorea JM, Washburna MP. Advances in shotgun proteomics and the analysis of membrane proteomes. J Proteomics 2010; 73:2078-2091.

29) Li X, Pizarro A, Grosser T. Elective affinities--bioinformatic analysis of proteomic mass spectrometry data. Arch Physiol Biochem 2009; 115:311-319.

30) Laemmli UK. Cleavage of structural proteins during the assembly of the head of bacteriophage T4. Nature 1970; 227:680-685.

31) Mitulovic G, Mechtler K. HPLC techniques for proteomics analysis—a short overview of latest developments. Briefings Funct Genomics Proteomics 2006;5:249-260.

32) Cox J, Mann M. Computational principles of determining and improving mass precision and accuracy for proteome measurements in an Orbitrap. J Am Soc Mass Spectrom 2009; 20:1477-1485.

33) Koulman A, Woffendin G, Narayana VK, Welchman H, Crone C, Volmer DA. High-resolution extracted ion chromatography, a new

tool for metabolomics and lipidomics using a second generation orbitrap mass spectrometer. Rapid Commun Mass Spectrom 2009; 23:1411-1418.

34) Mancuso F, Bunkenborg J, Wierer M, Molina H. Data extraction from proteomics raw data: An evaluation of nine tandem MS tools using a large Orbitrap data set. Proteomics 2012; 75:5293-5303.

35) Perkins DN, Pappin DJC, Creasy DM, Cottrell JS. Probability-based protein identification by searching sequence databases using mass spectrometry data. Electrophoresis 1999; 20:3551-3567.

36) Eng JK., McCormack AL, Yates JR III. An approach to correlate tandem mass spectral data of peptides with amino acid sequences in a protein database. J Am Soc Mass Spectrom 1994; 5:976-989.

37) Craig R, Beavis RC. TANDEM: matching proteins with tandem mass spectra. Bioinformatics. 2004; 20:1466-1467

38) Cunningham R, Ma D, Li L. Mass spectrometry-based proteomics and peptidomics for systems biology and biomarker discovery. Front Biol 2012; 7:313-335.

39) Colaert N, Barsnes H, Vaudel M, Helsens K, Timmerman E, Sickmann A, Gevaert K, Martens L. Thermo-msf-parser: An Open Source Java Library to Parse and Visualize Thermo Proteome Discoverer msf Files. J Proteome Res 2011; 10:3840-3843.

40) Keller A, Nesvizhskii AI, Kolker E, Aebersold R. Empirical statistical model to estimate the accuracy of peptide identifications made by MS/MS and database search. Anal Chem 2002; 74:5383-592.

41) Nesvizhskii AI, Keller A, Kolker E, Aebersold R. A statistical model for identifying proteins by tandem mass spectrometry. Anal Chem 2003; 75:4646-4658.
42) Reiter1 L, Claassen M, Schrimpf SP, Jovanovic M, Schmidt A, Buhmann JM, Hengartner MO, Aebersold R. Protein identification false discovery rates for very large proteomics datasets generated by tandem mass spectrometry. Mol Cell Proteomics 2009; 8:2405-2417.
43) Käll L, Storey JD, MacCoss MJ, Noble WS. Assigning Significance to Peptides Identified by Tandem Mass Spectrometry Using Decoy Databases. J Proteome Res 2008; 7:29-34.
44) Searle BC. Scaffold: a bioinformatic tool for validating MS/MS-based proteomic studies. Proteomics 2010; 10:1265-1269.
45) Patel VJ, Thalassinos K, Slade SE, Connolly JB, Crombie A, Murrell JC, Scrivens JH. A Comparison of Labeling and Label-Free Mass Spectrometry-Based Proteomics Approaches. J Proteome Res 2009; 8:3752-3759.
46) Neilson KA, Ali NA, Muralidharan S, Mirzaei M, Mariani M, Assadourian G, Lee A, van Sluyter SC, Haynes PA. Less label, more free: Approaches in label-free quantitative mass spectrometry. Proteomics 2011; 11:535-553.
47) Zhu W, Smith JW, Huang CM. Mass Spectrometry-Based Label-Free Quantitative Proteomics. J Biomed Biotechnol 2010; 2010 Article ID 840518, doi:10.1155/2010/840518.
48) Washburn MP, Wolters D, Yates JR III. Large-scale analysis of the yeast proteome by multidimensional protein identification technology. Nat Biotechnol 2001; 19:242-247.

49) Liu H, Sadygov RG, Yates JR III. A model for random sampling and estimation of relative protein abundance in shotgun proteomics. Anal Chem 2004; 76:4193-4201.

50) Keller A, Eng J, Zhang N, Li XJ, Aebersold R. A uniform proteomics MS/MS analysis platform utilizing open XML file formats. Mol Syst Biol 2005; 1:1-8.

51) Caracciolo G, Foglia P, Fuscoletti V, Giancanti P, Marianecci C, Pozzi D, Laganà A. Existence of hybrid structures in cationic liposome/DNA complexes revealed by their interaction with plasma proteins. Colloid Surf. B Biointerfaces 2011; 82:141-146.

52) Jefferis R, Kumararatne D S. Selective Igg subclass deficiency: Quantification and clinical relevance. Clin Exp Immunol 1990, 81:357-367.

53) Labarre D, Vauthier C, Chauvierre C, Petri B, Müller R, Chehimi MM. Interactions of blood proteins with poly(-isobutylcyanoacrylate) nanoparticles decorated with a polysaccharidic brush. Biomaterials 2005, 26:5075-5084.

54) Anderson NL, Anderson NG. The human plasma proteome: History, character, and diagnostic prospects. Mol Cell Proteomics 2002, 1:845-867.

55) Sitrin RG, Pan PM, Srikanth S, Todd RF 3rd. Fibrinogen activates NF-kappa B transcription factors in mononuclear phagocytes. J Immunol 1998, 161:1462-1470.

56) Rubel C, Fernandez GC, Dran G, Bompadre MB, Isturiz MA, Palermo MS. Fibrinogen promotes neutrophil activation and delays apoptosis. J Immunol 2001, 166:2002-2010.

57) Gardner WD, Haselby JA, Hoch SO. Identification of a major serum DNA-binding protein as factor B of the alternative complement pathway. J Immunol 1980, 124:2800-2806.

58) Zhang J, Liu F, Conwell CC, Tan Y, Huang L. Mechanistic Studies of Sequential Injection of Cationic Liposome and Plasmid DNA. Mol Ther 2006, 13:429-437.

59) Iwanami K, Matsumoto I, Yoshiga Y, Inoue A, Kondo Y, Yamamoto K, Tanaka Y, Minami R, Hayashi T, Goto D, Ito S, Nishimura Y, Sumida T. Altered peptide ligands inhibit arthritis induced byglucose-6-phosphate isomerase peptide. Arthritis Res.Ther. 2009, 11:1-14.

60) Köcher T, Pichler P, Swart R, Mechtler K. Quality control in LC-MS/MS. Proteomics 2011, 11:1026-1030.

61) Monopoli MP, Walczyk D, Campbell A, Elia G, Lynch I, Baldelli Bombelli F, Dawson KA. Physical-chemical aspects of protein corona: relevance to in vitro and in vivo biological impacts of nanoparticles. JACS 2011, 133:2525-2534.

62) Monopoli MP, Baldelli Bombelli F, Dawson KA. Nanobiotechnology: nanoparticle coronas take shape. Nat Nanotechnol 2011;6:11-22.

63) Walczyk D, Baldelli Bombelli F, Monopoli MP, Lynch I, Dawson KA. What the cell "sees" in bionanoscience. J Am Chem Soc 2010;132:5761-5768.

64) Yamada Y, Kogure K, Nakamura Y, Inoue K, Akita H, Nagatsugi F, Sasaki S, Suhara T, Harashima H. Development of efficient packaging method of oligodeoxynucleotides by a condensed nano

particle in lipid envelope structure. Biol Pharm Bull 2005, 28:1939-1942.

65) Li SD, Huang L. Surface-modified LPD nanoparticles for tumor targeting. Ann NY Acad Sci 2006, 1082:1-8.

66) Chen Y, Sen J, Bathula SR, Yang Q, Fittipaldi R, Huang L. Novel cationic lipid that delivers siRNA and enhances therapeutic effect in lung cancer cells. Mol. Pharmaceutics 2009, 6:696-705.

67) Caracciolo G, Pozzi D, Amenitsch H, Caminiti R. Multicomponent cationic lipid-DNA complex formation: role of lipid mixing. Langmuir 2005, 21:11582-11587.

68) Amenitsch H, Caracciolo G, Foglia P, Fuscoletti V, Giansanti P, Marianecci C, Pozzi D, Laganà A. Existence of hybrid structures in cationic liposome/DNA complexes revealed by their interaction with plasma proteins. Colloids Surf, B 2011, 82:141-146.

69) Lundqvist M, Stigler J, Elia G, Lynch I, Cedervall T, Dawson KA. Nanoparticle size and surface properties determine the protein corona with possible implications for biological impacts. Proc Natl Acad Sci USA 2008, 105:14265-14270.

70) Lynch I, Salvati A, Dawson KA. Protein-nanoparticle interactions: what does the cell see? Nat Nanotechnol 2009, 4:546-547.

71) Pozzi D, Caracciolo G, Caminiti R, Candeloro De Sanctis S, Amenitsch H, Marchini C, Montani M, Amici A. Toward the rational design of lipid gene vectors: shape coupling between lipoplex and anionic cellular lipids controls the phase evolution of lipoplexes and the efficiency of DNA release. ACS Appl Mater Interfaces 2009, 10:2237-2249.

72) Marchini C, Pozzi D, Montani M, Alfonsi C, Amici A, Amenitsch H, Candeloro De Sanctis S, Caracciolo G. Tailoring lipoplex composition to the lipid composition of plasma membrane: a Trojan horse for cell entry? Langmuir 2010, 26:13867-13873.

73) Caracciolo G, Marchini C, Pozzi D, Caminiti R, Amenitsch H, Montani M, Amici A. Structural stability against disintegration by anionic lipids rationalizes the efficency of cationic liposom/DNA complexes. Langmuir 2007, 23:4498-4508.

74) Mönkkönen J, Urtti A. Lipid fusion in oligonucleotide and gene delivery with cationic lipids. Adv Drug Delivery Rev 1998, 34:37-49.

75) Zuhorn IS, Visser WH, Bakowsky U, Engberts JB, Hoekstra D. Interference of serum with lipoplex_cell interaction: modulation of intracellular processing. Biochim. Biophys. Acta 2002, 1560:25-36.

76) Kogure K, Moriguchi R, Sasaki K, Ueno M, Futaki S, Harashima H. Development of efficient packaging method of oligodeoxynucleotides by a condensed nano particle in lipid envelope structure. J Controlled Release 2004, 98:317-323.

77) Tan Y, Whitmore M, Li S, Frederik P, Huang L. LPD nanoparticles—novel nonviral vector for efficient gene delivery. Methods Mol Med 2002, 69:73-81.

78) Chen Y, Bathula SR, Li J, Huang L. Multifunctional nanoparticles delivering small interfering RNA and doxorubicin overcome drug resistance in cancer. J Biol Chem 2010, 285:22639-22650.

79) Caracciolo G, Pozzi D, Caminiti R, Marchini C, Montani M, Amici A, Amenitsch A. On the correlation between phase evolution of

lipoplexes/anionic lipid mixtures and DNA release. Appl Phys Lett 2007, 91:143903.

80) Adler AF, Leong KW. Emerging links between surface nanotechnology and endocytosis: impact on nonviral gene delivery. Nano Today 2010, 5:553-569.

81) Almofti MR, Harashima H, Shinohara Y, Almofti A, Li WH, Kiwada H. Lipoplex size determines lipofection efficiency with or without serum. Mol Membr Biol 2003, 20:35-43.

82) Rejman J, Oberle V, Zuhorn IS, Hoekstra D. Size dependent internalization of particles via the pathways of clathrin- and caveole-mediated endocytosis. Biochem J 2004, 377:159-169.

83) Rejman J, Conese M, Hoekstra D. Gene transfer by means of lipo- and polyplexes: role of clathrin and caveole-mediated endocytosis. J Liposome Res 2006, 16:237-247.

84) Hoekstra D, Rejman J, Wasungu L, Shi F, Zuhorn I. Gene delivery by cationic lipids: in and out of an endosome. Biochem Soc Trans 2007, 35:68-71.

85) Yang JP, Huang L. Overcoming the in hibitory effect of serum on lipofection by increasing the charge ratio of cationic liposome to DNA. Gene Ther. 1997, 4, 950-960.

86) Zelphati O, Uyechi LS, Barron LG, Szoka FC Jr. Effect of serum components on the physico-chemical properties of cationic lipid/oligonucleotide complexes and on their interactions with cells. Biochim Biophys Acta 1998, 1390:119-133.

87) Caracciolo G, Pozzi D, Caminiti R, Congiu Castellano A. Structural characterization of a new lipid/DNA complex showing a selective

transfection efficiency in ovarian cancer cells. Eur Phys J E 2003, 10:331-336.

88) Yury S, Tarahovsky Y, Koynova R, MacDonald RC. DNA release from lipoplexes by anionic lipids: correlation with lipid mesomorphism, interfacial curvature, and membrane fusion. Biophys J 2004, 87:1054-1064.

89) Koynova R, Wang L, Tarahovsky Y, MacDonald RC. Lipid phase control of DNA delivery. Bioconjugate Chem 2005, 16:1335-1339.

90) Koynova R, MacDonald RC. Lipid transfer between cationic vesicles and lipidDNA lipoplexes: effect of serum. Biochim Biophys Acta 2005, 1714:63-70.

91) Koynova R, Wang L, MacDonald RC. An intracellular lamellarnonlamellar phase transition rationalizes the superior performance of some cationic lipid transfection agents. Proc Natl Acad Sci U S A 2006, 103:14373-14378.

92) Caracciolo G, Pozzi D, Amenitsch H, Caminiti R. Interaction of lipoplexes with anionic lipids resulting in DNA release is a two-stage process. Langmuir 2007, 23:8713-8717.

93) Yi EC, Marelli M, Lee H, Purvine SO, Aebersold R, Aitchison JD, Goodlett DR. Approaching complete peroxisome characterization by gas-phase fractionation, Electrophoresis 2002, 23:3205-3216.

94) Spahr CS, Davis MT, McGinley MD, Robinson JH, Bures EJ, Beierle J, Mort J, Courchesne PL, Chen K, Wahl RC, Yu W, Luethy R, Patterson SD. Towards defining the urinary proteome using liquid chromatography-tandem mass spectrometry. I. Profiling an unfractionated tryptic digest. Proteomics 2001, 1:93-107.

95) Koc EC, Burkhart W, Blackburn K, Moyer MB, Schlatzer DM, Moseley A, Spremulli LL. The large subunit of the mammalian mitochondrial ribosome. Analysis of the complement of ribosomal proteins present. J Biol Chem 2001, 276:43958-43969.

I

RESEARCH ARTICLE

DNA affects the composition of lipoplex protein corona: A proteomics approach

Anna L. Capriotti[1], Giulio Caracciolo[2], Giuseppe Caruso[1], Patrizia Foglia[1], Daniela Pozzi[2], Roberto Samperi[1] and Aldo Laganà[1]

[1] Dipartimento di Chimica, Sapienza Università di Roma, Roma, Italy
[2] Dipartimento di Medicina Molecolare, Sapienza Università di Roma, Roma, Italy

The distribution of drug delivery systems into the body is affected by plasma proteins adsorbed onto their surface. Furthermore, an exact understanding of the structure and morphology of drug carriers is fundamental to understand their role as gene delivery systems. In this work, the adsorption of human plasma proteins bound to cationic liposomes and to their relative DNA lipoplexes was compared. A shotgun proteomics approach based on HPLC coupled to high resolution MS was used for an efficient identification of proteins adsorbed onto liposome and lipoplex surfaces. The distinct pattern of proteins adsorbed helps to better understand the DNA compaction process. The experimental evidence leads us to hypothesize that polyanionic DNA is associated to the lipoplex surface and can interact with basic plasma proteins. Such a finding is in agreement with recent results showing that lipoplexes are multilamellar DNA/lipid domains partially decorated with DNA at their surface. Proteomics experiments showed that the lipoplex corona is rich of biologically relevant proteins such as fibronectin, histones and complement proteins. Our results provide novel insights to understand how lipoplexes activate the immune system and why they are rapidly cleared from the blood stream. The differences in the protein adsorption data detected in the presented experiments could be the basis for the establishment of a correlation between protein adsorption pattern and in vivo fate of intravenously administered nanoparticles and will require some consideration in the future.

Received: December 20, 2010
Revised: May 9, 2011
Accepted: May 12, 2011

Keywords:
Biomedicine / Differences analysis / Liposomes / LC-MS/MS / Nanomedicine / Plasma

1 Introduction

The development of safe and efficient drug delivery systems is one of the critical steps in achieving the full potential of the gene therapy in the treatment of many inherent and acquired diseases [1–3]. The majority of gene therapy experiments and clinical trials currently use viral delivery systems [4–6], but several aspects need to be improved for achieving therapeutic benefit in patients. These include better efficiency and reliability of procedures for the manufacture of virus, freedom from helper virus contamination [7], avoidance of immunogenicity of the viral particle itself and ways of overcoming the limitation of transgene size [8–10]. In several of these respects, non-viral delivery systems have clear advantages over viral delivery systems such as preparation reproducibility, lack of immunogenicity and almost no size limit to the piece of DNA carried into cells. Cationic liposomes (CLs) are the most promising non-viral candidates for in vitro and in vivo gene delivery

Correspondence: Dr. Anna L. Capriotti, Dipartimento di Chimica, Sapienza Università di Roma, Box no 34 - Roma 62, Piazzale Aldo Moro 5, 00185 Roma, Italy
E-mail: annalaura.capriotti@uniroma1.it
Fax: +39-06-490631

Abbreviations: CL, cationic liposome; **CT,** calf thymus; **DC-Chol,** 3-[*N*-(*N*,*N*-dimethylaminoethane)-carbamoyl] cholesterol; **DOPE,** dioleoylphosphatidylethanolamine; **LTQ,** linear quadrupole ion trap; **RT,** room temperature; **TPP,** trans-proteomic pipeline; ζ_p, ζ potential

applications [11–13]. Regarding the barriers to in vivo transfection, the inhibitory effect of plasma proteins binding to lipoplex surface nanoparticles has been reported. The immunological response to pathogens and foreign bodies is activated by specific plasma proteins that contribute to their clearance by the reticuloendothelial system, particularly in the liver. Plasma proteins such as albumin, lipoproteins, fibrinogen and heparin can bind to lipid membranes, causing aggregation of lipoplexes. Recent ground-breaking studies focused on what cells and organs barrier actually see when interacting with a nanoparticle dispersed in a biological medium [14]. Nanoparticles covered by plasma proteins interact with the cell surface and are internalized by nonspecific and/or highly specific pathways, such as receptor–ligand interactions. This protein-mediated binding can also affect the structure arrangement of the membrane itself [15]. It has been shown that such particle–biomolecule complexes can be physically isolated from the surrounding medium and studied in detail, without altering their structure. The way by which nanoparticles are processed by cells is strongly regulated by the identity and lifetime of proteins adsorbed on their surface. Most cellular internalization mechanisms are receptor-mediated. Therefore, a nanoparticle bare or covered by proteins that are not recognized by cell receptors cannot be efficiently engulfed by cells. Interestingly, the hard corona can evolve significantly as one passes from protein concentrations appropriate to in vitro cell studies to those present in in vivo studies [16]. A better knowledge of proteins adsorbed on nanoparticle surface is an urgent task for comprehending their biological responses. Moreover, the comprehension of the correlation between protein adsorption and in vivo organ distribution can be exploited to realize liposomes targeting different tissues. Since the adsorption of plasma proteins occurs at the surface level, proteomics technique is expected to clarify the surface properties of both CLs and lipoplexes.

In the present study, we have investigated the binding of human plasma proteins on the surface of lipoplexes made of the cationic lipid 3-[*N*-(*N*,*N*-dimethylaminoethane)-carbamoyl] cholesterol (DC-Chol), the neutral 'helper' lipid dioleoylphosphatidylethanolamine (DOPE) and DNA. DC-Chol-DOPE CLs were regarded as a control of the experiment. Since DC-Chol-DOPE/DNA lipoplexes and DC-Chol-DOPE CLs share the same lipid composition, this approach will also help us towards identifying proteins absorbed on the lipoplex surface as a consequence of the presence of complexed DNA. Proteins solely and specifically bound to lipoplex surface are extremely important because they determine the biological identity of lipoplexes in vivo. For this purpose, we have employed a shotgun proteomics approach with a nano-HPLC system coupled to a high resolution Orbitrap linear quadrupole ion trap (LTQ)-XL mass spectrometer. This combined approach is expected to develop a workflow specifically geared toward the efficient identification of protein adsorbed onto nanoparticles surface.

2 Materials and methods

2.1 Reagents and chemicals

The cationic lipid DC-Chol and the zwitterionic lipid DOPE were purchased from Avanti Polar Lipids (Alabaster, AL). Calf thymus (CT) Na-DNA was purchased from Sigma-Aldrich (St. Louis, MO). All organic solvents were purchased from Carlo Erba Reagents (Milan, Italy). Sodium chloride, iodoacetamide, EDTA, TRIS, polyacrylamide, DTT and ammonium bicarbonate were acquired from GE Healthcare (Amersham Biosciences, Uppsala, Sweden). Ultrapure water was obtained from distilled water by a Milli-Q system (Millipore Billerica, MA, USA). Protein LoBind tube were obtained from Eppendorf (Hamburg, Germany). Porcine trypsin (modified, sequencing grade) was commercialized by Promega (Madison, WI, USA).

2.2 CL preparation

Appropriate amounts of DC-Chol and DOPE were solved in $CHCl_3$ at a molar ratio of zwitterionic lipid in the bilayer was Φ = (neutral lipid/total lipid) (mol/mol) = 0.5. First, the solvent was removed by a gentle stream of nitrogen. To ensure solvent removal, samples were kept under vacuum for 12 h. The lipid film was hydrated with a solution 10 mmol/L Tris-HCl, pH 7.4, 150 mmol/L NaCl, 1 mmol/L EDTA (dissolving buffer).

The obtained liposome suspensions (1 mg/mL) were sonicated to clarity and stored at 30°C for 48 h to achieve full hydration.

2.3 Lipoplexes preparation

CT Na-DNA was employed. CT Na-DNA was solubilized in Tris-HCl buffer (1 mg/mL). Sonication for 5 min resulted in DNA fragmentation (length distribution between 500 and 1000 base pair, as determined by gel electrophoresis). Self-assembled DC-Chol- DOPE/DNA lipoplexes were obtained by mixing 24 μL of DNA solution to 200 μL of liposome dispersion and incubating at room temperature (RT) for 20 min.

2.4 Size and ζ potential measurements

Size and ζ potential (ζ_p) measurements of both CLs and lipoplexes were determined by a Zetasizer Nano ZS90 (Malvern, UK) at 25°C with a scattering angle of 90.0°. The neat vesicle dispersions was used for sizing measurements, while 1/10 diluted samples were employed for ζ_p measurements. For each sample, five measurements were replicated and averaged. All the data showed an unimodal distribution. The polydispersity index was directly calculated by the apparatus software.

2.5 Human plasma samples

Human whole blood was obtained from the Experimental Medicine Department ('Sapienza' University of Rome) by venipuncture of healthy volunteers aged 20–40 years, using BD™ P100 Blood Collection System (Franklin Lakes, NJ, USA) with K_2EDTA anticoagulant and protease inhibitors cocktail. After clot formation, blood samples were centrifugated at $1000 \times g$ for 5 min to pellet the blood cells. The supernatant plasma was collected and, after checking the absence of hemolysis, was pooled to keep down differences between individuals and reduce the overall subject-to-subject variation. Then pooled plasma was aliquoted and stored at 80°C in labeled Protein LoBind tubes to ensure plasma stability during storage. Before analysis, plasma aliquots were thawed at 4 °C and then warmed at RT.

2.6 CL and lipoplex incubation with plasma and centrifugation

Aliquots of 200 μL of plasma were incubated with 200 μL of CL suspension (1 mg/mL) in the dissolving buffer at 37°C for 1 h. The same procedure was used for lipoplexes. A robust centrifugation ($15\,000 \times g$ for 10 min) was used to pellet the nanoparticle–protein complexes. Each pellet was washed with 250 μL of the dissolving buffer, vortexed and then was transferred into a new Protein LoBind tubes. After washing, samples were newly centrifuged to remove proteins other than those constituting the hard protein corona. This procedure was repeated twice. After each washing step, tubes were changed to reduce contamination from plasma proteins. Figure 1 shows the protein profile adsorbed onto liposome and lipoplex surface after SDS-PAGE.

2.7 In-solution trypsin digestion

The nanoparticle–protein complexes were resuspended in 40 μL of 8 mol/L urea solution in 50 mmol/L NH_4HCO_3 and 2 μL of 200 mmol/L DTT and were incubated at 37°C for 1 h, under slight agitation, to denature proteins adsorbed onto liposome and lipoplex surface. Afterwards, 8 μL of 200 mmol/L iodoacetamide were added to the samples, and then they were incubated at RT for 1 h in the dark. Subsequently, 8 μL of 200 mmol/L DTT were added and incubated at 37°C for 1 h, under slight agitation, to consume any leftover alkylating agent and to avoid trypsin alkylation. The sample solutions were then diluted with 50 mmol/L NH_4HCO_3 to obtain a final urea concentration of 1 mol/L. Reconstituted trypsin solution (20 μg/mL in 50 mmol/L NH_4HCO_3) was added to ensure a minimum enzyme-to-substrate ratio of 1:20. The samples were allowed to digest rotating overnight at 37°C and the digestion was quenched by adding formic acid. Digested samples were desalted by using a SPE C18 column (BOND ELUT 1CC LRC-C18, VARIAN, Palo Alto, CA, USA) conditioned with acetonitrile and rinsed with 0.1% TFA. Peptides were eluted from the SPE column with 0.5 mL of ACN/H_2O (50:50, v/v) containing 0.05% TFA and were dried in a Speed-Vac SC 250 Express (Thermo Savant, Holbrook, NY, USA). Each sample was re-constituted with 100 μL of the 0.1% formic acid solution. Digested samples were stored at −80°C until analysis.

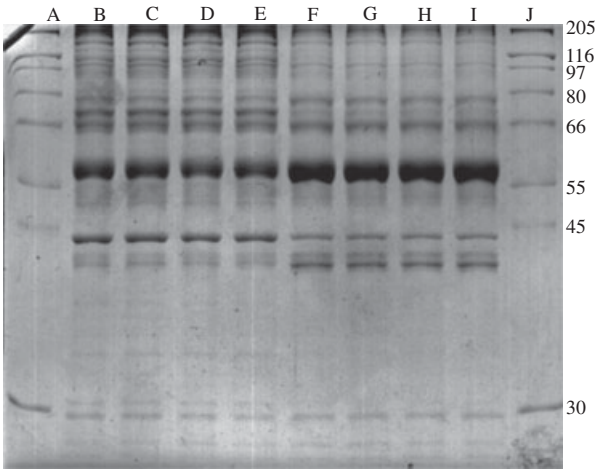

Figure 1. Proteins adsorbed onto DC-Chol-DOPE CLs (lanes B–E, respectively) and DC-Chol-DOPE/DNA lipoplexes (lanes F–I, respectively) surface were mixed with electrophoretic sample buffer, and boiled for 5 min prior to the electrophoretic run at 200 V constant voltage for 35 min. The proteins were visualized using Coomassie PhastGel Blue R-350. Lanes A and J are protein molecular weight markers (kDa).

2.8 NanoHPLC-MS analysis

A HPLC/MS system consisting of a Dionex Ultimate 3000 nano-LC system (Sunnyvale CA, USA) connected to a LTQ-Orbitrap XL mass spectrometer (Thermo Fisher Scientific, Bremen, Germany) equipped with a nanospray ion source was used to analyze tryptic peptides. Peptide mixtures were resolved on a Hypersil Gold C_{18} column (particle size 5 μm, 150 × 0.18 mm) at a flow rate of 1 μL/min. The LC gradient was optimized to detect the largest set of peptides, using H_2O/formic acid (99.9:0.1, v/v) as phase A and ACN/formic acid (99.9:0.1, v/v) as phase B. A 120 min gradient from 2 to 90% B was used. After an isocratic step at 2% B for 5 min, B was linearly increased to 35% in 80 min; afterwards, B was increased to 90% B in 5 min. To rinse the column such percentage was held constant for 2 min. Finally, the B content was to 2% over 2 min, and the column was re-equilibrated for 20 min. The loading pump for peptide enrichment was conducted at a flow-rate of 6 μL/min by premixed mobile phases H_2O/ACN (98:2, v/v) with 0.1% formic acid. A 10 μL aliquot of sample was injected. The mass spectrometer was operated in the data-dependent mode to automatically switch between Orbitrap-MS and

LTQ-MS/MS acquisition (*m/z* range 350–1800, resolution 60 000) using the 'TOP5 strategy'. In brief, a scan cycle was initiated with a full scan of high mass accuracy in the Orbitrap analyzer that was followed by MS/MS scans in the linear ion trap on the five most intense precursor ions with dynamic exclusion of previously selected ions. This dynamic exclusion consisted of two MS/MS spectra acquisitions of the most abundant ion for a period of 30 s and then excluding this ion for the followed fragmentations for 100 s. The activation type used was CID with a normalized collision energy set at 35 V. The experimental design provided replicate MS runs on the same sample. The runs, called technical replicates, help assess the additional variation introduced into the measurements by the experimental procedure and can increase the number of identified proteins. Therefore, a total of five LC-MS/MS runs for each sample (liposomes and lipoplexes) were analyzed.

2.9 Data processing and statistical validation

For database search, raw data files obtained from Xcalibur software were submitted in MASCOT Deamon (version 2.2.04, Matrix Science, London, UK) using the ThermoFinnigan LCQ/DECA RAW file data import filter. Data were searched against human entries in the SwissProt protein database (version 57.15, 20 266 sequences). Trypsin was specified as the proteolytic enzyme with a maximum of two missed cleavages, and fixed modification (carbamidomethyl) on cysteine (+57.0215 Da), and variable modifications (oxidation) on methionine (+15.9949 Da) were set for all searches. The monoisotopic mass tolerance for precursor ions and fragmentation ions were set to 10 ppm and 0.8 Da, respectively. Charge states of +2 or +3 were selected as precursor ions.

Peptide identification and protein assignment were statistically validated submitting the MASCOT result files (.dat) in the open source Trans-Proteomic Pipeline (TPP) software (Seattle Proteome Center, SPC, Proteomics Tools: http://tools.proteomecenter.org/software.php). After conversion of the output MASCOT files (.dat) in the.pepXML format, the PeptideProphet and and ProteinProphet tools [17–19], included in TPP, were employed.

Protein identifications have been submitted to the proteomics identifications database PRIDE, accession numbers 15915 and 15916.

3 Results and discussion

3.1 Size and ζ_p measurements

Size and ζ_p measurements showed that DC-Chol-DOPE CLs are cationic vesicles ($\zeta_p = 55.1 \pm 1.1$ mV) quite small in size (hydrodynamic radius, R_H, around 65 nm). Narrow particle size distribution (polydispersity index = 0.2) showed liposome suspensions to be monodisperse. The mix of DNA and CLs induced the formation of larger size lipoplexes ($R_H \sim 120$ nm). Surface charge DC-Chol-DOPE/DNA lipoplexes was slightly lower than that of free liposomes ($\zeta_p = 48.1 \pm 1.4$ mV). Such finding is most likely to be due to partial neutralization of the positive charge of cationic lipids by poly-anionic DNA.

3.2 Separation of nanoparticle–protein complex from plasma by centrifugation

In this study, we used centrifugation as a method of separation of the nanoparticle–protein complex because, according to previous findings [20], standard durations of washing and centrifugation give reproducible results. To date, most studies have used centrifugation as the method of separation of particle-associated proteins [21]. In particular, stringent washing conditions, suitable to investigate the so-called 'hard corona' [21, 22], were used. Therefore, three washes with the dissolving buffer were performed to remove all weakly bound proteins. Sedimentation of large proteins, formation of protein aggregates and co-precipitation were avoided by selecting a short centrifugation time (2 min). Despite the three vigorous washes, many proteins were identified (Table 1). Such finding indicates that most proteins of the protein corona remained tightly bound to liposomes The presence in the corona of proteins whose concentration in plasma is not high suggests that the interaction between liposomes and some plasma proteins is not dependent on their concentration, but it depends on their affinity for liposome surface, different for each protein.

3.3 Statistical data analysis for validation of peptide and protein identification using TPP

Following MASCOT searching of acquired MS/MS spectra, rather than interpreting the data solely on the basis of filtering by database search engine output scores (threshold approach), MASCOT output files were submitted to the recently developed statistical open source software, the TPP. PeptideProphet and ProteinProphet, the two new statistical tools of TPP, designed for such a purpose, were applied to peptide and protein identification, respectively. Figure 2 summarizes the data workflow for this process. Because the sensitivity (percentage of total correct identifications remaining after restricting data at a given probability threshold) and error rates (percentage of total false identification) for any data set modeled are directly related and are affected by the probability threshold set to filter the data sets, setting more or less stringent probability threshold is possible. The peptide and protein probability thresholds for running PeptideProphet and ProteinProphet were set at 0.7 and 0.9, respectively, for both sample data sets (liposomes and lipoplexes). The related values for the error rate and sensitivity were 0.6, 84.4% for liposomes and 0.8, 83.0% for

Table 1. Proteins identified exclusively onto liposome or lipoplex surface with the main search result parameters obtained after TPP validation, and their relative positive/negative charge at pH 7

Protein ID	Protein name	Protein probability	Coverage %	Unique peps	Charge pH 7
Liposomes					
O15027|SC16A_HUMAN	Protein transport protein Sec16A	0.9234	0.6	3	−51.3
O43866|CD5L_HUMAN	CD5 antigen-like	0.9846	18.7	4	−11.3
O95445|APOM_HUMAN	Apolipoprotein M	0.9873	9	2	−3.8
P01019|ANGT_HUMAN	Angiotensinogen	0.9999	8.9	2	−5.8
P01617|KV204_HUMAN	Ig κ chain V-II region TEW	0.9904	32.7	2	−0.9
P12259|FA5_HUMAN	Coagulation factor V	0.9623	1.1	2	−40.6
P21926|CD9_HUMAN	CD9 antigen	0.9889	15.4	2	0.4
P62256|UBE2H_HUMAN	Ubiquitin-conjugating enzyme E2 H	0.908	15.3	2	−13.3
Q13790|APOF_HUMAN	Apolipoprotein F	1	8.8	3	−6.7
Q9BWP8|COL11_HUMAN	Collectin-11	1	29.2	6	−6.3
Q9UK55|ZPI_HUMAN	Protein Z-dependent protease inhibitor	0.9995	7.9	2	4.1
Lipoplexes					
O00194|RB27B_HUMAN	Ras-related protein Rab-27B	0.9248	10.1	2	−2.9
O60361|NDK8_HUMAN	Putative nucleoside diphosphate kinase	0.9983	19	2	3.8
O60814|H2B1K_HUMAN	Histone H2B type 1-K	1	34.9	4	18.6
O95810|SDPR_HUMAN	Serum deprivation-response protein	0.9913	12.5	4	−18.3
P00747|PLMN_HUMAN	Plasminogen	0.9308	3.7	2	3.4
P01031|CO5_HUMAN	Complement C5	1	4.8	6	−9.8
P01042|KNG1_HUMAN	Kininogen-1	1	25.6	14	6.8
P02730|B3AT_HUMAN	Band 3 anion transport protein	0.9934	3.6	2	−27.7
P02751|FINC_HUMAN	Fibronectin	1	4.4	7	−45.3
P07357|CO8A_HUMAN	Complement component C8 α chain	0.9991	7.9	2	−3.7
P07360|CO8G_HUMAN	Complement component C8 γ chain	0.9953	16.3	2	3.1
P10412|H14_HUMAN	Histone H1.4	1	16.9	4	58.9
P10643|CO7_HUMAN	Complement component C7	0.9797	3.8	2	−6.6
P11142|HSP7C_HUMAN	Heat shock cognate 71 kDa protein	1	23.1	8	−11.4
P11169|GTR3_HUMAN	Solute carrier family 2, facilitated glucose transporter member 3	0.9999	8.1	3	0.4
P13645|K1C10_HUMAN	Keratin, type I cytoskeletal 10	1	25.7	8	−14.2
P18428|LBP_HUMAN	Lipopolysaccharide binding prot	0.9573	6	2	−1.7
P24844|MYL9_HUMAN	Myosin regulatory light polypeptide 9	1	55.8	8	−11.1
P30041|PRDX6_HUMAN	Peroxiredoxin 6	0.9869	16.1	2	−1.4
P30101|PDIA3_HUMAN	Protein disulfide-isomerase A3	0.9963	18.2	3	−4.0
P31146|COR1A_HUMAN	Coronin-1A	0.9984	13.4	3	−1.9
P52907|CAZA1_HUMAN	F Actin capping prot. Sub. α	0.9832	14	3	−7.2
P55209|NP1L1_HUMAN	Nucleosome assembly prot 1 like 1	0.9207	14.3	3	−52.6
Q00610|CLH1_HUMAN	Clathrin heavy chain	0.9036	1.6	2	−33.2
Q01518|CAP1_HUMAN	Adenylyl cyclase-associated protein 1	1	29.5	6	5.8
Q14766|LTBP1_HUMAN	Latent transforming G.F. β bind	0.9328	3.1	3	−36.8

lipoplexes. Protein identifications based on mass spectra correlating to at least two unique tryptic peptides were considered valid identifications. Applying these conditions, 110 and 125 proteins were identified as adsorbed onto liposome and lipoplex surface, respectively, with an overlap of 99 proteins. Further information on protein identification is provided in Supporting Information.

3.4 Serum proteins adsorbed onto nanoparticle surface

The shotgun proteomics strategy has been already adopted to identify the proteins adsorbed onto DC-Chol-DOPE CLs and onto DC-Chol-DOPE/DNA lipoplexes [20]. As Table 1 shows, individual proteins or protein classes, including HSA, various Igs, apolipoproteins, fibrinogen, proteins of the complement pathways and other proteins were identified. Our results confirm previous observations that nanoparticles can bind several classes of plasma proteins in various amounts [22]. In fact, upon exposure to biological fluids, nanoparticles are first covered by the most abundant plasma proteins that are subsequently replaced by the higher affinity ones [21]. HSA, the most abundant protein in plasma, was found to be associated both with DC-Chol-DOPE CLs [20], and DC-Chol-DOPE/DNA lipoplexes. Igs, identified as part of the protein corona around different nanoparticles, are involved in many biological processes, e.g.

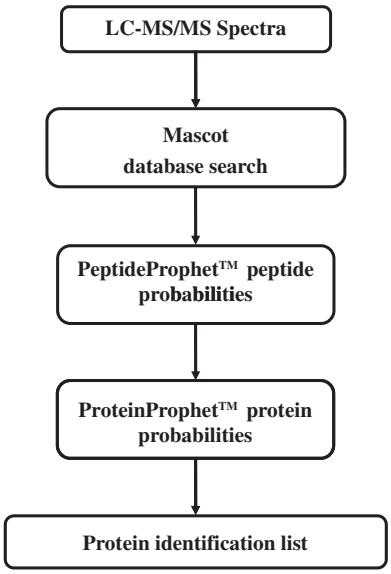

Figure 2. Acquired MS/MS spectra were submitted to MASCOT for searching protein sequence database. MASCOT results were subsequently converted to pepXML by MASCOT2XML, and evaluated by PeptideProphet. The resulting files were then analyzed by ProteinProphet, resulting in a single list of identified proteins.

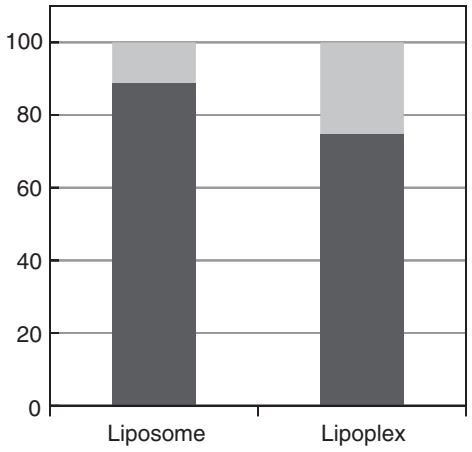

Figure 3. Percentage of proteins that are unique for each system (dark gray) as well as the fractions detected on both of them (light gray).

allergic reaction, immunity response and anaphylactic shock. IgG is also involved in transport across the placenta as well as in the opsonization process [23]. Apolipoproteins are the main constituents of the protein corona of particles with hydrophobic surface [21, 24]. Furthermore, they are involved in the lipid and cholesterol transportation throughout bloodstream [25] and, as such, are expected to greatly influence the intracellular trafficking, fate and transport of nanoparticles inside cells and animal body. The fibrinogen, a glycoprotein that is converted by thrombin into fibrin during blood coagulation, interacts with foreign surfaces and induces attachment of immune cells such as monocytes, macrophages and neutrophils. As a result of fibrinogen action, apoptosis is delayed and antibody-dependent cell cytotoxicity and phagocytosis are increased [26, 27]. Other acute-phase proteins were recognized in the protein corona suggesting that the nanoparticle–protein complex can activate various inflammatory responses. Most proteins related to the complement pathways that promotes neutrophil attachment to different surfaces were also identified [28]. It has been reported that classical pathways of the complement system can be activated by polystyrene latex particles modified with hydroxyethyl acrylate [29] and non-functionalized double-walled carbon nanotubes [30].

In Fig. 3 a general evaluation of the degree of similarity of the protein coronas around DC-Chol-DOPE CLs and DC-Chol-DOPE/DNA lipoplexes is presented where the fraction of proteins that are unique for each system (light gray) as well as the fractions detected on both of them (dark gray) are reported. More than 88% of the corona for CLs is constituted by proteins that are also in lipoplex corona. On the other hand, this percentage decreases to 74% of proteins for lipoplexes, which bind more identified proteins than liposomes. Since the first interaction between lipid nanovectors and plasma proteins is electrostatic, this finding is a striking confirmation that lipoplex surface is different from that of pure CLs. Bearing in mind that the lipid composition of CLs and lipoplexes is identical, such surface modification is probably due to the DNA condensation on the lipid surface. Thus, DNA may affect the biological impact of nanoparticles by modifying the composition of their protein corona. This is a key issue that must be evaluated in nanomedicine and nanosafety studies in vivo.

To find out a correlation between surface charge of lipid nanoparticles and composition of protein coronas, the charges at pH = 7 of all the proteins identified was calculated by a dedicated software (http://www.scripps.edu/~cdputnam/protcalc.html) and the values are listed in Table 1.

Figure 4A shows the fraction of negatively (dark gray) and positively (light gray) charged proteins in the overlap of the two protein coronas. As evident, the proteins common to both coronas are principally negative (66%). This is an expected result because both DC-Chol-DOPE CLs and DC-Chol-DOPE/DNA lipoplexes are positively charged nanoparticles that preferentially interact with oppositely charged proteins. Even though the relative abundance of identified proteins could not be determined, the strategy used in Fig. 4A might be useful to investigate how the surface charge properties of lipid nanoparticles influence the composition of the protein corona. Indeed, the relative protein abundance is not expected to reflect the biological impact; in terms of the biological response, the most abundantly associated proteins do not necessarily have the strongest effect. A less abundant protein with high affinity and specificity for a particular receptor may instead be a key

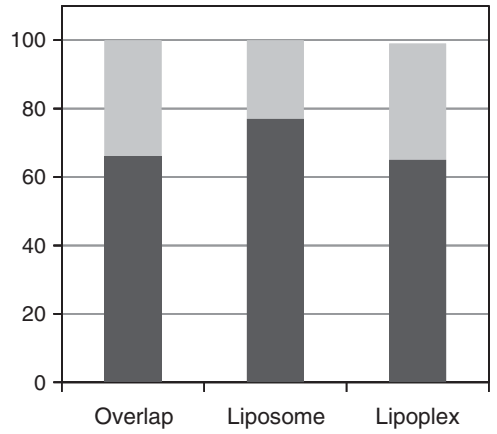

Figure 4. Fraction of negatively (dark gray) and positively (light gray) charged proteins.

player. It is therefore essential to develop methods, as that presented in this investigation, to identify both major and minor particle-associated proteins. The picture is different when unique proteins (i.e. that are not in common) are considered (Fig. 4B). In this case, the percentage of negative proteins was found to be about 77 and 65% for liposomes and lipoplexes, respectively. On the other hand, the average charge of the proteins found in the coronas was ~ -11 for DC-Chol-DOPE CLs and -6 for DC-Chol-DOPE/DNA lipoplexes. Aside from being a quantitative result, this finding is in agreement with ζ_p measurements showing that DC-Chol-DOPE CLs are more positively charged ($\zeta_p = 55.1 \pm 1.1$ mV) than DC-Chol-DOPE/DNA lipoplexes ($\zeta_p = 48.1 \pm 1.4$ mV). On average, the presence of more positively charged proteins in the lipoplex corona indicates that their surface is, at least locallynegatively charged. In previous investigations [31, 32], we have provided unambiguous evidence that DC-Chol-DOPE/DNA lipoplexes are onion-like structures made of tenths of alternating lipid and DNA layers. The most likely explanation of such observation is that a fraction of DNA is associated with the lipoplex surface and could interact with basic plasma proteins by charge attraction. This suggestion is supported by the recent study [31] showing that clusters of multilamellar lipoplexes connected by DNA coexist with DNA-decorated unbroken vesicles. Even though electrostatics plays a key role in the interaction of nanoparticles with plasma proteins, many other factors can influence the detailed nature of the nanoparticle protein corona. Among them, size, shape and surface hydrophilicity/hydrophobicity can affect the composition of the corona. With this respect, our DLS and ζ_p results showed that DC-Chol-DOPE CLs and DC-Chol-DOPE/DNA lipoplexes did not exhibit remarkable differences. Thus, minor changes, if any, in the above-mentioned chemical-physical properties could not be used to explain the observed differences in their corona composition. Growing evidence suggests that the adsorbed protein layer is a determining factor for the cellular uptake, trafficking and biodistribution of lipoplexes. A detailed knowledge of proteins specifically bound to lipoplexes might open up the way to understand molecular phenomena occurring upon lipoplex–protein interactions in vivo. Furthermore, a precise definition of these proteins is a vital piece of information for developing an effective and correctly addressed strategy of gene delivery. To address this issue, we mainly focused on the proteins present in the corona of lipoplexes. Some proteins were specifically found on the lipoplex corona (Table 1). The most significant ones were: (i) fibronectin; (ii) HSP70; (iii) histones; (iv) complement proteins. Fibronectin was not found on the liposome corona; thus it makes sense that this protein interacts with DNA molecules adsorbed at the lipoplex surface. This suggestion is in plain agreement with the existence of a DNA-binding domain in the fibronectin molecule. Fibronectin is a high-molecular weight ($\sim$440 kDa) protein involved in many biological processes such as cell adhesion, growth, migration and differentiation. Cellular fibronectin is assembled into the extracellular matrix and binds to membrane-spanning receptor proteins called integrins. In addition to integrins, fibronectin also binds extracellular matrix components such as collagen, fibrin and sulfate proteoglycans. Since the latter cellular components are known to promote the lipoplex–cell interaction, it could be hypothesized that fibronectin could also play a role in facilitating the lipoplex cell adhesion and internalization. According to this suggestion, some authors recently reported on the surface-mediated delivery of lipoplexes mixed with fibronectin [33]. The inclusion of fibronectin on the surface or in solution with the lipoplexes was found to enhance the substrate-mediated gene transfer efficiency.

HSP70 are a class of functionally related proteins whose expression is increased when cells are exposed to elevated temperatures or other stress. Among other functions, extracellular and membrane-bound HSPs are involved in binding antigens and presenting them to the immune system [34]. HSPs are useful as immunologic adjuvants in boosting the response to a vaccine [35]. Histone H1 (P10412) and H2B type 1-K (O60814) were identified. They are highly alkaline proteins found in eukaryotic cell nuclei, which package and order the DNA into structural units called nucleosomes. More in detail, Histone H1 is one of the most abundant proteins in the nucleus of eukaryotic cells. It has long been known as the 'linker histone', because it links the chromatosomal DNA that goes between the nucleosomes. Histone H2B type 1-K is one of the proteins involved in the structure of chromatin in eukaryotic cell. Aside from biological interpretations, finding Histone H1 and Histone H2B type 1-K in the lipoplex corona (and not in the liposome corona) is a striking confirmation of our suggestion that DNA is adsorbed at the lipoplex membrane is recognized by specific DNA-binding proteins.

Some other proteins found in the lipoplex corona were identified as immune-response proteins. Among them, the most relevant ones seemed to be the complement proteins.

Complement proteins make up the complement system, a part of the immune system that 'complements' the ability of antibodies and phagocytic cells to clear pathogens from an organism [36]. Complement activation by the classical pathway occurs when the rst component of complement, C1, binds, mainly via charge interactions to immune complexes (containing IgG or IgM) or directly to a non-Ig target surface. Remarkably, we observe that C1 was identified both on the liposome and the lipoplexes corona. Recent studies [37] have shown that C1 interacts favorably with phospholipids in CLs. According to these findings, our proteomics results are likely to suggest that those complement proteins that have been found in both the coronas are most likely to be bound to the lipid surface. On the other side, C5 (P01031), C7 (P10643) and the α (P07357) and γ (P07360) chain of C8 (Table 1) were found only on that of lipoplexes. Our proteomics results showing that these complement proteins are present at the DNA-rich surface of lipoplexes are in very good agreement with the existence of a domain with DNA-binding activity in the complement proteins [38]. From a biological point of view, complement proteins identified on the lipoplex corona play a key role in the activation of the alternative complement pathway. In particular, C5b initiates the membrane attack pathway, which leads to the formation of the membrane attack complex, consisting of C5b, C6, C7, C8 and polymeric C9, that is the cytolytic end-product of the complement cascade. It forms a transmembrane channel on the surface of intruding pathogenic cells, which causes their osmotic lysis and their final killing. In the context of gene delivery, it has reported that Kupffer cells and other macrophage cell types clear complement-coated pathogens. Thus, our proteomic results showing that lipoplexes are coated by several complement proteins might contribute to explain why lipoplexes are often rapidly cleared from the bloodstream and delivered to the Kupffer cells in the liver.

Recent in vivo studies [37, 38] have shown that the sequential injection of CLs and DNA strongly reduces the uptake by the liver and results in higher level of activity with respect to preformed CLs–DNA complexes. To explain results, the authors suggested that sequential injection of CLs and DNA might inhibit the binding of some opsonin proteins, thus reducing stimulation of phagocytosis by reticuloendothelial system. Remarkably, our results support such hypothesis because complement proteins were detected only in the corona of lipoplexes and not in the corona of CLs. This observation could, at least in part, explain the superior efficiency of transfection strategies based on such sequential injection.

Opsonization remains a severe obstacle to in vivo transfection and significant challenges remain before lipoplex-mediated gene delivery technique can be used technologically. Among unreturned questions, how lipoplexes can suppress the immune response is a mandatory task for successful gene delivery applications. However, to respond such query it is necessary to deeply understand the lipoplex-induced immune response. In the future, a precise characterization of the lipoplex protein corona composition, as that reported in this study, shall be used to attain quantitative data on the dynamics of the protein corona [39, 40]. Such knowledge will be extremely useful for a multitude of protein nanoscience applications.

4 Concluding remarks

The current work is the first study aiming to identify and compare proteins that bind onto DC-Chol-DOPE CLs and onto DC-Chol-DOPE/DNA lipoplexes. A distinct pattern of protein adsorbed onto liposomes and lipoplexes surface, as suggested by the results, helps to better understand the DNA compaction process. The experimental evidence leads us to hypothesize that poly-anionic DNA is associated with the lipoplex surface and can interact with positively charged plasma proteins. Our results are in agreement with the existence of clusters composed of multilamellar DNA/lipid domains coexisting with other multilamellar complexes or, alternatively, with intact vesicles stuck together by DNA. Even more remarkably, we have shown that the lipoplex corona is rich of histones and complement proteins. The former are DNA-binding proteins and their presence on the lipoplex surface confirms our suggestions that a part of DNA is bound to the lipid surface. Complement proteins compose the complement system, a part of the immune system that works against intruding pathogenic cells. Therefore, our results provide novel insights to understand how lipoplexes activate the immune system and why they are rapidly cleared from the blood stream. Since these proteins were found to be specifically bound to the lipoplex surface and not to the liposome one, new delivery strategies that protect delivered DNA making it inaccessible to plasma proteins are highly desirable.

Future work will be performed in that direction. In addition, these results show that shotgun proteomics analysis of proteins adsorbed onto nanoparticles surface can be useful in the design of better drug carriers for specific target cells or tissues. The differences in the protein adsorption data detected in the presented experiments could be the basis for the establishment of a correlation between protein adsorption pattern and in vivo fate of intravenously administered nanoparticles.

The authors have declared no conflict of interest.

5 References

[1] Dalgleish, A. G., Why: gene therapy? *Gene Ther.* 1997, *4*, 629–630.

[2] Factor, P., Gene therapy for acute diseases. *Mol. Ther.* 2001, *4*, 515–524.

[3] Nishikawa, M., Huang, L., Nonviral vectors in the new millennium: delivery barriers in gene transfer. *Hum. Gene Ther.* 2001, *12*, 861–870.

[4] Lu, D. R., Zhou, J. M., Zheng, B., Qiu, X. F. et al., Stage I clinical trial of gene therapy for hemophilia B. *Sci. China B Chem. Life Sci. Earth Sci.* 1993, *36*, 1342–1351.

[5] Kay, M. A., Manno, C. S., Ragni, M. V., Larson, P. J. et al., Evidence for gene transfer and expression of factor IX in haemophilia B patients treated with an AAV vector. *Nat. Genet.* 2000, *24*, 257–261.

[6] Fields, P. A., Arruda, V. R., Armstrong, E., Chu, K. et al., Risk and prevention of anti-factor IX formation in AAV-mediated gene transfer in the context of a large deletion of F9. *Mol. Ther.* 2001, *4*, 201–210.

[7] Drittanti, L., Jenny, C., Poulard, K., Samba, A. et al., Optimised helper virus-free production of high-quality adeno-associated virus vectors. *J. Gene Med.* 2001, *3*, 59–71.

[8] Nakai, H., Storm, T. A., Kay, M. A., Increasing the size of rAAV-mediated expression cassettes in vivo by intermolecular joining of two complementary vectors. *Nat. Biotechnol.* 2000, *18*, 527–532.

[9] Duan, D., Yue, Y., Yan, Z., Engelhardt, J. F., A new dual-vector approach to enhance recombinant adeno-associated virus-mediated gene expression through intermolecular cis activation. *Nat. Med.* 2000, *6*, 595–598.

[10] Sun, L., Li, J., Xiao, X., Overcoming adeno-associated virus vector size limitation through viral DNA heterodimerization. *Nat. Med.* 2000, *6*, 599–602.

[11] Tros de Ilarduya, C., Arangoa, M. A., Moreno-Aliaga, M. J., Düzgüne◦, N., Enhanced gene delivery in vitro and in vivo by tansferrin-lipoplexes. *Biochim. Biophys. Acta* 2002, *1561*, 209–221.

[12] De la Torre, L. G., Rosada, R. S., Fávaro Trombone, A. P., Frantz, F. G. et al., The synergy between structural stability and DNA binding controls the antibody production in EPC/DOTAP/DOPE liposomes and DOTAP/DOPE lipoplexes. *Colloids Surf. B Biointerfaces* 2009, *73*, 175–184.

[13] Rädler, J. O., Koltover, I., Salditt, T., Safinya, C. R., Structure of DNA-cationic liposome complexes: DNA intercalation in multilamellar membranes in distinct interhelical packing regimes. *Science* 1997, *275*, 810–814.

[14] Walczyk, D., Baldelli Bombelli, F., Monopoli, M. P., Lynch, I., Dawson, K. A., What the Cell ''Sees'' in Bionanoscience. *J. Am. Chem. Soc.* 2010, *132*, 5761–5768.

[15] Lynch, I., Salvati, A., Dawson, K. A., Protein-nanoparticle interactions: What does the cell see? *Nat. Nanotech.* 2009, *4*, 546–547.

[16] Monopoli, M. P., Walczyk, D., Campbell, A., Elia, G. et al., Physicalchemical aspects of protein corona: relevance to in vitro and in vivo biological impacts of nanoparticles. *J. Am. Chem. Soc.* 2011, *133*, 2525–2534.

[17] Keller, A., Nesvizhskii, A. I., Kolker, E., Aebersold, R., Empirical statistical model to estimate the accuracy of peptide identifications made by MS/MS and database search. *Anal. Chem.* 2002, *74*, 383–392.

[18] Keller, A., Eng, J., Zhang, N., Li, X. J. et al., A uniform proteomics MS/MS analysis platform utilizing open XML file formats. *Mol. Syst. Biol.* 2005, *1*, 1–8.

[19] Nesvizhskii, A. I., Keller, A., Kolker, E., Aebersold, R., A statistical model for identifying proteins by tandem mass spectrometry. *Anal. Chem.* 2003, *75*, 4646–4658.

[20] Capriotti, A. L., Caracciolo, G., Caruso, G., Cavaliere, C. et al., Analysis of plasma protein adsorption onto DC-Chol-DOPE cationic liposomes by HPLC-CHIP coupled to a Q-TOF mass spectrometer. *Anal. Bioanal. Chem.* 2010, *398*, 2895–2903.

[21] Cedervall, T., Lynch, I., Foy, M., Berggård, T. et al., Detailed identification of plasma proteins adsorbed on copolymer nanoparticles. *Angew. Chem. Int. Ed. Engl.* 2007, *119*, 5856–5858.

[22] Cedervall, T., Lynch, I., Lindman, S., Berggard, T. et al., Understanding the nanoparticle–protein corona using methods to quantify exchange rates and affinities of proteins for nanoparticles. *Proc. Natl. Acad. Sci. USA* 2007, *104*, 2050–2055.

[23] Jefferis, R., Kumararatne, D. S., Selective Igg subclass deficiency: Quantification and clinical relevance. *Clin. Exp. Immunol.* 1990, *81*, 357–367.

[24] Labarre, D., Vauthier, C., Chauvierre, C., Petri, B. et al., Interactions of blood proteins with poly(-isobutylcyanoacrylate) nanoparticles decorated with a polysaccharidic brush. *Biomaterials* 2005, *26*, 5075–5084.

[25] Anderson, N. L., Anderson, N. G., The human plasma proteome: History, character, and diagnostic prospects. *Mol. Cell. Proteomics* 2002, *1*, 845–867.

[26] Sitrin, R. G., Pan, P. M., Srikanth, S., Todd, R. F., Fibrinogen activates NF-kappa B transcription factors in mononuclear phagocytes. *J. Immunol.* 1998, *161*, 1462–1470.

[27] Rubel, C., Fernandez, G. C., Dran, G., Bompadre, M. B. et al., Fibrinogen promotes neutrophil activation and delays apoptosis. *J. Immunol.* 2001, *166*, 2002–2010.

[28] McNally, A. K., Anderson, J. M., Complement C3 participation in monocyte adhesion to different surfaces. *Proc. Natl. Acad. Sci. USA* 1994, *91*, 10119–10123.

[29] Luck, M., Schroder, W., Paulke, B. R., Blunk, T. et al., Complement activation by model drug carriers for intravenous application: determination by two-dimensional electrophoresis. *Biomaterials* 1999, *20*, 2063–2068.

[30] Salvador-Morales, C., Flahaut, E., Sim, E., Sloan, J., Complement activation and protein adsorption by carbon nanotubes. *Mol. Immunol.* 2006, *43*, 193–201.

[31] Caracciolo, G., Foglia, P., Fuscoletti, V., Giancanti, P. et al., Existence of hybrid structures in cationic liposome/DNA complexes revealed by their interaction with plasma proteins. *Colloid Surf. B* 2011, *82*, 141–146.

[32] Caracciolo, G., Callipo, L., Candeloro De Sanctis, S., Cavaliere, C. et al., Surface adsorption of protein corona controls the cell internalization mechanism of DC-Chol–DOPE/DNA lipoplexes in serum. *Biochim. Biophys. Acta* 2010, *1798*, 536–543.

[33] Iwanami, K., Matsumoto, I., Yoshiga, Y., Inoue, A. et al., Altered peptide ligands inhibit arthritis induced by

glucose-6-phosphate isomerase peptide. *Arthritis Res.Ther.* 2009, *11*, 1–14.

[34] Schubert, D., Schmidt, M., Zaiss, D., Jungblut, P. R., Kamradt, T., Autoantibodies against GPI and creatine kinase in rheumatoid arthritis. *Nat. Immunol.* 2002, *3*, 411.

[35] Doolittle, R. F., The multiplicity of domains in proteins. *Ann. Rev. Biochem.* 1995, *64*, 287–314.

[36] Gardner, W. D., Haselby, J. A., Hoch, S. O., Identification of a major serum DNA-binding protein as factor B of the alternative complement pathway. *J. Immunol.* 1980, *124*, 2800–2806.

[37] Tan, Y., Liu, F., Li, Z., Li, S., Huang, L., Sequential injection of cationic liposome and plasmid DNA effectively transfects the lung with minimal inflammatory toxicity. *Mol. Ther.* 2001, *3*, 673–682.

[38] Zhang, J., Liu, F., Conwell, C. C., Tan, Y. et al., Mechanistic Studies of Sequential Injection of Cationic Liposome and Plasmid DNA. *Mol. Ther.* 2006, *13*, 429–437.

[39] Deng, Z. J., Mortimer, G., Schiller, T., Musumeci, A. et al., Differential plasma protein binding to metal oxide nanoparticles. *Nanotechnology* 2009, *20*, 455101, 9pp.

[40] Lundqvist, M., Stigler, J., Elia, G., Lynch, I. et al., Nanoparticle size and surface properties determine the protein corona with possible implications for biological impacts. *Proc. Natl. Acad. Sci. USA* 2008, *105*, 14265–14270.

II

Anal Bioanal Chem (2011) 401:1195–1202
DOI 10.1007/s00216-011-5188-8

ORIGINAL PAPER

Shotgun proteomic analytical approach for studying proteins adsorbed onto liposome surface

Anna Laura Capriotti · Giulio Caracciolo · Chiara Cavaliere · Carlo Crescenzi · Daniela Pozzi · Aldo Laganà

Received: 29 April 2011 / Accepted: 14 June 2011 / Published online: 2 July 2011

Abstract The knowledge about the interaction between plasma proteins and nanocarriers employed for in vivo delivery is fundamental to understand their biodistribution. Protein adsorption onto nanoparticle surface (protein corona) is strongly affected by vector surface characteristics. In general, the primary interaction is thought to be electrostatic, thus surface charge of carrier is supposed to play a central role in protein adsorption. Because protein corona composition can be critical in modifying the interactive surface that is recognized by cells, characterizing its formation onto lipid particles may serve as a fundamental predictive model for the in vivo efficiency of a lipidic vector. In the present work, protein coronas adsorbed onto three differently charged cationic liposome formulations were compared by a shotgun proteomic approach based on nano-liquid chromatography–high-resolution mass spectrometry. About 130 proteins were identified in each corona, with only small differences between the different cationic liposome formulations. However, this study could be useful for the future controlled design of colloidal drug carriers and possibly in the controlled creation of biocompatible surfaces of other devices that come into contact with proteins into body fluids.

Keywords Cationic liposomes · Mass spectrometry · Nanoparticles · Plasma · Protein corona

Electronic supplementary material The online version of this article (doi:10.1007/s00216-011-5188-8) contains supplementary material, which is available to authorized users.

A. L. Capriotti · C. Cavaliere (✉) · A. Laganà
Dipartimento di Chimica, Sapienza Università di Roma,
Piazzale Aldo Moro 5,
00185 Rome, Italy
e-mail: chiara.cavaliere@uniroma1.it

G. Caracciolo · D. Pozzi
Dipartimento di Medicina Molecolare,
Sapienza Università di Roma,
Piazzale Aldo Moro 5,
00185 Rome, Italy

C. Crescenzi
Dipartimento di Scienze Farmaceutiche e Biomediche,
Università di Salerno,
Via Ponte Don Melillo,
84084 Fisciano (SA), Italy

Introduction

One of the problems posed by liposomes as carriers for drug delivery and gene therapy is a rapid clearance from the blood circulation. Various aspects of liposome architecture strongly influence the clearance behavior. Positively charged liposome containing equimolar amounts of cholesterol are particularly stable, as well as liposomes containing amphipathic phosphatidylethanolamine. During the last few decades, cationic liposomes (CLs) and their complexes with DNA (lipoplexes) have attracted a lot of scientific interest as their advantages as gene delivery vectors were recognized and they became the most widely used synthetic nanocarriers of genes both in vitro and in vivo, and the object of extensive physical–chemical characterizations [1–4].

A critical obstacle for extensive clinical application of lipid-mediated transfection (lipofection) is its low transfection efficiency. Among the potential factors regulating lipofection, membrane charge density of lipid bilayers, σ_M, has been identified as a key parameter regulating nanoparticle activity in vitro [5], and the existence of an optimal membrane charge density, σ_M^*, for in vivo transfection studies was demonstrated.

However, despite the success for in vitro transfection, nanocarriers often exhibit significant drawbacks when used for in vivo delivery. When nanoparticles enter in contact with human plasma, proteins compete for their surface leading to a rich protein "corona" that potentially dictates the fate in vivo [6, 7]. In general, the primary nanoparticle–protein interaction is electrostatic, thus surface charge of carrier is supposed to play a central role in protein adsorption. Because protein binding to nanoparticles can be critical in modifying the interactive surface that is recognized by cells, understanding how and why plasma proteins are adsorbed to lipid particles may serve as a fundamental predictive model for the in vivo efficiency of a lipidic vector. This is a point of great general interest, even though only marginally addressed so far, in view of future clinical application of lipoplexes. Therefore, the knowledge of the adsorbed proteins could be useful in the screening of new liposomal formulations which result more biocompatible.

In this study, we investigated the liposomes made of the cationic lipid (3-[*N*-(*N*,*N*-dimethylaminoethane)-carbamoyl])-cholesterol (DC-Chol), and the zwitterionic lipid dioleoyl-phosphatidylethanolamine (DOPE). The possible effect of membrane charge density on the composition of adsorbed protein coronas was also studied. The membrane charge density is the average charge per unit area of the membrane and it is controlled by the ratio of neutral to cationic lipid in the liposome formulation. Thus, it was varied by changing the neutral/total lipid molar ratio, "diluting" the cationic lipid in the membrane.

Liquid chromatography coupled on-line with electrospray ionization–mass spectrometry (LC/ESI-MS) is the technique of choice when analyzing proteins and peptides in biological samples. In particular, the most employed proteomics strategy is the "shotgun" approach which is based on the LC/ESI-MS analysis of tryptic digests of a whole protein sample.

In recent years, great impulse to proteomics has been provided by the improved performances of newly available mass spectrometers and chromatographic instrumentation, resulting in higher sensitivity, speed of analysis, and mass accuracy [8, 9]. However, the huge amount of data obtainable with these new analytical instrumentations have also required the development of dedicated softwares for handling and filtering the results.

In the present work, a shotgun proteomics approach based on high-resolution MS (by an Orbitrap instrument) coupled to nanoLC system was employed to identify the proteins adsorbed onto liposome surface after incubation with human plasma. Data were then submitted to a suitable result statistical validation.

Even if LC/MS has been already applied for investigating interactions between nanoparticle and proteins [6, 7, 10–12], this is the first study comparing three differently charged CL formulations.

Experimental

Chemicals and reagents

The cationic lipid DC-Chol and the neutral "helper" lipid DOPE were purchased from Avanti Polar Lipids (Alabaster, AL, USA).

Ethylenediaminetetraacetic acid (EDTA), tris (hydroxymethyl)aminomethane (Tris), sodium chloride, 1,4-dithiothreitol (DTT), iodoacetamide (IAA), ammonium bicarbonate, urea, trifluoroacetic acid (TFA) were purchased from Sigma Aldrich (St. Louis, MO, USA). All organic solvents were the highest grade available from Carlo Erba Reagents (Milan, Italy).

Ultrapure water was produced from distilled water by a Milli-Q system (Millipore Corporation, Billerica, MA, USA). Protein LoBind tube were obtained from Eppendorf (Hamburg, Germany). Modified porcine trypsin, sequencing grade, was commercialized by Promega (Madison, WI, USA). Solid-phase extraction (SPE) C18 cartridges were from BOND ELUT (Varian, Palo Alto, CA, USA).

Cationic liposomes preparation

DC-Chol and DOPE were used without further purifications. The liposome solutions were prepared solving appropriate amounts of DC-Chol and DOPE in $CHCl_3$ at three different molar ratios of neutral lipid in the bilayer of Φ (neutral lipid/total lipid, mol/mol)=0.3, 0.5, and 0.7, keeping constant the moles of cationic lipids (i.e., the overall charge). The solvent was evaporated under vacuum for 12 h, and the obtained lipid film was hydrated with a buffer 10 mmol L^{-1} Tris–HCl (pH 7.4), 150 mmol L^{-1} NaCl, 1 mmol L^{-1} EDTA. Small unilamellar vesicles were prepared by sonication and allowed to stay at 30 °C for 24 h to achieve full hydration.

Size and zeta potential measurements

All sizing and zeta potential (ζ_p) measurements were made on a Zetasizer Nano ZS90 (Malvern, U.K.) at 25°C with a scattering angle of 90.0°. Sizing measurements were made on the neat vesicle dispersions, whereas the samples were diluted 1/10 with distilled water for ζ_p measurements. For all samples investigated, the data show a unimodal distribution and represent the average of at least five different measurements carried out for each sample. The polydispersity index (pdi) was directly calculated by the apparatus software.

Human plasma samples

Human plasma samples were obtained from Department of Experimental Medicine (Sapienza University of Rome) according to institutional bioethics approval. Sample of human whole blood were obtained by venipuncture of ten healthy volunteers aged 20–40 years, by means of BD™ P100 Blood Collection System (Franklin Lakes, NJ, USA) with K_2EDTA anticoagulant and protease inhibitors cocktail. Human plasma was prepared as follows: after clot formation, the samples were centrifuged at 1,000 RCF for 5 min to pellet the blood cells, and the supernatant plasma was removed. After checking the absence of hemolysis, the plasma from each separate donor was pooled, split into 200 μL aliquots, and stored at −80 °C in labeled Protein LoBind tubes, until further use. For analysis, the aliquots were thawed at 4 °C and then allowed to warm at room temperature.

Incubation of cationic liposomes with human plasma

Plasma protein binding to nanoparticles was studied by incubating 200 μL of CL suspension in 10 mmol L^{-1} Tris–HCl (pH 7.4), 150 mmol L^{-1} NaCl, 1 mmol L^{-1} EDTA with 200 μL of plasma as already described [12]. The incubation was carried on at 37 °C for 1 h to promote aggregation. The sample was centrifuged at 15 kRCF for 10 min to pellet the CL–protein complexes. The pellet was washed with 250 μL of 10 mmol L^{-1} Tris–HCl (pH 7.4), 150 mmol L^{-1} NaCl, 1 mmol L^{-1} EDTA, using a vortex mixer, transferred into a new Protein LoBind tube, and centrifuged again to pellet the liposome–protein complexes. The entire procedure was repeated twice. The tubes were changed after each washing step to minimize contamination of plasma proteins bound to the tubes. A plasma aliquot not incubated with CLs was subjected to the same procedure as control to verify the absence of protein precipitation. Three experimental replicates were performed for each of the three CL formulations to ensure the reproducibility of the particle–protein complex formation.

Tryptic digestion and peptide desalting

After the incubation of nanoparticles with plasma, the obtained pellet was resuspended in 40 μL of 8 mol L^{-1} urea in 50 mmol L^{-1} NH_4HCO_3 (pH=7.8). Afterwards, the proteic solution was reduced with 2 μL 200 mmol L^{-1} DTT, alkylated with 8 μL 200 mmol L^{-1} IAA, and added with another 8 μL 200 mmol L^{-1} DTT. Finally, the sample solution was diluted with 50 mmol L^{-1} NH_4HCO_3 to obtain a final urea concentration of 1 mol L^{-1} and digested overnight with 2 μg of trypsin at 37 °C. The enzymatic reaction was stopped by adding TFA.

Digested sample was desalted using a SPE C18 silica cartridge. The cartridge was attached to a vacuum manifold apparatus, washed with 1 mL of acetonitrile, and conditioned with 1 mL of H_2O 0.1% (*v*/*v*) TFA. Then the tryptic digest was passed through the SPE column, and the peptides were slowly eluted with 500 μL of water/acetonitrile (50:50, *v*/*v*) 0.05% TFA.

After eluate lyophilization in a Speed-Vac SC 250 Express (Thermo Savant, Holbrook, NY, USA), the sample was re-constituted with 100 μL of 0.1% (*v*/*v*) HCOOH. All samples were stored at −80 °C until analysis.

LC/MS conditions

NanoLC was performed using a Dionex Ultimate 3000 instruments (Dionex, Sunnyvale, CA, USA) consisting of a nanopump with degasser, and a loading pump connected to a thermostatted microwell-plate autosampler.

Sample was enriched on-line on a 300 μm i.d. × 5 mm Acclaim PepMap 100 C18 (5 μm particle size, 100 Å pore size) μ-precolumn (Dionex), employing a premixed mobile phase H_2O:CH_3CN 98:2 (*v*/*v*; phase C) containing 0.1% (*v*/*v*) HCOOH at a flow rate of 10 μL min^{-1}. A 5-μL aliquot of sample was injected.

Peptides were separated on a Biobasic 18 (5 μm particle size, 300 Å pore size) 75 μm i.d. × 100 mm, 15 μm tip picofrit column (Thermo Scientific, Bellefonte, PA, USA) operated at a flow rate of 250 nL min^{-1}. Phase A was H_2O and phase B was CH_3CN, both containing 0.1% (*v*/*v*) HCOOH. A 120-min gradient was used: after an isocratic step at 5% B for 5 min, B was linearly increased to 30% within 75 min; afterwards, B was increased to 80% within 5 min, and to 95% within the following 10 min to rinse the column. Finally, B was reported to 5% over 1 min and the column re-equilibrated for 24 min.

The nanoLC system was coupled to an LTQ-Orbitrap XL hybrid mass spectrometer (Thermo Fisher Scientific, Bremen, Germany) via a nanoelectrospray ion source, operated in positive ionization mode, with spray and capillary voltage set at 2.90 kVand 42 V, respectively, and capillary temperature set at 180 °C.

Full MS spectra were acquired in profile mode in the *m*/*z* range 350–1,800 in the Orbitrap with resolution set at 60,000, whereas data-dependent MS/MS scan of the five most intense monoisotopic peaks in the spectra (top five strategy) was operated with collision-induced dissociation activation at low resolution in the LTQ. Rejection of +1, and unassigned charge states was enabled. All MS/MS spectra were collected using a normalized collision energy of 35%, and an isolation window of 2 *m*/*z*. Ion trap and Orbitrap maximum ion injection times were set to 1,000 and 200 ms, respectively. Automatic gain control was used to prevent overfilling of the ion traps and was set to 5×10^5

for full FTMS scan, and 1×10^4 ions in MS^n mode for the LTQ. To minimize redundant spectral acquisitions, dynamic exclusion was enabled with a repeat count of 1 and a repeat duration of 30 s.

The whole LC/MS system was managed by Xcalibur software (v.2.07, ThermoFisher Scientific).

Five technical replicates per sample were performed.

Data analysis

Thermo RAW data files were submitted to Mascot Deamon (v2.2.04, Matrix Science, London, UK) using the Thermo-Finnigan LCQ/DECA RAW file data import filter to perform database searches against the nonredundant Swiss-Prot database (v57.15; *Homo sapiens* species restriction, 20,266 sequences).

For the database search, trypsin was specified as the proteolytic enzyme with a maximum of two missed cleavages. Carbamidomethylation was set as fixed modification of cysteine, whereas variable modification was oxidation of methionine. The monoisotopic mass tolerance for precursor ions and fragmentation ions were set to 10 ppm and 0.8 Da, respectively. Charge states of +2, or +3 were selected as precursor ions.

Peptide identification and protein assignment were statistically validated submitting the Mascot result files (.dat) in the open source Trans-Proteomic Pipeline (TPP) software (v4.4 Vuvuzela, Seattle Proteome Center, Proteomics Tools: http://tools.proteomecenter.org/software.php). After conversion of the output Mascot files (.dat) in the .pepXML format, the PeptideProphet and ProteinProphet tools [13–15] included in TPP, were employed.

Results and discussion

DLS and zeta potential measurements

DLS and zeta potential measurements showed that DC-Chol–DOPE CLs are positively charged vesicles with the following ζ_p values: 60.1±1.2 mV for Φ=0.3; 56.3±1.3 mV for Φ=0.5; and 55.7±1.3 mV for Φ=0.7. The hydrodynamic radius, R_H, is ranged between 105 and 110 nm. Narrow particle size distribution (pdi=0.2) showed liposome suspensions to be monodisperse.

Separation of nanoparticle–protein complex from plasma

The suitability of centrifugation as a method of separation of the nanoparticle–protein complex, followed by suitable washing stringent conditions for characterizing the so-called hard corona has been already discussed in previous works [6, 12].

LC/MS condition optimization

For data-dependent MS/MS scan, the top five acquisition strategy was chosen, allowing the selection of the five most intense peaks (above a set threshold) in the spectrum for MS/MS analysis. Therefore, it is important to assure separation in those parts of chromatogram where most peptides are eluted, to avoid discarding some precursors. Peptide separation was optimized on the base of identified proteins; then, the Thermo RAW files were submitted to the freely available software RawMeat (v2.0, VAST Scientific, http://vastscientific.com/rawmeat/), a data quality assessment tool designed for Thermo MS data. By the aid of RawMeat, that compares the time dependent effects with MS and MS/MS chromatogram, the suitability of chromatographic separation was verified, in particular observing the top N spacing graph, showing the number of precursors selected per scan cycle.

Repeatability and reproducibility

Proteomics experiments are sensitive to both biological and technical variability, and recently the degree in variability from analysis-to-analysis for even relatively simple complex biological samples has been illustrated and discussed [16, 17].

Lack of reproducibility of MS results in proteomics can be caused by variations in sample preparation, proteolytic digestion, on-line separation of peptides, and MS data acquisition, analysis and interpretation. Additionally, some intrinsic properties of LC/MS/MS contribute to the problem such as the stochastic nature of peptide sampling [8].

The main parameters affecting repeatability and reproducibility between samples were investigated.

In order to analyze only the variables due to the analytical protocol and methodology, all plasma samples were aliquots from a pool of plasma obtained from ten different donors, thus avoiding any biological variability. In fact, blood composition can vary substantially, leading to different interactions between nanoparticles and proteins for different individuals [6].

The low complexity of samples under investigation allowed to employ a shotgun proteomics approach without needing any prefractionation step, this greatly reduced protein/peptide variable losses.

To assess variability due to sample preparation, three experimental replicates were performed. Figure 1 shows, for each CL formulation, the number of proteins identified analyzing the data obtained from each of the three single experiments (five LC/MS runs per sample) and from the three experiments considered all together (15 LC/MS runs in total). The proteins identified in all the three experiments respect to the total for CLs with Φ=0.3, 0.5, and 0.7 were,

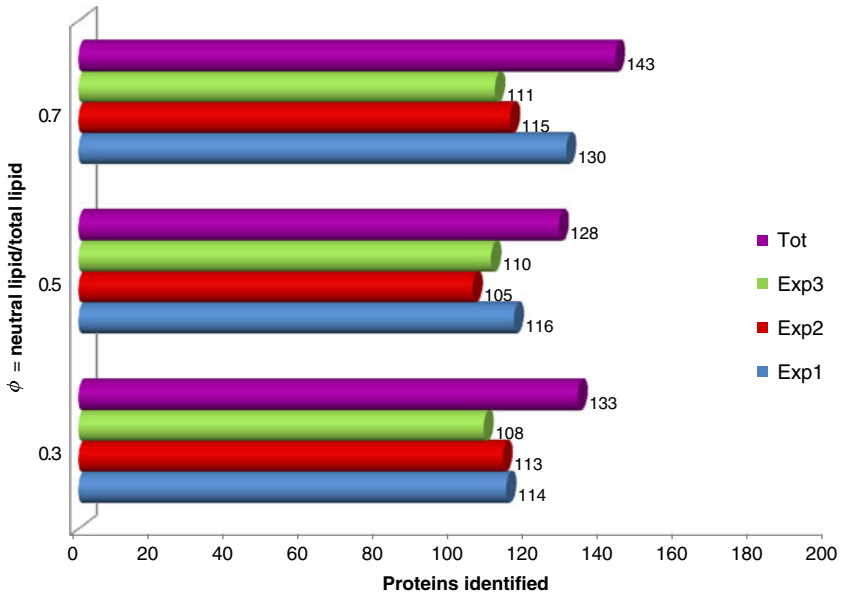

Fig. 1 For each cationic liposome formulation, it is shown the number of proteins identified from the data obtained in each of the three single experiments (five LC/MS runs per sample) and analyzing the three experiments all together (15 LC/MS runs in total)

respectively, 94/133 (71%), 92/128 (72%), and 96/143 (67%).

Another critical parameter in proteomics analysis is the enzyme amount needed to obtain a complete proteolytic digestion of the sample. The RawMeat charge distribution graph showed the presence in the full MS spectra of precursors with mass charge varying from +2 to +6, with +2 and +3 charge precursors representing about 85% of the total, and +4 charge precursors another 10%, indicating a satisfactory digestion yield in all the samples analyzed.

Technical variation is purely related to the analytical techniques being used, because every measurement technique has some intrinsic sources of variability that cannot be totally eliminated. However, technical replicates of the same sample allow to improve analysis precision. Indeed, replicate analyses of the same sample have been demonstrated to improve confidence in protein and peptide identifications [9, 18]. Therefore, five technical replicates were performed for all the samples (three samples for each CL formulation).

Retention time reproducibility was assessed by overlaying the total ion current of all the samples belonging to the same CL formulation and checking the alignment with RawMeat software. Good reproducibility was also obtained comparing retention times of some selected peaks eluting at different retention times present in samples belonging to different CL formulations, if the same chromatographic column was used.

At the end of each sample technical replicate batch, potential sample carryover was assessed by analyzing blank injections.

As regards MS data acquisition, repeatability and reproducibility between samples was evaluated comparing the number of MS and MS/MS scans, as well as average intensity of the full MS spectra in all the LC/MS runs. Results are reported in Table 1 and show that the mean number of scans presents in all cases a relative standard deviation below 5%.

As reported by Köcher et al. [8], until recently, there have been no common rules for MS-based protein identification. Responding to the concerns of the scientific community regarding high numbers of false-positive protein identifications in the literature, common guidelines were adopted by some scientific journals specialized in proteomics [19, 20]. However, these guidelines are mainly recommendations and are currently only required for publication in some proteomics journals, whereas they do not apply for publishing MS data in the majority of scientific journals. One of the most important requirements within these guidelines is to report the false discovery rate (FDR), a number estimating the uncertainty of protein identification. Among the different existing approaches on how calculate FDR [13, 15, 21, 22], the TPP software was employed to statistical validate peptide identification and protein assignment.

Protein identification and statistical data analysis by TPP software

After protein identification by Mascot search engine, the resulting output files (15 files for each CL formulation) were submitted to the statistical open source software TPP. The two new statistical tools of TPP, i.e., PeptideProphet and ProteinProphet, designed for such a purpose, were applied to peptide and protein identification, respectively.

Because the sensitivity (percentage of total correct identifications remaining after restricting data at a given proba-

Table 1 Mean values and relative standard deviation (RSD) of the number of MS and MS/MS scans, and spectrum average intensity obtained, for each of the three cationic liposome formulations, in the five technical replicates of single experiments and considering all the three experimental replicates

Φ		03			0.5			0.7		
		MS scan	MS2 scan	Avg int	MS scan	MS2 scan	Avg int	MS scan	MS2 scan	Avg int
Exp 1 (5 runs)	$Mean_1$	4103	5056	2.2×10^6	3914	5307	2.3×10^6	3574	6608	6.7×10^6
	RSD_1%	2.7%	2.7%	3.8%	0.6%	1.0%	5.8%	0.9%	0.5%	4.0%
Exp 2 (5 runs)	$Mean_2$	3903	5200	2.4×10^6	3862	5294	2.1×10^6	3645	6272	5.6×10^6
	RSD_2%	0.7%	1.4%	3.5%	0.3%	0.6%	3.1%	0.6%	0.7%	2.3%
Exp 3 (5 runs)	$Mean_3$	3818	4990	1.7×10^6	3755	5105	1.6×10^6	3646	5912	4.5×10^6
	RSD_3%	0,4%	0,4%	2.0%	0.9%	1.4%	1.1%	2.0%	2.6%	5.9%
Total (15 runs)	Mean	3941	5082	2.1×10^6	3843	5235	2.0×10^6	3622	6264	5.6×10^6
	RSD%	3.5%	2.4%	15.7%	1.9%	2.1%	15.4%	1.5%	4.9%	17.2%

bility threshold) and error rates (percentage of total false identification) for any dataset modeled are directly related and are affected by the probability threshold set to filter the datasets, it is possible setting more or less stringent probability threshold. The peptide and protein probability thresholds for running PeptideProphet and ProteinProphet were set at 0.7 and 0.9, respectively, for all sample data sets. The related values for FDR and sensitivity were, respectively, 0.5% and 86.9% for CLs with Φ=0.3; 0.6% and 89.0% for CLs with Φ=0.5; and 0.6% and 90.7% for CLs with Φ=0.7.

Following HUPO recommendation, protein identification was considered valid only if based on mass spectra correlating to at least two unique tryptic peptides. Applying these conditions, the proteins identified as adsorbed onto surface of CLs with Φ=0.3, 0.5, and 0.7 were, respectively, 133, 128, and 143, for a total of 169 proteins, with 106 common proteins (see Fig. 2). Proteins identified only in one CL formulation are reported in Table 2. Details about all the identified proteins are provided in Electronic Supplementary Material.

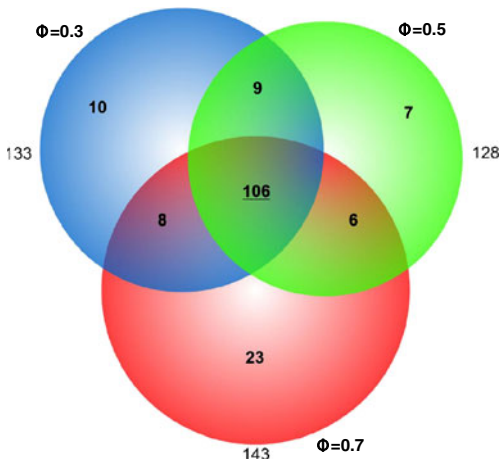

Fig. 2 Venn diagram representing the total number of proteins identified onto surface of cationic liposomes with Φ=0.3, 0.5 and 0.7, and the relative overlaps

Plasma proteins adsorbed onto liposome surface

Most of the 106 proteins common to the three CL formulation are related mainly to the immune or inflammatory (acute phase) response and to the blood coagulation processes, including platelet activation and degranulation, or in lipid transport functions (e.g., apolipoproteins).

As can be seen in Fig. 2 and Table 2, only few proteins had an exclusive binding with only one CL formulation.

Among proteins belonging only to corona of CLs with Φ=0.3, all the proteins but keratin (most likely deriving from a contamination during sample preparation) were identified with up to three unique peptides. The same situation occurred for proteins adsorbed onto CLs with Φ=0.5, except for tubulin beta-1 chain, identified with 13 unique peptides. Tubulin is the major constituent of microtubules, and is a heterodimer of alpha and beta chains. However, we did not find any explanation for this preferential interaction with CLs with Φ=0.5, either from the biological or electrostatic point of view.

The CLs with Φ=0.7 were able to bind more proteins and, as a consequence, were also the nanoparticles having the highest percentage of proteins adsorbed exclusively onto their surface (16% versus 7.5% and 5.4% of CLs with Φ, respectively, 0.3 and 0.5). This result is likely due to the different CL characteristics: because the moles of cationic lipids are fixed whereas the moles of neutral lipids is varied to obtain the different Φ values, CLs with higher Φ possess a larger surface area. On the other hand, to a higher Φ corresponds a smaller σ_M that, differently from our initial hypothesis, seems to have not a determinant role in protein adsorption. The proteins identified with the highest number of unique tryptic peptides were ceruplosamin (16), phospholipid transfer protein (PLTP) (14), antithrombin-III (9),

Table 2 Proteins identified in only one cationic liposome formulation with the relative main identification parameters and charge at pH 7

Uniprot protein ID	Protein name	Protein prob	Coverage%	Unique peps	Charge (pH 7)
Φ=0.3					
O43866 CD5L_HUMAN	CD5 antigen-like	1	26.5	3	−11.4
P02747 C1QC_HUMAN	Complement C1q subcomponent subunit C	0.9962	11.0	2	4.2
P06733 ENOA_HUMAN	Alpha-enolase	0.9816	17.7	3	1.3
P11597 CETP_HUMAN	Cholesteryl ester transfer protein	0.9969	5.7	2	−7.9
P25705 ATPA_HUMAN	ATP synthase subunit alpha, mitochondrial	0.9999	10.5	3	9.6
P35908 K22E_HUMAN	Keratin, type II cytoskeletal 2 epidermal	1	68.5	32	3.8
P48735 IDHP_HUMAN	Isocitrate dehydrogenase [NADP], mitochondrial	0.9827	6.2	2	10.9
P55072 TERA_HUMAN	Transitional endoplasmic reticulum ATPase	0.9175	3.7	2	−22.8
Q9BWP8 COL11_HUMAN	Collectin-11	1	17.3	3	−6.3
Q9ULV4 COR1C_HUMAN	Coronin-1 C	0.9951	12.0	2	0.5
Φ=0.5					
O00299 CLIC1_HUMAN	Chloride intracellular channel protein 1	0.9309	12.0	2	−7.5
P60174 TPIS_HUMAN	Triosephosphate isomerase	0.9966	16.9	2	−0.2
P61158 ARP3_HUMAN	Actin-related protein 3	0.9964	7.9	2	−7.1
P62937 PPIA_HUMAN	Peptidyl-prolyl *cis–trans* isomerase A	0.9999	19.4	2	1.8
P68366 TBA4A_HUMAN	Tubulin alpha-4A chain	1	37.1	3	−21.2
Q15942 ZYX_HUMAN	Zyxin	0.9715	9.8	2	−3
Q9H4B7 TBB1_HUMAN	Tubulin beta-1 chain	1	46.8	13	−18.2
Φ=0.7					
P00450 CERU_HUMAN	Ceruloplasmin	1	22.5	16	−32.5
P00747 PLMN_HUMAN	Plasminogen	1	16.2	5	3.4
P01008 ANT3_HUMAN	Antithrombin-III	1	35.8	9	−1
P01011 AACT_HUMAN	Alpha-1-antichymotrypsin	1	30.0	7	−9.9
P01625 KV402_HUMAN	Ig kappa chain V–IV region Len	0.9998	23.7	2	0.9
P01861 IGHG4_HUMAN	Ig gamma-4 chain C region	1	49.5	3	1.4
P02735 SAA_HUMAN	Serum amyloid A protein	1	66.4	8	−0.4
P02745 C1QA_HUMAN	Complement C1q subcomponent subunit A	0.9985	20.4	2	7.3
P02766 TTHY_HUMAN	Transthyretin	1	68.0	7	−3.9
P04217 A1BG_HUMAN	Alpha-1B-glycoprotein	1	18.8	3	−11.4
P05155 IC1_HUMAN	Plasma protease C1 inhibitor	1	18.0	4	−2.7
P05546 HEP2_HUMAN	Heparin cofactor 2	1	14.6	4	−0.7
P19652 A1AG2_HUMAN	Alpha-1-acid glycoprotein 2	1	31.3	5	−7.5
P25787 PSA2_HUMAN	Proteasome subunit alpha type-2	1	17.1	2	0.8
P25789 PSA4_HUMAN	Proteasome subunit alpha type-4	1	20.7	3	1.8
P36955 PEDF_HUMAN	Pigment epithelium-derived factor	0.9006	11.2	2	−3.2
P39060 COIA1_HUMAN	Collagen alpha-1(XVIII) chain	0.9995	5.3	2	−22.8
P43652 AFAM_HUMAN	Afamin	0.9887	7.3	2	−10.9
P49720 PSB3_HUMAN	Proteasome subunit beta type-3	1	8.8	2	−0.7
P55058 PLTP_HUMAN	Phospholipid transfer protein	1	38.9	14	0
P81605 DCD_HUMAN	Dermcidin	0.9956	22.7	2	−0.6
Q00610 CLH1_HUMAN	Clathrin heavy chain 1	0.9082	1.4	2	−33.2
Q6Q788 APOA5_HUMAN	Apolipoprotein A-V	1	5.5	2	−4.7

serum amyloid A protein (8), alpha-1-antichymotrypsin (7), and transthyretin (7).

Among these six proteins, four belong to the same biological processes of the most of 106 common proteins. In fact, PLTP is involved in cellular lipid metabolic process and lipid transport, and has been shown to interact with apoliprotein A-I and A-II [23]; recently [24], it has been observed that the level of PLTP in plasma increases during

acute inflammation, and complex formation with clusterin, coagulation factors and complement factors were demonstrated by immuno-isolation and shotgun proteomics. Serum amyloid A protein is a major acute phase reactant and an apolipoprotein of the HDL complex; and alpha-1-antichymotrypsin is also involved in acute phase response. Antithrombin-III is the most important serine protease inhibitor in plasma that regulates the blood coagulation cascade.

Different biological processes are interested for transthyretin (transport and hormone activity), and ceruloplasmin that is the major copper-carrying protein in the blood, and in addition plays a role in iron metabolism.

The eight proteins identified adsorbed only onto CLs with Φ=0.3 and 0.7, a deeper analysis of the number of unique peptides related to the proteins showed that, indeed, for seven, the differences were not very significant (e.g., five proteins were also present in CLs with Φ=0.5 with only one unique peptide and thus discarded). However, the tubulin beta chain, identified with 12 and 5 unique peptides, respectively, in CLs with Φ=0.3 and 0.7, was totally absent in CLs with Φ=0.5.

This protein is related to apoptosis and defense response processes.

Regarding the protein overlaps between CLs with Φ=0.3 and 0.5, and between CLs with Φ=0.5 and 0.7, as well as proteins common to all CL formulations, in most cases, a logical trend (i.e., the number of unique peptides and sequence coverage) is observed.

The biochemical rationale for some adsorbed proteins onto one or more of the CLs studied is hardly understandable. Protein interaction between them and with other molecules is a very complex phenomenon and, in this scenario, some unexpected specific interactions could be simply due to casual events rendering the surface "antigenic" for a specific protein. Nevertheless, this interaction might cause consequences at level of liposome to target cell interaction.

Acknowledgment This publication is based on work supported by Award No. KUK-F1-036-32, made by King Abdullah University of Science and Technology (KAUST).

References

1. Felgner PL, Ringold GM (1989) Nature 337:387–388
2. Safinya CR (2001) Curr Opin Struct Biol 11:440–448
3. McManus JJ, Rädler JO, Dawson KA (2003) Langmuir 19:9630–9637
4. McManus JJ, Rädler JO, Dawson KA (2003) J Phys Chem B 107:9869–9875
5. Ewert KK, Evans HM, Zidovska A, Bouxsein NF, Ahmad A, Safinya CR (2006) J Am Chem Soc 128:3998–4006
6. Cedervall T, Lynch I, Foy M, Berggård T, Donnely SC, Cagney G, Linse S, Dawson KA (2007) Angew Chem Int Ed 119:5856–5858
7. Cedervall T, Lynch I, Lindman S, Berggard T, Thulin E, Nilsson H, Dawson KA, Linse S (2007) Proc Natl Acad Sci USA 104:2050–2055
8. Köcher T, Pichler P, Swart R, Mechtler K (2011) Proteomics 11:1026–1030
9. Malmström J, Lee H, Aebersold R (2007) Curr Opin Biotechn 18:378–384
10. Lynch I, Cedervall T, Lundqvist M, Cabaleiro-Lago C, Linse S, Dawson KA (2007) Adv Colloid Interface Sci 134(135):167–174
11. Lundqvist M, Stigler J, Elia G, Lynch I, Cedervall T, Dawson KA (2008) Proc Natl Acad Sci USA 105:14265–14270
12. Capriotti AL, Caracciolo G, Caruso G, Cavaliere C, Pozzi D, Samperi R, Laganà A (2010) Anal Bioanal Chem 398:2895–2903
13. Keller A, Nesvizhskii AI, Kolker E, Aebersold R (2002) Anal Chem 74:383–392
14. Keller A, Eng J, Zhang N, Li XJ, Aebersold R (2005) Mol Syst Biol 1:1–8
15. Nesvizhskii AI, Keller A, Kolker E, Aebersold R (2003) Anal Chem 75:4646–4658
16. Geromanos SJ, Hughes C, Golick D, Ciavarini S, Gorenstein MV, Richardson K, Hoyes JB, Vissers JPC, Langridge JI (2011) Proteomics 11:1189–1211
17. Bell AW, Deutsch EW, Au CE, Kearney RE, Sechi S, Nilsson T, Bergeron JJM, HUPO Test Sample Working Group (2009) Nat Methods 6:423–430
18. Wu CC, MacCoss MJ, Howell KE, Yates JR (2003) Nat Biotechnol 21:532–538
19. Bradshaw RA, Burlingame AL, Carr S, Aebersold R (2006) Mol Cell Proteomics 5:787–788
20. Wilkins MR, Appel RD, Van Eyk JE, Chung MCM, Görg A et al (2006) Proteomics 6:4–8
21. Elias JE, Gygi SP (2007) Nat Methods 4:207–214
22. Moore RE, Young MK, Lee TD (2002) J Am Soc Mass Spectrom 13:378–386
23. Pussinen PJ, Jauhiainen M, Metso J, Pyle LE, Marcel YL, Fidge NH, Ehnholm C (1998) J Lipid Res 39:152–161
24. Cheung MC, Vaisar T, Han X, Heinecke JW, Albers JJ (2010) Biochem 49:7314–7322

III

JOURNAL OF PROTEOMICS 75 (2012) 1924–1932

Available online at www.sciencedirect.com

SciVerse ScienceDirect

www.elsevier.com/locate/jprot

Do plasma proteins distinguish between liposomes of varying charge density?

Anna Laura Capriotti[a], *Giulio Caracciolo*[b], *Chiara Cavaliere*[a,*], *Patrizia Foglia*[a], *Daniela Pozzi*[b], *Roberto Samperi*[a], *Aldo Laganà*[a]

[a]*Dipartimento di Chimica, Sapienza Università di Roma, Piazzale Aldo Moro 5, 00185 Rome, Italy*
[b]*Dipartimento di Medicina Molecolare, Sapienza Università di Roma, Piazzale Aldo Moro 5, 00185 Rome, Italy*

ARTICLE INFO

Article history:
Received 18 October 2011
Accepted 4 January 2012
Available online 14 January 2012

Keywords:
Cationic liposomes
Label-free quantitative analysis
Plasma proteins
Proteomics
NanoLC–MS/MS

ABSTRACT

Cationic liposomes (CLs) are one of the most employed nonviral nanovector systems in gene therapy. However, their transfection efficiency is strongly affected by interactions with plasma components, that lead to the formation of a "protein corona" onto CL surface. The interactions between nanoparticles entering the body and biomolecules have an essential role for their biodistribution. Because the knowledge of proteins adsorbed onto vector surface could be useful in the screening of new, more efficient and more biocompatible liposomal formulations, the behavior of three CLs with different membrane charge densities was investigated. The proteins of the three coronas were identified by nano-liquid chromatography–tandem mass spectrometry, and quantified with label-free spectral counting strategy. Fibrinogen displayed higher association with CLs with high membrane charge density, while apolipoproteins and C4b-binding protein with CLs with low membrane charge density. These results are discussed in terms of the different lipid compositions of CLs and may have a deep biological impact for in vivo applications. Surface charge of nanoparticles is emerging as a relevant factor determining the corona composition after interaction with plasma proteins. Remarkably, it is also shown that the charge of the protein corona formed around CLs is strongly related to their membrane charge density.

1. Introduction

Gene therapy, consisting in the introduction of new genetic materials to hosts, is attracting a growing interest to study gene function and its regulation, to establish and most of all to explore potential therapeutic applications to various acquired or inherited diseases [1] caused by the defect of the absence of one or more genes. Therefore, the development of suitable vectors for an efficient transfection is of fundamental importance in gene therapy.

Starting from the first application in 1987 [2], cationic liposome (CL)-mediated gene transfer has been the most extensively investigated and commonly used nonviral gene delivery approach [1,3–6]. Several different lipids, all sharing the common structure, i.e. positively charged hydrophilic head and hydrophobic tail connected via a linker, have been developed and tested for lipofection. The positively charged head group (generally amines or quaternary ammonium salts) serves to interact with DNA (lipoplexes) or other anionic biomolecules, while the hydrophobic part is the "helper" lipid. The structure of CL (including surface charge density and colipid) strongly affects its transfection efficiency [1].

However, one of the major problems using nanovectors for drug or gene delivery is their interaction with blood

* *Corresponding author*. Tel.: +39 06 49913748; fax: +39 06 490631.
E-mail address: chiara.cavaliere@uniroma1.it (C. Cavaliere).

1874-3919/$ – see front matter © 2012 Elsevier B.V. All rights reserved.
doi:10.1016/j.jprot.2012.01.003

components, that can provoke vector rapid clearance from the blood circulation. Indeed, when nanoparticles enter into blood circulation, plasma proteins are adsorbed onto their surface to form a "protein corona" [7–12]. These interactions with blood biomolecules have been shown to have an essential role in nanoparticle biodistribution [10], and clearance behavior is strongly affected by nanocarrier architecture [11,13]. Therefore, protein binding to nanoparticles can be critical in modifying the interactive surface that is recognized by cells [14,15], and understanding how and why plasma proteins are adsorbed to lipid particles may serve as a fundamental predictive model for the in vivo efficiency of the vector, in view of future clinical applications.

Because the knowledge of plasma proteins adsorbed onto vector surface could be useful in the screening of new, more efficient and more biocompatible liposomal formulations, in a previous work [16] we investigated the behavior of three CLs with different membrane charge densities. In particular, we characterized from the qualitative point of view the three protein coronas by nano-liquid chromatography–tandem mass spectrometry (nanoLC–MS/MS). No significant differences were found in the composition of protein coronas. However, some quantitative differences could be inferred from the Exponentially Modified Protein Abundance Index (emPAI) values [17] provided by the search engine Mascot. For this reason, we decided to perform a quantitative analysis to have a deeper insight and better investigate about a possible specific absorption of plasma proteins onto the different CL surfaces.

MS-based quantitative proteomics can be performed employing both stable isotope labeling and label-free approaches [18–20]. Labeled methods allow the simultaneous quantification of several samples, however present also some drawbacks, such as incomplete labeling, sample dilution (rendering difficult the detection of low abundance proteins), and are associated with high costs. For these reasons, label-free strategies are widely used in biomarker studies [21]. Label-free MS measurement of peptides (and therefore of their parent protein) relies on peak intensity measurements (comparing the direct MS signal intensity for any given peptide on the basis of its retention time, and m/z ratio) or spectral counting (SC) [22–24]. In SC approach, the number of acquired MS/MS spectra matching to a specific peptide is considered an indicator of its abundance in a given sample [20,23]. SCs of peptides associated with a protein are then summed and compared across the samples, often after normalization.

In the present work, a label-free quantification of plasma proteins adsorbed onto the surface of the three liposome formulations previously investigated was performed. According to recent findings [25], CLs are excellent model systems of lipid nanoparticles in which an inner core made of DNA precondensed by oppositely charged macromolecules (e.g. polycations, cationic proteins etc.) is coated with a lipid envelope. After nanoLC–MS/MS analysis and Mascot database search, protein identification was statistically validated with Scaffold software. The same software was also used to evaluate quantitative differences between the three protein coronas with SC method.

Very recently, a few papers on MS-based quantification of protein coronas on different nanoparticle surfaces have been published [11,12,26], however this is the first study on quantification of the plasma proteins adsorbed onto different CLs.

2. Material and methods

2.1. Chemicals and standards

All chemicals were purchased from Sigma Aldrich (St. Luis, Mo, USA) unless otherwise stated. The sequencing grade modified trypsin was from Promega (Madison, WI, USA). All organic solvents were the highest grade available from Carlo Erba Reagents (Milan, Italy). Ultrapure water (resistivity 18.2 MΩ cm) was obtained by an Arium water purification system (Sartorius, Florence, Italy).

The cationic lipid 3β-[N-(N′, N′-dimethylaminoethane)-carbamoyl])-cholesterol (DC-Chol), and the neutral lipid dioleoylphosphatidylethanolamine (DOPE) were purchased from Avanti Polar Lipids (Alabaster, AL, USA).

Solid phase extraction (SPE) C18 cartridges were BOND ELUT (Varian, Palo Alto, CA, USA).

2.2. Preparation of cationic liposomes

The solutions of liposomes were prepared as already described [16] by solving suitable amounts of DC-Chol and DOPE in $CHCl_3$, keeping constant the moles of cationic lipids, to obtain three different molar ratios of neutral lipid in the bilayer Φ (neutral lipid/total lipid, mol/mol)=0.3, 0.5, and 0.7.

After solvent removal (under vacuum for 12 h), the resulting lipid film was hydrated with 10 mmol L^{-1} Tris–HCl pH 7.4, 150 mmol L^{-1} NaCl, 1 mmol L^{-1} EDTA (buffer A). Small unilamellar vesicles were prepared by sonication and allowed to stay at 30 °C for 24 h to achieve full hydration.

The characterization of the resulting vesicle dispersions and samples was made by means of size and zeta potential measurements, respectively [16].

2.3. Samples

Sample of human whole blood were obtained by venipuncture of ten healthy volunteers aged 20–40 years; K_2EDTA anticoagulant and protease inhibitors cocktail were immediately added. Human plasma (HP) samples were prepared at the Department of Experimental Medicine (Sapienza Università di Roma) in accordance with the institutional bioethics code.

HP from each donor was pooled, split into aliquots, and stored at −80 °C in Protein LoBind tubes (Eppendorf, Hamburg, Germany) until further use. For analysis, the aliquots were thawed at 4 °C and then allowed to warm at room temperature.

2.4. Human plasma-cationic liposome incubation

Incubation of HP with CLs was conducted as described in a previous work [27]. Briefly, 200 μL of HP were incubated with 200 μL of CL suspension in buffer A, at 37 °C for 1 h. After centrifugation (15,000 RCF for 10 min) the pellet, constituted by CL-protein complexes, was washed twice with 250 μL buffer A. For each of the three CL formulations, three experimental replicates were performed.

2.5. Protein digestion and peptide desalting

The protein–nanoparticle complex pellet was redissolved in 40 μL of 8 mol L^{-1} urea in 50 mmol L^{-1} NH_4HCO_3 (pH=7.8). Afterwards, protein tryptic digestion was conducted following the protocol already described elsewhere, employing 2 μg of trypsin [16].

The digestion was stopped by adding TFA. Then, the resulting peptide mixture was passed through a SPE C18 silica cartridge for desalting, washed and eluted with 500 μL of water/acetonitrile (50:50, v/v) 0.05% TFA.

After solvent removal in a Speed-Vac apparatus (mod. SC 250 Express; Thermo Savant, Holbrook, NY, USA), sample residue was reconstituted with 100 μL H_2O 0.1% (v/v) HCOOH. All samples were stored at −80 °C until analysis.

2.6. NanoLC–MS/MS analysis

NanoLC system was Dionex Ultimate 3000 (Dionex, Sunnyvale, CA, USA), equipped with a degasser and a thermostatted microwell-plate autosampler.

Peptides were preconcentrated injecting 5 μL aliquot of sample onto a 300 μm i.d.×5 mm Acclaim PepMap 100 C18 (5 μm particle size, 100 Å pore size) μ-precolumn (Dionex); the loading pump was then operated for 5 min with H_2O: CH_3CN 98:2 (v/v) containing 0.1% (v/v) HCOOH at flow-rate of 10 μL min^{-1}. Peptide mixture was separated on a Biobasic 18 (5 μm particle size, 300 Å pore size) 75 μm i.d.×100 mm, 15 μm tip picofrit column (Thermo Scientific, Bellefonte, PA, USA) operated at a flow rate of 250 nL min^{-1}. Phase A was H_2O and phase B was CH_3CN, both with 0.1% (v/v) HCOOH. After an isocratic step at 5% B for 5 min, B was linearly increased to 30% within 75 min; then, B was increased to 80% within 5 min, and to 95% within the following 10 min to rinse the column.

Mass spectrometry detection was performed by an LTQ-Orbitrap XL instrument (ThermoFisher Scientific, Bremen, Germany) with a nanospray source, operated in positive ion mode. Spray and capillary voltage were set at 2.90 kV and 42 V, respectively; capillary temperature was 180 °C.

Full MS spectra were acquired in profile mode in the *m*/z range 350–1800 in the Orbitrap with resolution set at 60,000, whereas data-dependent MS/MS scan of the 5 most intense monoisotopic peaks in the spectra (top 5 strategy) was operated with collision-induced dissociation (CID) activation at low resolution in the LTQ. Rejection of +1, and unassigned charge states was enabled. All MS/MS spectra were collected using a normalized collision energy of 35%, and an isolation window of 2 *m*/z. Automatic gain control was used to prevent overfilling of the ion traps, and dynamic exclusion was enabled to minimize redundant spectral acquisitions.

The whole LC–MS system was managed by Xcalibur software (v.2.07, ThermoFisher Scientific).

Five technical replicates per sample were performed.

2.7. Data analysis

Thermo RAW data files were submitted to Mascot Deamon (v2.3.2, Matrix Science, London, UK) using the ThermoFinnigan LCQ/DECA RAW file data import filter to perform database searches against the nonredundant UniProtKB/Swiss-Prot database (release 57.15 of 2 March 2010; Homo sapiens species restriction, 20,266 sequences).

For the database search, trypsin was specified as the proteolytic enzyme with up to two missed cleavages. Carbamidomethylation of cysteine and oxidation of methionine were set as fixed and variable modification, respectively. The monoisotopic mass tolerance for precursor ions and fragmentation ions was set to 10 ppm and 0.8 Da, respectively.

To validate protein identifications derived from MS/MS sequencing results, the Mascot output files (.dat) were submitted in the commercial software Scaffold (v3.1.2, Proteome Software, Portland, Oregon, USA; http://www.proteomesoftware.com/) [28], that employs independent implementation of Bayesian statistical algorithms developed by the Institute for Systems Biology, i.e. PeptideProphet™ and ProteinProphet® [29–31]. Scaffold tool to integrate Mascot identification results with X!Tandem search engine results (performed in automatic with the same parameters settled for Mascot) was used.

3. Results and discussion

3.1. Size, polidispersity and charge of CLs

Size, polidispersity (pdi), and ζ Potential (ζ_P) of DC-Chol-DOPE CLs at the three different molar ratios of neutral lipid in the bilayer were measured before and after incubation with HP (Table 1). Dynamic light scattering and ζ_P measurements showed that all the three DC-Chol-DOPE CLs investigated are positively charged vesicles (ζ_P in the range 54.3–60.5 mV) with a hydrodynamic radius (R_H) around 100 nm. Narrow particle size distribution (pdi ~0.2) showed CL suspensions to be monodisperse. After incubation with plasma, formation of larger size nanoparticles (depending on CL typology) occurred. The very large R_H increase of CLs with Φ=0.7 after incubation with plasma shows that a more pronounced aggregation phenomenon occurred [14,32].

Table 1 – Size (*D*), polidispersity (pdi), and ζ Potential (ζ_P) of DC-Chol-DOPE liposomes at three different molar ratios of neutral lipid in the bilayer, Φ, before and after incubation with human plasma (HP).

	DC-Chol-DOPE	DC-Chol-DOPE/HP
Φ=0.3		
D (nm)	102±4	450±23
pdi	0.243	0.459
ζ_P (mV)	54.3±0.7	−9.0±0.9
Φ=0.5		
D (nm)	109±2	360±31
pdi	0.212	0.345
ζ_P (mV)	56.3±1.3	−11.4±0.8
Φ=0.7		
D (nm)	105±1	1761±400
pdi	0.239	0.513
ζ_P (mV)	60.5±1.3	−27.4±0.7

3.2. Sample analysis

Optimization of parameters affecting LC–MS/MS analysis, as well as repeatability and reproducibility between samples, has been already illustrated [16].

Because the focus of the work is the evaluation of quantitative differences in protein coronas of the differently charged CL formulations, and it is known that difference in blood composition can lead to different interactions between nanoparticles and proteins [7], the biological variability was avoided by pooling HP samples from all the ten donors.

Three experimental replicates were performed for each CL typology, and five technical replicates were carried out for each sample. To assure good chromatogram alignment and retention times reproducibility between the three experiments of each CL formulation, as well as between all the three CL formulation experimental batches, it was fundamental to use the same chromatographic column.

3.3. Protein identification

The resulting output files obtained by Mascot search engine (15 files for each CL formulation) were submitted to the software Scaffold. Peptide identification assigned by Mascot was verified using the X!Tandem database searching program (integrated into Scaffold) to increase the confidence. Then, the software probabilistically validated these peptide identifications and derived corresponding protein probabilities using PeptideProphet and ProteinProphet, respectively.

Scaffold results were filtered applying the condition to consider valid only protein identifications based on mass spectra correlating to at least two unique tryptic peptides. Minimum peptide identification probability was set at 95% (the highest available value), whereas protein identification probability was set at 99%. Applying these filters, a false discovery rate (FDR) <0.1% was obtained, and a total of 177 proteins were identified in the protein coronas of the three CL formulations, 152 for CLs with Φ=0.3, and 143 for both CLs with Φ=0.5 and 0.7, with 117 proteins in common (as shown in Fig. 1). Further details on identification parameters and the full list of proteins and peptides can be found in Supplementary Tables S1 and S2.

In the previous work [16], data obtained from Mascot were statistically validated with the open source Trans-Proteomic Pipeline (TPP) software (v4.4 Vuvuzela, Seattle Proteome Center, Proteomics Tools: http://tools.proteomecenter.org/software.php), that employs the PeptideProphet and ProteinProphet algorithms, the same successively adopted by Scaffold. In that case, applying for all sample data sets 70% and 90% as peptide and protein probability thresholds, the proteins identified as adsorbed onto surface of CLs with Φ=0.3, 0.5, and 0.7 were, respectively, 133, 128, and 143, for a total of 169 proteins, with 106 common proteins. The different results obtained in the present work are very likely due to the slight modifications of the algorithms and to the employment of X!Tandem as second search engine (see Supplementary Figs. S1 and S2).

Regarding to FDR estimate, there are several ways to calculate it. Because MS/MS peak list data have not been searched against a decoy database, Scaffold calculated the FDR with a probabilistic method used by the TPP and the Protein Prophet algorithm, based on the assigned protein probabilities.

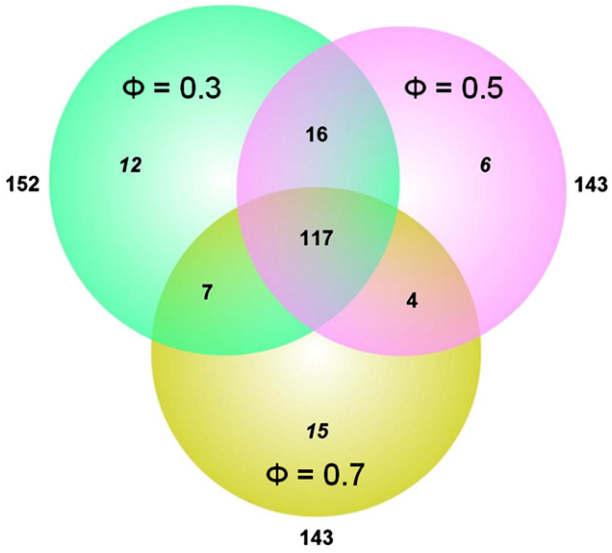

Fig. 1 – Venn diagram reporting the number of proteins identified onto the surface of the three cationic liposome formulations.

After validation, a good agreement in proteins identified in the three different experimental replicates of the single CL formulation was obtained (see Supplementary Table S1).

Most of the 117 proteins common to the three CL formulations are involved in cellular process, biological regulations, response to stimulus, and metabolic processes (Fig. 2).

3.4. Protein quantitative analysis and relation with CL membrane charge density

Identification and quantification of the proteins that bind to CLs in biological environments, i.e. the protein corona, can provide insights into their biocompatibility and biodistribution in vivo. It is now emerging the concept that it is the protein relative abundance within protein corona which is the most important outcome of the protein-nanoparticle binding. It is thus essential to quantify both major and minor particle-associated proteins. Such knowledge will constitute the basis for future efforts to establish mathematical models for predicting nanoparticle surface chemistry interactions.

For protein quantitative analysis, Scaffold software allows the normalization of the SC (NSC) and offers various statistical tests to identify significant abundance differences in two or more categories. Quantitative data showed that CLs with Φ=0.3 and Φ=0.5 had a similar protein abundance for almost all the identified proteins (see Fig. 3 and Supplementary Table S3). This finding means that the composition of these two CL formulations is roughly the same. On the other side, the comparison between the abundance of proteins bound to the coronas of CLs with Φ=0.3 and Φ=0.7 showed relevant differences. Therefore, in the following text, discussion of results will be restricted to the comparison of CLs with Φ=0.3 and Φ=0.7.

For the two CL formulations considered, the mean value of NSCs obtained in the three experimental replicates for each protein was further normalized to the protein mass (*MWNSC*)

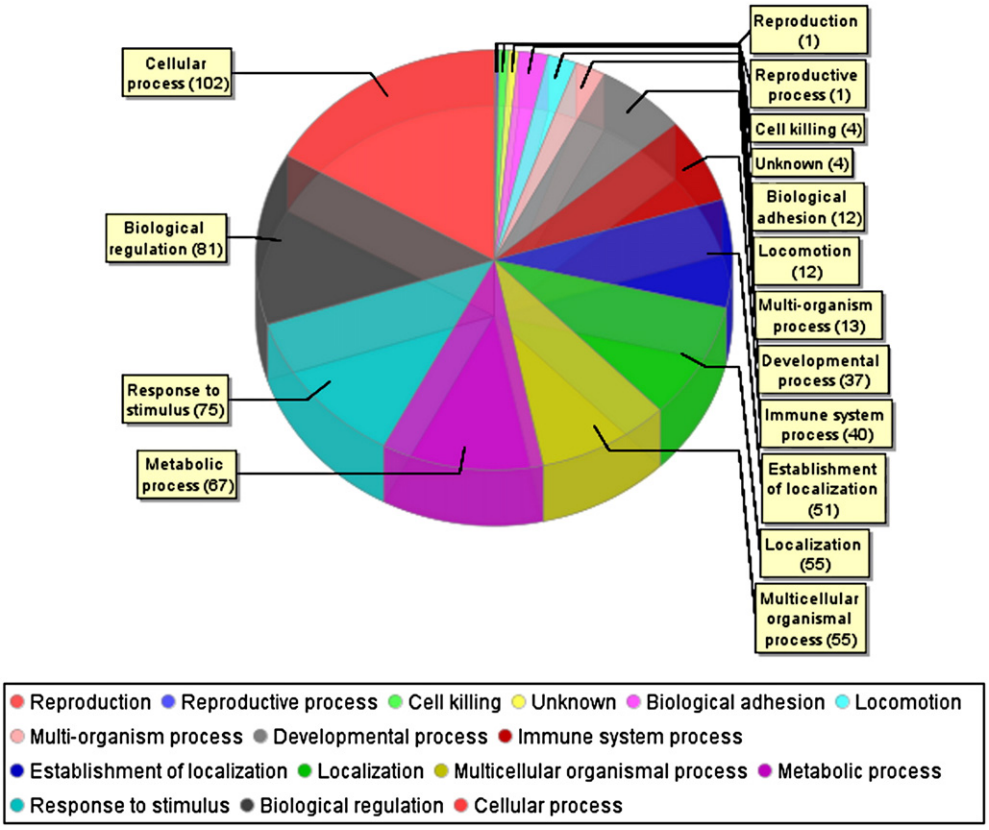

Fig. 2 – Pie chart showing the biological processes in which the 117 common proteins identified in all the three cationic liposome formulations are involved. One protein can belong to more than one biological process.

and expressed as the relative protein quantity by applying the following equation:

$$MWNSC_k = \left(\frac{(NSC/MW)_k}{\sum_{i=1}^{n} (NSC/MW)_i} \right) \times 100 \qquad (1)$$

where $MWNSC_k$ is the percentage molecular weight normalized NSC for protein k (i.e. the relative protein abundance in the 'hard corona' [12]), and MW is the molecular weight in kDa for protein k. This correction takes into account the protein size and evaluates the actual contribution of each protein to the hard corona composition [12]. By using Eq. (1), the relative protein abundance for the CL formulations selected (i.e. CLs with Φ=0.3, and 0.7) could be calculated (Supplementary Table S4).

It is worth mentioning that protein abundance does not necessarily reflect the biological impact. Indeed, a less abundant protein with high affinity and specificity may be a key player in several biological processes. However, proteins whose relative protein abundance is extremely low are not expected to be a determining factor for the fate and impact of the particles [12–14]. To make data interpretation simpler and more meaningful, the analysis was thereby restricted to those proteins whose $MWNSC_k$ was $\geq$1 either in the corona of CLs with Φ=0.3 or in that of CLs with Φ=0.7. Relative protein abundance of proteins satisfying such criterion is reported in Fig. 4. As Fig. 4 clearly shows, the relative protein abundance was found to be strictly dependent on the CL formulation. According to previous findings [12–14], size and chemical surface properties are among the most relevant influential factors of nanoparticle bound protein abundance. In this regard, while both the size and the zeta potential of CLs with Φ=0.3 and 0.7 are pretty similar (Table 1), the lipid compositions of these formulations are really different from each other. Given the remarkable differences in the relative protein abundance shown in Fig. 4, it appeared that, under the experimental conditions of this study, the lipid composition of the nanoparticle surface was more impactful on the protein absorption than did their size. To better decipher data, we calculated the relative protein abundance ratio, R, defined as $R = MWNSC_k(\Phi=0.3)/MWNSC_k(\Phi=0.7)$ (Fig. 5). Finally, we considered significant only $R>2$ and $R<0.5$. Fig. 5 clearly shows that fibrinogen displays higher rate of association with the surface of CLs with Φ=0.3 ($R>2$) with respect to all other identified proteins. On the other side, apolipoproteins and C4b-binding protein alpha chain are the proteins most abundantly associated in the corona of CLs with Φ=0.7 ($R<0.5$). Bearing in mind that CLs with Φ=0.7 are definitely richer in DOPE than that their counterpart with Φ=0.3, we corroborate previous findings showing that phospholipid-lipoprotein binding is a general feature of lipid-based nanoparticles under physiological conditions. Accordingly, our findings suggest that apolipoproteins have hydrophilic groups of phospholipids that can more favorably interact with the phospholid moiety of DOPE rather than with the less hydrophilic head group of DC-

Chol. This information may be particularly important since lipoprotein phospholipids play a critical role in the normal functioning and integrity of the lipid transport system [33].

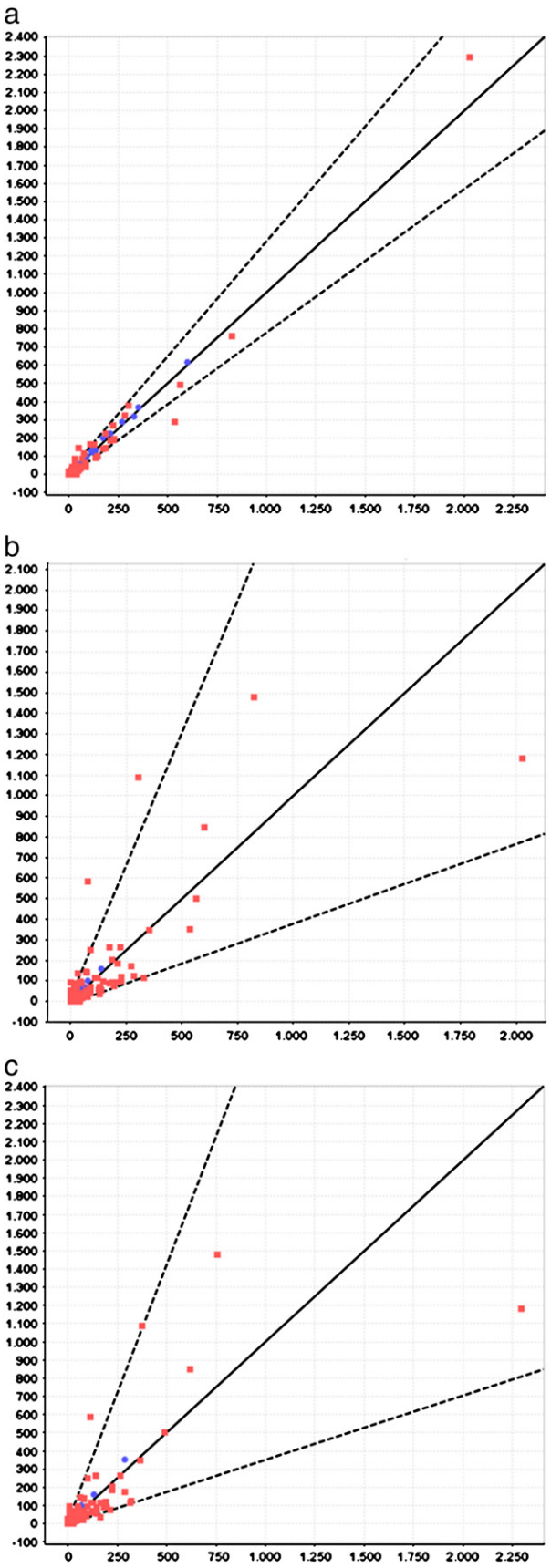

It is important to underline that such a remarkable difference in the composition of the coronas of CLs with Φ=0.3 and Φ=0.7 may have a deep biological impact. Indeed, it has been recently hypothesized that adsorbed protein layer may affect cellular uptake and may affect trafficking, while in vivo, specific binding of proteins influences biodistribution and blood clearance. Adsorption of opsonins like fibrinogen (abundantly associated to CLs with Φ=0.3), IgG, and complement factors, is supposed to promote rapid clearance from the bloodstream, while binding of dysopsonins like apolipoproteins (largely abundant in the corona of CLs with Φ=0.7) etc. promotes prolonged circulation time in blood [12–14]. Apolipoproteins are also involved in the transportation of lipids and cholesterol in the bloodstream and, as such, are expected to greatly affect the intracellular trafficking, fate, and transport of nanoparticles in cells and animals. It has been also proposed that apolipoprotein enrichment on CL surfaces, as that observed in the case of CLs with Φ=0.7, might stimulate interaction with low-density lipoprotein receptors, resulting in transport across the blood–brain barrier. The behavior of C4b-binding protein, more adsorbed onto CLs with Φ=0.7 than onto CLs with Φ=0.3, does not represent a contradiction to this scenario, considering the inhibitory role of the protein in the complement system.

This specific adsorption of CLs, at different Φ is also confirmed observing the list of proteins detected only in the corona of CLs with Φ=0.7 and the proteins detected only in the protein coronas of CLs with Φ=0.3 (Supplementary Table S5). Proteins bound to CLs with Φ=0.7 are expressed or synthesized almost in the liver, and are involved in blood coagulation process and complement pathway. The proteins that have been found only in the coronas of CLs with Φ=0.3 have binding functions and are localized mostly in cytoplasm. Therefore, proteins expressed in an organ rich in lipids as the liver seem to have a preferential adsorption on surface of CLs with the major lipophilic characteristic (Φ=0.7). However, results reported in Supplementary Table S5 shows that the relative protein abundance of such 'exclusive proteins' is lower than 1% in both the coronas. As discussed above, such percentages are too low to suppose such proteins are key players.

Fig. 3 – Quantitative Scatterplot graph plotting each protein as a point on a two dimensional Q–Q scatterplot. The x-axis is the normalized spectral count (NSC) for the protein for all samples in one category, and the y-axis is the NSC in a second category: a) NSC for CLs with Φ=0.3 vs NSC for CLs with Φ=0.5; b) NSC for CLs with Φ=0.3 vs NSC for CLs with Φ=0.7; and c) NSC for CLs with Φ=0.5 vs NSC for CLs with Φ=0.7. Proteins with similar abundances in both categories are plotted as points near the 45 degree line. The two dashed lines represent two standard deviations (depending on the number of spectra), then proteins that plot outside these lines are differentially expressed. Proteins plotted as red points are those labeled as significantly different between categories by quantitative analysis Fisher's Exact test. Proteins plotted as blue points are those labeled as insignificant.

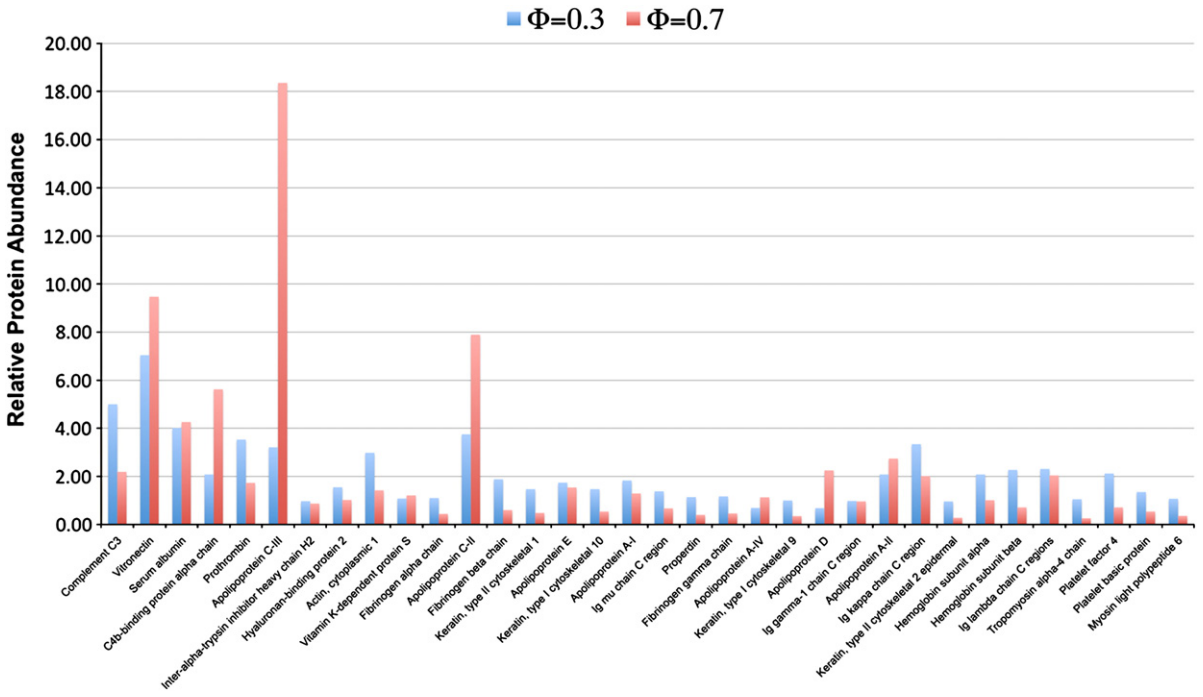

Fig. 4 – Relative protein abundance of proteins (normalized to molecular weight, MWNSC) satisfying the criterion that $MWNSC_k \geq 1$ either in the corona of CLs with $\Phi = 0.3$ or in that of CLs with $\Phi = 0.7$.

Lastly, surface charge of nanoparticles has been suggested as a relevant factor determining the corona composition after interaction with plasma proteins. Thus, we asked whether a correlation between the surface charge of CLs and the composition of the resulting protein coronas could actually exist. To this end, the charges at pH 7.4 of the above mentioned

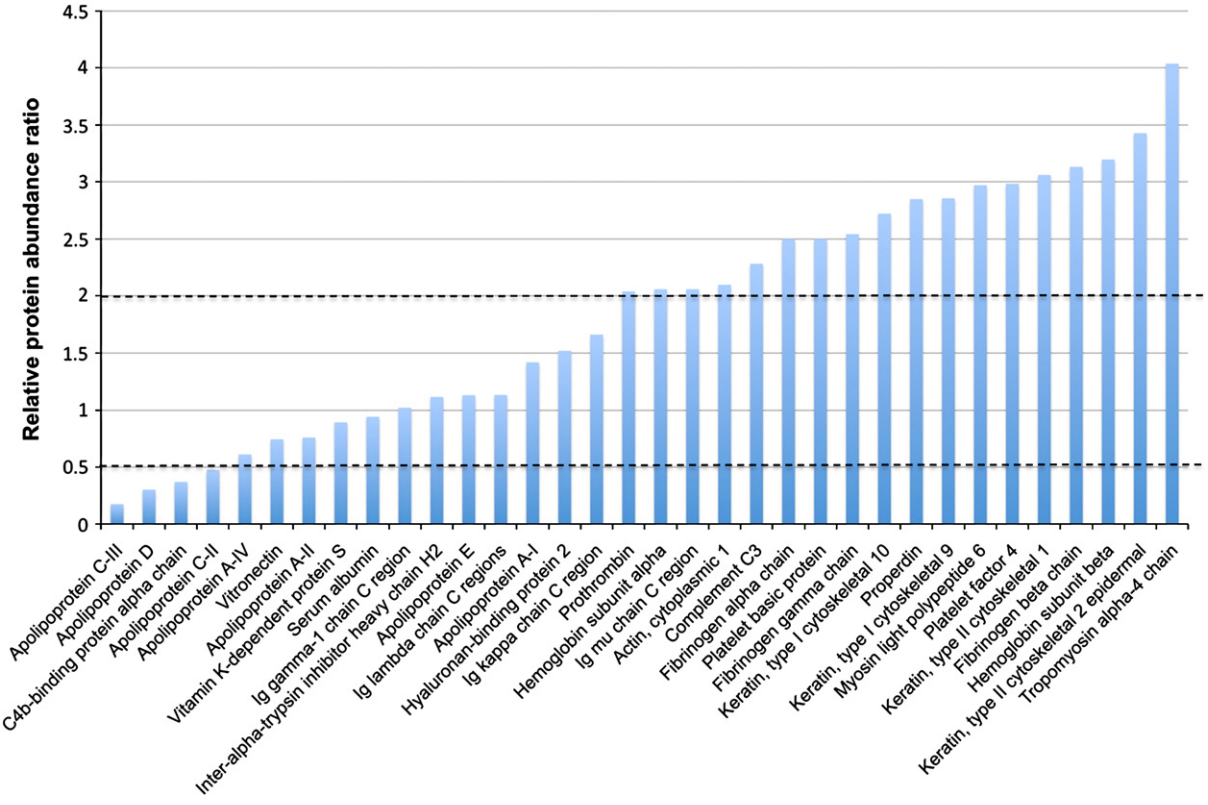

Fig. 5 – Relative protein abundance ratio, R, defined as the ratio between relative protein abundance of protein k($MWNSC_k$) in CLs with $\Phi = 0.3$ and $MWNSC_k$ in CLs with $\Phi = 0.7$.

proteins were calculated by a dedicated software (http://www.scripps.edu/~cdputnam/protcalc.html). The charge of statistically significant proteins (those proteins with $MWNSC_k \geq 1$ either in the corona of CLs with $\Phi=0.3$ or in that of CLs with $\Phi=0.7$) is reported in Supplementary Table S6. The relative charge, a measure of the relative amount of the charge on the protein corona, was calculated by multiplying the total charge on the protein k, q_k, for its relative protein abundance, $MWNSC_k$. It reads:

$$Q(\Phi) = \sum_{k=1}^{n} q_k \times MWNSC_k(\Phi). \quad (2)$$

By applying Eq. (2) we found that: (i) The relative charge of both the coronas is negative; (ii) $Q(\Phi=0.3) < Q(\Phi=0.7)$. The former result is quite obvious in that it confirms that the cationic surface of CLs preferably interacts with negatively charged proteins. On the other hand, considering that CLs at $\Phi=0.3$ are more positively charged with respect to their counterpart with $\Phi=0.7$, the latter finding indicates that the charge of the protein corona and the membrane charge density of cationic lipid membranes are strongly related to each other. The low membrane charge density of CLs at $\Phi=0.7$ (rich in the neutral DOPE and poor in cationic DC-Chol) could result in a low electrostatic repulsion barrier that could be overcome by basic proteins with the result that short-range attractive van der Waals forces prevail on electrostatic repulsion thereby inducing membrane aggregation and nanoparticle clustering. Such suggestion is in very good agreement with the results of Table 1 showing that, upon interaction with human plasma, CLs with $\Phi=0.7$ largely aggregate. Aside from clarifying the molecular mechanisms of opsonization, the present results are likely to indicate that the molar fraction of DOPE in the CL formulations may have a determinant role by regulating both the surface properties and the membrane charge density of cationic membranes.

4. Conclusions

Because nanoparticle interactions with plasma proteins strongly affect the distribution of the vectors into the body, understanding of these interactions could be useful in developing nanocarriers with surface, size and shape able to drive them to target organs. The employment of a quantitative strategy to determine the proteins adsorbed onto the surface of three CLs formulations, characterized by a different lipid composition and membrane charge density, has shown a preferential absorption for some classes of proteins. Our results indicate that, for lipid gene vectors as those used in the present study (e.g., cationic liposomes, lipid nanoparticles), lipid composition does control the surface properties of nanoparticles that, in turn, is able to entirely change the nature of the biologically active proteins in the corona, and thereby possibly also the biological impacts. The role of these proteins in driving nanoparticle biodistribution is not completely clear. Nevertheless, the proposed approach is applicable to other nanoparticle typologies, and can support in designing and testing new carriers for possible clinical employment.

Supplementary materials related to this article can be found online at doi:10.1016/j.jprot.2012.01.003.

Acknowledgments

This publication is based on work supported by Award No. KUK-F1-036-32, made by King Abdullah University of Science and Technology (KAUST).

We kindly thank Francesco Di Pascasio for his helpful assistance in data software elaboration.

REFERENCES

[1] Al-Dosari MS, Gao X. Nonviral gene delivery: principle, limitations, and recent progress. AAPS J 2009;11:671–81.
[2] Felgner PL, Gadek TR, Holm M, Roman R, Chan HW, Wenz M, et al. Lipofection: a highly efficient, lipid-mediated DNA-transfection procedure. Proc Natl Acad Sci U S A 1987;84:7413–7.
[3] Morille M, Passirani C, Vonarbourg A, Clavreul A, Benoit JP. Progress in developing cationic vectors for non-viral systemic gene therapy against cancer. Biomaterials 2008;29:3477–96.
[4] Kamimura K, Suda T, Zhang G, Liu D. Advances in gene delivery systems. Pharm Med 2011;25:293–306.
[5] Abu Lila AS, Ishida T, Kiwada H. Targeting anticancer drugs to tumor vasculature using cationic liposomes. Pharm Res 2010;27:1171–83.
[6] Bhattacharya S, Bajaj A. Advances in gene delivery through molecular design of cationic lipids. Chem Commun 2009;31:4632–56.
[7] Cedervall T, Lynch I, Foy M, Berggård T, Donnely SC, Cagney G, et al. Detailed identification of plasma proteins adsorbed on copolymer nanoparticles. Angew Chem Int Ed 2007;119:5854–6.
[8] Lundqvist M, Stigler J, Cedervall T, Elia G, Lynch I, Dawson K. Nanoparticle size and surface properties determine the protein corona with possible implications for biological impacts. Proc Natl Acad Sci U S A 2008;105:14265–70.
[9] Lynch I, Dawson KA. Protein–nanoparticle interactions. Nano Today 2008;3:40–7.
[10] Aggarwal P, Hall JB, McLeland CB, Dobrovolskaia MA, McNeil SE. Nanoparticle interaction with plasma proteins as it relates to particle biodistribution, biocompatibility and therapeutic efficacy. Adv Drug Deliv Rev 2009;61:428–37.
[11] Tenzer S, Docter D, Rosfa S, Wlodarski A, Kuharev J, Rekik A, et al. Nanoparticle size is a critical physicochemical determinant of the human blood plasma corona: a comprehensive quantitative proteomic analysis. ACS Nano 2011;5:7155–67.
[12] Monopoli MP, Walczyk D, Campbell A, Elia G, Lynch I, Baldelli Bombelli F, et al. Physical–chemical aspects of protein corona: relevance to in vitro and in vivo biological impacts of nanoparticles. JACS 2011;133:2525–34.
[13] Monopoli MP, Baldelli Bombelli F, Dawson KA. Nanobiotechnology: nanoparticle coronas take shape. Nat Nanotechnol 2011;6:11–2.
[14] Walczyk D, Baldelli Bombelli F, Monopoli MP, Lynch I, Dawson KA. What the cell "sees" in bionanoscience. J Am Chem Soc 2010;132:5761–8.
[15] Allen LT, Tosetto M, Miller I, O'Connor D, Penney SC, Lynch I, et al. Surface induced changes in protein adsorption and implications for cell-surface response. Biomaterials 2006;27:3096–108.
[16] Capriotti AL, Caracciolo G, Cavaliere C, Crescenzi C, Pozzi D, Laganà A. Shotgun proteomic analytical approach for studying proteins adsorbed onto liposome surface. Anal Bioanal Chem 2011;401:1195–202.
[17] Ishihama Y, Oda Y, Tabata T, Sato T, Nagasu T, Rappsilber J, et al. Exponentially modified protein abundance index

(emPAI) for estimation of absolute protein amount in proteomics by the number of sequenced peptides per protein. Mol Cell Proteomics 2005;4:1265–72.
[18] Nefedov AV, Gilski MJ, Sadygov RG. Bioinformatics tools for mass spectrometry-based high-throughput quantitative proteomics platforms. Curr Proteomics 2011;8:125–37.
[19] Neilson KA, Ali NA, Muralidharan S, Mirzaei M, Mariani M, Assadourian G, et al. Less label, more free: approaches in label-free quantitative mass spectrometry. Proteomics 2011;11:535–53.
[20] Mueller LN, Brusniak MY, Mani DR, Aebersold R. An assessment of software solutions for the analysis of mass spectrometry based quantitative proteomics data. J Proteome Res 2008;7:51–61.
[21] Sandin M, Krogh M, Hansson K, Levander F. Generic workflow for quality assessment of quantitative label-free LC–MS analysis. Proteomics 2011;11:1114–24.
[22] Lundgren DH, Hwang SI, Wu L, Han DK. Role of spectral counting in quantitative proteomics. Expert Rev Proteomics 2010;7:39–53.
[23] Katz E, Fon M, Eigenheer RA, Phinney BS, Fass JN, Lin D, et al. A label-free differential quantitative mass spectrometry method for the characterization and identification of protein changes during citrus fruit development. Proteome Sci 2010;8:68–86.
[24] Yao X. Derivatization or not: a choice in quantitative proteomics. Anal Chem 2011;83:4427–39.
[25] Caracciolo G, Pozzi D, Capriotti AL, Marianecci C, Carafa M, Marchini C, et al. Factors determining the superior performance of lipid/DNA/protammine nanoparticles over lipoplexes. J Med Chem 2011;54:4160–71.
[26] Simberg D, Park JH, Karmali PP, Zhang WM, Merkulov S, McCrae K, et al. Differential proteomics analysis of the surface heterogeneity of dextran iron oxide nanoparticles and the implications for their in vivo clearance. Biomaterials 2009;30:3926–33.
[27] Capriotti AL, Caracciolo G, Caruso G, Cavaliere C, Pozzi D, Samperi R, et al. Analysis of plasma protein adsorption onto DC-Chol-DOPE cationic liposomes by HPLC-CHIP coupled to a Q-TOF mass spectrometer. Anal Bioanal Chem 2010;398: 2895–903.
[28] Searle BC. Scaffold: a bioinformatic tool for validating MS/MS-based proteomics studies. Proteomics 2010;10:1265–9.
[29] Keller A, Nesvizhskii AI, Kolker E, Aebersold R. Empirical statistical model to estimate the accuracy of peptide identifications made by MS/MS and database search. Anal Chem 2002;74:383–92.
[30] Nesvizhskii AI, Keller A, Kolker E, Aebersold R. A statistical model for identifying proteins by tandem mass spectrometry. Anal Chem 2003;75:4646–58.
[31] Keller A, Eng J, Zhang N, Li XJ, Aebersold R. A uniform proteomics MS/MS analysis platform utilizing open XML file formats. Mol Syst Biol 2005;1:1–8.
[32] Urbanija J, Tomšič N, Lokar M, Ambrožič A, Čučnik S, Rozmanc B, et al. Coalescence of phospholipid membranes as a possible origin of anticoagulant effect of serum proteins. Chem Phys Lipids 2007;150:49–57.
[33] Dergunov AD, Taveirne J, Vanloo B, Caster H, Rosseneu M. Structural organization of lipid phase and protein–lipid interface in apolipoprotein-phospholipid recombinants: influence of cholesterol. Biochim Biophys Acta 1997;1346: 131–46.

IV

Langmuir

ARTICLE

pubs.acs.org/Langmuir

Evolution of the Protein Corona of Lipid Gene Vectors as a Function of Plasma Concentration

Giulio Caracciolo,*[,†] Daniela Pozzi,[†] Anna Laura Capriotti,[‡] Chiara Cavaliere,[‡] Patrizia Foglia,[‡] Heinz Amenitsch,[§] and Aldo Laganà[‡]

[†]Department of Molecular Medicine, "Sapienza" University of Rome, Viale Regina Elena 324, 00161, Rome, Italy

[‡]Department of Chemistry, "Sapienza" University of Rome, P.le A. Moro 5, 00185 Rome, Italy

[§]Institute of Biophysics and Nanosystems Research, Austrian Academy of Sciences, Schmiedelstrasse 6, A-8042 Graz, Austria

Supporting Information

ABSTRACT: The concept that the effective unit of interest in the cell−nanomaterial interaction is the particle and its corona of associated proteins is emerging. Here we investigate the compositional evolution of the protein corona of 1,2-dioleoyl-3-trimethylammonium propane (DOTAP) cationic liposomes (CLs) and DOTAP/DNA lipoplexes over a wide range of plasma concentrations (2.5−80%). The composition of the hard corona of lipoplexes is quite stable, but that of CLs does evolve considerably. We show that the protein corona of CLs is made of both low-affinity and competitive-binding proteins whose relative abundance changes with the plasma concentration. This result may have deep biological implications for the application of lipid-based gene vectors both in vitro and in vivo.

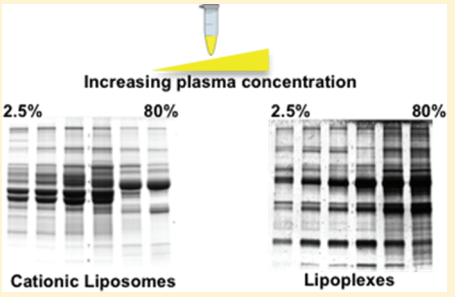

1. INTRODUCTION

Gene delivery holds great promise as a therapeutic agent for a vast array of disorders such as cancer and genetic and acquired diseases. Among the most promising nonviral candidates, cationic liposomes/DNA complexes (lipoplexes) have been widely used[1−3] because of their low immunogenicity, safety, ability to package large DNA molecules, and ease of preparation. Over the last two decades, consistent efforts have been made with respect to the development of lipoplex formulations that would exhibit cell specificity, minimal immune response, the efficient release of DNA into cells, and a large DNA capacity. Unfortunately, a deep knowledge of the physical−chemical properties of these systems in simple solvents did not result in the formulation of lipid vectors that were as efficient as their viral counterparts. This may be due to the main difference existing between the nanocarrier and its modified version after interacting with biological media. Recently, a series of pioneering studies[4−8] have radically changed our way of thinking about nanocarries for in vitro and in vivo gene delivery applications. It has been shown that the effective unit of interest in the cell−nanomaterial interaction is not the nanoparticle itself but the particle and its hard corona of associated proteins from plasma or other bodily fluids. This corona of proteins at the surface of the particle is sufficiently long-lived that actually the entity is "seen" and processed by living cells. In a recent seminal paper,[9] Monopoli et al. demonstrated that the composition of the hard corona of silica nanoparticles at low protein concentration (appropriate to in vitro cell studies) can be very different with respect to its counterpart at high protein concentration (typical of in vivo studies). This is a key issue that has broad implications for in vitro−in vivo extrapolations[9] and will determine the future road map of nanomedicine and perhaps impact the overall field of nanoscience.[4]

Here we investigate the compositional evolution of the protein corona of 1,2-dioleoyl-3-trimethylammonium propane (DOTAP) cationic liposomes (CLs) and DOTAP/DNA lipoplexes as a function of increasing plasma concentration. According to recent findings,[10] CLs are excellent model systems of lipid nanoparticles (LNP) in which a DNA/polycation core is coated with a lipid envelope.[11−13] This study allowed us to elucidate more quantitatively the degree to which the protein corona of lipid gene vectors can change, depending on the biological environment. Although the hard corona of lipoplexes is quite stable, we find that the hard corona of CLs can evolve quite considerably as one passes from protein concentrations appropriate to in vitro cell studies to those present in in vivo studies. As a consequence, the biological identity of lipid gene vectors whose surfaces are entirely lipidic (e.g., LNP) may change dramatically as the amount of protein in the environment changes. This result may have deep biological implications for the application of lipid-based gene vectors both in vitro and in vivo.[4−10]

2. EXPERIMENTAL SECTION

2.1. Liposome and Lipoplex Preparation. Cationic DOTAP was purchased from Avanti Polar Lipids (Alabaster, AL) and used without further purification. Calf thymus (CT) DNA was obtained from Sigma-Aldrich (St. Louis, MO) and was used without further purification. A solution of CT-DNA (1 mg/mL) was sonicated for 15 min to produce fragments with typical length distributions of between 500 and

Received: July 27, 2011
Revised: September 15, 2011
Published: November 01, 2011

1000 base pairs as determined by electrophoresis on agarose gels. Unilamlellar DOTAP CLs (1 mg/mL) were prepared according to standard protocols.[14] Positively charged DOTAP/DNA lipoplexes were prepared by mixing 100 μL of DOTAP CLs with 50 μL of CT-DNA at a cationic lipid/DNA charge ratio of $\rho = 1$.[15]

2.2. Sizing and ζ-Potential Measurements. All sizing and ζ-potential measurements were made on a Zetasizer Nano ZS90 (Malvern, U.K.) at 25 °C with a scattering angle of 90°. Sizing measurements were made on the neat vesicle dispersions, whereas the samples were diluted 1:10 with distilled water for the zeta potential experiments to obtain reliable and accurate measurements. For all of the samples investigated, the data show a unimodal distribution and represent the average of at least five different measurements carried out for each sample. More accurate experimental details can be found in ref 10.

2.3. Synchrotron Small-Angle X-ray Scattering Measurements. Synchrotron small-angle X-ray scattering (SAXS) measurements were performed at the Austrian SAXS station of the ELETTRA synchrotron light source (Trieste, Italy).[16] SAXS patterns were recorded with gas detectors based on the delay line principle covering the q ranges from $q_{min} = 0.4$ nm^{-1} to $q_{max} = 5$ nm^{-1} with a beam size at the sample position of 5×10^{-3} nm^{-1} (fwhm). The angular calibration of the detectors was performed with silver behenate powder (with a d spacing of 5.838 nm). The data have been normalized for variations in the primary beam intensity and corrected for the detector efficiency, and the background has been subtracted. Exposure times were typically 300 s. No evidence of radiation damage was observed in the X-ray diffraction patterns. In both experimental sessions, the sample was held in a 1 mm glass capillary (Hilgenberg, Malsfeld, Germany) and the measurements were performed at 25 °C with a precision of 0.1 °C.

2.4. Proteomics Experiments. Human plasma was prepared as described elsewhere.[17] Both CLs and lipoplex suspensions (final lipid concentration for both suspensions 0.75 mg/mL) were incubated in different plasma concentrations (2.5, 5, 10, 20, 50, and 80%) in a saline buffer (pH 7.4). After incubation, the samples were centrifuged to pellet the particle/protein complexes. The pellet was resuspended in the saline buffer, transferred into a new vial, and centrifuged again to pellet the particle/protein complexes; this procedure was repeated twice.[18] For separation by 1D polyacrilamide gel electrophoresis (1D-PAGE), the proteins were eluted from the particles by adding sodium dodecyl sulfate (SDS)-PAGE sample buffer to the pellet and boiling the solution. A 12% polyacrylamide gel was employed to separate the proteins as reported elsewhere.[19] Coomassie PhastGel Blue R-350 was used to stain the gels with gentle agitation, in accordance with the manufacturer's manual (GE Healthcare, Milan, Italy). All experiments were conducted four times to ensure the reproducibility of the particle/protein complex pellet sizes, general pattern, and band intensities on the 1D gels. To determine the molecular weights (MWs) of proteins after an electrophoretic run, protein molecular weight markers were used. The molecular weights were finally obtained by means of Kodak dedicated software (Rochester, NY). For protein identification by liquid chromatography-tandem mass spectrometry (LC-MS/MS), the pellet nanoparticles−proteins were resuspended in urea−NH_4HCO_3 buffer. Afterward, the proteic solution was handled and enzimatically digested with trypsin as described in previous work.[18,19] The resulting peptide mixture was analyzed by LC-MS/MS, and the protein identity was assigned by employing Mascot (v2.2.04, Matrix Science) as a database search engine. Protein identity statistical validation and relative quantitative analysis were performed with Scaffold software (v. 3.1.2, Proteome Software).

3. RESULTS AND DISCUSSION

To investigate the protein corona−nanoparticle complex better, we performed a preliminary physical−chemical characterization of both DOTAP CLs and DOTAP/DNA lipoplexes. Sizing and

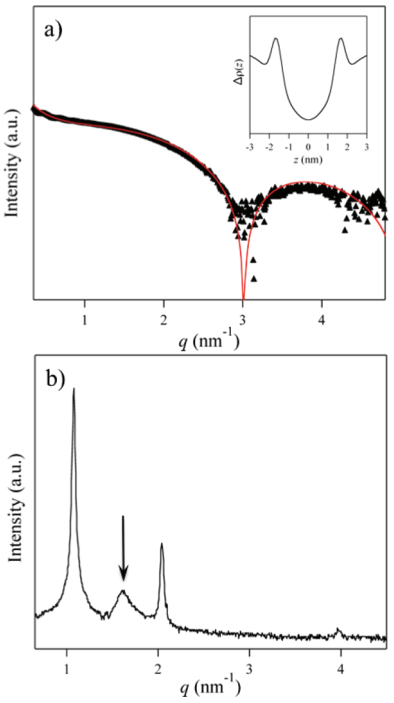

Figure 1. (a) SAXS pattern of DOTAP cationic liposomes. The pattern has been fitted using eq 1 (solid line). (Inset) Electron density profile calculated from the SAXS pattern reported in panel a. (b) SAXS pattern of DOTAP/DNA lipoplexes. Bragg peaks arise from the multilayered lipid membrane/DNA structure. The black arrow indicates the DNA peak arising from the 1D DNA−DNA in-plane correlation.

ζ-potential measurements showed that DOTAP CLs are small, positively charged vesicles (hydrodynamic radius, $R_H = 61.2 \pm 2.5$ nm; ζ potential = 55.1 ± 1.2 mV). DOTAP/DNA lipoplexes are larger with respect to neat DOTAP CLs ($R_H = 125.5 \pm 4.5$ nm). DNA addition also results in a lowering of the surface charge (ζ potential = 40.0 ± 1.1 mV).

Synchrotron SAXS was used to investigate the structure of DOTAP CLs and DOTAP/DNA lipoplexes on the nanoscale. Figure 1a shows the SAXS pattern of DOTAP CLs. The system exhibited only pure diffuse scattering, and quasi-Bragg peaks were not observed. Such a SAXS pattern is typical of uncorrelated bilayers (e.g., unilamellar vesicles). The scattering intensity was therefore fitted with a simple unilamellar vesicle model using the Gaussian-type representation of the electron density profile (EDP) as described in ref 20

$$I(q) = 2\pi \frac{\left[2\sigma_H \exp\left(-\frac{\sigma_H^2 q^2}{2}\right)\cos(qz_H) - \sigma_C \rho \exp\left(-\frac{\sigma_C^2 q^2}{2}\right)\right]^2}{q^2} \quad (1)$$

where σ_H is the half width at half-maximum of the Gaussian representing the polar region that can be assumed to be a realistic estimate of the headgroup size, z_H is the distance between the headgroup and the center of the bilayer, σ_C is the standard deviation of the Gaussian at the center of the bilayer accounting for the hydrocarbon chains, and ρ is the ratio of the methyl terminus electron density amplitude to the headgroup. In Table 1, we report the coefficient values obtained by fitting the SAXS profile of DOTAP CLs to eq 1.

dx.doi.org/10.1021/la202912f |Langmuir 2011, 27, 15048–15053

The resulting EDP was calculated as explained in ref 20 and is given in the inset of Figure 1a. The more-electron-dense regions (i.e., the two maxima in the EDP of Figure 1a) represent the headgroup regions. The fwhm of the Gaussian representing the headgroup has been assumed to be a realistic estimate of the headgroup size, $d_H = 2\sigma_H$.[20,21] According to this definition, the bilayer thickness can be determined directly from the electron density profile by $d_B = 2(z_H + \sigma_\square)$. From the EDP of Figure 1a, the bilayer thickness, $d_B = 3.68 \pm 0.2$ nm, and the extension of the headgroup region, $d_H = 0.54 \pm 0.03$ nm, were determined.[21]

The SAXS pattern of Figure 1b shows that DOTAP/DNA lipoplexes are multilamellar aggregates with a periodicity of $d = 2\pi/q_{001} = 6.00 \pm 0.01$ nm. The lamellar periodicity, d, is the sum of the bilayer thickness, d_B, and the layer occupied by fully hydrated DNA rods, d_W (≈ 2.5 nm).[14,15] As a consequence, the bilayer thickness of the lipoplexes was calculated from $d_B = d - d_W = 3.5$ nm. This value, within experimental error, is in good agreement with the thickness of pure DOTAP bilayers estimated from the EDP of Figure 1a. From the DNA peak (marked by an arrow), an interhelical spacing of $d_{DNA} = 2\pi/q_{DNA} = 4.01$ nm was calculated. This indicates that the DNA rods are densely packed within lamellar DOTAP/DNA lipoplexes. From the fwhm of the first-order lamellar Bragg peaks, a lamellar domain size of about $L_m = 2\pi/\text{fwhm} \approx 200$ nm could be estimated. Given the lamellar repeat unit of $d = 6.00$ nm, this finding suggests that DOTAP/DNA lipoplexes are multilamellar onionlike structures made of more than 30 lipid bilayer/DNA monolayer repeat units. Within experimental error, such a calculation gives a rough estimation of the ratio of the exposed area of unilamellar DOTAP CLs to that of multilamellar DOTAP/DNA lipoplexes.

Table 1. Coefficient Values Obtained by Fitting the SAXS Profile of DOTAP CLs Reported in Figure 1a with the Unilamellar Vesicle Model Based on the Gaussian-Type Representation of the Electron Density Profile (Equation 1)[20]

σ_H (nm)	0.27 ± 0.03
z_H (nm)	1.57 ± 0.08
σ_C (nm)	1.02 ± 0.05
ρ	0.80 ± 0.07

Combined sizing, ζ-potential, and SAXS results well support the accepted model of the DNA-induced restructuring of CLs upon lipoplex formation.[22] Taken together, these data confirm the recent suggestion that lipoplexes are hybrid structures with the lipid surface partially decorated by negatively charged DNA chains.[23] Such a nanostructure would have a deep impact on the adsorption of plasma proteins, which is to a large extent an electrostatically driven phenomenon.[4−9]

To focus on the evolution of the protein corona that forms around both CLs and lipoplexes upon exposure to plasma, 1D SDS/PAGE experiments were performed. Figure 2a,b shows 1D SDS/PAGE gel results in which DOTAP CLs and DOTAP/DNA lipoplexes were incubated in plasma concentrations from 2.5 to 80%. With increasing plasma concentration, the protein pattern for DOTAP CLs changes considerably (Figure 2a), whereas for lipoplexes the intensity of the protein bands seem to increase monotonously with increasing plasma concentration (Figure 2b). To provide insight into the evolution of the total protein content as a function of the plasma concentration, the total band intensities of proteins recovered from DOTAP CLs (Figure 2c) and DOTAP/DNA lipoplexes (Figure 2d) were

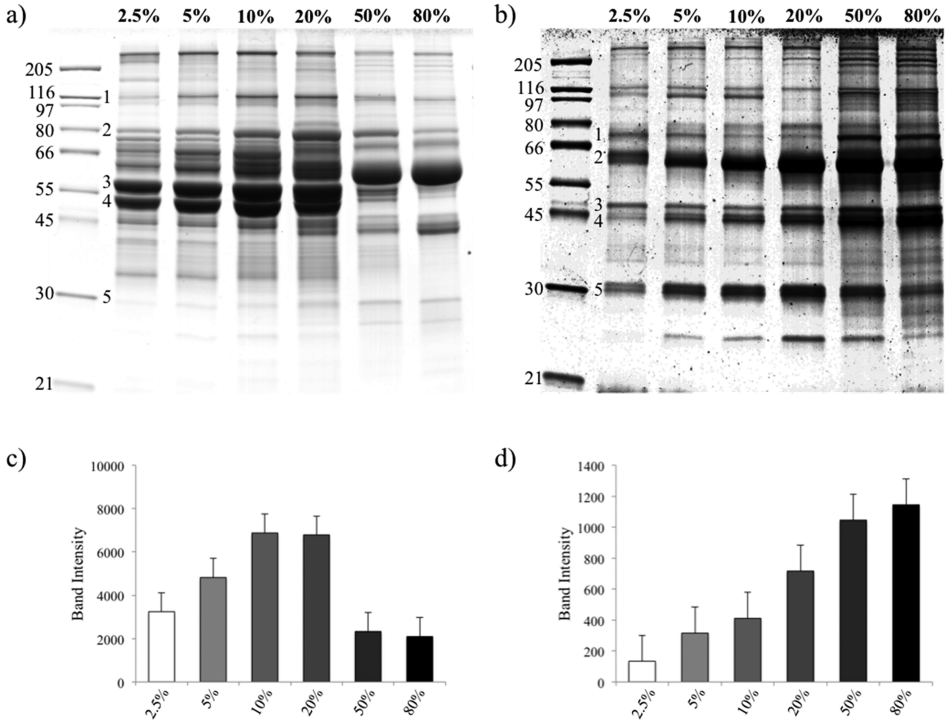

Figure 2. One-dimensional SDS-PAGE gel of human plasma proteins obtained from (a) DOTAP cationic liposome−protein complexes and (b) DOTAP/DNA lipoplex−protein complexes following incubation at different plasma concentrations. The molecular weights of the proteins on the standard ladder are reported on the left for reference. Histograms representing the total band intensity of proteins recovered from (c) DOTAP cationic liposomes and (d) DOTAP/DNA lipoplexes incubated with 2.5, 5, 10, 20, 50, and 80% plasma concentration.

dx.doi.org/10.1021/la202912f |*Langmuir* 2011, 27, 15048–15053

calculated.[9] Figure 2c shows that, for DOTAP CLs, the total amount of protein is maximized at ~20% plasma and decreases at lower and higher plasma concentrations. According to the literature,[4−9] this evolving trend may indicate that the most abundant proteins (i.e., those having been bound first) are progressively displaced by those with a higher affinity. Alternatively, this could be an effect of the aggregation of CLs.[6] In this case, we underline that the results may be different from the results reported in this article.

On the other side, the total band intensity of proteins recovered from DOTAP/DNA lipoplexes increases with increasing plasma concentration (Figure 2d). This result is most likely to suggest that more proteins of the same type bind at higher concentrations. There are many factors influencing the detailed nature of the biomolecule corona. Among them, the nanoparticle size, surface charge, and surface curvature may affect protein adsorption such that the coronas associated with nanoparticles of the same material can vary in composition.[4−9] Bearing in mind that DOTAP CLs and DOTAP/DNA lipoplexes mainly differ in the presence of DNA, we suggest that DNA molecules play a key role in the formation of the protein corona of lipoplexes even at low plasma concentration. This suggestion is supported by our results that DNA is partially located at the lipoplex surface and therefore available for protein adsorption.

We also observe that at fixed plasma concentrations the total intensity of each lane is higher for CLs than for lipoplexes. Because the signal intensity within each scan is proportional to the vesicle surface area available to plasma protein adsorption, this result indicates that the lipid membrane area of CLs that is available for binding is larger than that of lipoplexes. This finding is in agreement with the results of the physical−chemical characterization showing that the lipoplex is a multilamellar structure. Indeed, multilamellarity[3,14,15] is known to reduce the fraction of the lipid available on the outer surface of the vesicle population for the initial binding of oppositely charged macromolecules. To give further support to such a conclusion, the total intensity of each lane (i.e., at a fixed plasma concentration) from the gel reported in Figure 2b was divided by the total intensity of the corresponding lane from the gel reported in Figure 2d. The calculated ratio, R_I, is reported in Figure S1a. At the lowest plasma concentration (2.5%), R_I was found to be ~25. Such a value is in very good agreement with the ratio of the exposed surface area of the DOTAP CLs to that of the DOTAP/DNA lipoplexes. Even though the ratio of the exposed surface area of the DOTAP CLs to that of the DOTAP/DNA lipoplexes was constant in our experiments, R_I was found to decrease with increasing plasma concentration. To compare results, experimental data should be collected by keeping the ratio of the plasma concentration to the total particle surface area/mL, R_{CA}, the same.[6] Although our data were collected at different R_{CA} ratios, the two investigated regions were practically contiguous (Table S1). However, when the total intensity of each lane from gels reported in Figure 2a,b is plotted against R_{CA}, no clear trend is found (Figure S1b). As evident, the interpretation of the data reported in Figure S1a is not trivial and is complicated by the fact that (i) the exposed surface area of CLs is roughly 30-fold higher than that of lipoplexes and the effective area per protein decreases with increasing protein concentration; (ii) the particle size, which is known to affect the protein adsorption,[6] of CLs and lipoplexes is different; and (iii) the surfaces of CLs are completely lipidic whereas those of lipoplexes are partially decorated with DNA molecules. All of these observations suggest that, upon interaction with plasma proteins, the compositions of the coronas of CLs and lipoplexes can change in different ways from each other. As a result, a quantitative comparison between the coronas of CLs and lipoplexes is much less obvious than one would expect.

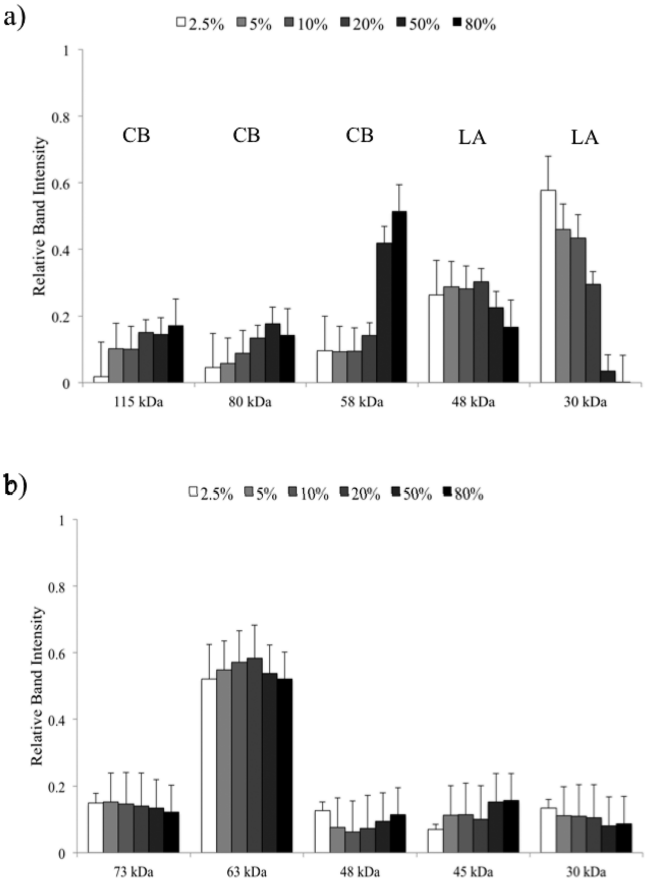

Figure 3. Relative amounts of the most abundant proteins (marked by numbers in Figure 2) adsorbed in the hard corona complexes of (a) DOTAP cationic liposomes and (b) DOTAP/DNA lipoplexes from plasma solutions at different concentrations (legend) after 1 h of incubation. The results are extracted as the relative intensities from the gels shown in Figure 2a,b, respectively. Proteins whose relative amounts in the corona decrease with increasing plasma concentration are labeled as low-affinity (LA) proteins, and those whose relative amounts in the corona increase are labeled as competitive-binding (CB) proteins.

To investigate the evolution of the protein corona of both CLs and lipoplexes better, a semiquantitative densitometry analysis was performed. In Figure 3a,b, we show the relative densitometry results (the intensity of each protein band is divided by the total intensity of the lane)[9] of five major bands from the gels in Figure 2a,b as a function of the plasma concentration during incubation. Within the limits of gel separation methodologies, this provides a semiquantitative description of the variations in the band intensities that are visible in Figure 2. In Figure 3a, we could distinguish both low-affinity (LA) proteins, whose relative amount in the corona decrease, and competitive-binding (CB) proteins, whose relative amount in the corona increases with increasing plasma concentration. Aside from clarifying the exact mechanism of protein corona formation, it is clear that the corona composition of DOTAP CLs is not stable, with its composition

probably being affected by a cooperative phenomenon.[9] However, for DOTAP/DNA lipoplexes, the relative intensities of all bands did not change appreciably. This result indicates that the protein corona of lipoplexes increases from 2.5 to 80% plasma whereas its protein composition remained largely unchanged.

The compositional evolution of the coronas of CLs and lipoplexes can be compared by calculating an average of standard deviations for the relative band intensities reported in Figure 3a, b. Each population consists of the five relative intensities at fixed MW. To this end, we first calculated the standard deviation of each intensity population, defined as

$$\sigma = \sqrt{\frac{\sum_{i=1}^{N} (x_i - \bar{x})^2}{N-1}} \qquad (2)$$

where x_i is the ith band intensity of a given intensity population, $\bar{x}$ is the average of an intensity population, and N is the number of elements in the population. Standard deviations calculated for DOTAP CLs were much larger than those obtained from the intensity populations of DOTAP/DNA lipoplexes (Figure S1). The average of the standard deviations calculated for DOTAP CLs ($\langle\sigma\rangle$ = 0.11) was about 5-fold higher than its counterpart calculated for DOTAP/DNA lipoplexes ($\langle\sigma\rangle$ = 0.02).

The identities of the proteins were last determined by mass spectrometry analysis of selected bands cut from the gels reported in Figure 2a,b. Identified proteins are reported in Table S1. Even though an accurate protein quantification is beyond the scope of the present study and is currently in progress, some systematic effects were detected. The most abundant plasma proteins such albumin, fibrinogen (alpha, beta, and gamma chains), complement C5, apolipoprotein A-I, transferrin, vitronectin, and fibronectin were identifed on both coronas. On the other side, the corona of DOTAP/DNA lipoplexes was found to be richer in immunoglobulins (Ig) than was that of DOTAP CLs. In particular, a large number of Ig gamma proteins (Ig-Gs) were identified by their mass. Ig-Gs are involved in many processes (e.g., immunity responses). In particular, it has been reported that Ig-Gs can promote the phagocytosis of DNA-loaded nanovectors by macrophages and other phagocytic cells such as hepatic Kupffer cells. This is consistent with several observations that lipoplexes primarily accumulate in the liver following intravenous administration.[24−26] Because Ig-Gs are mainly basic proteins (i.e., with pK >7), proteomics results suggest that the surface charge of lipoplexes may locally deviate from being positively charged. This suggestion is supported by sizing, ζ-potential, and SAXS results showing that a fraction of DNA is adsorbed at the lipoplex membrane and can interact electrostatically with cationic molecules. Another class of plasma proteins exclusively found in the lipoplex corona was histones. Histones are alkaline proteins found in eukaryotic cell nuclei that package and order the DNA into structural units called nucleosomes. In particular, histones H1.4, H3.1, H4, and H2B type 1-K were identified (Table S2). Histone H1 is one of the most abundant proteins in the nucleus of eukaryotic cells. It has long been known as the linker histone because it links the chromatosomal DNA that goes between the nucleosomes. Histone H2B type 1-K is one of the proteins involved in the structure of chromatin in eukaryotic cells. Finding such proteins in the lipoplex corona may confirm our suggestion that some plasma proteins can specifically recognize the DNA molecule at the lipoplex surface. The proteins normally found inside the nucleus should not be found in a significant amount in plasma. Thus, we cannot exclude the possibility that the commercial calf thymus DNA was contamined by histones.

The biochemical rationale for protein corona formation is still unclear. Recent studies[27−29] have shown that the nanoparticle protein corona can evolve over time. This temporal evolution might cause consequences at the level of liposomes to target cell interaction and needs further investigation to predict the actual biological identity of the protein−LNP complex as far as the protein layer is built up.

4. CONCLUSIONS

It is now clearly emerging that the primary defining element of nanoparticles in biological media is their protein corona that dictates the biodistribution and final fate in vivo, which is the entity actually seen by target cells both in vitro and in vivo. We have combined studies on the composition of the protein corona at different plasma concentrations (mimicking in vitro and in vivo conditions) with structural data on the complexes. We have shown that the protein corona of CLs is made of both low-affinity and competitive-binding proteins whose relative abundance changes with the plasma concentration. Such effects may be so striking that the biological identity of lipid gene vectors with DNA cargo confined in the interior space (e.g., LNP) may change dramatically as the amount of protein in the environment changes. In particular, nanoparticle−protein complexes in vitro (at low serum dilutions) may poorly correlate with those that exist in vivo. On the other side, passing from low to high plasma concentrations, the protein corona of lipoplexes changes in abundance but not in composition. By correlating such evolution trends with the distinctive physical−chemical properties of lipoplexes, we conclude that the evolution of the protein corona passing from in vitro to in vivo conditions is severely affected by the presence of DNA. This aspect should be carefully considered for the rational design of lipid gene vectors.

■ ASSOCIATED CONTENT

Supporting Information. Ratio of the total band intensity of each lane from the gel reported in Figure 2b,f to the corresponding lane from the gel reported in Figure 2d as a function of the plasma concentration. Total band intensity of each lane from gels reported in Figure 2a,b against the ratio of the plasma concentration to the total particle surface area/mL. Standard deviations for the relative band intensities reported in Figure 3a,b of DOTAP CLs and DOTAP/DNA lipoplexes. Ratio of the plasma concentration to the total particle surface area/mL of the dispersion. Proteins identified on nanoparticle surfaces determined by mass spectrometry analysis of selected bands cut from the gels reported in Figure 2a,b. This material is available free of charge via the Internet at http://pubs.acs.org.

■ AUTHOR INFORMATION

Corresponding Author

*E:mail: giulio.caracciolo@uniroma1.it.

■ REFERENCES

(1) Felgner, P. L.; Ringold, G. M. Cationic liposome-mediated transfection. *Nature* **1989**, *337*, 387–388.

(2) Ramezani, M.; Khoshhamdam, M.; Dehshari, A.; Malaekeh-Nikouei, B. The influence of size, lipid composition and bilayer fluidity of cationic liposomes on the transfection efficiency of nanolipoplexes. *Colloids Surf., B* **2009**, *72*, 1–5.

(3) Pozzi, D.; Caracciolo, G.; Caminiti, R.; Candeloro De Sanctis, S.; Amenitsch, H.; Marchini, C.; Montani, M.; Amici, A. Toward the rational design of lipid gene vectors: shape coupling between lipoplex and anionic cellular lipids controls the phase evolution of lipoplexes and the efficiency of DNA release. *ACS Appl. Mater. Interfaces* **2009**, *10*, 2237–2249.

(4) Cedervall, T.; Lynch, I.; Lindman, S.; Berggård, T.; Thulin, E.; Nilsson, H.; Dawson, K. A.; Linse, S. Understanding the nanoparticle–protein corona using methods to quantify exchange rates and affinities of proteins for nanoparticles. *Proc. Natl. Acad. Sci. U.S.A.* **2007**, *104*, 2050–2055.

(5) Cedervall, T.; Lynch, I.; Foy, M.; Berggård, T.; Donnelly, S. C.; Cagney, G.; Linse, S.; Dawson, K. A. Detailed identification of plasma proteins adsorbed on copolymer nanoparticles. *Angew. Chem., Int. Ed.* **2007**, *46*, 5754–5756.

(6) Lundqvist, M.; Stigler, J.; Elia, G.; Lynch, I.; Cedervall, T.; Dawson, K. A. Nanoparticle size and surface properties determine the protein corona with possible implications for biological impacts. *Proc. Natl. Acad. Sci. U.S.A.* **2008**, *105*, 14265–14270.

(7) Lynch, I.; Salvati, A.; Dawson, K. A. Protein-nanoparticle interactions: what does the cell see? *Nat Nanotechnol.* **2009**, *4*, 546–547.

(8) Walczyk, D.; Baldelli Bombelli, F.; Monopoli, M. P.; Lynch, I.; Dawson, K. A. What the cell "sees" in bionanoscience. *J. Am. Chem. Soc.* **2010**, *132*, 5761–5768.

(9) Monopoli, M. P.; Walczyk, D.; Campbell, A.; Elia, G.; Lynch, I.; Baldelli Bombelli, F.; Dawson, K. A. Physical–chemical aspects of protein corona: relevance to in vitro and in vivo biological impacts of nanoparticles. *J. Am. Chem. Soc.* **2010**, *133*, 2525–2534.

(10) Caracciolo, G.; Pozzi, D.; Capriotti, A. L.; Marianecci, C.; Carafa, M.; Marchini, C.; Montani, M.; Amici, A.; Amenitsch, H.; Digman, M. A.; Gratton, E.; Sanchez, S. S.; Laganà, A. Factors determining the superior performance of lipid/DNA/protammine nanoparticles over lipoplexes. *J. Med. Chem.* **2011**, *54*, 4160–4171.

(11) Kogure, K.; Moriguchi, R.; Sasaki, K.; Ueno, M.; Futaki, S.; Harashima, H. Development of efficient packaging method of oligodeoxynucleotides by a condensed nano particle in lipid envelope structure. *J. Controlled Release* **2004**, *98*, 317–323.

(12) Li, S. D.; Huang, L. Surface-modified LPD nanoparticles for tumor targeting. *Ann. N.Y. Acad. Sci.* **2006**, *1082*, 1–8.

(13) Chen, Y.; Sen, J.; Bathula, S. R.; Yang, Q.; Fittipaldi, R.; Huang, L. Novel cationic lipid that delivers siRNA and enhances therapeutic effect in lung cancer cells. *Mol. Pharmaceutics* **2009**, *6*, 696–705.

(14) Marchini, C.; Pozzi, D.; Montani, M.; Alfonsi, C.; Amici, A.; Amenitsch, H.; Candeloro De Sanctis, S.; Caracciolo, G. Tailoring lipoplex composition to the lipid composition of plasma membrane: a Trojan horse for cell entry? *Langmuir* **2010**, *26*, 13867–13873

(15) Caracciolo, G.; Marchini, C.; Pozzi, D.; Caminiti, R.; Amenitsch, H.; Montani, M.; Amici, A. Structural stability against disintegration by anionic lipids rationalizes the efficency of cationic liposom/DNA complexes. *Langmuir* **2007**, *23*, 4498–4508.

(16) Amenitsch, H.; Rappolt, M.; Kriechbaum, M.; Mio, H.; Laggner, P.; Bernstorff, S. First performance assessment of the small-angle X-ray scattering beamline at ELETTRA. *J. Synchrotron Radiat.* **1998**, *5*, 506–508.

(17) Caracciolo, G.; Callipo, L.; Candeloro De Sanctis, S.; Cavaliere, C.; Pozzi, D.; Laganà, A. Surface adsorption of protein corona controls the cell internalization mechanism of DC-Chol–DOPE/DNA lipoplexes in serum. *Biochim. Biophys. Acta* **2010**, *1798*, 536–543.

(18) Capriotti, A. L.; Caracciolo, G.; Cavaliere, C.; Crescenzi, C.; Pozzi, D.; Laganà, A. Shotgun proteomics analytical approach for studying proteins adsorbed onto liposome surface. *Anal. Bioanal. Chem.* **2011**, *401*, 1195–1202.

(19) Capriotti, A. L.; Caracciolo, G.; Caruso, G.; Cavaliere, C.; Pozzi, D.; Samperi, R.; Laganà, A. Analysis of plasma protein adsorption onto DC-Chol-DOPE cationic liposomes by HPLC-CHIP coupled to a Q-TOF mass spectrometer. *Anal. Bioanal. Chem.* **2010**, *398*, 2895–2903.

(20) Pabst, G.; Rappolt, M.; Amenitsch, H.; Laggner, P. Structural information from multilamellar liposomes at full hydration: full *q*-range fitting with high quality x-ray data. *Phys. Rev. E* **2000**, *62*, 4000–4009.

(21) Caracciolo, G.; Pozzi, D.; Amenitsch, H.; Caminiti, R. One-dimensional thermotropic dilatation area of lipid headgroups within lamellar lipid/DNA complexes. *Langmuir* **2006**, *22*, 4267–4273.

(22) Caracciolo, G.; Pozzi, D.; Amenitsch, H.; Caminiti, R. Multicomponent cationic lipid–DNA complex formation: role of lipid mixing. *Langmuir* **2005**, *21*, 11582–11587.

(23) Amenitsch, H.; Caracciolo, G.; Foglia, P.; Fuscoletti, V.; Giansanti, P; Marianecci, C.; Pozzi, D.; Laganà, A. Existence of hybrid structures in cationic liposome/DNA complexes revealed by their interaction with plasma proteins. *Colloids Surf., B* **2011**, *82*, 141–146.

(24) Litzinger, D. C.; Brown, J. M.; Wala, I.; Kaufman, S. A.; Van, G. Y.; Farrell, C. L.; Collins, D. Fate of cationic liposomes and their complex with oligonucleotide in vivo. *Biochim. Biophys. Acta* **1996**, *1281*, 139–149.

(25) de Wolf, H. K.; Snel, C. J.; Verbaan, F. J.; Schiffelers, R. M.; Hennink, W. E.; Storm, G. Effect of cationic carriers on the pharmacokinetics and tumor localization of nucleic acids after intravenous administration. *Int. J. Pharm.* **2007**, *331*, 167–175.

(26) Khoury, M.; Louis-Plence, P.; Escriou, V.; Noel, D.; Largeau, C.; Cantos, C.; Scherman, D.; Jorgensen, C.; Apparailly, F. Efficient new cationic liposome formulation for systemic delivery of small interfering RNA silencing tumor necrosis factor alpha in experimental arthritis. *Arthritis Rheum.* **2006**, *54*, 1867–1877.

(27) Maiorano, G.; Sabella, S.; Sorce, B.; Brunetti, V.; Malvindi, M. A.; Cingolani, R.; Pompa, P. P. Effects of cell culture media on the dynamic formation of protein–nanoparticle complexes and influence on the cellular response. *ACS Nano* **2010**, *4*, 7481–7491.

(28) Dell'Orco, D.; Lundqvist, M.; Oslakovic, C.; Cedervall, T.; Linse, S. Modeling the time evolution of the nanoparticle-protein corona in a body fluid. *PLoS One* **2010**, *5*, e10949.

(29) Casals, E.; Pfaller, T.; Duschl, A.; Oostingh, G. J.; Puntes, V. Time evolution of the nanoparticle protein corona. *ACS Nano* **2010**, *4*, 3623–3632.

V

Journal of Medicinal Chemistry

ARTICLE

pubs.acs.org/jmc

Factors Determining the Superior Performance of Lipid/DNA/Protammine Nanoparticles over Lipoplexes

Giulio Caracciolo,[*,†] Daniela Pozzi,[†] Anna Laura Capriotti,[‡] Carlotta Marianecci,[§] Maria Carafa,[§] Cristina Marchini,[∥] Maura Montani,[∥] Augusto Amici,[∥] Heinz Amenitsch,[⊥] Michelle A. Digman,[#] Enrico Gratton,[#] Susana S. Sanchez,[#,∞] and Aldo Laganà[‡]

[†]Department of Molecular Medicine, "Sapienza" University of Rome, Viale Regina Elena, 324, 00161, Rome, Italy

[‡]Department of Chemistry, "Sapienza" University of Rome, P.le A. Moro 5, 00185 Rome, Italy

[§]Department of Drug Chemistry and Technologies, Faculty of Pharmacy, "Sapienza" University of Rome, P.le A. Moro 5, 00185 Rome, Italy

[∥]Department of Bioscience and Biotechnology, University of Camerino, Via Gentile III da Varano, 62032 Camerino (MC), Italy

[⊥]Institute of Biophysics and Nanosystems Research, Austrian Academy of Sciences, Schmiedelstrasse 6, A-8042 Graz, Austria

[#]Laboratory for Fluorescence Dynamics, Department of Biomedical Engineering, University of California, Irvine, 3120 Natural Sciences 2, Irvine, California 92697-2715, United States

[∞]Microscopy and Dynamic Imaging Unit, Centro Nacional de Investigaciones Cardiovasculares, Fundación CNIC-Carlos III, Madrid, Spain

Supporting Information

ABSTRACT: The utility of using a protammine/DNA complex coated with a lipid envelope made of cationic 1,2-dioleoyl-3-trimethylammonium propane (DOTAP) for transfecting CHO (Chinese hamster ovary cells), HEK293 (human embryonic kidney cells), NIH 3T3 (mouse embryonal cells), and A17 (murine cancer cells) cells was examined. The widely used DOTAP/DNA lipoplex was employed as a reference. In all the tested cell lines lipid/protamine/DNA (LPD) nanoparticles were more efficient in transfecting cells than lipoplexes even though the lipid composition of the lipid envelope was the same in both devices. Physical−chemical properties were found to control the ability of nanocarriers to release DNA upon interaction with cellular membranes. LPD complexes easily release their DNA payload, while lipoplexes remain largely intact and accumulate at the cell nucleus. Collectively, these data explain why LPD nanoparticles often exhibit superior performances compared to lipoplexes in trasfecting cells and represent a promising class of nanocarriers for gene delivery.

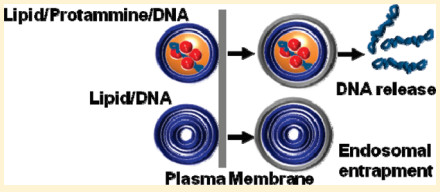

Gene therapy research is still problematic owing to a paucity of acceptable vector systems to deliver nucleic acids to patients for therapy.[1−3] Viral vectors are efficient but may be dangerous for routine clinical use. Synthetic nonviral vectors are fundamentally safer but are currently not efficient enough to be clinically viable. A possible solution for gene therapy lies with improved synthetic nonviral vectors based upon well-established platform technologies and a thorough understanding of the barriers to efficient gene delivery and expression (transfection) relevant to clinical applications of interest. One of the most common nonviral gene delivery vectors are DNA−cationic lipid complexes (lipoplexes). On the basis of freeze−fracture electron micrographs and X-ray diffraction studies, it was suggested that lipoplexes are multilamellar onion-like systems with DNA sandwiched between opposing lipid bilayers.[4−8] Once inside the cell, such multilamellar structure offers protection from DNA degradation but do not often allow for an adequate DNA release from endosomal compartments. If gene payload is not released from endosomes, it is shuttled to the lysosomes, where it is degraded by the abundant nucleases and transfection may fail.[9−11] To overcome this problem, lipid/DNA/polycation (LDP) complexes, in which plasmid DNA (pDNA) condensed with a polycation is encapsulated by a lipid envelope, have recently been developed.[12] Kogure et al.[12] demonstrated that the luciferase activity of a DNA−poly-L-lysine complex (DPC) with a lipid envelope was 10 times higher than only DPC in NIH 3T3 cells, suggesting that the lipid coating is important and critical for efficient gene delivery. Recent studies showed superiority of LPD-mediated gene transfer over conventional liposomes for delivering a gene to the liver.[13] Over the past few years several efforts to improve the delivery efficiency of LPD systems have been made.[14−18] The composition of the lipid envelope of LPD systems has been modified with novel chemical compounds, while the surface has been functionalized with several polymers and ligands. In a recent study a new lysine based cationic lipid containing a guanidine group that serves simultaneously as a delivery component and a therapeutic agent was reported.[16] Such

Received: March 1, 2011
Published: May 13, 2011

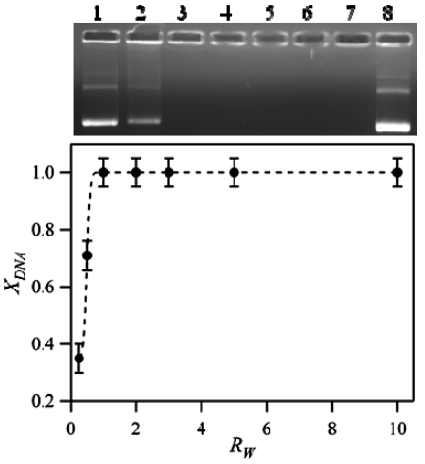

Figure 1. (Top) Digital photograph of protammine/DNA complexes (P/DNA) with increasing P/DNA weight ratio R_W: R_W = 0.1 (lane 1), R_W = 0.5 (lane 2), R_W = 1 (lane 3), R_W = 2 (lane 4), R_W = 3 (lane 5), R_W = 5 (lane 6), R_W = 10 (lane 7), and control DNA (lane 8). Experiments revealed two major bands for naked DNA (lane 8). The high-mobility band was attributed to the most compact (supercoiled) form, and the less-intense one was considered to be the non-super-coil content in the plasmid preparation. (Bottom) Molar fraction of plasmid DNA protected by protamine, X_{DNA}, against the P/DNA weight ratio, R_W.

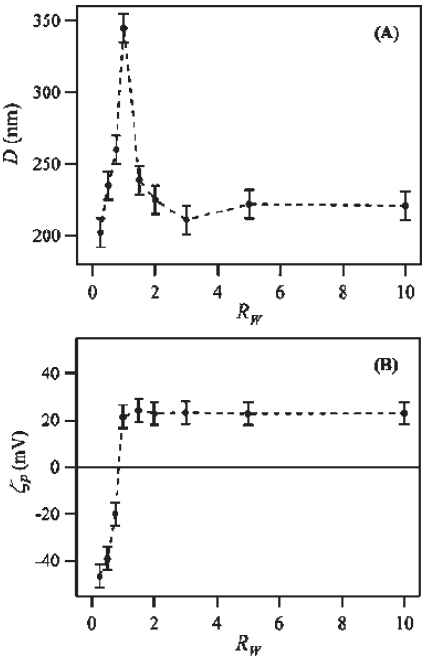

Figure 2. (A) Diameter of P/DNA complexes, D_H, as a function of the P/DNA weight ratio, R_W. This behavior is typical of the reentrant condensation effect. (B) ζ-Potential of P/DNA complexes as a function of R_W. The charge inversion effect occurring for 0.5< R_W <1 changes the overall charge of the aggregates from negative (DNA excess) to positive (protamine excess).

novel formulation resulted in enhanced cellular uptake, gene silencing, and tumor growth inhibition. Systemic tumor-targeted delivery remains the most challenging issue in the drug delivery field. In vivo data of tissue distribution demonstrated the potential of surface-modified LPD nanoparticles for tumor targeting.[15] Whether the superior performance of LPD systems over the consolidated lipoplex strategy does correlate with distinct physical−chemical properties of LPD complexes is an open question that needs to be answered. Generally, lipoplex dispersions are heterogeneous and polydisperse, consisting of a variety of structures in dynamic equilibrium. Recently, the existence of hybrid structures made of multilamellar lipoplexes stuck together by DNA has been reported.[19] Because physical−chemical properties of gene vectors may determine their interaction with cells and tissues, a precise knowledge of these properties may be important for predicting their biological response both in vitro and in vivo. Comparative studies of pDNA-encapsulation type and lipoplex type gene vectors would therefore provide useful information to decipher the relationship between the physical−chemical properties of gene vectors and their mechanisms of interaction with the cell's components. This knowledge is expected to drive the rational design of highly efficient gene delivery systems.

In the present study, we show that the transfection efficiency (TE) of protammine/DNA complexes coated with a lipid envelope made of cationic 1,2-dioleoyl-3-trimethylammonium propane (DOTAP) is from 3 to 20 times higher than that of DOTAP/DNA lipoplexes. We asked whether such remarkable difference in TE did correlate with particulate features of complexes. To answer this question, we investigated complex formation, DNA protection ability, surface properties, nanostructure, ability to release DNA upon interaction with cellular lipids, and intracellular trafficking. We present findings showing that the superior efficiency of LPD complexes over lipoplexes does correlate with their distinctive physical−chemical properties.

RESULTS

Complex Formation. Gel retardation assay was carried out to evaluate the condensing ability of P/DNA, LPD complexes, and lipoplexes.[20−24] The complete retardation of the binary P/DNA complex can be observed when the P/DNA weight ratio, R_W, was above 0.5 (Figure 1, top part). Starting from R_W = 0.75, the molar fraction of plasmid DNA completely protected by protamine, X_{DNA} (Figure 1, bottom part), was maximum (i.e., X_{DNA} = 1). P/DNAcomplex formation was investigated by measuring the average hydrodynamic radius, R_D, and the electrophoretic mobility of the diffusing complexes in the solution. The combined use of these two techniques allowed us to study both of the two typical phenomena occurring in these systems, namely, the reentrant condensation and the charge inversion effect.[25,26] In Figure 2 the average dimensions and the ζ-potential of P/DNA particles are plotted against R_W. As can be seen, with the increase in R_W, complex formation begins and the diameter of complexes, D_H, gradually increases until a maximum is reached at $R_W \approx 1$. Our results are in good agreement with previous studies showing that P/DNA particles show a neutral charge at R_W = 0.9.[27] Further increase in the P content determines the formation of decreasing-size complexes until the size of the original P/DNA core is approximately reached again (reentrant condensation). Aggregates also undergo the charge inversion effect, documented by the ζ-potential values whose sign changes for 0.5 < R_W <1, differentiating negatively and positively charged aggregates. On the basis of these results, P/DNA complex at R_W = 0.75 was therefore chosen because it guaranteed complete DNA protection, exhibited negative charge (−20 mV), and had appropriate dimensions (260 nm) with the minimum P content. Then the preassembled negatively charged P/DNA core was coated with a

dx.doi.org/10.1021/jm200237p | J. Med. Chem. 2011, 54, 4160–4171

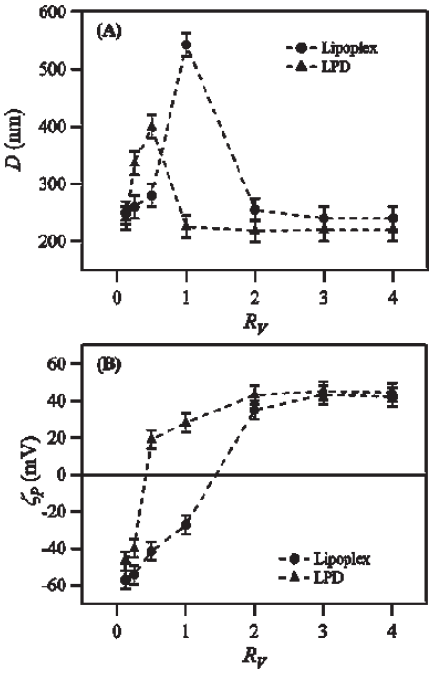

Figure 3. (A) Diameter of LPD complexes (triangles) and lipoplexes (circles) as a function of the lipid/DNA volume ratio, R_V. (B) ζ-Potential of LPD complexes (triangles) and lipoplexes (circles) as a function of R_V.

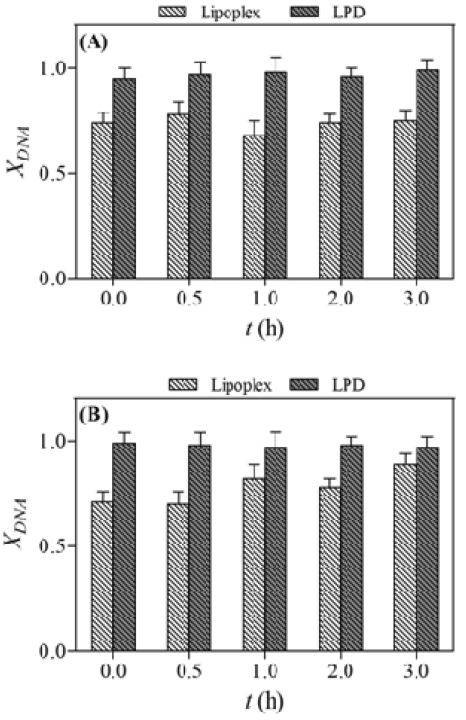

Figure 4. Molar fraction of DNA protected, X_{DNA}, by LPD nanoparticles and lipoplexes over incubation with buffer (A) and serum (B).

lipid envelope through membrane fusion of positively charged DOTAP small unilamellar vesicles (SUVs) (55 mV, R_H = 61.2 nm), triggered by the electrostatic attraction around the negatively charged core. The main results are summarized in Figure 3 where we show the diameter D_H (part A, triangles) and the ζ-potential ζ_p (part B, triangles) of DOTAP/P−DNA LPD complexes as a function of the lipid/DNA volume ratio, R_V. As can be seen, with the increase of R_V, complexation begins and the size of the complexes gradually increases until a maximum is reached ($D_H \approx 500$ nm at $R_V = 0.5$). Increasing the lipid content ($R_V > 0.5$) results in the formation of decreasing-size complexes. Aggregates also undergo the charge inversion effect, recognizable by the ζ-potential values (Figure 3b, triangles) whose sign changes around $R_V = 0.5$, differentiating negatively and positively charged aggregates. This trend shows three different ζ potential regions: (i) the region where the net charge of LPD complexes is negative and almost constant at (−31 mV); (ii) the region where the inversion of ζ potential sign takes place (around $R_V = 0.5$); and (iii) the region where the net charge of the LPD complexes is positive (47.8 mV). We observe that condensed P/DNA core (260 nm) is larger in size than the final LPD complex (~220 nm). This finding suggests that the P/DNA core is partly disassembled upon DNA−lipid interaction. Upon disassembling, some free DNA may give rise to a minor fraction of lipoplexes, if any, in the final dispersion. Even though the polydispersity index was low (pdi <0.25), this possibility cannot be excluded. In Figure 3 D_H (part A, circles) and ζ_p, (part B, circles) of DOTAP/DNA lipoplexes plotted against R_V are also reported. As evident, both the re-entrant condensation and the charge inversion effect occurred, but at R_V values larger than those observed in the case of LPD complexes. Dynamic investigation of size and ζ potential showed that both LPD nanoparticles and lipoplexes were fairly stable over 24 h (Supporting Information). The LPD complex at $R_V = 2$ was finally chosen because it exhibited positive charge (47.8 mV) as well as the lowest colloidal dimensions (220 nm) and the lowest polydispersity index (pdi = 0.22).

DNA condensation was also investigated by UV−vis absorption measurements by which the binding constants for both LPD complexes and lipoplexes were estimated ($K_{LPD} = (2.1 \pm 0.5) \times 10^4\ M^{-1}$ and $K_{Lipoplex} = (1.3 \pm 0.3) \times 10^4\ M^{-1}$; details are given in the Supporting Information). A slightly stronger lipid/DNA interaction for LPD systems was observed. Since the stability of lipid−DNA complexes is related to charge neutralization, our findings are most likely to indicate that protammine contributes to a better DNA charge neutralization.[28]

DNA Protection Ability. The DNA protection ability of both LPD nanoparticles and lipoplexes was investigated by electrophoresis on agarose gel. In Figure 4A we report the molar fraction of DNA protected by either lipoplexes and LPD nanoparticles, X_{DNA}, over the incubation period with cells. The starting point ($t = 0$) refers to the time when lipid vectors are usually given to cells, i.e., about 20 min of incubation after lipid−DNA mixing. At $t = 0$, the protection ability of LPD is almost complete while some free DNA is present in the lipoplex formulation ($X_{DNA} \approx 0.25$). Such values of protection remained the same over 3 h of incubation. The presence of serum in the transfection media has been found to be inhibitory to gene transfer.[29] This inhibition has been mainly attributed to serum−lipid membrane interaction resulting in destabilization of the lipid structure. Such structural degradation is often accompanied by lipid−DNA dissociation and release leading to a decrease in the DNA protection ability of complexes. We therefore investigated the protection ability of both LPD nanoparticles and lipoplexes in serum. As can be seen in Figure 4B, no relevant changes in the molar fraction of protected DNA, X_{DNA}, occurred. This indicates that the DNA-protection capacity of complexes was not modified by serum.

dx.doi.org/10.1021/jm200237p | J. Med. Chem. 2011, 54, 4160–4171

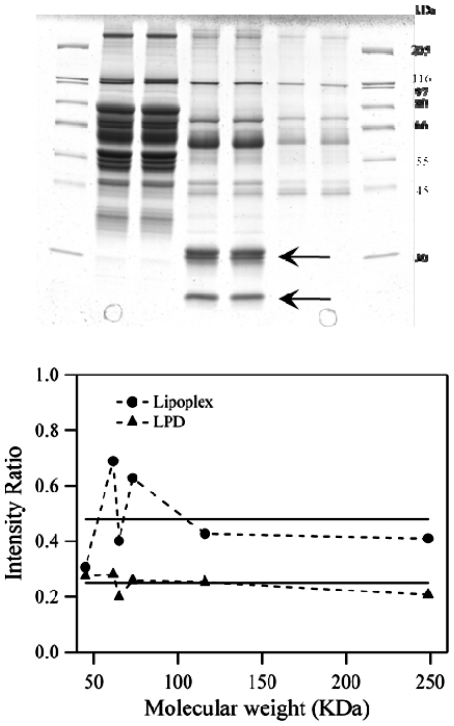

Figure 5. (Top) Photograph of an SDS−PAGE (12% gel) of human plasma proteins retrieved from DOTAP CLs (lanes 1 and 2), LPD complexes (lanes 3 and 4), and lipoplexes (lanes 5 and 6). Lane 7 is a protein molecular weight marker. The black arrows indicate the bands of human plasma proteins that were found to be much more abundantly associated with lipoplexes than with cationic liposomes. (Bottom) Intensity of protein band identified in the patterns of both lipid nanoparticles, I_{LPD}, and lipoplexes, $I_{Lipoplex}$, compared to the that of corresponding band identified in the patterns of DOTAP CLs, I_{DOTAP}. Intensity ratios (I_{LPD}/I_{DOTAP}, triangles) and ($I_{Lipoplex}/I_{DOTAP}$, circles) are plotted against the molecular weight of several protein bands, M_W. In the case of LPD complexes approximately uniform intensity ratios were observed, whereas intensity ratios of lipoplexes exhibited a random variation.

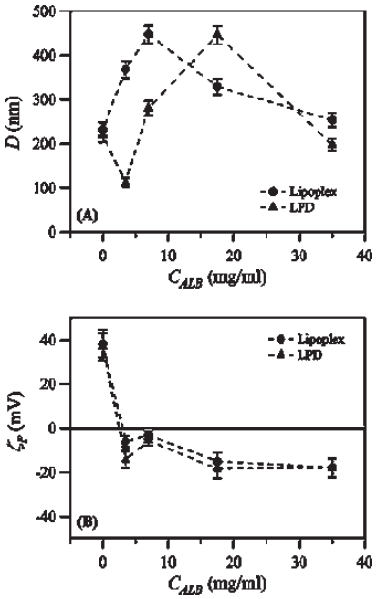

Figure 6. (A) Diameter of LPD complexes (triangles) and lipoplexes (circles) as a function of albumin concentration, C_{ALB}. (B) ζ-Potential of LPD complexes (triangles) and lipoplexes (circles) as a function of albumin concentration, C_{ALB}.

Surface Properties. Recent pioneering studies[30−34] have reported on the existence of a rich protein layer associated with the surface of nanoparticles after treatment with biological fluids (e.g., human plasma, HP). Here we perform proteomics experiments to investigate the "protein corona" associated with the surface of DOTAP cationic liposomes (CLs), LPD complexes, and lipoplexes after interaction with HP. Figure 5 (top part) shows one-dimensional sodium dodecyl sulfate−polyacrylamide gel electrophoresis (1D SDS−PAGE) (12% gels) of plasma proteins retrieved from DOTAP CLs (lanes 1 and 2), DOTAP/DNA lipoplexes (R_V = 2) (lanes 3 and 4), and LPD complexes (R_V =2) (lanes 5 and 6). As Figure 5 shows, 1D SDS−PAGE experiments were highly reproducible. Even though an accurate protein analysis is beyond the scope of the present study and will be given in detail elsewhere, some systematic effects were detected. We observe that the intensities of almost all protein bands of CLs (lanes 1 and 2) were higher than those of both lipoplexes (lanes 3 and 4) and lipid nanoparticles (lanes 5 and 6). Since the signal intensity within each scan is proportional to the vesicle surface available to plasma protein adsorption, this result indicates that the lipid membrane area of CLs that is available for binding is larger than that of lipoplexes and lipid nanoparticles. To find a surface similarity between the different surfaces, the intensity of each protein band identified in the patterns of both lipid nanoparticles, I_{LPD}, and lipoplexes, $I_{Lipoplex}$, was compared to that of the corresponding band identified in the patterns of DOTAP CLs, I_{DOTAP}. A comparative intensity analysis is reported in Figure 5 (bottom part) where the intensity ratios (I_{LPD}/I_{DOTAP}) and ($I_{Lipoplex}/I_{DOTAP}$) are plotted against the molecular weight of several protein bands, M_W. In the case of LPD complexes a series of approximately uniform intensity ratios was observed (Figure 5, bottom part, triangles). On the other hand, intensity ratios of lipoplexes (Figure 5, bottom part, circles) exhibited a random variation. This finding is most likely to suggest that the surface of LPD complexes has a high degree of similarity with that of pure DOTAP CLs, while that of lipoplexes has not. Furthermore, a protein band observed in the protein pattern of lipoplexes (indicated by black arrow in Figure 5, top part) was not detected in the pattern of CLs or in that of LPD nanoparticles. This high-intensity band was centered around 23 kDa. In this band a large number of Ig-Gs were identified by their mass (proteomics data not reported). Ig-Gs are basic proteins involved in many processes such as immunity response.[33] This finding indicates that the surface charge of lipoplexes differs, at least locally, from being positive. The latter observation is most likely to suggest that negatively charged DNA is adsorbed at the lipoplex surface and can interact with basic plasma proteins. In summary, our findings suggest that (i) the surface area of LPD complexes available to protein adsorption resembles that of DOTAP CLs (i.e., it is mainly lipidic) but it is smaller than that of pure DOTAP SUVs; (ii) the surface of lipoplexes is partly decorated with DNA molecules, while that of LPD is not.

We therefore asked ourselves whether the observed differences in the surface properties of lipoplexes and LPD nanoparticles may also affect their size and ζ-potential upon interaction with plasma proteins. To model the interaction of complexes with plasma proteins, albumin from bovine serum

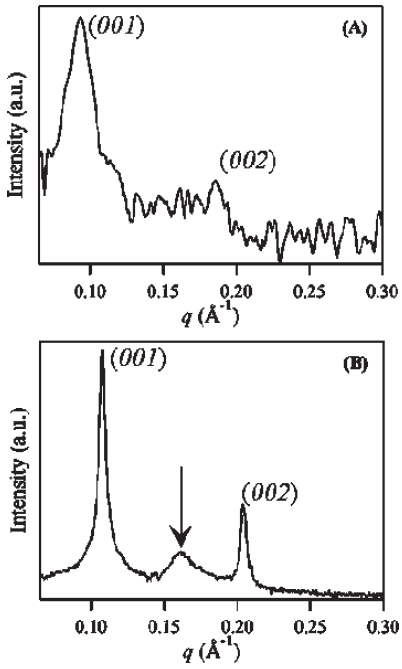

Figure 7. (A) Synchrotron SAXS pattern of LPD complexes at a lipid/DNA volume ratio, $R_V = 2$. Two broad Bragg peaks, corresponding to a periodicity $d = 2\pi/q_{001} = 7.10$ nm, were detected and larger than those commonly observed in most DOTAP/DNA complexes (typically 5.5−6.2 nm). (B) Synchrotron SAXS pattern of DOTAP/DNA lipoplexes ($R_V = 2$). The sharp periodically spaced peaks at q_{001} are caused by alternating lipid bilayer−DNA−monolayer structure with periodicity $d = 2\pi/q_{001} = 6.01 \pm 0.01$ nm. The middle peak (marked by an arrow) results from one-dimensional (1D) ordering of the DNA sandwiched between the lipid bilayers and corresponds to a DNA interhelical spacing $d_{DNA} = 2\pi/q_{DNA} = 4.01$ nm.

(Sigma-Aldrich, St. Louis, MO) was employed. Albumin is the main protein of HP and is negatively charged at physiological pH. Size and ζ-potential of complexes were investigated as a function of increasing albumin concentration, C_{ALB}, from zero up to its typical concentration in plasma (35 mg/mL). Figure 6A shows that upon interaction with albumin, the size of both lipoplexes and LPD nanoparticles increased with increasing albumin concentration, passed throughout a maximum, and finally reached a plateau value. On the other side, the ζ potential (Figure 6B) changed from positive (∼40 mV) to negative values (about −20 mV). Even though albumin changed the ζ-potential of lipoplexes and LPD nanoparticles to negative, gel electrophoresis showed that albumin was never able to release pDNA from the complexes (data not shown). Such finding is in very good agreement with the results of Figure 4B showing that the DNA protection ability of complexes is not affected by serum.

Nanostructure. Figure 7A shows the synchrotron SAXS pattern of LPD complexes ($R_V = 2$). As evident, two broad Bragg peaks, corresponding to a periodicity $d = 2\pi/q_{001} = 7.10$ nm, were detected. The large peak width, which is characteristic of a system with a short scattering correlation length, is an indication that the bilayers are weakly bound. Further, the lamellar periodicity, d, is larger than that commonly observed in most DOTAP/DNA complexes (typically 5.5−6.2 nm).[4−7] This suggests that the lipid membranes are in a highly swollen state due to electrostatic repulsion between adjacent charged DOTAP bilayers. From the full width at half-maximum (fwhm) of the

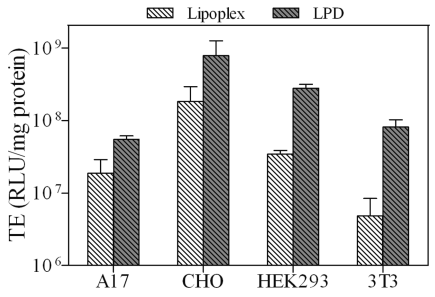

Figure 8. Transfection efficiency of LPD complexes and lipoplexes at the same lipid/DNA ratio ($R_V = 2$). Luciferase activity is expressed as relative light units/mg of protein in the cell lysate.

first-order lamellar Bragg peaks, a domain lamellar size of $L_m = 2\pi/\text{fwhm} \approx 70$ nm could be estimated. These observations are consistent with a model of LPD complexes made of a P/DNA core coated with a lipid envelope made of about 10 DOTAP bilayers.

We next examined the nanostructure of DOTAP/DNA lipoplexes. Figure 5, top, shows the SAXS pattern of DOTAP/DNA lipoplexes ($R_V = 2$). The sharp periodically spaced peaks at q_{001} are caused by alternating lipid bilayer−DNA−monolayer structure with periodicity $d = 2\pi/q_{001} = 6.01 \pm 0.01$ nm. This result is in agreement with previous experimental evidence of the DNA-induced liposome restructuring upon lipoplex formation provided by different techniques such as X-ray diffraction and cryoelectron microscopy.[4−8] The middle peak (marked by an arrow) results from one-dimensional (1D) ordering of the DNA sandwiched between the lipid bilayers.[23,24] It is usually referred to as "DNA peak" and corresponds to a DNA interhelical spacing $d_{DNA} = 2\pi/q_{DNA} = 4.01$ nm. From the fwhm of the first-order lamellar Bragg peaks, a domain lamellar size of about $L_m = 2\pi/\text{fwhm} \approx 200$ nm could be estimated. Given the lamellar d-spacing, $d = 6.00$ nm, this finding suggests that DOTAP/DNA lipoplexes are multilamellar onion-like structures made of more than 30 repeating lipid bilayer/DNA monolayer repeat units.[4−8]

Transfection Efficiency. To compare the ability of LPD nanoparticles and lipoplexes ($R_V = 2$) to deliver plasmid DNA, TE experiments were performed in NIH 3T3, CHO, Hek293, and A17 cells. TE results are reported in Figure 8. According to the literature, TE was found to be dependent on the given cell line. The CHO cell line was much more easily transfected than the A17 one, while intermediate levels of transfection were obtained with Hek 293 NIH 3T3 and cells. Even though different cell lines exhibited varying levels of TE, Figure 8 clearly shows the superior performance of LPD nanoparticles over lipoplexes in all the tested cell lines. TE was found to increase by a factor of ∼3 in A17, ∼4 in CHO, ∼8 in Hek293, and ∼20 in NIH 3T3 cells.

Interaction with Cellular Lipids. A viewpoint now emerging is that a critical factor in the lipid-mediated gene delivery is the structural evolution of lipoplexes upon interaction and mixing with anionic cellular lipids.[20,21,35−38] Such a structural rearrangement is supposed to play a central role in the DNA escape process, i.e., in how DNA dissociates from lipoplexes and is released into the cytoplasm and eventually into the nucleus. Thus, we were particularly interested in whether the DNA release from complexes upon interaction with cellular lipids might correlate with the TE data reported in Figure 8. Electrophoretic experiments (digital photographs not reported for space consideration) allowed us to quantify the molar fraction of DNA that

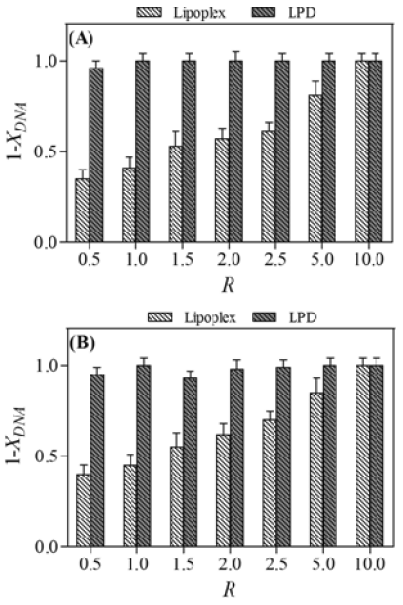

Figure 9. Molar fraction of DNA, $1 - X_{DNA}$, that is no longer electrostatically associated with LPD complexes and lipoplexes after interaction with DOPG (A) and DOPA (B) cellular lipids of as a function of the anionic/cationic charge ratio, *R*.

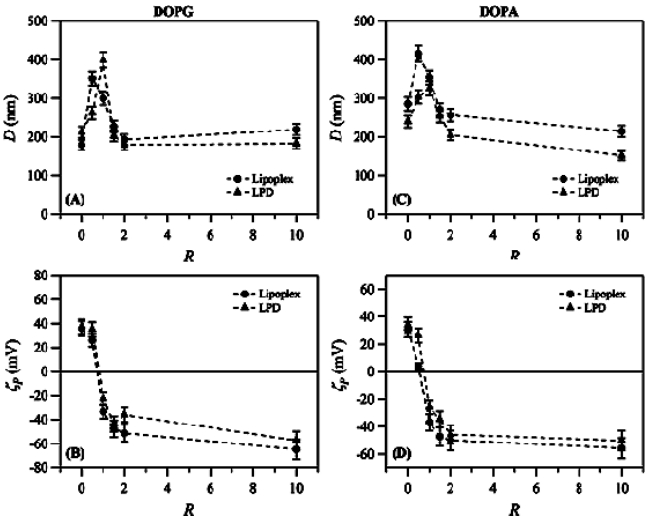

Figure 10. (A) Diameter of LPD complexes (triangles) and lipoplexes (circles) upon interaction with DOPG as a function of the anionic/cationic charge ratio, *R*. (B) ζ-Potential of LPD complexes (triangles) and lipoplexes (circles) upon interaction with DOPG as a function of the anionic/cationic charge ratio, *R*. (C) Diameter of LPD complexes (triangles) and lipoplexes (circles) upon interaction with DOPA as a function of the anionic/cationic charge ratio, *R*. (D) ζ-Potential of LPD complexes (triangles) and lipoplexes (circles) upon interaction with DOPG as a function of the anionic/cationic charge ratio, *R*.

is no longer electrostatically associated with cationic lipids, $1 - X_{DNA}$, as a function of the anionic/cationic charge ratio *R* upon interaction with DOPG (Figure 9A) and DOPA (Figure 9B) cellular lipids. At the lowest *R* ($R = 0.5$), DNA is almost completely dissociated from LPD complexes ($1 - X_{DNA} \approx 1$), while a large fraction of DNA is still protected by lipoplexes ($1 - X_{DNA}$ of ∼0.35 and ∼0.45 for DOPG and DOPA, respectively). Figure 9 also shows that DNA released from lipoplexes, $1 - X_{DNA}$, increases with increasing *R* and reaches 1 at $R \approx 10$. These findings suggest that a much lower amount of anionic lipids (ALs) is needed to promote complete DNA dissociation from LPD complexes.

Size and ζ-potential of lipoplexes and LPD nanoparticles upon interaction with cellular lipids are reported in Figure 10. Addition of ALs to cationic complexes results in a marked increase in size until a maximum is reached (at *R* of ∼0.5 and ∼1 for lipoplexes and LPD systems, respectively). Upon further addition of anionic charge, vesicle size reverted to control values. The observed increase in size of complexes for $R < 1$ can be either associated with van der Waals attractions overcoming weak electrostatic repulsions (reentrant condensation) or to vesicle fusion. Aggregates also undergo the charge inversion effect, documented by the ζ-potential values whose sign changes for $0.5 < R < 1$, differentiating positively and negatively charged aggregates. Size and ζ-potential of complexes after interaction with ALs were pretty stable over 24 h (data not reported for space consideration). On the basis of the analysis reported in Figure 10, it is difficult to correlate the extent of DNA release (Figure 9) with the size and ζ-potential of complexes emerging from interaction with cellular lipids. Electrophoresis results (Figure 9) show that for $R < 0.5$ DNA is almost completely released from LPD systems, while it is still largely protected by lipoplexes. As a whole, these results indicate that the size and ζ-potential of complexes interacting with cellular lipids are mainly regulated by the anionic/cationic charge ratio, *R*, while the ability of the investigated formulations to release DNA is controlled by factors other than *R*. The DNA release ability may be connected with the membrane fusion rate of complexes with cellular membranes that is, in turn, inversely related to the multilamellarity of lipid aggregates. Such suggestion is in good agreement with SAXS findings (Figure 7) showing that lipoplexes are multilamellar systems, while LPD nanoparticles are made of a few membranes and are therefore more disposed to fuse with ALs mimicking cellular membranes and to release their gene cargo.

Cell Imaging. Confocal images of CHO-K1 cells 4 h after incubation with LPD complexes and DOTAP/DNA lipoplexes ($R_V = 2$) are shown in Figure 11. We observe that green fluorescence from lipids forming LPD nanoparticles was clearly localized, while DNA (red fluorescence) had visibly spread into the cytoplasm (Figure11A). It may be reasonable to judge such spreading red regions as due to plasmid DNA exiting from the endosomal or lysosomal stage into the cytoplasm. Over the same time scale, CHO-K1 cells incubated with DOTAP/DNA lipoplexes were mainly distributed throughout the cytoplasm and to some extent at the cell periphery (Figure 11B). Complexes appeared almost devoid of cytoplasmic plasmid DNA, suggesting that such binary formulation is defective in facilitating endosomal escape of nucleic acids, resulting in entrapment of plasmid DNA in endosomes. Since there is a possibility that lipoplexes exhibit DNA release with different kinetics than LPD complexes, the distribution was followed at various time points (4, 6, 8, 10, 12, 24, 36, and 48 h). Over such time scale, significant cytosolic DNA release from lipoplexes as that observed for LPD nanoparticles was not detected.

■ DISCUSSION

This study represents a direct comparison between a pDNA-encapsulated system (LPD) and a complex system (lipoplex) on

dx.doi.org/10.1021/jm200237p |*J. Med. Chem.* 2011, 54, 4160–4171

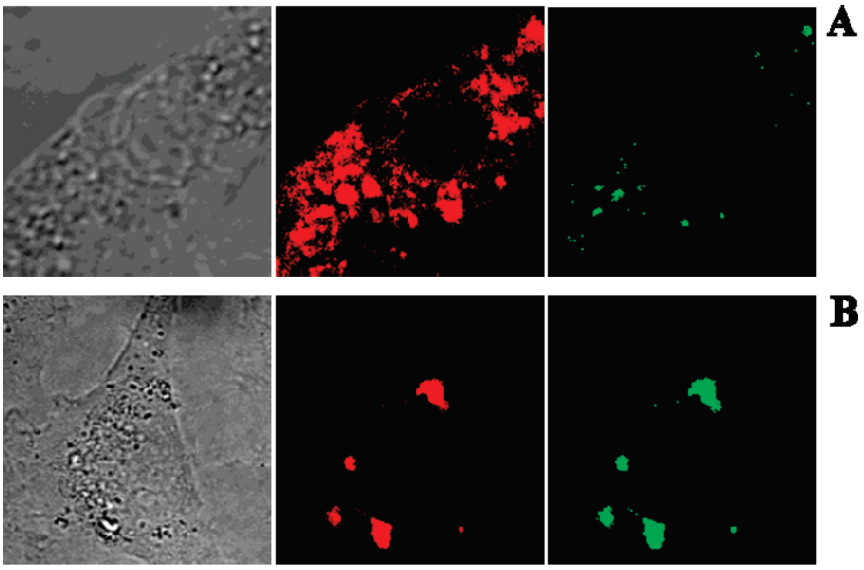

Figure 11. Confocal microscopy of CHO-K1 cells 4 h after treatment with LPD complexes (A) and lipoplexes (B). Green fluorescence from NBD lipids forming LPD complexes was clearly localized, while DNA (red fluorescence) had visibly spread into the cytoplasm. DOTAP/DNA lipoplexes were distributed throughout the cytoplasm and to some extent at the cell periphery. Colocalization of green and red fluorescence signals suggests that lipoplexes are intact with DNA trapped within.

the basis of the same lipid composition. Crucial to the mechanism of gene delivery is likely the relative ease by which the gene and amphiphile dissociate. Insight into parameters that determine stabilization and destabilization of these complexes, which are intricately related to their efficiency in gene delivery, requires an understanding of factors that govern amphiphile−DNA interaction and subsequent complex formation. Upon complex formation, reentrant condensation and charge inversion[20,21] occurred in both systems (Figure 3). Both charge inversion and charge and size saturation of LPD complexes were found to occur at R_V values smaller than those observed when lipoplexes were used. This finding means that complete encapsulation of protamine/DNA core by a lipid envelope requires a lower amount of cationic lipid than that needed to condense the same amount of DNA by a lipoplex system. Toxicity of the complex, as described for many such complexes, may depend upon the amount of cationic lipid used to transfect cells. Pertinent to sustaining such toxicity effects may be their biodegradability and the cell's capacity to eliminate cationic lipids. Thus, LPD complexes, because of the lower amount of cationic lipid needed to protect DNA, are potentially less toxic than lipoplexes.

We found that TE of LPD nanoparticles was higher than that of lipoplexes in all the tested cell lines (Figure 8). DNA complexes must overcome a series of barriers to gain access to the membrane surface, cytoplasmic compartment, and nucleus of a target cell and to translate transgenes into protein. As particles encounter each of these barriers, they are subject to a certain probability of success or failure in overcoming each. The cumulative probability of success for the entire journey is reflected in the transfection efficiency for a given system.[39] A number of physical−chemical properties of lipoplexes have been proposed as factors regulating success in overcoming such transfection barriers such as size,[40−43] ζ-potential,[44,45] nanostructure,[22,46] propensity to be disintegrated by anionic lipids,[20,21,35−38,47] and ability to release DNA both in the cytosol and in the nucleus.

Upon arrival near the cell, complexes associate electrostatically with mammalian cells, which contain surface proteoglycans with negatively charged sulphated groups. Since the first interaction between nanocarriers and cells is charge-mediated and not specific, complexes with high ζ-potential are supposed to be better internalized. A preferential binding should result in subsequent efficient cellular internalization of the carrier−DNA complex that is crucial to nonviral gene transfer. However, ζ-potential of LPD complexes and lipoplexes were found to be roughly the same (ζ_p = 47.5 and 44.4 mV, respectively). Thus, charge-mediated efficient binding played a minor role, if any, in differentiating efficiency levels of the two carriers.

Nonviral vectors can be transported to the cytoplasmic compartment by a diversity of endocytic mechanisms.[39] Each of these pathways may support a different level of transfection mediated by a given delivery system. An emerging paradigm for the design of effective gene carriers is the modification of particulate parameters to encourage entry via a preferable endocytic pathway.[48,49] The endocytic machinery and cell membrane have well-defined geometries and flexibility that may restrict entry of incompatibly large or small particles.[40−43] Recently, a size-dependent mechanism of lipoplex internalization has been proposed.[41] Accordingly, complexes with a size of approximately 200 nm or less are supposed to enter cells basically via the clathrin-coated pathway, while larger complexes are internalized via caveolae-mediated pathways. Our DLS data show that both LPD complexes and lipoplexes used in the present study are larger than 200 nm in size. Even though a precise determination of the internalization mechanisms of LPD complexes and lipoplexes is beyond the scope of the present study, we claim that potential differences in their internalization efficiency, if any, should not be size regulated. In summary, size and surface charge of complexes could not be taken into account to justify differences in TE.

It is the surface of the gene delivery system that is recognized and processed by cells, and this has important implications for safety considerations and the practice of nanomedicine.[30−33] From this point of view, surface properties of LPD complexes and lipoplexes were found to be largely different from each other.

Proteomics experiments (Figure 5, top) showed that surface of LPD complexes resembles that of pure DOTAP CLs while that of lipoplexes is partly decorated with adsorbed DNA molecules. The latter finding is in very good agreement with the recent suggestion that the position of the negatively charged DNA is not controlled in the lipoplex system.[19] This aspect is potentially detrimental for in vivo application because interactions between negatively charged DNA and positively charged serum components have been found to result in the formation of large aggregates and would also result in undesirable lung accumulation. On the other side, encapsulating pDNA in the lipid envelope would be an ideal strategy to shield the mutual interactions between DNA and basic serum proteins.[10,12−18]

When in the cytosol, the ability of a nonviral vector to escape from the endosomal compartment determines the carrier's transfection ability. Exposure to the acidic and degradative lysosomal compartment reduces the transfection efficiency of nonviral vectors. Therefore, enhanced escape from the acidic endosomes by the proton sponge effect[50] or by chemical and physical endosomolytic agents[51] has been pursued to help surmount this cytoplasmic barrier. Most lipid/DNA complexes are ordered structures. In cells, they may be presumed to interact with a number of cellular membranes, during which DNA may be released gradually only after the lipoplex has acquired enough anionic lipids to neutralize the cationic charge and to rearrange into a structure from which the DNA can escape. Thus, intermixing of cellular lipids with lipoplex lipids is presumed to be a necessary step in transfection.[52] Upon nanocarrier−cellular membrane interaction, anionic cellular lipids laterally diffuse into the complex and locally neutralize cationic lipids.[52] Formation of cationic/anionic mixed bilayers is expected to weaken the electrostatic attraction between cationic lipoplex lipids and anionic DNA molecules. Only when the membrane charge density of cationic membranes is completely neutralized by anionic lipids does DNA start to escape from complexes appreciably.[53] SAXS measurements showed that DNA is not present in the lipid envelope of LPD complexes, but it is confined in the central core. Thus, anionic cellular lipids can interact with cationic lipids of LPD complexes without competing with DNA molecules. According to electrostatic interaction models,[52,53] we hypothesize that the absence of electrostatic competition between ALs and DNA molecules would result in the high incorporation efficiency of ALs within LPD membranes, resulting in the efficient DNA cytoplasmic release observed by confocal microscopy experiments (Figure 11). Numerous contacts visualized by electron microscopy between lipoplexes and various cellular membranes[54] support a concept of gradual lipoplex peeling and DNA release. SAXS measurements reported in Figure 7 show that LPD complexes are made of about 10 lipid layers in a highly swollen state, while lipoplexes are well ordered multilamellar structures made of more than 30 alternating lipid/DNA layers. Given the need for intermixing of anionic cellular lipids and cationic carrier lipids,[52−58] our findings take on a particular significance because the ability of ALs to initiate DNA release could depend on the extent of membrane fusion (strictly, lipid mixing) between anionic cellular membranes and lipid carriers. All these suggestions are well supported by results reported in Figure 9 showing a plain correlation between complexes and their ability to release DNA upon interaction with cellular lipids.

Figure 12 summarizes our present understanding of mechanisms occurring upon complex−cell interaction. Because of similar size and ζ-potential, as well as identical lipid composition, it is reasonable that complexes enter the cell using similar internalization mechanisms. However, after complex internalization within cells, both LPD complexes and lipoplexes must fuse with the negatively charged cellular membrane to escape endosomes. LPD complexes are more fusogenic than lipoplexes, a phenomenon that is presumably related to higher interaction between cationic and anionic cellular lipids due to the absence of competing DNA in the lipid envelope and to the lower number of lipid layers to be peeled off. If poor DNA release from lipoplexes proves to be a critical attribute of poor transfection, an intelligent strategy to achieve efficient dissociation of pDNA is desirable. Collectively, these data support the hypothesis that the encapsulation of pDNA in the lipid envelope has a distinct advantage for releasing DNA in the cytosol. As for intranuclear disposition of the DNA cargo, coating the core with the minimum number of fusogenic lipid envelopes ensuring complete DNA protection is ideal for decoating and for facilitated release.

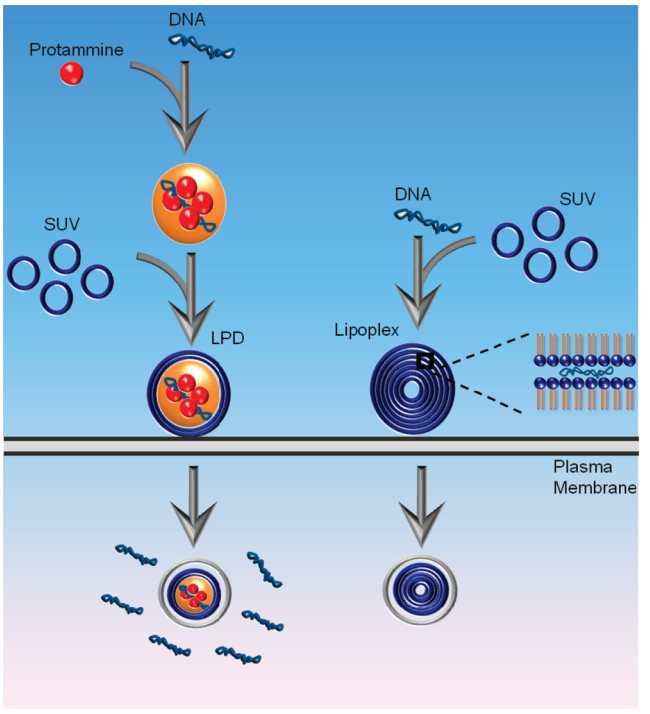

Figure 12. Because of comparable size and ζ-potential, as well as identical lipid composition, it is reasonable to judge that LPD complexes and lipoplexes enter the cell using similar internalization mechanisms. However, after complex internalization, both LPD complexes and lipoplexes fuse with the negatively charged endosomal membrane. LPD complexes are more fusogenic than lipoplexes, a phenomenon that is presumably related to higher interaction between cationic and anionic cellular lipids due to the absence of competing DNA in the lipid envelope and to the lower number of lipid layers to be peeled off. DNA release from endosomes is not a relevant barrier for LPD complexes, while DOTAP/DNA lipoplexes remained largely intact and accumulated at the nuclear membrane without releasing DNA abundantly.

CONCLUSIONS

The findings reported herein indicate that a LPD system is more efficient in transfecting cells if compared to the consolidated lipoplex strategy. Such a system has evident advantage in terms of endosomal escape and DNA release. Encapsulating

pDNA in the lipid envelope would also be an ideal strategy to shield the mutual interactions between DNA and basic serum proteins for in vivo applications as well as to better investigate the interaction between nanocarriers and cellular compartments. The findings reported in this study promise to be useful for the development of efficient gene delivery systems for both in vitro and in vivo applications. In the near future, the very same packaging strategy will be applied to develop a proper LPD system equipped with functional devices to control intracellular fate and intranuclear DNA release. This functionalized envelope-type system will be able to compete with the efficiency of viral vectors.

EXPERIMENTAL SECTION

Liposomes. Cationic 1,2-dioleoyl-3-trimethylammonium propane (DOTAP) and fluorescently labeled NBD-DOTAP were purchased from Avanti Polar Lipids (Alabaster, AL) and used without further purification. DOTAP cationic liposomes (CLs) were prepared according to standard protocols.[59] In brief, the proper amount of DOTAP was dissolved in chloroform and the solvent was evaporated under vacuum for at least 24 h. The obtained lipid films were hydrated with the appropriate amount of Tris-HCl buffer solution (10^{-2} M, pH 7.4) to achieve the desired final concentration (1 mg/mL). The same experimental protocol was used to prepare negatively charged liposomes made of anionic lipids dioleoylphosphatidylglycerol (DOPG) and dioleoylphosphatidic acid (DOPA). Liposome dispersions were sonicated to clarity to prepare SUVs.

LPD Complexes. Protamine sulfate salt (P) from salmon (MW = 5.1 kDa) was purchased from Sigma-Aldrich (St. Louis, MO). For dynamic light scattering, synchrotron small-angle X-ray scattering (SAXS), and electrophoresis experiments, calf thymus DNA was used. For confocal fluorescence microscopy experiments, Cy3-labeled 2.7 kbp plasmid DNA (Mirus Bio Corporation, Madison, WI) was used. Positively charged P/DNA microspheres were prepared at seven protamine/DNA weight ratios R_W = 0.25, 0.5, 1, 2, 3, 5, and 10. Positively charged P/DNA microspheres at R_W = 0.5 were mixed with DOTAP SUVs at nine lipid/DNA volume ratios, R_V = 0.25, 0.5, 1, 1.25, 1.75, 2, 3, 5, and 10.

Lipoplexes. When adequate amounts of the DNA solutions were mixed with suitable volumes of DOTAP liposome dispersions, self-assembled DOTAP/DNA lipoplexes at nine volume ratios R_V = 0.25, 0.5, 1, 1.25, 1.75, 2, 3, 5, and 10 were obtained.

Size and ζ-Potential. The size and size distribution of CLs, LPD, and lipoplexes were measured at 25 °C by a Malvern NanoZetaSizer spectrometer equipped with a 5 mW HeNe laser (wavelength λ = 632.8 nm) and a digital logarithmic correlator. The normalized intensity autocorrelation functions were detected at 90° and analyzed by using the CONTIN method, which analyzes the autocorrelation function through an inverse Laplace transform[60,61] in order to obtain the distribution of the diffusion coefficient D of the particles. This coefficient is converted into an effective hydrodynamic radius R_H by using the Stokes−Einstein relationship $R_H = K_BT/(6\pi\eta D)$, where K_BT is the thermal energy and η the solvent viscosity. Our clusters invariably show a size distribution, and the values of the radii reported here correspond to the so-called "intensity weighted" average.[62] The electrophoretic mobility measurements were carried out by means of the laser Doppler electrophoresis technique, the same apparatus used for size measurements. The mobility u was converted into the ζ-potential using the Smoluchowski relation $\zeta = u\eta/\varepsilon$, where η and ε are the viscosity and the permittivity of the solvent phase, respectively.

One-Dimensional Polyacrylamide Gel Electrophoresis (1D-PAGE). Human plasma was prepared as described elsewhere.[63] An amount of 100 μL of CL, LPD, and lipoplex suspensions (1 mg/mL) were incubated with 100 μL of plasma on ice. The samples were centrifuged to pellet the particle−protein complexes. The pellet was resuspended in phosphate buffered saline (PBS), transferred into a new vial, and centrifuged again to pellet the particle−protein complexes; this procedure was repeated twice. The proteins were eluted from the particles by adding sodium dodecyl sulfate (SDS) sample buffer to the pellet and boiling the solution. Then the proteins were separated by 10% 1D SDS−PAGE gels. Coomassie PhastGel Blue R-350 was used to stain the gels with gentle agitation, in accordance with the manufacturer's manual (GE Healthcare, Milan, Italy). All experiments were conducted four times to ensure reproducibility of the particle−protein complex pellet sizes, general pattern, and band intensities on the 1D gels. To determine molecular weights of proteins after electrophoretic run, protein molecular weight markers were used. The molecular weights were finally obtained by means of the dedicated software Kodak (Rochester, NY).

Synchrotron Small Angle X-ray Scattering. SAXS measurements were performed at the Austrian SAXS station of the synchrotron light source ELETTRA (Trieste, Italy).[64] SAXS patterns were recorded with gas detectors based on the delay line principle covering the q-ranges from q_{min} = 0.04 Å^{-1} to q_{max} = 0.5 Å^{-1} with a resolution of 5×10^{-4} Å^{-1} (fwhm). The angular calibration of the detectors was performed with silver behenate powder (d-spacing of 58.38 Å). The data have been normalized for variations of the primary beam intensity, corrected for the detector efficiency, and the background has been subtracted. Exposure times were typically 300 s. No evidence of radiation damage was observed in the X-ray diffraction patterns. In both experimental sessions the sample was held in a 1 mm glass capillary (Hilgenberg, Malsfeld, Germany) and the measurements were performed at 25 °C with a precision of 0.1 °C.

Transfection Efficiency. Transfection efficiency is evaluated by the expression of reporter firefly luciferase gene and measured by the luciferase reporter assay. Fibroblasts 3T3 NIH, CHO, Hek293, and A17[65] cells were cultured in Dulbecco's modified Eagle's medium (DMEM) with GlutaMAX-I (Invitrogen) supplemented with 10% fetal bovine serum (FBS, Invitrogen) at 37 °C and 5% CO_2 atmosphere, splitting cells every 2−4 days to maintain monolayer coverage. Twenty-four hours before transfection 150 000 cells were seeded per well into 24-well culture plates in order to reach 70−80% confluence during transfection. For transfection experiments, plasmid DNA (pGL3 control vector, which codifies for firefly luciferase under the control of SV40 promoter) (Promega, Madison, WI) was employed. Both LPD nanoparticles and lipoplexes were prepared at a fixed lipid/DNA volume ratio, R_V = 2. This value was chosen because it corresponds to a typical plateau value. LPD complexes and lipoplexes were prepared in Optimem (Invitrogen) by mixing, for each well of 24-well plates, 0.5 μg of pDNA, condensed or not with protamine, with 10 μL of sonicated lipid dispersion (0.5 mg/mL). These complexes were left for 20 min at room temperature before adding them to the cells. The cells were incubated with lipoplexes in Optimem (Invitrogen) for 3 h to permit transient transfection before they were incubated in 1 mL of growth medium for 24 h. Finally, cells were whashed in PBS and harvested in 200 μL of 1× reporter lysis buffer (Promega). Of the cell suspension 20 μL was diluted in 100 μL of luciferase reaction buffer (Promega), and the luminescence was measured after 10 s using a luminometer (Berthold). Results were espressed as relative light units per mg of cell proteins as determined by Bio-Rad protein assay dye reagent (Bio-Rad). Each condition was performed in quadruplicate and repeated three times.

Electrophoresis on Agarose Gels. Electrophoresis studies were conducted on 1% agarose gel containing ethidium bromide in Tris−borate−EDTA (TBE) buffer as elsewhere described.[58] LPD complexes and lipoplexes were prepared by mixing 4 μg of pDNA, condensed or not with protamine, with 45 μL of lipid dispersion (1 mg/mL DOTAP). These complexes were left for 20 min at room temperature before

incubating them with (i) Tris-HCl buffer solution (incubation time 0−3 h), (ii) fetal bovine serum (FBS) (incubation time 0−3 h), and negatively charged liposomes (DOPA, DOPG) (incubation time 1 h). Naked plasmid DNA, P/DNA microspheres, LPD complexes, and lipoplexes (upon interaction with Tris-HCl buffer solution, serum, and cellular lipids at different *R* values) were analyzed by electrophoresis. For this purpose, 10 μL of each sample was mixed with 2 μL of loading buffer (glycerol 30%, bromophenol blue 0.25%) and subjected to agarose gel electrophoresis for 1 h at 80 V. The electrophoresis gel was visualized and digitally photographed using a Kodak image station, model 2000 R (Kodak, Rochester, NY). Digital photographs were enhanced using dedicated software (Kodak MI, Kodak).[66]

Confocal Fluorescence Microscopy Experiments. Chinese hamster ovary (CHO-K1) cells were cultured and maintained in a humidified, 5% CO_2 atmosphere at 37 °C in Dulbecco's modified Eagle's medium (Gibco, Paisley, U.K.) supplemented with 10% fetal bovine serum and nonessential amino acids, splitting the cells every 2−4 days to maintain monolayer coverage. For transfection experiments, lipoplexes were prepared in PBS (Invitrogen, Carlsbad, CA) by mixing 0.5 μg of Cy3-labeled plasmid DNA with 10 μL of sonicated lipid dispersions. These complexes were left for 20 min at room temperature before adding them to the cells. Confocal fluorescence microscopy experiments were performed with the Olympus Fluoview 1000 (Olympus, Melville, NY) confocal microscope.

■ ASSOCIATED CONTENT

Supporting Information. DNA condensation by lipoplexes and LPD nanoparticles from UV−vis absorption measurements; size and ζ potential of complexes followed in time over 24 h. This material is available free of charge via the Internet at http://pubs.acs.org.

■ AUTHOR INFORMATION

Corresponding Author
*Phone: 39 06 49693271. Fax: 39 06 490631. E-mail: giulio.caracciolo@uniroma1.it.

■ ACKNOWLEDGMENT

This work was partially supported by the Italian Minister for University and Research (MIUR) (Futuro in Ricerca, Grant No. RBFR08TLPO).

■ ABBREVIATIONS USED

LDP, lipid/DNA/polycation; TE, transfection efficiency; CL, cationic liposome; SDS−PAGE, sodium dodecyl sulfate−polyacrylamide gel electrophoresis; AL, anionic lipid

■ REFERENCES

(1) Felgner, P. L.; Ringold, G. M. Cationic liposome-mediated transfection. *Nature* **1989**, *337*, 387–388.
(2) Marshall, E. Gene therapy: what to do when clear success comes with an unclear risk?. *Science* **2002**, *288*, 951–952.
(3) Ramezani, M.; Khoshhamdam, M.; Dehshari, A.; Malaekeh-Nikouei, B. The influence of size, lipid composition and bilayer fluidity of cationic liposomes on the transfection efficiency of nanolipoplexes. *Colloids Surf., B* **2009**, *72*, 1–5.
(4) Raëdler, J. O.; Koltover, I.; Salditt, T.; Safinya, C. R. Structure of DNA−cationic liposome complexes: DNA intercalation in multilamellar membranes in distinct interhelical packing regimes. *Science* **1997**, *275*, 810–814.
(5) Salditt, T.; Koltover, I.; Raëdler, J. O.; Safinya, C. R. Two-dimensional smectic ordering of linear DNA chains in self-assembled DNA−cationic liposome mixtures. *Phys. Rev. Lett.* **1997**, *79*, 2582–2585.
(6) Artzner, F.; Zantl, R.; Rapp, G.; Raëdler, J. O. Observation of a rectangular columnar phase in condensed lamellar cationic lipid−DNA complexes. *Phys. Rev. Lett.* **1998**, *81*, 5015–5018.
(7) Caracciolo, G.; Caminiti, R.; Natali, F.; Castellano, A. C. A new approach for the study of cationic lipid−DNA complexes by energy dispersive X-ray diffraction. *Chem. Phys. Lett.* **2002**, *366*, 200–204.
(8) Sternberg, B.; Sorgi, F. L.; Huang, L. New structures in complex formation between DNA and cationic liposomes visualized by freeze−fracture electron microscopy. *FEBS Lett.* **1994**, *356*, 361–366.
(9) Mönkkönen, J.; Urtti, A. Lipid fusion in oligonucleotide and gene delivery with cationic lipids. *Adv. Drug Delivery Rev.* **1998**, *34*, 37–49.
(10) Zuhorn, I. S.; Visser, W. H.; Bakowsky, U.; Engberts, J. B; Hoekstra, D. Interference of serum with lipoplex−cell interaction: modulation of intracellular processing. *Biochim. Biophys. Acta* **2002**, *1560*, 25–36.
(11) Elouahabi, A.; Ruysschaert, J. M. Formation and intracellular trafficking of lipoplexes and poliplexes. *Mol. Ther.* **2005**, *11*, 336–347.
(12) Kogure, K.; Moriguchi, R.; Sasaki, K.; Ueno, M.; Futaki, S.; Harashima, H. Development of efficient packaging method of oligodeoxynucleotides by a condensed nano particle in lipid envelope structure. *J. Controlled Release* **2004**, *98*, 317–323.
(13) Yamauchi, J.; Hayashi, Y.; Kajimoto, K.; Akita, H.; Harashima, H. Comparison between a multifunctional envelope-type nano device and lipoplex for delivery to the liver. *Biol. Pharm. Bull.* **2010**, *33*, 926–929.
(14) Tan, Y.; Whitmore, M.; Li, S.; Frederik, P.; Huang, L. LPD nanoparticles—novel nonviral vector for efficient gene delivery. *Methods Mol. Med.* **2002**, *69*, 73–81.
(15) Li, S. D.; Huang, L. Surface-modified LPD nanoparticles for tumor targeting. *Ann. N.Y. Acad. Sci.* **2006**, *1082*, 1–8.
(16) Chen, Y.; Sen, J.; Bathula, S. R.; Yang, Q.; Fittipaldi, R.; Huang, L. Novel cationic lipid that delivers siRNA and enhances therapeutic effect in lung cancer cells. *Mol. Pharmaceutics* **2009**, *6*, 696–705.
(17) Chen, Y.; Bathula, S. R; Li, J.; Huang, L. Multifunctional nanoparticles delivering small interfering RNA and doxorubicin overcome drug resistance in cancer. *J. Biol. Chem.* **2010**, *285*, 22639–22650.
(18) Yang, X.; Peng, Y.; Yu, B.; Yu, J.; Zhou, C.; Mao, Y.; Lee, L. J.; Lee, R. J. A covalently stabilized lipid−polycation−DNA (sLPD) vector for antisense oligonucleotide delivery. *Mol Pharmaceutics* [Online early access]. DOI: 10.1021/mp100272k. Published Online: Mar 2, **2011**.
(19) Amenitsch, H.; Caracciolo, G.; Foglia, P.; Fuscoletti, V.; Giansanti, P; Marianecci, C.; Pozzi, D.; Laganà, A. Existence of hybrid structures in cationic liposome/DNA complexes revealed by their interaction with plasma proteins. *Colloid Surf., B* **2011**, *82*, 141–146.
(20) Caracciolo, G.; Pozzi, D.; Caminiti, R.; Marchini, C.; Montani, M.; Amici, A.; Amenitsch, A. On the correlation between phase evolution of lipoplexes/anionic lipid mixtures and DNA release. *Appl. Phys. Lett.* **2007**, *91*, 143903.
(21) Caracciolo, G.; Marchini, C.; Pozzi, D.; Caminiti, R.; Amenitsch, H.; Montani, M.; Amici, A. Structural stability against disintegration by anionic lipids rationalizes the efficency of cationic liposom/DNA complexes. *Langmuir* **2007**, *23*, 4498–4508.
(22) Pozzi, D.; Caracciolo, G.; Caminiti, R.; Candeloro De Sanctis, S.; Amenitsch, H.; Marchini, C.; Montani, M.; Amici, A. Toward the rational design of lipid gene vectors: shape coupling between lipoplex and anionic cellular lipids controls the phase evolution of lipoplexes and the efficiency of DNA release. *ACS Appl. Mater. Interfaces* **2009**, *10*, 2237–2249.
(23) Caracciolo, G.; Pozzi, D.; Amici, A.; Amenitsch, H. Universality of DNA adsorption behavior on the cationic membranes of nanolipoplexes. *J. Phys. Chem. B* **2010**, *114*, 2028–2032.
(24) Caracciolo, G.; Caminiti, R. DNA−DNA electrostatic interactions within cationic lid/DNA lamellar complexes. *Chem. Phys. Lett.* **2004**, *400*, 314–319.

(25) Zuzzi, S.; Cametti, C.; Onori, G. Polyion-induced aggregation of lipidic-coated solid polystyrene spheres: the many facets of complex formation in low-density colloidal suspensions. *Langmuir* **2008**, *24*, 6044–6049.

(26) Zuzzi, S.; Cametti, C.; Onori, G.; Sennato, S.; Tacchi, S. Polyion-induced cluster formation in different colloidal polyparticle aqueous suspensions. *Langmuir* **2009**, *25*, 5910–5917.

(27) Dunne, M.; Bibby, D. C.; Jones, J. C.; Cudmore, S. Encapsulation of protamine sulphate compacted DNA in polylactide and polylactide-*co*-glycolide microparticles. *J. Controlled Release* **2003**, *92*, 209–219.

(28) Marty, R.; N'soukpoé-Kossi, C. N.; Charbonneau, D.; Weinert, C. M.; Kreplak, L.; Tajmir-Riah, H.-A. Structural analysis of DNA complexation with cationic lipids. *Nucleic Acids Res.* **2009**, *37*, 849–857.

(29) Chesnoy, S.; Huang, L. Structure and function of lipid-DNA complexes for gene delivery. *Annu. Rev. Biophys. Biomol. Struct.* **2000**, *29*, 27–47.

(30) Cedervall, T.; Lynch, I.; Lindman, S.; Berggård, T.; Thulin, E.; Nilsson, H.; Dawson, K. A.; Linse, S. Understanding the nanoparticle–protein corona using methods to quantify exchange rates and affinities of proteins for nanoparticles. *Proc. Natl. Acad. Sci. U.S.A.* **2007**, *104*, 2050–2055.

(31) Lundqvist, M.; Stigler, J.; Elia, G.; Lynch, I.; Cedervall, T.; Dawson, K. A. Nanoparticle size and surface properties determine the protein corona with possible implications for biological impacts. *Proc. Natl. Acad. Sci. U.S.A.* **2008**, *105*, 14265–14270.

(32) Monopoli, M. P.; Walczyk, D.; Campbell, A.; Elia, G.; Lynch, I.; Baldelli Bombelli, F.; Dawson, K. A. Physical–chemical aspects of protein corona: relevance to in vitro and in vivo biological impacts of nanoparticles. *J. Am. Chem. Soc.* **2010**, *133*, 2525–2534.

(33) Caracciolo, G.; Callipo, L.; Candeloro De Sanctis, S.; Cavaliere, C.; Pozzi, D.; Laganà, A. Surface adsorption of protein corona controls the cell internalization mechanism of DC-Chol–DOPE/DNA lipoplexes in serum. *Biochim. Biophys. Acta* **2010**, *1798*, 536–543.

(34) Deng, Z. J.; Mortimer, G.; Schiller, T.; Musumeci, A.; Martin, D.; Minchin, R. F. Differential plasma protein binding to metal oxide nanoparticles. *Nanotechnology* **2009**, *20*, 455101.

(35) Yury, S.; Tarahovsky, Y.; Koynova, R.; MacDonald, R. C. DNA release from lipoplexes by anionic lipids: correlation with lipid mesomorphism, interfacial curvature, and membrane fusion. *Biophys. J.* **2004**, *87*, 1054–1064.

(36) Koynova, R.; Wang, L.; Tarahovsky, Y.; MacDonald, R. C. Lipid phase control of DNA delivery. *Bioconjugate Chem.* **2005**, *16*, 1335–1339.

(37) Koynova, R.; MacDonald, R. C. Lipid transfer between cationic vesicles and lipid–DNA lipoplexes: effect of serum. *Biochim. Biophys. Acta* **2005**, *1714*, 63–70.

(38) Koynova, R.; Wang, L.; MacDonald, R. C. An intracellular lamellar–nonlamellar phase transition rationalizes the superior performance of some cationic lipid transfection agents. *Proc. Natl. Acad. Sci. U.S.A.* **2006**, *103*, 14373–14378.

(39) Adler, A. F.; Leong, K. W. Emerging links between surface nanotechnology and endocytosis: impact on nonviral gene delivery. *Nano Today* **2010**, *5*, 553–569.

(40) Almofti, M. R.; Harashima, H.; Shinohara, Y.; Almofti, A.; Li, W. H.; Kiwada, H. Lipoplex size determines lipofection efficiency with or without serum. *Mol. Membr. Biol.* **2003**, *20*, 35–43.

(41) Rejman, J.; Oberle, V.; Zuhorn, I. S.; Hoekstra, D. Size-dependent internalization of particles via the pathways of clathrin- and caveole-mediated endocytosis. *Biochem. J.* **2004**, *377*, 159–169.

(42) Rejman, J.; Conese, M.; Hoekstra, D. Gene transfer by means of lipo- and polyplexes: role of clathrin and caveole-mediated endocytosis. *J. Liposome Res.* **2006**, *16*, 237–247.

(43) Hoekstra, D.; Rejman, J.; Wasungu, L.; Shi, F.; Zuhorn, I. Gene delivery by cationic lipids: in and out of an endosome. *Biochem. Soc. Trans.* **2007**, *35*, 68–71.

(44) Yang, J. P.; Huang, L. Overcoming the inhibitory effect of serum on lipofection by increasing the charge ratio of cationic liposome to DNA. *Gene Ther.* **1997**, *4*, 950–960.

(45) Zelphati, O.; Uyechi, L. S.; Barron, L. G.; Szoka, F. C., Jr. Effect of serum components on the physico-chemical properties of cationic lipid/oligonucleotide complexes and on their interactions with cells. *Biochim. Biophys. Acta* **1998**, *1390*, 119–133.

(46) Caracciolo, G.; Pozzi, D.; Caminiti, R.; Congiu Castellano, A. Structural characterization of a new lipid/DNA complex showing a selective transfection efficiency in ovarian cancer cells. *Eur. Phys. J. E* **2003**, *10*, 331–336.

(47) Caracciolo, G.; Pozzi, D.; Caminiti, R.; Marchini, C.; Montani, M.; Amici, A.; Amenitsch, H. Transfection efficiency boost by designer multicomponent lipoplexes. *Biochim. Biophys. Acta* **2007**, *1768*, 2280–2292.

(48) Akita, H.; Kudo, A.; Minoura, A.; Yamaguti, M.; Khalil, I. A.; Moriguchi, R.; Masuda, T.; Danev, R.; Nagayama, K.; Kogure, K.; Harashima, H. Multi-layered nanoparticles for penetrating the endosome and nuclear membrane via a step-wise membrane fusion process. *Biomaterials* **2009**, *30*, 2940–2949.

(49) Akita, H.; Kogure, K.; Moriguchi, R.; Nakamura, Y.; Higashi, T.; Nakamura, T.; Serada, S.; Fujimoto, M.; Naka, T.; Futaki, S.; Harashima, H. Nanoparticles for ex vivo siRNA delivery to dendritic cells for cancer vaccines: programmed endosomal escape and dissociation. *J. Controlled Release* **2010**, *143*, 311–317.

(50) Sonawane, N. D.; Szoka, F. C., Jr.; Verkman, A. S. Chloride accumulation and swelling in endosomes enhances DNA transfer by polyamine–DNA polyplexes. *J. Biol. Chem.* **2003**, *278*, 44826–44831.

(51) Wagner, E. Effects of membrane-active agents in gene delivery. *J. Controlled Release* **1998**, *53*, 155–158.

(52) Xu, Y. H.; Szoka, F. C. Mechanism of DNA release from cationic liposome/DNA complexes used in cell transfection. *Biochemistry* **1996**, *35*, 5616–5623.

(53) Caracciolo, G.; Pozzi, D.; Amenitsch, H.; Caminiti, R. Interaction of lipoplexes with anionic lipids resulting in DNA release is a two-stage process. *Langmuir* **2007**, *23*, 8713–8717.

(54) Koynova, R.; Tarahovsky, Y.; Wang, L.; MacDonald, R. C. Lipoplex formulation of superior efficacy exhibits high surface activity and fusogenicity, and readily releases DNA. *Biochim. Biophys. Acta* **2007**, *1768*, 375–386.

(55) Kozlov, M. M.; Markin, V. S. On the theory of membrane fusion. The adhesion–condensation mechanism. *Gen. Physiol. Biophys.* **1984**, *5*, 379–402.

(56) Pantazatos, D. P.; Pantazatos, S. P.; MacDonald, R. C. Bilayer mixing, fusion, and lysis following the interaction of populations of cationic and anionic phospholipid bilayer vesicles. *J. Membr. Biol.* **2003**, *194*, 129–139.

(57) Hed, G.; Safran, S. A. Attractive instability of oppositely charged membranes induced by charge density fluctuations. *Phys. Rev. Lett.* **2004**, *93*, 138101.

(58) Marchini, C.; Pozzi, D.; Montani, M.; Alfonsi, C.; Amici, A.; Amenitsch, H.; Candeloro De Sanctis, S.; Caracciolo, G. Tailoring lipoplex composition to the lipid composition of plasma membrane: a Trojan horse for cell entry?. *Langmuir* **2010**, *26*, 13867–13873.

(59) Caracciolo, G.; Pozzi, D.; Caminiti, R. Lipid mixing upon deoxyribonucleic acid-induced liposomes fusion investigated by synchrotron small-angle X-ray scattering. *Appl. Phys. Lett.* **2005**, *87*, 133901.

(60) Provencher, S. W. A constrained regularization method for inverting data represented by linear algebraic or integral equations. *Comput. Phys. Commun.* **1982**, *27*, 213–227.

(61) Provencher, S. W. CONTIN: a general purpose constrained regularization program for inverting noisy linear algebraic and integral equations. *Comput. Phys. Commun.* **1982**, *27*, 229–242.

(62) Berne, B. J.; Pecora, R. *Dynamic Light Scattering: With Applications to Chemistry, Biology, and Physics*; Dover Publications Inc.: New York, 2003.

(63) Caracciolo, G.; Callipo, L.; Candeloro De Sanctis, S.; Cavaliere, C.; Pozzi, D.; Laganà, A. Surface adsorption of protein corona controls the cell internalization mechanism of DC-Chol–DOPE/DNA lipoplexes in serum. *Biochim. Biophys. Acta* **2010**, *1798*, 536–543.

(64) Amenitsch, H.; Rappolt, M.; Kriechbaum, M.; Mio, H.; Laggner, P.; Bernstorff, S. First performance assessment of the small-angle X-ray scattering beamline at ELETTRA. *J. Synchrotron Radiat.* **1998**, *5*, 506–508.

(65) Galiè, M.; D'Onofrio, M.; Montani, M.; Amici, A.; Calderan, L.; Marzola, P.; Benati, D.; Merigo, F.; Marchini, C.; Sbarbati, A. Tumor vessel compression hinders perfusion of ultrasonographic contrast agents. *Neoplasia* **2005**, *7*, 528–536.

(66) Caracciolo, G.; Pozzi, D.; Caminiti, R.; Marchini, C.; Montani, M.; Amici, A.; Amenitsch, H. DNA release from cationic liposome/DNA complexes by anionic lipids. *Appl. Phys. Lett.* **2006**, *89*, 233903.

VI

Analytical Biochemistry 419 (2011) 180–189

Contents lists available at SciVerse ScienceDirect

Analytical Biochemistry

journal homepage: www.elsevier.com/locate/yabio

Differential analysis of "protein corona" profile adsorbed onto different nonviral gene delivery systems

Anna Laura Capriotti [a], Giulio Caracciolo [b], Giuseppe Caruso [a], Patrizia Foglia [a,*], Daniela Pozzi [b], Roberto Samperi [a], Aldo Laganà [a]

[a] Dipartimento di Chimica, Sapienza Università di Roma, Piazzale Aldo Moro 5, 00185 Rome, Italy
[b] Dipartimento di Medicina Molecolare, Sapienza Università di Roma, Piazzale Aldo Moro 5, 00185 Rome, Italy

ARTICLE INFO

Article history:
Received 24 May 2011
Received in revised form 29 July 2011
Accepted 2 August 2011
Available online 9 August 2011

Keywords:
Proteomics
Mass spectrometry
Protein corona
Liposome
Nanomedicine

ABSTRACT

A shotgun proteomics approach was used to characterize and compare the proteins that lead to the formation of a rich "protein corona" adsorbed onto the surfaces of cationic liposomes (CLs), lipoplexes, and lipid/polycation/DNA (LPD) complexes, when they come into contact with plasma. After separation of the nanoparticle–protein complex from plasma, the protein mixture was digested, and peptides were analyzed by nanoliquid chromatography–Orbitrap LTQ-XL mass spectrometry. The number of proteins bound to lipoplexes was double that of those identified in the corona of CLs (208 vs 105), while 77 proteins were common to both coronas. The number of proteins bound to the surface of the LPD complexes (158, 133 of which are common to lipoplexes) is intermediate between those found in the protein corona of both CLs and lipoplexes. About half of them were found in the protein corona of CLs. By overlapping the three formulations, it can be seen that only 12 proteins are peculiar to LPD complexes. These results may help in designing gene delivery systems capable of binding the minimum possible quantity of proteins that influence transfection negatively, binding selectively proteins capable of helping in steering *in vivo* the vector toward the target, and obtaining more efficient and effective gene therapy.

One of the most important requirements in gene therapy is the development of safe and efficient gene delivery systems. Retroviruses, adenoviruses, and adeno-associated viruses are viral vectors that have shown a high transfection efficiency and are used in many clinical trials, but may be dangerous for routine clinical use [1]. In the past two decades, because of the advantages of their nonimmunogenicity, convenience of handling, and high capability for the delivery of genetic materials [2,3], nonviral vectors have attracted a growing interest in the scientific community. Cationic liposomes (CLs)[1] have been extensively studied as nonviral vectors since the first lipofection was reported in 1987 [4]. One of the most common nonviral gene delivery vectors is the DNA–cationic lipid complex (lipoplex). Much work has been done, with different experimental techniques, toward determining the lipoplex microstructure and stability, as well as on its transfection efficiency [5–14]. The cationic lipids used as transfection agents are indeed readily and easily metabolized by the target tissues [15–17]. One critical element for efficient gene delivery is the lipid composition of cationic liposomes, and many quaternary ammonium surfactants have been tried, including compounds with alkyl, ether, and ester bonds. Monocationic lipids are widely used to make most cationic carriers [17–19], and 1,2-dio-leoyl-3-trimethylammonium-propane (DOTAP), a double chain quaternary ammonium surfactant, is the most popular cationic lipid used in lipoplex formation. When cationic lipids are used as carriers of nucleic acids (RNA, DNA), periodic multilayer structures with DNA chains adsorbed between lipid membranes are often formed [7,20]. This multilayer structure offers protection from DNA degradation inside the cell; on the other hand, the DNA is not properly released from endosomal compartments. Recently, this problem was overcome by developing the lipid/polycation/DNA (LPD) complex, where the plasmid DNA (pDNA) is condensed with a polycation and encapsulated by a lipid envelope [21]. It has been shown that the gene transfer mediated by the LPD complex works better than the conventional gene transfer using liposomes for delivering a gene into the liver [22]. Medical administration of these gene delivery vectors is frequently carried out by parenteral injection. Therefore, on exposure to biological media, the administered gene delivery vectors are immediately covered by plasma proteins that lead to the formation of a rich "protein corona" [23–25]. Recent studies have shown that the binding of plasma

* Corresponding author. Address: Dipartimento di Chimica, Sapienza Università di Roma, Box n 34–Roma 62, Piazzale Aldo Moro 5, 00185 Rome, Italy. Fax: +39 06 490631.
E-mail address: patrizia.foglia@uniroma1.it (P. Foglia).

[1] *Abbreviations used:* CLs, liposomes; CT, calf thymus; DOTAP, 1,2-dio-leoyl-3-trimethylammonium-propane; DTT, 1,4-dithiothreitol; IAA, iodoacetamide; LPD, lipid/polycation/DNA; MPS, mononuclear phagocytic system; SUVs, small unilamellar liposomes; TFA, trifluoroacetic acid; Tris, tris(hydroxymethyl)aminomethane.

0003-2697/$ - see front matter © 2011 Elsevier Inc. All rights reserved.
doi:10.1016/j.ab.2011.08.003

proteins to nanoparticles, such as gene delivery vectors, is a critical step in determining their fate in vivo [26,27]. Moreover, plasma proteins play an important role in the identification of foreign bodies in the bloodstream. Macrophages of the mononuclear phagocytic system (MPS) remove unprotected nanoparticles from the bloodstream within seconds of intravenous administration, thus rendering them ineffective as site-specific drug delivery devices [28]. Several methods have been developed to camouflage or mask nanoparticles, allowing them to temporarily bypass recognition by the MPS and increase their blood circulation half-life [28–30]. From these examples it is clear that nanoparticle–protein interactions are important for understanding the circulation, clearance rates, blood half-life, stability, immunogenicity, and organ biodistribution of nanoparticles. Moreover, in order to fully realize the biomedical value of the gene delivery vectors it is important to improve their functionality in the biological environment by studying the nanoparticle–protein interactions.

In the present study, we compare the binding of human plasma proteins onto the surface of DOTAP CLs, DOTAP/DNA lipoplexes, and DOTAP/protamine/DNA complexes. For this purpose, we have employed a shotgun proteomics approach based on centrifugation for separating the nanoparticle–protein complex, followed by "in-solution" proteolytic digestion of the whole protein mixture, and determination of the resulting peptides by nano-high-performance liquid chromatography (nano-HPLC) coupled with a high-resolution Orbitrap LTQ-XL mass spectrometer.

To the authors' best knowledge, this is the first study using this approach to characterize the protein corona of cationic liposomes, lipoplexes, and lipid/polycation/DNA complexes. We found that these nanoparticles are capable of binding different plasma protein categories with important biological functions, such as lipoproteins, immunoglobulins, acute-phase proteins, proteins which play an essential role in protein synthesis, proteins strongly related to cellular activity, and proteins involved in complement pathways and coagulation. These results could help in designing gene delivery systems capable of binding selectively certain proteins rather than others, and of steering their biodistribution *in vivo* so as to obtain a more efficient and effective gene therapy.

Materials and methods

Reagents and chemicals

DOTAP was purchased from Avanti Polar Lipids (Alabaster, AL), and used without further purification. Calf thymus (CT) Na–DNA and protamine sulfate salt (P) from salmon (MW = 5.1 kDa) were purchased from Sigma–Aldrich (St. Louis, MO). Tris(hydroxymethyl)aminomethane (Tris), sodium chloride, polyacrylamide ethylenediaminetetraacetic acid (EDTA), iodoacetamide (IAA), 1,4-dithiothreitol (DTT), ammonium bicarbonate, and Coomassie PhastGel Blue R-350 were purchased from GE Healthcare (Amersham Biosciences, Uppsala, Sweden). All organic solvents were the highest grade available from Carlo Erba Reagents (Milan, Italy). Ultrapure water was produced from distilled water by a Milli-Q system (Millipore Corporation, Billerica, MA, USA). Protein LoBind tubes were obtained from Eppendorf (Hamburg, Germany). Porcine trypsin (modified, sequencing grade) was commercialized by Promega (Madison, WI, USA).

Human plasma collection, preparation, and storage

Human whole blood was obtained from the Experimental Medicine Department (Sapienza University of Rome) by venipuncture of healthy volunteers aged 20–40 years, by means of a BD P100 Blood Collection System (Franklin Lakes, NJ, USA), with protease inhibitors cocktail and K_2EDTA anticoagulant. Each tube was turned upside down 10 times to ensure mixing of blood with the K_2EDTA and, immediately after sediment formation, centrifuged for 10 min at 1000*g* for 5 min to pellet the blood cells. After verifying the absence of hemolysis, the supernatant plasma was removed and pooled to reduce the overall subject-to-subject variation and to reduce differences between individuals. The pooled plasma was split into 200-μL aliquots, and stored at −80 °C in labeled Protein LoBind tubes to ensure plasma stability during storage. When plasma was used for experiments, aliquots were thawed at 4 °C and then allowed to warm at room temperature (RT).

Liposomes

DOTAP CLs were prepared according to standard protocols [31]. Briefly, 5 mg of DOTAP was dissolved in 100 μL of chloroform and then evaporated under vacuum for at least 24 h. Then the lipid films obtained were hydrated with 5 mL of 10 mmol L^{-1} Tris–HCl (pH 7.4), 150 mmol L^{-1} NaCl, 1 mmol L^{-1} EDTA to achieve the desired final lipid concentration (1 mg mL^{-1}). Small unilamellar liposomes (SUVs), with mean diameter around 100 nm, were produced by sonication to clarity.

Lipoplexes

Self-assembled DOTAP/DNA lipoplexes, at a single lipid/DNA volume ratio (R_v) (R_v = DOTAP/DNA (vol/vol) = 1) were obtained by mixing 20 μL of the 1 mg mL^{-1} CT DNA solution to 100 μL of CLs SUVs dispersion. At this volume ratio, lipoplexes exhibited the lowest colloidal dimensions (about 200 nm, data not reported) and were positively charged (about 50 mV, data not reported) [32].

LPD complexes

Negatively charged P/DNA microspheres were prepared at a protamine/DNA weight ratio (R_w) of 0.5 [32]. LPD complexes were prepared by mixing P/DNA microspheres with DOTAP SUVs at a single lipid/DNA volume ratio (R_v = DOTAP/DNA (vol/vol) = 1). At this volume ratio, LPD systems exhibited the lowest colloidal dimensions (about 200 nm, data not reported), and were positively charged (about 45 mV, data not reported).

Incubation of CLs, lipoplexes, and LPD complexes with plasma and centrifugation

The incubation procedure was conducted as previously described [32], with minor modifications. Two hundred microliters of CL suspension (1 mg mL^{-1}) was added to 200 μL of plasma in the dissolving buffer and incubated at 37 °C for 1 h to promote aggregation of the plasma proteins onto the surface of nanoparticles. The same procedure was used for lipoplexes and LPD complexes. The samples were centrifuged at 15,000*g* for 10 min to pellet the nanoparticle–protein complexes. The pellet was washed three times with 250 μL of the dissolving buffer, using a vortex mixer, and then the sample was transferred into a new Protein LoBind tube and centrifuged again to pellet the nanoparticle–protein complexes. The tubes were changed after each washing step to minimize contamination from plasma proteins bound to the tube walls, and plasma without nanoparticles was used as a control to ensure there was no protein precipitation.

In-solution trypsin digestion

The enzymatic digestion procedure was conducted as previously described [32]. Briefly, the nanoparticle–protein complexes were resuspended in 40 μL of 8 mol L^{-1} urea solution in

50 mmol L^{-1} NH_4HCO_3 and 2 μL of 200 mmol L^{-1} DTT, and were incubated at 37 °C for 1 h under slight agitation to denature proteins adsorbed onto the nanoparticle surface. Afterward, 8 μL of 200 mmol L^{-1} IAA was added to the samples that were then incubated at RT for 1 h in the dark. Subsequently, 8 μL of 200 mmol L^{-1} DTT was added and incubated at 37 °C for 1 h, under slight agitation, to consume any leftover alkylating agent and to avoid trypsin alkylation. The sample solutions were then diluted with 50 mmol L^{-1} NH_4HCO_3 to obtain a final urea concentration of 1 mol L^{-1}. Reconstituted trypsin solution (20 μg mL^{-1} in 50 mmol L^{-1} NH_4HCO_3) was added to ensure a minimum enzyme-to-substrate ratio of 1/20. The samples were allowed to digest rotating overnight at 37 °C. The digestion was quenched by adding HCOOH. Digested samples were desalted by using an SPE C18 column (Bond Elut 1CC LRC-C18, Varian, Palo Alto, CA, USA) conditioned with acetonitrile and rinsed with 0.1% TFA. Peptides were eluted from the SPE column with 0.5 mL of CH_3CN/H_2O (50/50, v/v) containing 0.05% TFA and were dried in a Speed-Vac SC 250 Express (Thermo Savant, Holbrook, NY, USA). Each sample was reconstituted with 500 μL of the 0.1% HCOOH solution. Digested samples were stored at −80 °C until analysis. Three experimental replicates were performed for each type of nanoparticle, CLs, lipoplexes, and LPD complexes, to identify the proteins adsorbed on their surface forming the protein corona, and to allow assessment of the reproducibility and reliability of this approach.

Nano-HPLC–mass spectrometry analysis

A Dionex Ultimate 3000 nano-LC system (Sunnyvale, CA, USA) connected to a linear quadrupole ion trap-orbitrap (LTQ-Orbitrap XL) mass spectrometer (Thermo Scientific, Bremen, Germany) equipped with a nanospray ion source was used to analyze tryptic peptides. Peptide mixtures were enriched injecting a 5-μL aliquot of the sample on a 300 μm i.d. × 5 mm Acclaim PepMap 100 C18 (5 μm particle size, 100 Å pore size) μ-precolumn (Dionex), employing a premixed mobile phase H_2O/CH_3CN 98/2 (v/v) (phase C) containing 0.1% (v/v) HCOOH at a flow rate of 10 μL min^{-1}. Peptides were separated on a Biobasic 18 (5 μm particle size, 300 Å pore size) 75 μm i.d. × 100 mm, 15 μm tip picofrit column (Thermo Scientific, Bellefonte, PA, USA) connected in series with the concentrator column and operated at a flow rate of 250 nL min^{-1}. LC gradient was optimized to detect the largest set of peptides using H_2O/HCOOH (99.9/0.1, v/v) as phase A and CH_3CN/HCOOH (99.9/0.1, v/v) as phase B. A 120-min gradient was used; after an isocratic step at 5% B for 5 min, B was linearly increased to 30% within 75 min; afterward, B was increased to 80% within 5 min, and to 95% within the following 10 min to rinse the column. Finally, B was restored to 5% over 1 min and the column reequilibrated for 24 min. The mass spectrometer was operated in data-dependent mode to automatically switch between Orbitrap-MS and LTQ-MS/MS acquisition (m/z range 350–1800, resolution 60,000) using the "TOP5 strategy." In brief, a scan cycle was initiated with a full scan of high mass accuracy in the Orbitrap analyzer and followed by MS/MS scans in the linear ion trap on the five most intense precursor ions with dynamic exclusion of previously selected ions. This dynamic exclusion consisted of two MS/MS spectra acquisitions of the most abundant ions during a period of 30 s, and then the exclusion of these ions for the followed fragmentations for 100 s. The activation type used was CID with a normalized collision energy set at 35 V. Therefore, a total of five LC-MS/MS runs for each sample (CLs, lipoplexes, and LPD complexes) were analyzed.

Data processing and statistical validation

Raw data files, obtained from Xcalibur software, were submitted in Mascot Deamon (2.2.04 version, Matrix Science, London, UK) for database search using the ThermoFinnigan LCQ/DECA RAW file data import filter. Data were searched against human entries in the SwissProt protein database (57.15 version, 20266 sequences). Trypsin was specified as the proteolytic enzyme with a maximum of two missed cleavages, and fixed modification (carbamidomethyl) on cysteine (+57.0215 Da), and variable modifications (oxidation) on methionine (+15.9949 Da) were set for all searches. The monoisotopic mass tolerance for precursor ions and fragmentation ions were set to 10 ppm and 0.8 Da, respectively. Charge states of +2, +3, or unknown were selected as precursor ions. Peptide identification and protein assignment were statistically validated submitting the Mascot result files (.dat) in the statistical open source Trans-Proteomic Pipeline (TPP) software (Seattle Proteome Center, SPC, Proteomics Tools: http://tools.proteomecenter.org/software.php). After conversion of the output Mascot files (.dat) in the .pepXML format files, the PeptideProphet and ProteinProphet tools [33–35], included in TPP, were employed.

Results and discussion

Sample preparation

The nanoparticle–protein complex, formed by the protein corona and the nanoparticle in the plasma, is the unit actually concerned in biodistribution of the nanoparticles throughout the body [25]. Therefore, the method used to separate the nanoparticle–protein complex from excess plasma proteins must not destroy the complex or induce additional protein binding. For this reason, we used centrifugation for the separation of the nanoparticle–protein complex. This approach was chosen in accordance with previous findings showing that, if performed under controlled conditions of washing and centrifugation, it does not destroy the complex, and does not induce the binding of additional proteins [32]. Since we are working on proteins strongly adsorbed onto liposomes, the so-called "hard corona," the nanoparticle–protein complex pellet was washed vigorously three times in 250 μL of 10 mmol L^{-1} Tris–HCl, pH 7.4, 150 mmol L^{-1} NaCl, and 1 mmol L^{-1} EDTA, using a vortex mixer to remove all unbound proteins. We also used a short centrifugation time (2 min), to avoid sedimentation of large proteins, formation of protein aggregates, and coprecipitation. Despite the stringent washing conditions and the rapid spin a large number of proteins remained bound to the nanoparticle surface as components of the protein corona.

LC-MS/MS and data analysis

We performed experimental and technical replicates to assess the accuracy, reproducibility, and reliability of identification of the protein corona adsorbed onto the surface of CLs, lipoplexes, and LPD complexes by a shotgun proteomics approach. Three experimental replicates were performed for each type of nanoparticle. The experimental design provided five LC-MS/MS runs on the same sample. The runs, called technical replicates, allow the assessment of the additional variation introduced by the experimental procedure. Then Mascot output files were submitted to TPP software. To validate the peptide and protein identifications, two new statistical tools of TPP, namely Peptide Prophet and Protein Prophet, were applied. The peptide and protein probability thresholds for running Peptide Prophet and Protein Prophet were set at 0.75 and 0.90, respectively. Table 1 shows the values of sensitivity (percentage of total correct identifications after restricting data at a given probability threshold) and error rate (percentage of total false identifications) of each experimental replicate (5 LC runs) for each system investigated. Sensitivity and error rate for any dataset are both affected by the probability threshold, and

Table 1
Protein identification sensitivity and error rate determined by TPP of each experimental replicate (5 LC runs) for each system investigated, calculated with peptide probability ⩾ 0.75 and protein probability ⩾ 0.90.

Experimental replicate	Sensitivity	Error rate
CLs experimental replicate 1 (5 LC runs)	95.4%	0.3%
CLs experimental replicate 2 (5 LC runs)	92.5%	0.5%
CLs experimental replicate 3 (5 LC runs)	93.7%	0.4%
Lipoplexes experimental replicate 1 (5 LC runs)	88.8%	0.6%
Lipoplexes experimental replicate 2 (5 LC runs)	91.2%	0.6%
Lipoplexes experimental replicate 3 (5 LC runs)	94.2%	0.7%
LPD complexes experimental replicate 1 (5 LC runs)	87.5%	0.8%
LPD complexes experimental replicate 2 (5 LC runs)	81.0%	0.7%
LPD complexes experimental replicate 3 (5 LC runs)	86.2%	0.7%

strongly connected to each other. At best (experimental replicate 1 of CLs), the chosen thresholds resulted in a low false-positive rate (error rate of 0.3%), and in an extremely high percentage of correct identifications (95.4%). On the other hand, in the worst instance (experimental replicate 2 of LPD complexes), the false-positive rate was 0.7%, and a good percentage of correct identifications was still achieved (81.0%). The results show a high degree of reproducibility with very similar sensitivities, as well as similar values of the error rate for all sets of analyses. Since the goal of this study is the differential proteomic analysis of the protein corona adsorbed onto the surface of the three different lipid-based systems, the acquisition of an accurate protein profile of each corona is a key step toward the correct interpretation of the data. When using a proteomic approach for studying protein mixtures, the reanalysis of the same sample under the same experimental conditions can lead to the identification of a different set of proteins from that previously identified [36–38]. The degree of overlap between two chromatographic runs of the same sample varies depending on the complexity of the sample, ranging from 100% overlap (actually very rare) in not very complex samples to about 20% overlap in very complex samples. So the presence (or absence) of a protein in a sample can be due simply to an incomplete determination rather than to a biological difference between samples. With this in mind we decided to perform three experimental replicates, and five technical replicates. This procedure allowed us to increase the number of identified proteins for each protein corona of the three investigated systems. Moreover, in order to increase the confidence of the differential proteomics analysis, proteins identified by a single unique peptide were not considered. Comparing the data obtained (Table 2) with those found in the literature [39,40], we can affirm that the percentage of these proteins can be considered low. This observation makes us confident that relevant biological information was not missed, neglecting protein identified with a single peptide. Lastly, the protein identification in the three experimental replicates, each of them achieved from the five technical replicates, was compared.

Table 3 shows the overlap between the proteins identified on the surface of the three systems in the three experimental replicates, and the percentage of proteins identified in each experimental replicate versus the total proteins of the three combined experimental replicates. The latter parameter (percentage) ranges from 69.6% (experimental replicate 2 of LPD complexes) to 90.5% (experimental replicate 2 of CLs). A more thorough reading of the data shown in Table 3 prompts two relevant observations. First, the number of proteins overlapping, among the proteins identified on the surface of the three systems in the three experimental replicates, is very high. This is certainly due to the low complexity of protein mixtures, combined with the high number of chromatographic runs. Second, the variation in the percentage of proteins identified was found to be larger in the case of LPD complexes. This result indicates that the type of proteins that bind onto the surface of LPD complexes changes slightly between experimental replicates. This is probably due to the presence of protamine that could make the nanoparticles dynamically unstable. On the other hand, neither CLs nor lipoplexes contain protamine and are supposed to be more stable systems. Accordingly, the percentages of overlap among the three experimental replicates are very close to each other.

In Fig. 1, a Venn diagram showing the relationship among the proteins identified in the corona of CLs, lipoplexes, and LPD nanoparticles is reported. We observed that lipoplexes bind a number of proteins larger than those identified on the liposome surface. This finding can be explained considering that a fraction of DNA is located on the surface of nanoparticles. DNA molecules can bind additional proteins, such as DNA-binding proteins and/or basic proteins that do not interact with cationic lipid membranes. We also observed that the number of proteins bound to the surface of the LPD complexes is intermediate between those found in the protein corona of both CLs and lipoplexes. In principle, LPD complexes protect inside them the DNA carried; in fact, plasmid DNA is condensed with protamine and encapsulated by a lipid envelope. However, the possibility cannot be ruled out that, when CLs are added to the protamine/DNA dispersion, a fraction of precondensed DNA is subtracted by cationic lipids with the result that some intermediate structures with DNA available to protein adsorption are formed. This suggestion is further supported by the observation that the largest percentage of overlap is observed for lipoplexes and LPD complexes, probably because both these systems contain DNA. Further information on protein identification is provided in supporting data were also the proteins identified on just one unique peptide are shown.

Proteins identified on the surfaces of CLs, lipoplexes, and LPD complexes

Identified proteins are reported in Table 4. Proteins bound to lipoplexes were twice the amount of those identified in the corona

Table 2
Summary of proteins identified in the "protein corona" for each single experimental replicate of the three systems (the percentage of proteins identified with only one unique peptide is included).

	Experimental replicate 1		Experimental replicate 2		Experimental replicate 3	
Proteins onto CLs	Total proteins	110	Total proteins	118	Total proteins	114
	Proteins with 1 unique Pep	20	Proteins with 1 unique Pep	23	Proteins with 1 unique Pep	20
	% Proteins with 1 unique Pep	18.2%	% Proteins with 1 unique Pep	19.5%	%Proteins with 1 unique Pep	17.5%
Proteins onto lipoplexes	Total proteins	234	Total proteins	236	Total proteins	233
	Proteins with 1 unique Pep	58	Proteins with 1 unique Pep	50	Proteins with 1 unique Pep	65
	% Proteins with 1 unique Pep	24.2%	% Proteins with 1 unique Pep	21.2%	% Proteins with 1 unique Pep	27.9%
Proteins onto LPD complexes	Total proteins	168	Total proteins	127	Total proteins	137
	Proteins with 1 unique Pep	33	Proteins with 1 unique Pep	17	Proteins with 1 unique Pep	21
	% Proteins with 1 unique Pep	19.6%	% Proteins with 1 unique Pep	13.4%	% Proteins with 1 unique Pep	15.3%

Table 3
Overlap of identified proteins on the surface of the three systems in the three experimental replicates, each of them achieved from the five technical replicates (the percentage of proteins identified in each experimental replicate versus the total proteins of the three experimental replicates combined is also reported).

	Experimental replicate 1	Experimental replicate 2	Experimental replicate 3	Combined	Overlap	Not Overlap	Only experimental replicate 1	Only experimental replicate 2	Only experimental replicate 3
Proteins onto CLs	90 (85.7%)	95 (90.5%)	94 (89.5%)	105	82	13	1	5	7
Proteins onto Lipoplexes	176 (84.6%)	186 (89.4%)	168 (80.8%)	208	140	26	9	10	7
Proteins onto LPD complexes	135 (85.4%)	110 (69.6%)	116 (73.4%)	158	92	47	26	6	15

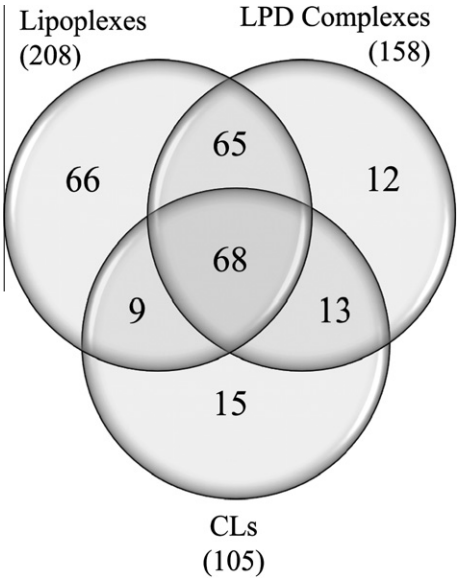

Fig.1. Venn diagram representing the total number of proteins identified on nanoparticle surfaces, and their respective overlaps.

of CLs (208 vs 105), and 77 proteins were common to both coronas (see also Fig. 1). The majority of them were apolipoproteins, which interact with lipids forming lipoproteins; immune response-related proteins, such as complement system proteins, which are part of the innate immune system; immunoglobulins; acute-phase proteins; coagulation-related proteins; and cell adhesion proteins. Most of the proteins found were secreted, but there were some proteins coming from cellular compartments. Among the proteins exclusively present in the protein corona of CLs, kininogen1 was found. Kininogen1 is a multidomain and multifunctional glycoprotein, mainly known as precursor of kinins and bradykinin, important mediators of inflammatory responses [41]. It has been recently shown that a fragment within D3 has antibacterial activity and a fragment within D5 possesses cell-binding and heparin-binding sites, and may be a modulator of the innate immunity system [42]. Also Lumican was found. Lumican is a glycoprotein, which contains 4 sulfotyrosin; thus its adsorption might be secondary to kininogen1 (heparin is a sulfate-rich glycosaminoglycan), although a "role of lumican" in the innate immune system has been also hypothesized [43]. Mannan-binding lectine serine protease1 exerts its function in the lectin pathway of complement, which performs a key role in the innate immunity system.

It is interesting to observe that most of the proteins specifically bound to lipoplex were low-abundance proteins, either secreted or coming from cellular compartments. These proteins are related to immune response, inflammatory response, blood coagulation, acute phase, and stress, and they cover most aspects of the cellular functions and processes, including cell cycle control, cell motility, nucleotide metabolism, DNA replication, protein synthesis, glycolysis, and transport. Some groups of metabolically related proteins found together seem to outline an unexpected scenario. Actin is one of the most abundant proteins present in multicellular organisms and is the monomeric subunit of microfilaments, one of the major components of cytoskeleton, which play a very important role in cytokinesis, cell motility, cell signaling, cell division, etc. Several studies have revealed a plethora of actin-binding proteins controlling the variety of actin-based processes [44,45]. Many of these proteins have been found only in the lipoplexes protein corona (Table 4), while alpha actinin-1 and pleckstrin are present also in CLs. In the lipoplexes protein corona, proteins related to DNA replication, proteins related to nucleotide and RNA synthesis, DNA or RNA binding, and cell cycle control are also present (Table 4). All these proteins are strongly related to cellular activity. While the majority are nonsecreted proteins, many of them are typically nuclear or nuclear/cytosolic proteins and are expected to be present in human plasma at very low levels. This could mean that a complex interaction among proteins and the DNA carried by lipoplexes takes place. In addition to histones and other proteins involved in chromatin dynamic-like nucleophosmin [46], proteins that play an essential role in protein synthesis, like the elongation factors [47], are also present.

The surface of LPD complexes was found to bind 158 proteins, the largest part of which (133) were common to lipoplexes. About half of them were found in the protein corona of CLs (81). By overlapping the three formulations, it can be seen that only 12 proteins are peculiar to LPD complexes (see also Fig. 1 for these data). Among them, keratin type1 cuticolar may be a contamination, and ceruloplasmin, a protein able to bind up to 7 copper ions, may co-complex Cu^{2+} with protamine. The remaining 10 proteins were identified by only two peptides. By comparing the number of peptides per protein, which is related to the protein concentration [48], we have concluded that the LPD complexes protein corona composition is about half way between the two formulations.

Conclusion

A wide range of nanostructured systems, both viral and nonviral, capable of delivering any type of genetic material of different size is available to date. Among nonviral gene carriers, CLs have been extensively studied. However, there is still an open question about the mechanisms of their biodistribution in the body. A key role in determining the biodistribution of any nanostructured system is surely played by the plasma proteins adsorbed onto their surface. Although the exact role of each of the proteins adsorbed onto the surface of the nanoparticles in the clearance and biodistribution is still not clear, it is essential to identify the plasma proteins of the protein corona that forms when the nanoparticles are in contact with body fluids such as plasma. Therefore, studies aimed at characterizing the protein corona are fundamental for

Table 4
Identified proteins on nanoparticle surface (the three systems in the three experimental replicates, each of them achieved from the five technical replicates); proteins identified by a single unique peptide are not considered.

Protein	Protein probability	Percentage coverage	Unique peptides	Description	CLs	Lipoplexes	LPD complexes
A6NIZ1|RP1BL_HUMAN	1	7.6	2	Ras-related protein Rap-1b-like protein	X		X
B2RPK0|HGB1A_HUMAN	0.9967	12.8	3	Putative high mobility group protein B1-like 1			X
O00299|CLIC1_HUMAN	0.9999	15.8	3	Chloride intracellular channel protein 1		X	
O14791|APOL1_HUMAN	0.9302	6.5	2	Apolipoprotein L1	X	X	X
O14818|PSA7_HUMAN	0.9999	13.3	2	Proteasome subunit alpha type-7		X	
O14950|ML12B_HUMAN	0.9999	16.4	2	Myosin regulatory light chain 12B		X	
O15144|ARPC2_HUMAN	0.9988	14.3	2	Actin-related protein 2/3 complex subunit 2		X	X
O43707|ACTN4_HUMAN	0.9873	3.4	2	Alpha-actinin-4	X		
O43866|CD5L_HUMAN	1	32.9	4	CD5 antigen-like		X	
O60234|GMFG_HUMAN	0.9822	19	2	Glia maturation factor gamma		X	
O60361|NDK8_HUMAN	0.999	13.9	2	Putative nucleoside diphosphate kinase		X	
O60814|H2B1K_HUMAN	1	38.1	7	Histone H2B type 1-K		X	X
O75083|WDR1_HUMAN	1	17.3	3	WD repeat-containing protein 1		X	X
O75874|IDHC_HUMAN	0.9999	8.9	2	Isocitrate dehydrogenase [NADP] cytoplasmic		X	
O76009|KT33A_HUMAN	0.9977	9.9	3	Keratin, type I cuticular Ha3-I			X
O95445|APOM_HUMAN	1	26.1	4	Apolipoprotein M	X		
P00450|CERU_HUMAN	0.9994	8.1	4	Ceruloplasmin			X
P00488|F13A_HUMAN	0.999	6	2	Coagulation factor XIII A chain	X	X	
P00558|PGK1_HUMAN	1	26.1	8	Phosphoglycerate kinase 1		X	X
P00734|THRB_HUMAN	1	60.6	73	Prothrombin	X	X	X
P00736|C1R_HUMAN	1	9.1	2	Complement C1r subcomponent	X		X
P00738|HPT_HUMAN	1	29.6	5	Haptoglobin	X	X	X
P00739|HPTR_HUMAN	0.9997	9.8	2	Haptoglobin-related protein		X	
P00740|FA9_HUMAN	1	47.9	21	Coagulation factor IX	X		X
P00742|FA10_HUMAN	1	36.1	17	Coagulation factor X	X		
P00747|PLMN_HUMAN	1	33.6	10	Plasminogen		X	X
P00751|CFAB_HUMAN	1	25.1	12	Complement factor B	X	X	X
P01009|A1AT_HUMAN	1	41.4	16	Alpha-1-antitrypsin	X	X	X
P01011|AACT_HUMAN	1	14.7	2	Alpha-1-antichymotrypsin		X	X
P01023|A2MG_HUMAN	0.9984	3	2	Alpha-2-macroglobulin	X	X	X
P01024|CO3_HUMAN	1	72.2	154	Complement C3	X	X	X
P01031|CO5_HUMAN	1	14.5	15	Complement C5	X	X	X
P01042|KNG1_HUMAN	1	32.1	33	Kininogen-1	X		X
P01591|IGJ_HUMAN	0.9996	23.3	2	Immunoglobulin J chain		X	
P01620|KV302_HUMAN	0.9991	31.2	2	Ig kappa chain V-III region SIE		X	X
P01625|KV402_HUMAN	0.9986	23.7	2	Ig kappa chain V-IV region Len		X	
P01765|HV304_HUMAN	1	16.5	2	Ig heavy chain V-III region TIL		X	X
P01766|HV305_HUMAN	1	16	2	Ig heavy chain V-III region BRO		X	
P01834|IGKC_HUMAN	1	82.1	11	Ig kappa chain C region	X	X	X
P01842|LAC_HUMAN	1	65.7	7	Ig lambda chain C regions	X	X	X
P01857|IGHG1_HUMAN	1	41.5	10	Ig gamma-1 chain C region	X	X	X
P01859|IGHG2_HUMAN	1	39	6	Ig gamma-2 chain C region		X	X
P01860|IGHG3_HUMAN	1	53.1	3	Ig gamma-3 chain C region		X	X
P01861|IGHG4_HUMAN	1	39.1	2	Ig gamma-4 chain C region		X	X
P01871|IGHM_HUMAN	1	44.5	16	Ig mu chain C region	X	X	X
P01876|IGHA1_HUMAN	1	34.8	10	Ig alpha-1 chain C region	X	X	X
P02647|APOA1_HUMAN	1	41.2	11	Apolipoprotein A-I	X	X	X
P02649|APOE_HUMAN	1	50.5	16	Apolipoprotein E	X	X	X
P02652|APOA2_HUMAN	1	69	13	Apolipoprotein A-II	X	X	X
P02654|APOC1_HUMAN	0.9998	24.1	2	Apolipoprotein C-I		X	X
P02655|APOC2_HUMAN	1	52.5	7	Apolipoprotein C-II	X	X	X
P02656|APOC3_HUMAN	1	58.6	8	Apolipoprotein C-III	X	X	X
P02671|FIBA_HUMAN	1	49.2	73	Fibrinogen alpha chain	X	X	X
P02675|FIBB_HUMAN	1	75.6	81	Fibrinogen beta chain	X	X	X
P02679|FIBG_HUMAN	1	62	55	Fibrinogen gamma chain	X	X	X
P02730|B3AT_HUMAN	0.9998	5.5	2	Band 3 anion transport protein		X	
P02735|SAA_HUMAN	1	27.9	2	Serum amyloid A protein	X	X	X
P02741|CRP_HUMAN	0.9784	11.2	3	C-reactive protein			X
P02745|C1QA_HUMAN	1	41.2	19	Complement C1q subcomponent subunit A		X	X
P02746|C1QB_HUMAN	1	49.8	22	Complement C1q subcomponent subunit B		X	X
P02747|C1QC_HUMAN	1	50.6	15	Complement C1q subcomponent subunit C		X	X
P02748|CO9_HUMAN	1	18.6	9	Complement component C9	X	X	X
P02749|APOH_HUMAN	1	22	4	Beta-2-glycoprotein 1		X	X
P02751|FINC_HUMAN	1	3.3	4	Fibronectin	X	X	X
P02760|AMBP_HUMAN	1	25.3	7	Protein AMBP	X	X	X
P02763|A1AG1_HUMAN	0.9994	12.4	3	Alpha-1-acid glycoprotein 1			X
P02765|FETUA_HUMAN	0.9993	19.3	3	Alpha-2-HS-glycoprotein	X	X	X
P02766|TTHY_HUMAN	1	68	9	Transthyretin	X	X	X
P02768|ALBU_HUMAN	1	69	63	Serum albumin	X	X	X
P02774|VTDB_HUMAN	0.9998	5.5	2	Vitamin D-binding protein		X	X
P02775|CXCL7_HUMAN	0.9988	30.5	3	Platelet basic protein	X	X	X
P02776|PLF4_HUMAN	1	35.6	3	Platelet factor 4	X	X	

(*continued on next page*)

Table 4 (*continued*)

Protein	Protein probability	Percentage coverage	Unique peptides	Description	CLs	Lipoplexes	LPD complexes
P02787|TRFE_HUMAN	1	15	6	Serotransferrin	X	X	X
P02788|TRFL_HUMAN	0.998	3	2	Lactotransferrin		X	
P02790|HEMO_HUMAN	0.9999	7.4	3	Hemopexin		X	X
P04003|C4BPA_HUMAN	1	62.5	37	C4b-binding protein alpha chain	X	X	X
P04004|VTNC_HUMAN	1	44.1	34	Vitronectin	X	X	X
P04070|PROC_HUMAN	1	31.2	13	Vitamin K-dependent protein C	X		
P04075|ALDOA_HUMAN	0.9999	16.2	4	Fructose-bisphosphate aldolase A		X	
P04114|APOB_HUMAN	1	34.8	112	Apolipoprotein B-100	X	X	X
P04196|HRG_HUMAN	1	10.5	4	Histidine-rich glycoprotein	X	X	
P04220|MUCB_HUMAN	1	44	2	Ig mu heavy chain disease protein	X	X	
P04264|K2C1_HUMAN	1	13.2	8	Keratin, type II cytoskeletal 1	X	X	X
P04275|VWF_HUMAN	0.9994	1.1	2	von Willebrand factor		X	
P04350|TBB4_HUMAN	1	11.5	2	Tubulin beta-4 chain	X		X
P04406|G3P_HUMAN	1	7.2	2	Glyceraldehyde-3-phosphate dehydrogenase	X	X	X
P05090|APOD_HUMAN	1	10.1	4	Apolipoprotein D	X		X
P05106|ITB3_HUMAN	0.9903	3.2	2	Integrin beta-3	X	X	
P05154|IPSP_HUMAN	0.9953	6.2	2	Plasma serine protease inhibitor			X
P05546|HEP2_HUMAN	1	60.3	28	Heparin cofactor 2	X	X	X
P06396|GELS_HUMAN	1	44.4	25	Gelsolin	X	X	X
P06576|ATPB_HUMAN	1	9.1	2	ATP synthase subunit beta, mitochondrial		X	
P06702|S10A9_HUMAN	0.9993	13.2	2	Protein S100-A9		X	
P06727|APOA4_HUMAN	1	51.5	18	Apolipoprotein A-IV	X	X	X
P06733|ENOA_HUMAN	1	34.6	10	Alpha-enolase		X	X
P06744|G6PI_HUMAN	1	2.7	2	Glucose-6-phosphate isomerase		X	
P06748|NPM_HUMAN	0.9999	7.1	2	Nucleophosmin		X	X
P06753|TPM3_HUMAN	1	5.2	2	Tropomyosin alpha-3 chain	X	X	X
P07195|LDHB_HUMAN	1	20.7	6	L-lactate dehydrogenase B chain		X	X
P07225|PROS_HUMAN	1	46.9	31	Vitamin K-dependent protein S	X	X	X
P07339|CATD_HUMAN	0.9996	11.2	2	Cathepsin D		X	X
P07355|ANXA2_HUMAN	0.9999	8.8	2	Annexin A2		X	
P07357|CO8A_HUMAN	1	5.1	2	Complement component C8 alpha chain	X	X	X
P07358|CO8B_HUMAN	0.9997	9.1	2	Complement component C8 beta chain	X	X	X
P07360|CO8G_HUMAN	1	33.2	4	Complement component C8 gamma chain	X	X	X
P07437|TBB5_HUMAN	1	18.9	4	Tubulin beta chain	X	X	X
P07737|PROF1_HUMAN	1	44.3	8	Profilin-1		X	X
P07900|HS90A_HUMAN	1	34.8	18	Heat shock protein HSP 90-alpha		X	X
P07996|TSP1_HUMAN	1	6	4	Thrombospondin-1	X	X	X
P08134|RHOC_HUMAN	0.9998	13.5	2	Rho-related GTP-binding protein RhoC		X	
P08514|ITA2B_HUMAN	1	6.9	3	Integrin alpha-IIb	X	X	X
P08519|APOA_HUMAN	1	43.9	27	Apolipoprotein(a)	X	X	X
P08567|PLEK_HUMAN	1	13.7	4	Pleckstrin	X	X	
P08571|CD14_HUMAN	1	14.7	4	Monocyte differentiation antigen CD14		X	X
P08603|CFAH_HUMAN	1	9.2	7	Complement factor H		X	X
P08697|A2AP_HUMAN	0.9999	14.7	3	Alpha-2-antiplasmin		X	X
P08709|FA7_HUMAN	1	14.2	4	Coagulation factor VII	X		
P08758|ANXA5_HUMAN	0.9989	9.7	2	Annexin A5		X	
P09429|HMGB1_HUMAN	1	23.3	4	High mobility group protein B1		X	X
P09651|ROA1_HUMAN	1	25.3	5	Heterogeneous nuclear ribonucleoprotein A1		X	X
P09871|C1S_HUMAN	1	48	29	Complement C1s subcomponent	X		X
P09874|PARP1_HUMAN	1	7.3	4	Poly [ADP-ribose] polymerase 1		X	
P0C0L4|CO4A_HUMAN	1	45	60	Complement C4-A	X		
P0C0L5|CO4B_HUMAN	1	45	61	Complement C4-B	X	X	X
P10412|H14_HUMAN	1	13.1	4	Histone H1.4		X	X
P10643|CO7_HUMAN	1	14.7	8	Complement component C7	X	X	X
P10809|CH60_HUMAN	0.9993	7.5	2	60 kDa heat shock protein, mitochondrial		X	
P10909|CLUS_HUMAN	1	41.4	33	Clusterin	X	X	X
P11021|GRP78_HUMAN	1	10.1	4	78 kDa glucose-regulated protein		X	
P11142|HSP7C_HUMAN	1	38.4	19	Heat shock cognate 71 kDa protein		X	X
P11597|CETP_HUMAN	0.9785	8.7	2	Cholesteryl ester transfer protein	X	X	X
P11908|PRPS2_HUMAN	0.9913	10.4	2	Ribose-phosphate pyrophosphokinase 2		X	
P12004|PCNA_HUMAN	1	16.1	3	Proliferating cell nuclear antigen		X	X
P12259|FA5_HUMAN	1	15.5	21	Coagulation factor V	X		
P12814|ACTN1_HUMAN	1	12.8	9	Alpha-actinin-1		X	
P13639|EF2_HUMAN	1	21.6	9	Elongation factor 2		X	X
P13645|K1C10_HUMAN	1	18.5	6	Keratin, type I cytoskeletal 10	X	X	X
P13671|CO6_HUMAN	1	6.6	3	Complement component C6	X	X	X
P13796|PLSL_HUMAN	1	12	3	Plastin-2		X	X
P14618|KPYM_HUMAN	1	41.1	18	Pyruvate kinase isozymes M1/M2		X	X
P14625|ENPL_HUMAN	1	7.2	2	Endoplasmin		X	
P15311|EZRI_HUMAN	0.9991	16.6	4	Ezrin			X
P17987|TCPA_HUMAN	0.9992	12.9	2	T-complex protein 1 subunit alpha		X	
P18206|VINC_HUMAN	0.9995	6.7	4	Vinculin	X	X	
P18428|LBP_HUMAN	1	29.9	12	Lipopolysaccharide-binding protein	X	X	X
P19338|NUCL_HUMAN	0.9999	9.4	2	Nucleolin		X	X

Table 4 (*continued*)

Protein	Protein probability	Percentage coverage	Unique peptides	Description	CLs	Lipoplexes	LPD complexes
P19823|ITIH2_HUMAN	1	48.7	52	Inter-alpha-trypsin inhibitor heavy chain H2	X	X	X
P19827|ITIH1_HUMAN	1	41.9	39	Inter-alpha-trypsin inhibitor heavy chain H1	X	X	X
P20618|PSB1_HUMAN	0.9982	15.8	2	Proteasome subunit beta type-1		X	
P20851|C4BPB_HUMAN	1	30.2	7	C4b-binding protein beta chain	X		X
P21333|FLNA_HUMAN	0.9995	0.9	2	Filamin-A	X	X	X
P21926|CD9_HUMAN	0.9991	15.4	2	CD9 antigen		X	
P22314|UBA1_HUMAN	0.9999	7.5	5	Ubiquitin-like modifier-activating enzyme 1		X	
P22626|ROA2_HUMAN	1	10.2	2	Heterogeneous nuclear ribonucleoproteins A2/B1		X	
P22891|PROZ_HUMAN	1	23.5	9	Vitamin K-dependent protein Z	X		
P23528|COF1_HUMAN	1	31.9	4	Cofilin-1		X	X
P25787|PSA2_HUMAN	1	26.5	5	Proteasome subunit alpha type-2		X	X
P26038|MOES_HUMAN	1	35.7	15	Moesin		X	X
P27169|PON1_HUMAN	1	74.1	33	Serum paraoxonase/arylesterase 1	X	X	X
P27797|CALR_HUMAN	0.9974	18	3	Calreticulin		X	X
P27918|PROP_HUMAN	1	19.8	10	Properdin	X	X	X
P28066|PSA5_HUMAN	1	12.9	2	Proteasome subunit alpha type-5			X
P28838|AMPL_HUMAN	0.9999	7.7	3	Cytosol aminopeptidase		X	X
P29401|TKT_HUMAN	0.9937	7.7	2	Transketolase		X	
P30101|PDIA3_HUMAN	1	12.5	4	Protein disulfide-isomerase A3		X	
P31146|COR1A_HUMAN	1	23.9	7	Coronin-1A		X	X
P31939|PUR9_HUMAN	1	8.4	2	Bifunctional purine biosynthesis protein PURH		X	
P31946|1433B_HUMAN	0.9779	8.9	2	14-3-3 protein beta/alpha			X
P32119|PRDX2_HUMAN	0.9899	14.6	3	Peroxiredoxin-2			X
P34096|RNAS4_HUMAN	0.9993	21.8	2	Ribonuclease 4		X	
P35443|TSP4_HUMAN	1	5.9	2	Thrombospondin-4	X		
P35527|K1C9_HUMAN	1	17.8	6	Keratin, type I cytoskeletal 9	X	X	X
P35542|SAA4_HUMAN	0.9772	17.7	2	Serum amyloid A-4 protein	X	X	X
P35579|MYH9_HUMAN	1	8.2	10	Myosin-9	X	X	X
P35908|K22E_HUMAN	1	12.8	5	Keratin, type II cytoskeletal 2 epidermal	X	X	X
P36873|PP1G_HUMAN	0.9894	10.8	2	Serine/threonine-protein phosphatase PP1-gamma catalytic subunit		X	
P37802|TAGL2_HUMAN	1	32.7	4	Transgelin-2		X	
P40227|TCPZ_HUMAN	0.9991	7.5	2	T-complex protein 1 subunit zeta		X	
P40925|MDHC_HUMAN	0.9999	15	3	Malate dehydrogenase, cytoplasmic		X	
P46777|RL5_HUMAN	1	11.8	2	60S ribosomal protein L5		X	
P47756|CAPZB_HUMAN	1	24.5	4	F-actin-capping protein subunit beta		X	X
P48740|MASP1_HUMAN	1	18.5	7	Mannan-binding lectin serine protease 1	X		
P49720|PSB3_HUMAN	1	25.9	5	Proteasome subunit beta type-3		X	X
P49747|COMP_HUMAN	1	15.5	7	Cartilage oligomeric matrix protein	X		X
P50395|GDIB_HUMAN	1	18.9	8	Rab GDP dissociation inhibitor beta		X	X
P51884|LUM_HUMAN	1	36.4	14	Lumican	X		
P51991|ROA3_HUMAN	0.9971	9	2	Heterogeneous nuclear ribonucleoprotein A3		X	
P52209|6PGD_HUMAN	0.9999	4.8	2	6-phosphogluconate dehydrogenase, decarboxylating		X	
P52907|CAZA1_HUMAN	1	22	4	F-actin-capping protein subunit alpha-1		X	X
P55056|APOC4_HUMAN	0.9896	20.5	2	Apolipoprotein C-IV		X	
P55058|PLTP_HUMAN	1	15.8	4	Phospholipid transfer protein		X	X
P55209|NP1L1_HUMAN	1	17.1	3	Nucleosome assembly protein 1-like 1		X	
P59665|DEF1_HUMAN	0.9129	20.2	2	Neutrophil defensin 1		X	
P60174|TPIS_HUMAN	1	18.1	3	Triosephosphate isomerase		X	X
P60660|MYL6_HUMAN	1	19.2	3	Myosin light polypeptide 6	X	X	
P60709|ACTB_HUMAN	1	60.5	10	Actin, cytoplasmic 1	X	X	X
P60900|PSA6_HUMAN	1	15.9	3	Proteasome subunit alpha type-6		X	X
P60953|CDC42_HUMAN	0.9962	25.7	2	Cell division control protein 42 homolog		X	
P61158|ARP3_HUMAN	1	19.9	4	Actin-related protein 3		X	X
P61204|ARF3_HUMAN	0.9995	9.9	2	ADP-ribosylation factor 3		X	
P61224|RAP1B_HUMAN	1	35.3	4	Ras-related protein Rap-1b		X	X
P61978|HNRPK_HUMAN	1	9.5	2	Heterogeneous nuclear ribonucleoprotein K		X	
P62805|H4_HUMAN	1	41.7	5	Histone H4		X	X
P62937|PPIA_HUMAN	1	58.8	10	Peptidyl-prolyl cis-trans isomerase A		X	X
P63104|1433Z_HUMAN	1	29	5	14-3-3 protein zeta/delta		X	X
P67936|TPM4_HUMAN	1	29	5	Tropomyosin alpha-4 chain		X	
P68104|EF1A1_HUMAN	1	46.8	11	Elongation factor 1-alpha 1		X	X
P68363|TBA1B_HUMAN	0.9995	7.1	2	Tubulin alpha-1B chain	X		X
P68366|TBA4A_HUMAN	0.9991	7.4	2	Tubulin alpha-4A chain	X		
P68431|H31_HUMAN	0.9985	19.9	3	Histone H3.1		X	
P68871|HBB_HUMAN	1	82.3	9	Hemoglobin subunit beta	X	X	X
P69905|HBA_HUMAN	1	76.8	11	Hemoglobin subunit alpha	X	X	X
P78371|TCPB_HUMAN	0.998	12	2	T-complex protein 1 subunit beta		X	
P78386|KRT85_HUMAN	0.9999	14.2	10	Keratin, type II cuticular Hb5			X
Q00839|HNRPU_HUMAN	1	12.7	7	Heterogeneous nuclear ribonucleoprotein U		X	X
Q01105|SET_HUMAN	0.9992	8.3	2	Protein SET			X
Q01518|CAP1_HUMAN	1	26.3	6	Adenylyl cyclase-associated protein 1		X	
Q06033|ITIH3_HUMAN	1	41.3	42	Inter-alpha-trypsin inhibitor heavy chain H3	X		X

(*continued on next page*)

Table 4 (*continued*)

Protein	Protein probability	Percentage coverage	Unique peptides	Description	CLs	Lipoplexes	LPD complexes
Q06830|PRDX1_HUMAN	1	31.2	5	Peroxiredoxin-1		X	X
Q09028|RBBP4_HUMAN	0.9999	17.2	4	Histone-binding protein RBBP4		X	
Q12905|ILF2_HUMAN	1	9.5	2	Interleukin enhancer-binding factor 2		X	
Q13103|SPP24_HUMAN	1	17.5	3	Secreted phosphoprotein 24		X	X
Q13201|MMRN1_HUMAN	1	3.7	3	Multimerin-1		X	
Q13418|ILK_HUMAN	0.9632	11.7	2	Integrin-linked protein kinase		X	
Q13790|APOF_HUMAN	1	24.4	8	Apolipoprotein F	X		X
Q14103|HNRPD_HUMAN	0.9997	9.9	2	Heterogeneous nuclear ribonucleoprotein D0		X	X
Q14520|HABP2_HUMAN	1	34.1	22	Hyaluronan-binding protein 2	X	X	X
Q14624|ITIH4_HUMAN	1	9	4	Inter-alpha-trypsin inhibitor heavy chain H4		X	X
Q15404|RSU1_HUMAN	0.9996	24.2	2	Ras suppressor protein 1		X	
Q16658|FSCN1_HUMAN	0.9937	4.5	2	Fascin		X	X
Q6Q788|APOA5_HUMAN	0.9999	15.6	3	Apolipoprotein A-V		X	
Q86UX7|URP2_HUMAN	1	16.6	5	Fermitin family homolog 3		X	
Q92688|AN32B_HUMAN	1	25.1	4	Acidic leucine-rich nuclear phosphoprotein 32 family member B		X	X
Q92928|RAB1C_HUMAN	0.9998	8.5	2	Putative Ras-related protein Rab-1C		X	
Q92954|PRG4_HUMAN	0.9994	3.6	2	Proteoglycan 4		X	
Q96KN2|CNDP1_HUMAN	1	60.9	28	Beta-Ala-His dipeptidase	X		
Q96PD5|PGRP2_HUMAN	1	12.3	3	*N*-acetylmuramoyl-L-alanine amidase		X	
Q99832|TCPH_HUMAN	1	8.7	2	T-complex protein 1 subunit eta		X	X
Q9BTT0|AN32E_HUMAN	0.996	12.3	2	Acidic leucine-rich nuclear phosphoprotein 32 family member E		X	X
Q9BWP8|COL11_HUMAN	1	18.8	4	Collectin-11	X	X	
Q9BXR6|FHR5_HUMAN	1	32	7	Complement factor H-related protein 5		X	X
Q9H299|SH3L3_HUMAN	0.999	31.2	2	SH3 domain-binding glutamic acid-rich-like protein 3		X	
Q9H4B7|TBB1_HUMAN	1	14	3	Tubulin beta-1 chain	X		
Q9HBI1|PARVB_HUMAN	0.9998	8	2	Beta-parvin		X	
Q9NQ79|CRAC1_HUMAN	0.999	6.5	2	Cartilage acidic protein 1	X		
Q9UK55|ZPI_HUMAN	1	21.4	4	Protein Z-dependent protease inhibitor	X		X
Q9UQ80|PA2G4_HUMAN	1	18	3	Proliferation-associated protein 2G4		X	
Q9Y490|TLN1_HUMAN	1	11.1	14	Talin-1	X	X	X
Total proteins					105	208	158

the identification of a correlation between the composition of the adsorbed protein corona and the complex biodistribution *in vivo*. Such investigations can therefore help those who are engaged in the construction of gene delivery nanocarriers. When the relationship between the physical–chemical properties of nanovectors and the composition of the adsorbed corona is elucidated, it will be possible to design gene delivery vectors capable of binding selectively certain proteins rather than others. In this way, it will be possible to steer their biodistribution in order to carry out efficient and effective gene therapy.

Appendix A. Supplementary data

Supplementary data associated with this article can be found, in the online version, at doi:10.1016/j.ab.2011.08.003.

References

[1] E. Marshall, Gene therapy. What to do when clear success comes with an unclear risk?, Science 298 (2002) 510–511
[2] T.I. Kim, M. Ou, M. Lee, S.W. Kim, Arginine-grafted bioreducible poly(disulfide amine) for gene delivery systems, Biomaterials 30 (2009) 658–664.
[3] M.A. Mintzer, E.E. Simanek, Nonviral vectors for gene delivery, Chem. Rev. 109 (2009) 259–302.
[4] P.L. Felgner, T.R. Gadek, M. Holm, R. Roman, H.W. Chan, M. Wenz, J.P. Northrop, G.M. Ringold, M. Danielsen, Lipofection: a highly efficient, lipid-mediated DNA-transfection procedure, Proc. Natl. Acad. Sci. USA 84 (1987) 7413–7417.
[5] H. Gershon, R. Ghirlando, S.B. Guttman, A. Minsky, Mode of formation and structural features of DNA-cationic liposome complexes used for transfection, Biochemistry 32 (1993) 7143–7151.
[6] J. Gustafsson, G. Arvidson, G. Karlsson, M. Almgren, Complexes between cationic liposomes and DNA visualized by cryo-TEM, Biochim. Biophys. Acta Biomembr. 1235 (1995) 305–312.
[7] I. Koltover, T. Salditt, J.O. Radler, C.R. Safinya, An inverted hexagonal phase of cationic liposome–DNA complexes related to DNA release and delivery, Science 281 (1998) 78–81.
[8] D.D. Lasic, H. Strey, M.C.A. Stuart, R. Podgornik, P.M. Frederik, The structure of DNA–liposome complexes, J. Am. Chem. Soc. 119 (1997) 232–233.
[9] J.O. Radler, I. Koltover, T. Salditt, C.R. Safinya, Structure of DNA–cationic liposome complexes: DNA intercalation in multilamellar membranes in distinct interhelical packing regimes, Science 275 (1997) 791–792.
[10] H.E.J. Hofland, L. Shephard, S.M. Sullivan, Formation of stable cationic lipid/DNA complexes for gene transfer, Proc. Natl. Acad. Sci. USA 93 (1996) 7305–7309.
[11] N. Ballas, N. Zakai, I. Sela, A. Loyter, A. Loyter, Liposomes bearing a quaternary ammonium detergent as an efficient vehicle for functional transfer of TMV-RNA into plant protoplasts, Biochim. Biophys. Acta Biomembr. 939 (1988) 8–18.
[12] B. Li, S. Li, Y. Tan, D.B. Stolz, S.C. Watkins, L.H. Block, L. Huang, Lyophilization of cationic lipid–protamine–DNA (LPD) complexes, J. Pharm. Sci. 89 (2000) 355–364.
[13] K. Hong, W. Zheng, A. Baker, D. Papahadjopoulos, Stabilization of cationic liposome–plasmid DNA complexes by polyamines and poly(ethylene glycol)-phospholipid conjugates for efficient in vivo gene delivery, FEBS Lett. 400 (1997) 233–237.
[14] P.C. Ross, M.L. Hensen, R. Supabphol, S.W. Hui, Multilamellar cationic liposomes are efficient vectors for in vitro gene transfer in serum, J. Liposome Res. 8 (1998) 499–520.
[15] R. Leventis, J.R. Silvius, Interactions of mammalian cells with lipid dispersions containing novel metabolizable cationic amphiphiles, Biochim. Biophys. Acta Biomembr. 1023 (1990) 124–132.
[16] J.K. Rose, L. Buonocore, M.A. Witt, A new cationic liposome reagent mediating nearly quantitative transfection of animal cells, BioTechniques 10 (4) (1991) 520–525.
[17] X. Gao, L. Huang, A novel cationic liposome reagent for efficient transfection of mammalian cells, Biochem. Biophys. Res. Commun. 179 (1991) 280–285.
[18] P.L. Felgner, T.R. Gadek, M. Holm, R. Roman, H.W. Chan, M. Wenz, J.P. Northrop, G.M. Ringold, N. Danielsen, Lipofection: a highly efficient, lipid-mediated DNA-transfection procedure, Proc. Natl. Acad. Sci. USA 84 (1987) 7413–7417.
[19] J.H. Felgner, R. Kumar, C.N. Sridhar, C.J. Wheeler, Y.J. Tsai, R. Border, P. Ramsey, M. Martin, P.L. Felgner, Enhanced gene delivery and mechanism studies with a novel series of cationic lipid formulations, J. Biol. Chem. 269 (1994) 2550–2561.
[20] G. Caracciolo, R. Caminiti, D. Pozzi, M. Friello, F. Boffi, A.C. Castellano, Self-assembly of cationic liposomes–DNA complexes: a structural and thermodynamic study by EDXD, Chem. Phys. Lett. 351 (2002) 222–228.
[21] K. Kogure, R. Moriguchi, K. Sasaki, M. Ueno, S. Futaki, H. Harashima, Development of efficient packaging method of oligodeoxynucleotides by a

condensed nano particle in lipid envelope structure, J. Controlled Release 98 (2004) 317–323.
[22] J. Yamauchi, Y. Hayashi, K. Kajimoto, H. Akita, H. Harashima, Comparison between a multifunctional envelope-type nano device and lipoplex for delivery to the liver, Biol. Pharm. Bull. 33 (2010) 926–929.
[23] T. Cedervall, I. Lynch, S. Lindman, T. Berggard, E. Thulin, H. Nilsson, K.A. Dawson, S. Linse, Understanding the nanoparticle–protein corona using methods to quantify exchange rates and affinities of proteins for nanoparticles, Proc. Natl. Acad. Sci. USA 104 (2007) 2050–2055.
[24] B. Sahoo, M. Goswami, S. Nag, S. Maiti, Spontaneous formation of a protein corona prevents the loss of quantum dot fluorescence in physiological buffers, Chem. Phys. Lett. 445 (2007) 217–220.
[25] I. Lynch, K.A. Dawson, Protein–nanoparticle interactions, NanoToday 3 (2008) 40–47.
[26] I. Lynch, T. Cedervall, M. Lundqvist, C. Cabaleiro-Lago, S. Linse, K.A. Dawson, The nanoparticle–protein complex as a biological entity: a complex fluids and surface science challenge for the 21st century, Adv. Colloid Interface Sci. 134/135 (2007) 167–74.
[27] D.E. Owens III, N.A. Peppas, Opsonization, biodistribution, and pharmacokinetics of polymeric nanoparticles, Int. J. Pharm. 307 (2006) 93–102.
[28] R. Gref, Y. Minamitake, M.T. Peracchia, V. Trubetskoy, V. Torchilin, R. Langer, Biodegradable long-circulating polymeric nanospheres, Science 263 (1994) 1600–1603.
[29] L. Illum, S.S. Davis, The organ uptake of intravenously administered colloidal particles can be altered using a non-ionic surfactant (Poloxamer-338), FEBS Lett. 167 (1984) 79–82.
[30] G. Kaul, M. Amiji, Long-circulating poly(ethylene glycol)-modified gelatin nanoparticles for intracellular delivery, Pharm. Res. 19 (2002) 1061–1067.
[31] G. Caracciolo, D. Pozzi, R. Caminiti, Lipid mixing upon deoxyribonucleic acid-induced liposomes fusion investigated by synchrotron small-angle X-ray scattering, Appl. Phys. Lett. 87 (2005) 133901–133903.
[32] A.L. Capriotti, G. Caracciolo, C. Caruso, D. Pozzi, R. Samperi, A. Laganà, Analysis of plasma protein adsorption onto DC-Chol-DOPE cationic liposomes by HPLC-CHIP coupled to a Q-TOF mass spectrometer, Anal. Bional. Chem. 389 (2010) 2777–2894.
[33] A. Keller, A.I. Nesvizhskii, E. Kolker, R. Aebersold, Empirical statistical model to estimate the accuracy of peptide identifications made by MS/MS and database search, Anal. Chem. 74 (2002) 383–392.
[34] A. Keller, J. Eng, N. Zhang, X.J. Li, R. Aebersold, A uniform proteomics MS/MS analysis platform utilizing open XML file formats, Mol. Syst. Biol. 1 (2005) 1–8.
[35] A.I. Nesvizhskii, A. Keller, E. Kolker, R. Aebersold, A statistical model for identifying proteins by tandem mass spectrometry, Anal. Chem. 75 (2003) 4646–4658.
[36] E.C. Yi, M. Marelli, H. Lee, S.O. Purvine, R. Aebersold, J.D. Aitchison, D.R. Goodlett, Approaching complete peroxisome characterization by gas-phase fractionation, Electrophoresis 23 (2002) 3205–3216.
[37] C.S. Spahr, M.T. Davis, M.D. McGinley, J.H. Robinson, E.J. Bures, J. Beierle, J. Mort, P.L. Courchesne, K. Chen, R.C. Wahl, W. Yu, R. Luethy, S.D. Patterson, Towards defining the urinary proteome using liquid chromatography-tandem mass spectrometry. I. Profiling an unfractionated tryptic digest, Proteomics 1 (2001) 93–107.
[38] E.C. Koc, W. Burkhart, K. Blackburn, M.B. Moyer, D.M. Schlatzer, A. Moseley, L.L. Spremulli, The large subunit of the mammalian mitochondrial ribosome. Analysis of the complement of ribosomal proteins present, J. Biol. Chem. 276 (2001) 43958–43969.
[39] N.V. Welham, M. Yamashita, S.H. Choi, C. Ling, Cross-sample validation provides enhanced proteome coverage in rat vocal fold mucosa, PLoS One 6 (2011) e17754.
[40] P.D. von Haller, E. Yi, S. Donohoe, K. Vaughn, A. Keller, A.I. Nesvizhskii, J. Eng, X. Li, D.R. Goodlett, R. Aebersold, J.D. Watts, The application of new software tools to quantitative protein profiling via isotope-coded affinity tag (ICAT) and tandem mass spectrometry, Mol. Cell. Proteomics 2 (2003) 428–442.
[41] J.N. Sharma, G.J. Al-Sherif, The kinin system: present and future pharmacological targets, Am. J. Biomed. Sci. 3 (2) (2011) 156–169.
[42] G. Lalmanach, C. Naudin, F. Lecaille, H. Fritz, Kininogens: more than cysteine protease inhibitors and kinin precursors, Biochimie 92 (2010) 1568–1579.
[43] F. Wu, N. Vij, L. Roberts, S. Lopez-Briones, S. Joyce, S. Chakravarti, A novel role of the lumican core protein in bacterial lipopolysaccharide-induced innate immune response, J. Biol. Chem. 282 (2007) 26409–26417.
[44] A. Disanza, A. Steffen, M. Hertzog, E. Frittoli, K. Rottnerd, G. Scita, Actin polymerization machinery: the finish line of signaling networks, the starting point of cellular movement, Cell. Mol. Life Sci. 62 (2005) 955–970.
[45] J. Saarikangas, H. Zhao, P. Lappalainen, Regulation of the actin cytoskeleton-plasma membrane interplay by phosphoinositides, Physiol. Rev. 90 (2010) 259–289.
[46] S.S. Gadad, P. Senapati, S.H. Syed, R.E. Rajan, J. Shandilya, V. Swaminathan, S. Chatterjee, E. Colombo, S. Dimitrov, P.G. Pelicci, U. Ranga, T.K. Kundu, The multifunctional protein nucleophosmin (NPM1) is a human linker histone H1 chaperone, Biochemistry 50 (2011) 2780–2789.
[47] R. Jørgensen, A.R. Merrill, G.R. Andersen, The life and death of translation elongation factor 2, Biochem. Soc. Trans. 34 (2006) 1–6.
[48] Y. Ishihama, Y. Oda, T. Tabata, T. Sato, T. Nagasu, J. Rappsilber, M. Mann, Exponentially modified protein abundance index (emPAI) for estimation of absolute protein amount in proteomics by the number of sequenced peptides per protein, Mol. Cell Proteomics 4 (2005) 1265–1272.

VII

Anal Bioanal Chem
DOI 10.1007/s00216-011-5691-y

ORIGINAL PAPER

Label-free quantitative analysis for studying the interactions between nanoparticles and plasma proteins

Anna Laura Capriotti · Giulio Caracciolo · Giuseppe Caruso · Chiara Cavaliere · Daniela Pozzi · Roberto Samperi · Aldo Laganà

Received: 24 October 2011 / Revised: 19 December 2011 / Accepted: 21 December 2011

Abstract A shotgun proteomics approach was used to compare human plasma protein binding capability with cationic liposomes, DNA–cationic lipid complexes (lipoplexes), and lipid–polycation–DNA (LPD) complexes. Nano-high-performance liquid chromatography coupled with a high-resolution LTQ Orbitrap XL mass spectrometer was used to characterize and compare their protein corona. Spectral counting and area under curve methods were used to perform label-free quantification. Substantial qualitative and quantitative differences were found among proteins bound to the three different systems investigated. Protein variety found on lipoplexes and LPD complexes was richer than that found on cationic liposomes. There were also significant differences between the amounts of protein. Such results could help in the design of gene-delivery systems, because some proteins could be more selectively bound rather than others, and their bio-distribution could be driven in vivo for more efficient and effective gene therapy.

Keywords Label-free quantification · Proteomics · Mass spectrometry · Protein corona · Liposome · Lipoplexes · DOTAP · Gene delivery

Published in the special issue *Analytical Science in Italy* with guest editor Aldo Roda.

Electronic supplementary material The online version of this article (doi:10.1007/s00216-011-5691-y) contains supplementary material, which is available to authorized users.

A. L. Capriotti (✉) · G. Caruso · C. Cavaliere · R. Samperi · A. Laganà
Dipartimento di Chimica,
Sapienza Università di Roma,
Box no. 34 - Roma 62, Piazzale Aldo Moro 5,
00185 Roma, Italia
e-mail: annalaura.capriotti@uniroma1.it

G. Caracciolo · D. Pozzi
Dipartimento di Medicina Molecolare,
Sapienza Università di Roma,
Piazzale Aldo Moro 5,
00185 Roma, Italia

Introduction

A major objective of gene therapy is to obtain targeted vectors that could efficiently transfer genes to specific cell types. Unfortunately, until now, the lack of such delivery systems has impeded the introduction of gene therapy into clinical applications. Ideally, a gene-delivery system should be stable, biocompatible, nontoxic, and cost effective, and it should be able to transfer exogenous highly anionic genetic materials to a tissue-specific site. Viral vectors, including retroviruses, adenoviruses, and adeno-associated viruses, have high transfection efficiency and have been used in multiple clinical trials, but may ultimately be too dangerous for routine clinical use [1].

In the past two decades, much attention has been devoted to non-viral vectors: cationic liposomes (CLs) have been extensively studied [2], and DNA–cationic lipid complexes (lipoplexes) are among the favourite non-viral gene-delivery vectors. Monocationic lipids are widely used for fabrication of cationic carriers [3–5]. 1,2-Dioleoyl-3-trimethylammoniumpropane (DOTAP), a double chain quaternary ammonium surfactant, is the most popular for lipoplex formation. X-ray scattering techniques suggest that when cationic lipids are used as carriers of nucleic acids (DNA), periodic multilayer structures are often formed with DNA chains adsorbed between lipid membranes [6, 7]. Once inside the cell, such multilayer structures offer protection from DNA degradation,

Published online: 25 January 2012

but often prevent adequate DNA release from the endosomal compartments. To overcome this problem, lipid–polycation–DNA (LPD) complexes, in which plasmid DNA (pDNA) condensed with a polycation is encapsulated by a lipid envelope, have recently been developed [8]. Recent studies have demonstrated the superiority of LPD-mediated gene transfer over conventional liposomes in delivering a gene to the liver [9].

Both lipoplexes and LPD complexes are frequently given via parenteral administration. As with any foreign material, the body mounts a biological response to such administered gene-delivery vectors. Upon contact with human plasma, lipid–DNA complexes are immediately coated by proteins, and a protein corona is formed around the complexes [10–12]. Recently, the binding of plasma proteins to nanoparticles, for example gene-delivery vectors, has been identified as a critical step in determining their fate in vivo [13, 14]. First experiments were directed at isolation and identification of particle-associated proteins. These studies provided information about relevant issues, for example opsonization, suggesting possible strategies for suppressing immune responses. More recent findings [15] have revealed that the average composition of the protein corona does not reflect the relative abundance of proteins in human plasma. Over time, those with higher affinity may displace the more abundant proteins, and the resulting biomolecule "hard corona" may contain only a few proteins in a relatively immobile layer, with a more loosely bound layer that is less well understood. This is a point of substantial general interest because the most abundantly associated proteins do not necessarily have the most profound effect. Instead, a less abundant protein with high affinity and specificity for a particular receptor may be extremely important. Information on binding affinities and stoichiometry for different combinations of protein corona and nanoparticles would be highly relevant to classification of the biological effect of the complexes. Furthermore, ranking of the affinities of proteins that coexist in specific bodily fluids or cellular compartments would add valuable information. Such accurate quantitative determination could be the basis for the establishment of a correlation between protein-adsorption pattern and in vivo fate of intravenously administered nanoparticles. As a result, protein quantification is the only strategy we have to reveal the molecular basis of cell–nanoparticle interactions.

The development of non-gel-based shotgun proteomic techniques, for example multidimensional protein identification technology, has provided powerful tools for studying large scale protein expression and characterization of complex biological systems [16]. Because of the development of mass spectrometers with high resolution and high mass accuracy, label-free quantification of liquid chromatography–mass spectrometry (LC–MS) data has become a very appealing approach for quantitative analysis of biological samples. Tandem mass spectrometry (MS–MS) label-free quantification can be performed by two distinct methods:

1. spectral counting, in which the number of spectra matched to peptides from a protein is used as a surrogate measure of protein abundance; and
2. area under the curve (AUC) or signal intensity measurement, in which protein abundance is derived from the extracted ion chromatograms.

The spectral counting method relies on the simple concept that an increase in protein abundance can increase the number of its detectable proteolytic peptides, i.e. the total number of MS–MS spectra that are acquired for that peptide. Liu et al. have demonstrated a linear relationship between the spectral count and relative protein abundance over a dynamic range of two orders of magnitude [17]. The AUC method, based on precursor ion signal intensity, compares the chromatographic peaks of peptide precursor ion measurements belonging to a specific protein extracted from an LC–MS–MS run [18–20].

In this study we used a shotgun proteomics approach to characterize differences between the binding of human plasma proteins to the surface of DOTAP CLs, DOTAP–DNA lipoplexes, and LPD complexes [21]. LC–MS–MS was selected as the most suitable method for analysis of the protein adsorption patterns. This method has been used successfully in areas such as protein analysis of cell and body fluids in general and, subsequently, in clinical diagnosis. Recently, LC–MS–MS was established for analysis of adsorbed proteins on nanoparticles for gene delivery [22]. Nano-high-performance liquid chromatography (nano-HPLC) coupled with a high-resolution LTQ Orbitrap XL (Thermo Fisher Scientific) mass spectrometer was used for SC and AUC label-free relative quantification of the investigated samples. Label-free comparative proteomics is a relatively new approach that has been used successfully for different systems (humans, yeast, fly, etc.) [23–26]; as far as we are aware its application to nanoparticle–protein interactions has not yet been investigated.

Experimental

Chemicals and reagents

DOTAP cationic lipid was purchased from Avanti Polar Lipids (Alabaster, AL, USA) and used without further purification. Calf thymus (CT) Na-DNA and protamine sulfate salt (P) from salmon (m.w.=5.1 kDa) were purchased from Sigma–Aldrich (St Louis, MO, USA). Ethylenediaminetetraacetic acid (EDTA), tris(hydroxymethyl)aminomethane (TRIS), sodium chloride, polyacrylamide, 1,4-dithiothreitol

(DTT), iodoacetamide (IAA), ammonium bicarbonate, protein molecular weight standards, and Coomassie PhastGel Blue R-350 were all purchased from GE Healthcare (Amersham Biosciences, Uppsala, Sweden). All organic solvents were the highest grade available from Carlo Erba Reagents (Milan, Italy). Ultrapure water was produced from distilled water by use of a Milli-Q system (Millipore Corporation, Billerica, MA, USA). Protein LoBind tubes were obtained from Eppendorf (Hamburg, Germany). Porcine trypsin (modified, sequencing grade) was obtained from Promega (Madison, WI, USA).

Human plasma collection, preparation and storage

Human whole blood was provided by the Dipartimento di medicina sperimentale of Sapienza Università di Roma. Blood was extracted by venipuncture from healthy 20–40-year-old volunteers, by use of the BD P100 Blood Collection System (Franklin Lakes, NJ, USA) with K_2EDTA as anticoagulant and a protease inhibitors cocktail. Immediately after blood extraction, each tube was inverted ten times to ensure mixing of the components, and subsequently centrifuged for 10 min at 1,000*g* to pellet the blood cells. Supernatant plasma was drawn and the absence of haemolysis was checked. Plasma specimens were then mixed to reduce differences between individuals and overall subject-to-subject variation. Mixed plasma was split into 200-μL volumes and stored at −80 °C in labelled Protein LoBind tubes, to ensure plasma stability until further use. When used for experiments, aliquots were thawed at 4 °C and then left to warm at RT.

Liposomes

CLs were prepared in accordance with standard procedures [27]. Chloroform (100 μL) was used to dissolve DOTAP (5 mg) and was then removed under vacuum for 24 h. The lipid films obtained were hydrated with 5 mL of a dissolving buffer (Tris–HCl, pH 7.4, 10 mmol L^{-1}; NaCl, 150 mmol L^{-1}; EDTA, 1 mmol L^{-1}) to achieve a final concentration of 1 mg mL^{-1}. Small unilamellar liposomes (SUVs) were produced by sonication to clarity (mean diameter approx. 100 nm) [21].

Lipoplexes

Self-assembled DOTAP–DNA lipoplexes at a single lipid-to-DNA volume ratio, R_V=1, were obtained by mixing 20 μL CT DNA solution (1 mg mL^{-1}) with 100 μL of SUVs dispersion. At this volume ratio, lipoplexes are positively charged and have the lowest colloidal dimensions [21].

LPD complexes

Negatively charged P–DNA microspheres were prepared at a protamine-to-DNA weight ratio R_W=0.5 [26]. P–DNA microspheres were mixed with SUVs at a single lipid-to-DNA volume ratio, R_V=1, to compare protein binding capacity of lipoplexes and LPD complexes properly. At this volume ratio, LPD complexes are positively charged and have the lowest colloidal dimensions [21].

CLs, lipoplexes, and LPD complexes incubation with plasma and centrifugation

The incubation procedure was conducted as described elsewhere [22]. Plasma-protein binding to CLs, lipoplexes, and LPD complexes was investigated by incubating 200 μL of each system, separately, with an equal amount of plasma in the dissolving buffer at 37 °C for 1 h. Solutions were then centrifuged at 15,000*g* for 10 min to separate the nanoparticle–protein complexes. Pellets were washed with 250 μL dissolving buffer, by use of a vortex mixer, transferred to a new Protein LoBind tube, and centrifuged again. To reduce contamination from plasma proteins bound to the tube wall, three washings were performed for each pellet. To check the reproducibility of nanoparticle–protein corona complex formation, three experimental replicates were performed for each system. A plasma aliquot not incubated with nanoparticles was subjected to the same procedure as control, to verify the absence of protein precipitation.

In-solution trypsin digestion

Protein denaturation and disulfide bonds reduction was performed with a solution prepared with 40 μL urea (8 mol L^{-1})–ammonium bicarbonate (50 mmol L^{-1}) and 2 μL 1,4-dithiothreitol (200 mmol L^{-1}), in which nanoparticle–protein systems were suspended and kept in incubation at 37 °C for 1 h under slight agitation. Carbamidomethylation of thiol groups was accomplished by addition of iodoacetamide (8 μL, 200 mmol L^{-1}) and incubation at RT for 1 h in the dark. Subsequently, to consume any leftover alkylating agent and to avoid trypsin alkylation, 8 μL 1,4-dithiothreitol (200 mmol L^{-1}) was added and samples were incubated at 37 °C for 1 h, with slight agitation. Solutions were then diluted with ammonium bicarbonate (50 mmol L^{-1}) to obtain a final urea concentration of 1 mol L^{-1}, and were incubated overnight at 37 °C with a solution of trypsin (20 μg mL^{-1})–ammonium bicarbonate (50 mmol L^{-1}) to ensure a minimum enzyme-to-substrate ratio of 1:20. Enzymatic digestion was quenched acidifying with formic acid.

Digested samples were desalted by use of an SPE C_{18} column (Bond Elut 1 cc LRC-C18; Varian, Palo Alto, CA, USA) conditioned with acetonitrile and rinsed with 0.1% TFA.

Table 1 Number of validated proteins found for each sample according to Proteome Discoverer and Scaffold analysis

	CLs	Lipoplexes	LPD Complexes	Overall
Proteome Discoverer	104	227	186	306
Scaffold	110	231	189	268

Peptides were eluted from the SPE column with 0.5 mL acetonitrile–water (50:50, *v*/*v*) containing 0.05% TFA and were dried in a Speed-Vac SC 250 Express (Thermo Savant, Holbrook, NY, USA). Each sample was re-constituted with formic acid (500 μL, 0.1%) and stored at −80 °C until analysis.

Nano HPLC–mass spectrometric analysis

Tryptic peptides were analyzed by use of a Dionex (Sunnyvale CA, USA) Ultimate 3000 nano-LC system connected to a linear quadrupole ion-trap Orbitrap (LTQ Orbitrap XL) mass spectrometer (ThermoScientific, Bremen, Germany) equipped with a nanospray ion source.

Peptide mixtures were enriched by injecting 5 μL sample, on-line, on to a 300 μm i.d.×5 mm Acclaim PepMap 100 C_{18} (5 μm particle size, 100 Å pore size) μ-precolumn (Dionex), using a premixed mobile phase H_2O–CH_3CN 98:2 (*v*/*v*) (phase C) containing 0.1% (*v*/*v*) HCOOH at a flow-rate of 10 μL min^{-1}.

Peptides were separated on a Biobasic 18 (5 μm particle size, 300 Å pore size) 75 μm i.d.×100 mm, 15 μm tip picofrit column (Thermo Scientific, Bellefonte, PA, USA) with a flow rate of 250 nL min^{-1}. The LC gradient was optimized to detect the largest set of peptides by using H_2O–HCOOH (99.9:0.1, *v*/*v*) as phase A and CH_3CN–HCOOH (99.9:0.1, *v*/*v*) as phase B. A 120-min gradient was used; after an isocratic step at 5% B for 5 min, B was linearly increased to 30% within 75 min; afterwards, B was increased to 80% within 5 min, and to 95% within the following 10 min to rinse the column. Finally, B was reduced to 5% over 1 min and the column re-equilibrated for 24 min. The mass spectrometer was operated in the data-dependent mode to automatically switch between Orbitrap-MS and LTQ-MS–MS acquisition (*m*/*z* range 400–1,800, 60,000 resolution) using the data-dependant acquisition, DDA, "TOP5 strategy". In brief, each scan cycle begins with a full scan at high resolution and high mass accuracy in the Orbitrap analyzer, followed by MS–MS scans in the linear ion trap on the five most intense precursor ions. Dynamic exclusion consists of two MS–MS spectra acquisitions of the most abundant ions during a period of 30 s and then excluding the ion from subsequent fragmentations for 100 s. The activation type used was CID with a normalized collision energy set at 35 V. To assess the additional variation introduced into the measurements by the experimental

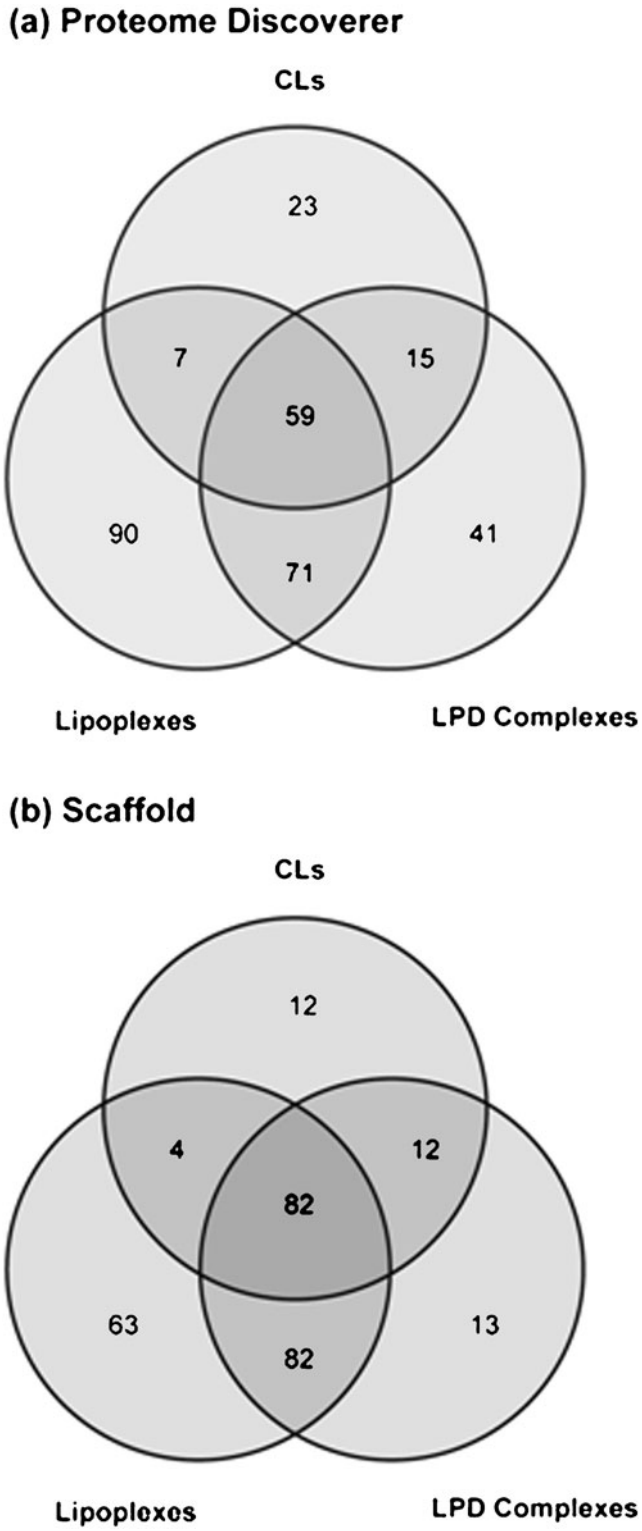

Fig. 1 Venn diagram representing the distribution of (**a**) number of validated proteins according to Proteome Discoverer, (**b**) number of validated proteins according to Scaffold

Table 2 SIEVE relative quantitative analysis results showing protein abundance (signal intensity) ratios for proteins having CV lower than 10%, *P* values lower than 0.001, Mascot scores higher than 25, peptides unique assignment, and abundance ratio higher than 2 or lower than 0.5 with a coefficient of variance lower than 0.33. Values in parentheses refer to proteins that do not satisfy SIEVE's restriction but do satisfy Scaffold's

Protein name	Accession no.	Lipoplexes/Cls abundance ratio	LPD complexes/CLs abundance ratio	LPD complexes/ lipoplexes abundance ratio
HSPA5 HSPA5 protein	IPI00003362			0.20±0.04
SAA4 Serum amyloid A_4 protein	IPI00019399			0.16±0.04
Prothrombin (Fragment)	IPI00019568	0.010±0.003		
PLG Plasminogen	IPI00019580		4.5±1.5	0.44±0.09
C4BPA C4b_binding protein alpha chain	IPI00021727	0.04±0.01		
APOE Apolipoprotein E	IPI00021842		(1.3±0.2)	0.29±0.03
APOA2 Apolipoprotein A_II	IPI00021854			0.33±0.06
APOC2 Apolipoprotein C_II	IPI00021856			0.7±0.1
APOB Apolipoprotein B_100	IPI00022229	2.7±0.1	(0.59±0.07)	0.29±0.02
C1QC Complement C1q subcomponent subunit C	IPI00022394			0.003±0.001
C9 Complement component C9	IPI00022395	(1.8±0.3)		0.28±0.04
PF4 Platelet factor 4	IPI00022446	(1.6±0.4)		0.07±0.01
LPA Apolipoprotein(a)	IPI00029168	2.2±0.2		0.49±0.06
Complement C5	IPI00032291			(2.6±1.0)
LBP Lipopolysaccharide_binding protein	IPI00032311	3.0±0.6		0.20±0.06
PFN1 Profilin_1	IPI00216691	13±4		0.18±0.05
PON1 Serum paraoxonase/arylesterase 1	IPI00218732	(2.0±1.6)	0.010±0.003	
THBS1 Thrombospondin_1	IPI00296099			0.12±0.02
VTN Vitronectin	IPI00298971	(1.5±0.1)		0.15±0.01
TLN1 Talin_1	IPI00298994	2.1±0.3		0.09±0.01
HIST4H4 Histone H4	IPI00453473			0.33±0.07
C3 Complement C3 (Fragment)	IPI00783987	2.1±0.4	(0.9±0.2)	
C6 Complement component 6 precursor	IPI00879709	0.45±0.06		

procedure and to increase the number of identified proteins, the experimental design provided five replicate (LC–MS–MS runs) for each of the three experimental replicates.

Identification of proteins

Raw MS–MS data files from Xcalibur software (version 2.0.7 SP1; Thermo Fisher Scientific) were submitted to Mascot Deamon (version 2.2.04, Matrix Science, London, UK) for database search against the IPI human database (version 3.79). A ThermoFinnigan LCQ/DECA RAW file data import filter was used. In brief, two missed cleavages were allowed and a precursor mass tolerance of 10 ppm was used in combination with 0.8 Da fragment mass tolerance; acetylation (N-term), oxidation (M), and deamidation (N, Q) were used as dynamic modifications; carbamidomethylation (C) was used as static modification. Mascot ion scores >25 on unique peptides were used for further processing, with a significance threshold >0.05.

Proteome Discoverer and SIEVE analysis

Proteome Discoverer software (version 1.3.0.339; Thermo Fisher Scientific) was used to validate identification of Mascot proteins. Proteins containing at least two identified peptides were accepted.

SIEVE software (version 1.3; Thermo Fisher Scientific) was used to execute differential quantitative analysis on validated proteins. Alignment and framing (peak detection) were performed as follows: data were processed in the interval 13–80 min of the chromatographic separation (also processed for peptide identification), frames from MS–MS scans were used, a maximum of 200,000 frames was set together with 10^5 as signal threshold, and peptides with MZStart 400 and MZStop 1,800, MZWidth 0.01, and RTWidth 2.5 were used.

Scaffold analysis

Scaffold [28] (version 3.1.2; Proteome Software, Portland, OR, USA) was also used to validate MS–MS based peptide

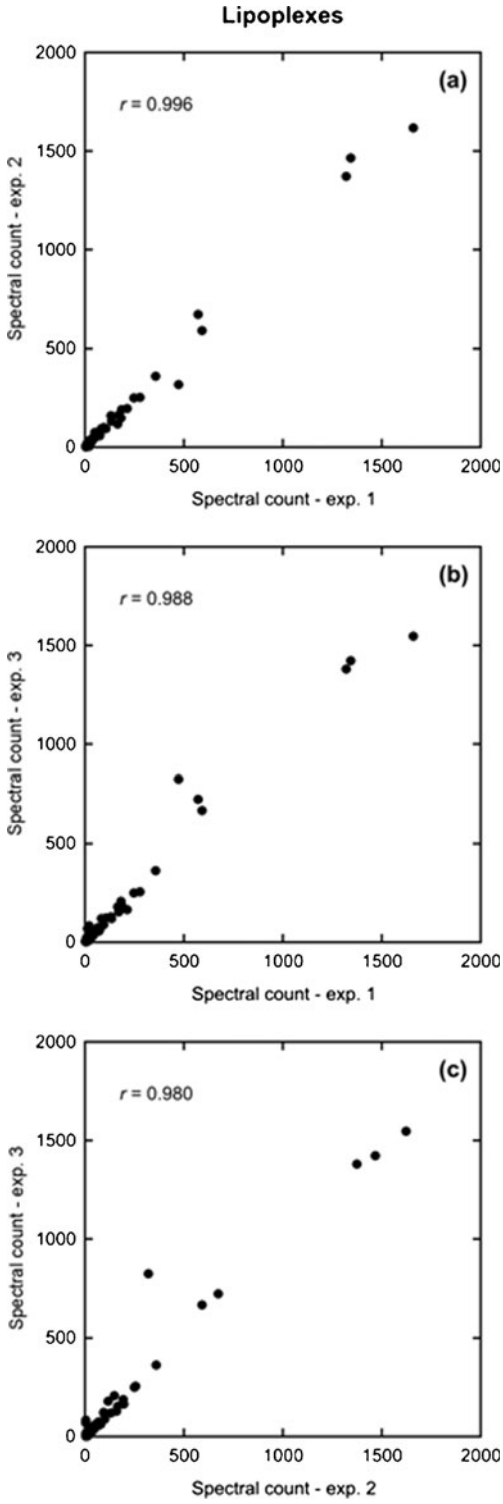

Fig. 2 Correlation between spectrum count in the three experiments conducted on the lipoplexes sample: (**a**) experiment 2 vs experiment 1, (**b**) experiment 3 vs experiment 1, and (**c**) experiment 3 vs experiment 2. Proteins with grouping ambiguity are not represented. In each plot, Pearson's product is indicated as *r*

and protein identification, and to execute differential quantitative analysis. Peptide identifications were accepted if they could be established at greater than 95% probability as specified by the Peptide Prophet algorithm [29]. Protein identifications were accepted if they could be established at greater than 99.0% probability and contained at least two identified peptides. Protein probabilities were assigned by the Protein Prophet algorithm [30]. Proteins that contained similar peptides and could not be differentiated on the basis of MS–MS analysis alone were grouped to satisfy the principles of parsimony. False discovery was found to be 0.1% for proteins and 0.5% for peptides.

Unweighted spectrum count (USC) was used to assess the consistency of experimental replicates in quantitative analysis, and normalized spectrum count (NSC) was used to retrieve protein abundance. The SC normalization is an option available in Scaffold by means of which spectral counts are multiplied by a fractional amount across samples, so that the total number of spectra are the same within each category and then across all categories. Fisher's exact test was used to identify significant differences and to calculate *P* values. Ratios between NSCs were used to perform differential quantitative analysis.

Gene ontology [31] (GO) terms for the validated proteins were retrieved from the NCBI online database [32] by using Scaffold's built-in facility. GO uses a controlled vocabulary to depict biological molecules or gene products in terms of biological process, molecular function, and cellular component.

Results and discussion

Sample preparation

The separation of the nanoparticle–protein complexes, the effective unit of interest in biodistribution of the nanoparticles throughout the body [12], from excess plasma proteins must not destroy the complex or induce additional protein binding. Therefore, centrifugation was chosen as separation method to avoid such possibilities [22]. Furthermore, because our interest focuses on those proteins strongly adsorbed on to nanoparticles, the so-called "hard corona", nanoparticle–protein complex pellet was washed vigorously three times with 250 μL 10 mmol L^{-1} Tris–HCl, pH 7.4, 150 mmol L^{-1} NaCl, and 1 mmol L^{-1} EDTA, using a vortex mixer to remove all unbound proteins, and centrifuging for a short time (2 min), to avoid sedimentation of large proteins, formation of protein aggregates, and co-precipitation.

Proteome Discoverer and SIEVE analysis results

Complete lists of the proteins validated by Proteome Discoverer over the all fifteen MS–MS files for each sample are available in the Electronic Supplementary Material (please refer to the Supporting Excel file).

Table 3 Scaffold relative quantitative analysis results showing protein abundance (NSC) ratios for proteins having no grouping ambiguity, a *P* value smaller than 0.001, and abundance ratio higher than 2 or lower than 0.5 with a coefficient of variance lower than 0.33. Proteins containing peptide sequences identical with other isoforms are reported as one accession number followed by parentheses containing the relative number of isoforms. Values in parentheses refer to proteins that do not satisfy Scaffold's restriction but do satisfy SIEVE's

Protein name	Accession no.	Lipoplexes/Cls abundance ratio	LPD complexes/CLs abundance ratio	LPD complexes/lipoplexes abundance ratio
Complement component C8 gamma chain	IPI00011261		3.8±0.6	2.1±0.6
Prothrombin (Fragment)	IPI00019568	(0.01±0.004)		
PLG Plasminogen	IPI00019580			(1.6±0.5)
cDNA FLJ55673, highly similar to Complem. fact. B	IPI00019591 (+2)		2.1±0.3	2.5±0.3
Properdin	IPI00021364			2.39±0.23
C4b-binding protein alpha chain	IPI00021727	0.09±0.01		
Apolipoprotein A-I	IPI00021841	2.3±0.5	5.1±0.7	2.3±0.3
Apolipoprotein E	IPI00021842	3.0±0.6	3.4±0.6	(1.1±0.3)
Apolipoprotein C-III	IPI00021857 (+1)		2.9±0.4	2.2±0.3
Isoform 1 of Fibrinogen alpha chain	IPI00021885	0.13±0.03	0.26±0.02	2.0±0.4
Apolipoprotein B-100	IPI00022229	2.8±0.3	3.0±0.5	(1.6±0.5)
Complement C1q subcomponent subunit A	IPI00022392			0.03±0.01
Complement C1q subcomponent subunit C	IPI00022394			0.06±0.02
Complement component C9	IPI00022395	2.8±0.6	3.6±0.8	(1.3±0.3)
Protein AMBP	IPI00022426	0.13±0.02		
Platelet basic protein	IPI00022445	4.8±0.5		
Platelet factor 4	IPI00022446	4.2±0.8		
Apolipoprotein(a)	IPI00029168	2.4±0.2	4.0±0.4	(1.7±0.1)
Complement C5	IPI00032291			2.7±0.8
Lipopolysaccharide-binding protein	IPI00032311	3.3±0.9	2.42±0.56	
Isoform HMW of Kininogen-1	IPI00032328		0.14±0.03	
PFN1 Profilin_1	IPI00216691			(0.4±0.1)
Isoform 2 of Phospholipid transfer protein	IPI00217778 (+2)			0.48±0.06
Serum paraoxonase/arylesterase 1	IPI00218732	0.09±0.02	0.08±0.02	
Isoform 1 of Vinculin	IPI00291175 (+1)	3.1±0.1		
Isoform 1 of Clusterin	IPI00291262 (+2)	0.38±0.06	0.5±0.1	
Inter-alpha-trypsin inhibitor heavy chain H1	IPI00292530	0.17±0.02	0.34±0.08	
Inter-alpha-trypsin inhibitor heavy chain H1	IPI00292530			2.0±0.6
Vitamin K-dependent protein S	IPI00294004		0.15±0.04	
Isoform 1 of Integrin alpha-IIb	IPI00295976	2.5±0.5		
Fibrinogen beta chain	IPI00298497	0.10±0.02	0.19±0.03	
Thrombospondin-1	IPI00296099	2.4±0.4		
Vitronectin	IPI00298971	2.5±0.3		(0.5±0.1)
Talin-1	IPI00298994	3.9±0.7		(0.08±0.05)
Isoform 2 of Filamin-A	IPI00302592 (+2)	10±2		0.18±0.06
Hyaluronan-binding protein 2	IPI00746623 (+1)	2.2±0.4		
Complement C3 (Fragment)	IPI00783987	(1.27±0.06)	2.4±0.1	

Three-hundred and six proteins were validated and accepted. The number of proteins found in each sample is summarized in Table 1. Lipoplex protein coronas were the richest in terms of qualitative composition, whereas that of the CLs was the poorest. In fact, the number of proteins found in the former is more than twice as large as that found in the latter, and it is only approximately 20% greater than the corresponding value for LPD complexes. On the other hand, the number of proteins found in LPD complexes "corona" is approximately 1.8 times the number found in

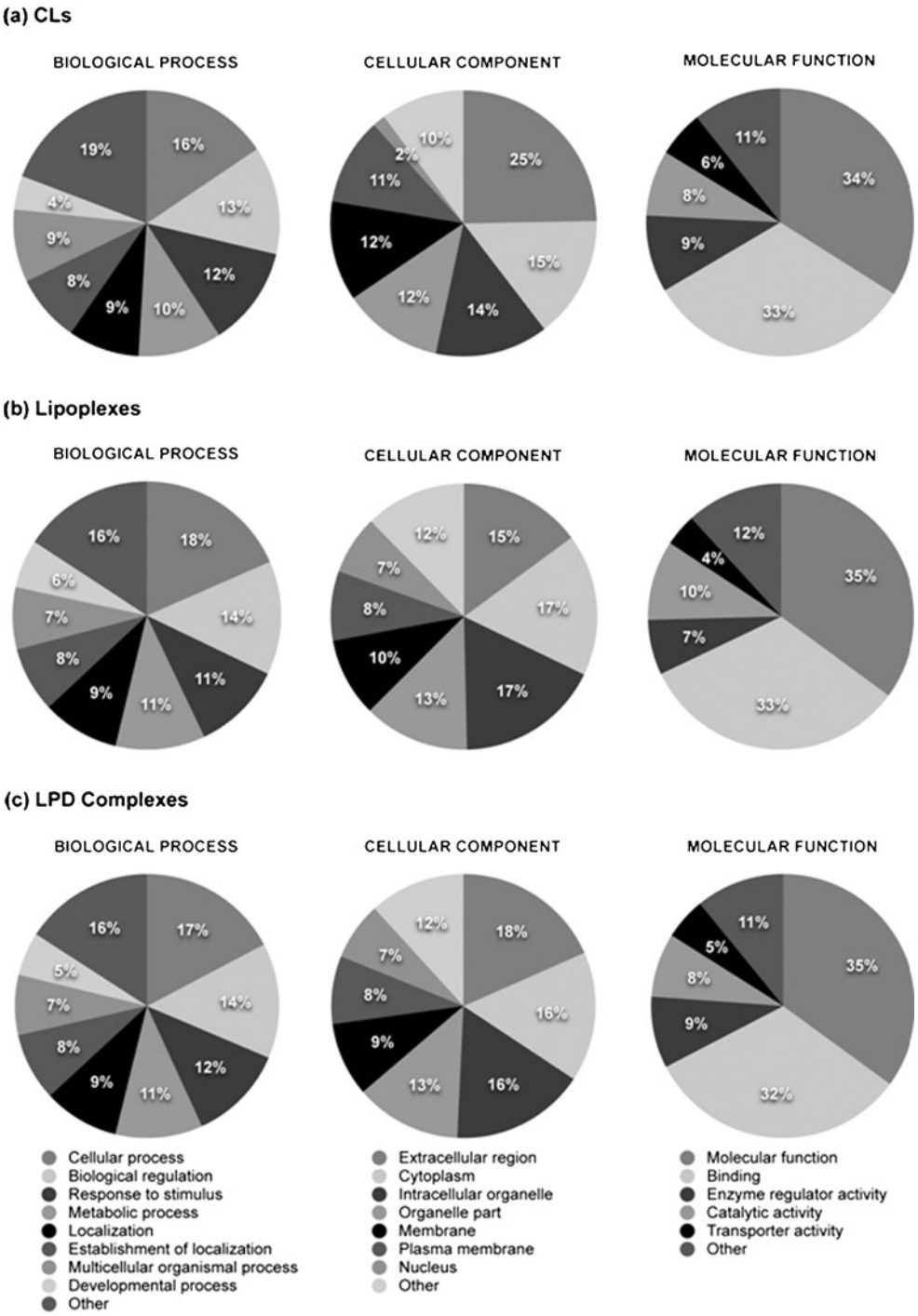

Fig. 3 Gene ontology classification of validated proteins found in (**a**) CLs, (**b**) lipoplexes, and (**c**) LPD complexes. Proteins with grouping ambiguity were excluded from the classification

that of the CLs. The situation can be further clarified by observing the distribution of the above numbers among samples using Venn diagrams, as shown in Fig. 1a. If we exclude the 59 proteins shared by all samples, protein overlap between lipoplexes and LPD complexes is 10 times and approximately 5 times the protein overlap found between lipoplexes and CLs, and between LPD complexes and CLs, respectively.

Relative quantitative analysis was performed on two samples at a time, each time taking into account the shared proteins only. For these proteins, the change in abundance was expressed as the ratio of protein signal intensity measured for one sample to the signal intensity measured for the other. Changes were considered significant if the following conditions were met: CV was lower than 10%, *P* value was lower than 0.001, Mascot score was higher than 25, and peptides had

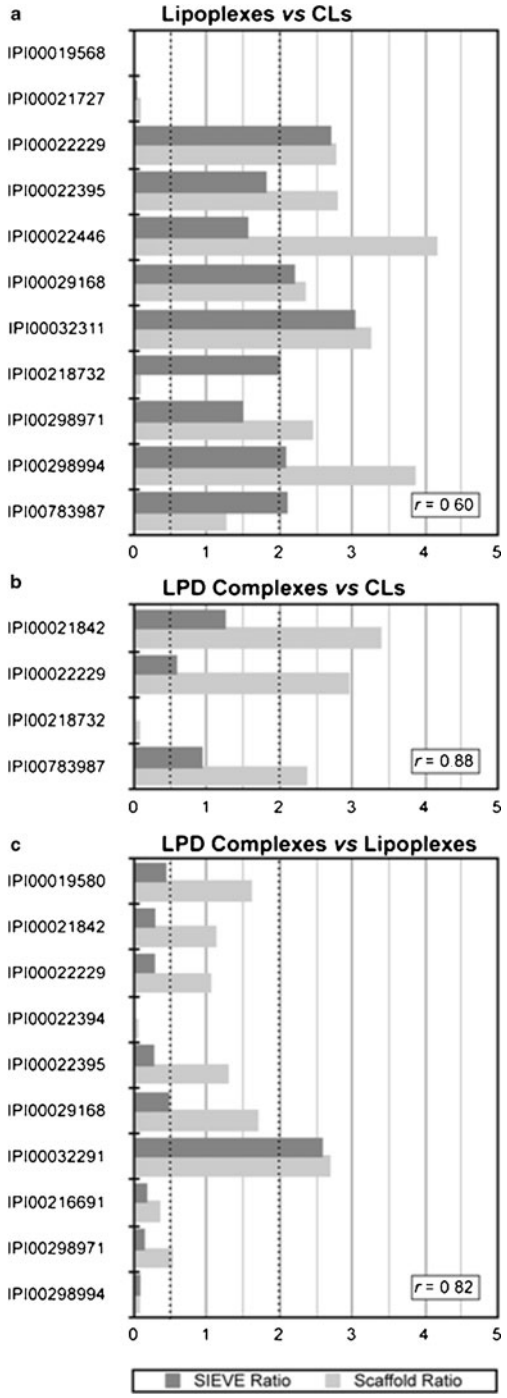

Fig. 4 Comparisons between relative abundance ratios as obtained by SIEVE and by Scaffold. Solely validated proteins for which at least one method has identified a significant relative ratio are shown. Pearson's product is indicated as *r*

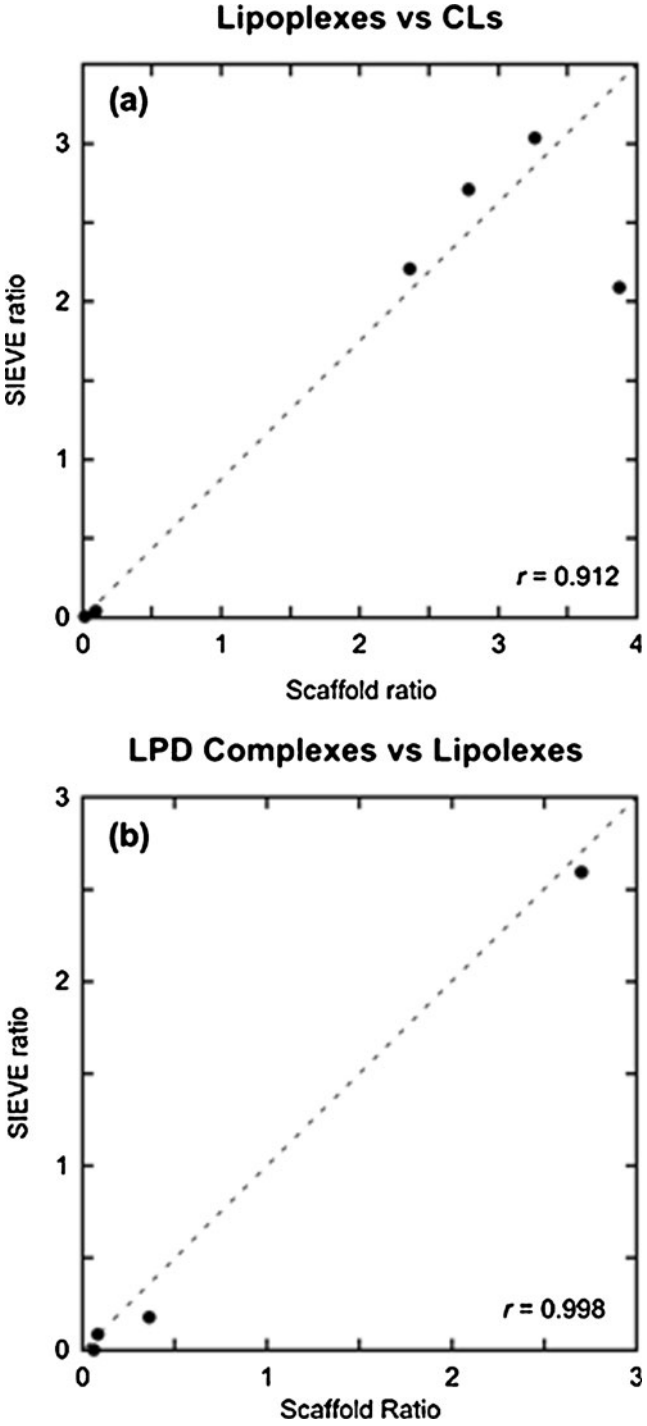

Fig. 5 Comparisons between relative abundance ratios as obtained by SIEVE and by Scaffold. Solely validated proteins for which both methods have identified a significant relative ratio, irrespective of the coefficient of variance, are shown. (**a**) From left to right: IPI00019568, IPI00021727, IPI00029168, IPI00022229, IPI00032311, and IPI00298994. (**b**) From left to right: IPI00022394, IPI00298994, IPI00216691 and IPI00032291. Pearson's product is indicated as *r*

unique protein assignment. Moreover, signal intensity (abundance) ratios had to be higher than 2 or lower than 0.5 with a coefficient of variance lower than 0.33. The numbers of proteins found to satisfy the above conditions in the analysis of lipoplexes vs CLs, LPD complexes vs CLs, and lipoplexes vs LPD complexes were 9, 2 and 17, respectively. Results are shown in Table 2.

Scaffold analysis results

The fifteen MS–MS spectra acquired for each sample were loaded and analyzed with Scaffold using the MuDPIT option (all spectra were combined in one analysis). A total of 268 proteins were validated. The complete list of identified proteins is available in the Electronic Supplementary Material (Table S1; also, for protein grouping ambiguities, number of assigned spectra, unique peptides and sequences coverage).

In comparing the number of proteins found in each sample, as summarized in Table 1, it is found again that the lipoplex protein corona is the richest in qualitative composition whereas that of the CLs is the poorest; protein number ratios for one sample to another are also very close to those found in Proteome Discoverer analysis. The distribution of proteins among samples are shown by use of Venn diagrams in Fig. 1b. Here we can see that—excluding the 82 proteins shared by all the samples—protein overlap between lipoplexes and LPD complexes is approximately 20 times and 7 times protein overlap found between lipoplexes and CLs, and between LPD complexes and CLs, respectively.

Proteins abundance was retrieved from spectral counts. Each experimental replicate was analyzed independently, combining all technical replicates in one analysis (using Scaffold's MuDPIT option). The consistency of replicate experiments was checked by comparing, among replicates, the unweighted spectrum count (USC) obtained for each protein. Figure 2 shows the correlation found between the three experiments carried out for the lipoplexes sample; correlations for the two other samples are available in the Electronic Supplementary Material (Figs. S1 and S2). Pearson's product was calculated and the results indicate that USCs obtained in the experimental replicates were highly reproducible. Therefore, NSC mean value (with the corresponding standard deviation) was calculated for each protein and used to perform relative quantitative analysis. Comparisons were made between two samples at a time, each time taking into account shared proteins only. Ratios between NSC mean values were calculated only for those proteins having no grouping ambiguity and having a P value smaller than 0.001. The numbers of proteins found to have an NSC ratio higher than 2 or lower than 0.5, with a coefficient of variance lower than 0.33, in the comparison of lipoplexes vs CLs, LPD complexes vs CLs and lipoplexes vs LPD complexes were 22, 17 and 12, respectively. Results are reported in Table 3.

Validated proteins were also classified by GO to be reasonably representative of the various cellular compartments, biological processes, and molecular functions they are involved in. Figure 3 summarizes GO classification for the (Fig. 3a) CLs, (Fig. 3b) lipoplexes, and (Fig. 3c) LPD complexes samples. Only small differences were found among samples in the distributions of values for the biological processes and the molecular functions. In fact, differences of 1–2% only are observed among more represented terms. It might be worth noticing that, among less represented biological process terms—not reported in Fig. 3—"growth" was found solely in lipoplexes, a single item, whereas "viral reproduction" was found in lipoplexes and LPD complexes only, 7 and 6 items, respectively. Regarding terms for less represented molecular functions, "electron carrier activity" occurred once in both lipoplexes and LPD complexes, and "translation regulator activity" occurred, respectively, twice and once; "transcription regulator activity" was found—5 times—in lipoplexes only. In contrast, some consistent differences were found in the distribution of the cellular component terms: "extracellular region" and "nucleus" have different representation in CLs samples compared with lipoplexes and LPD complexes, larger and smaller, respectively.

Conclusions

Proteome Discoverer and Scaffold analysis were found to validate an almost equal number of proteins. In particular, the number of identified proteins in each sample and the relative overlaps, as obtained by the two software packages, were found to be highly congruent.

CLs, lipoplexes, and LPD complexes protein coronas seem to be different in terms of qualitative composition. It was confirmed [33] that those of lipoplexes and LPD complexes are more variable than those of CLs, whereas there are small differences between those of lipoplexes and LPD complexes.

Both NSC Scaffold and AUC SIEVE analysis revealed there are quantitative differences also; approximately 10% of the validated proteins differ significantly in their amounts in the three coronas. Assuming the two methods of analysis to be complementary [34], the relative amount (signal intensity and abundance ratio) of validated proteins for which at least one method has identified a significant difference are compared in Fig. 4. A good correlation between ratios obtained by the two analytical methods was found for LPD complexes vs CLs and LPD complexes vs lipoplexes, whereas a lower correlation was found for lipoplexes vs CLs, as stated by Pearson's product. On the other hand, correlation is substantially increased by taking into account only those proteins identified by both methods with a significant difference, irrespective of the coefficient of variance, as shown in Fig. 5.

Such results could help in designing gene-delivery systems, because some proteins could be more selectively bound than others, and their bio-distribution could be driven in vivo for more efficient and effective gene therapy.

Acknowledgments We sincerely thank Dr Madalina Oppermann, Thermo Fisher Scientific, for her technical support and assistance. We would also like to acknowledge and thank Sapienza University of Rome Scientific Research 2010.

References

1. Marshall E (2002) What to do when clear success comes with an unclear risk? Science 298:510–511
2. Felgner PL, Gadek TR, Holm M, Roman R, Chan HW, Wenz M, Northrop JP, Ringold GM, Danielsen M (1987) Lipofection: a highly efficient, lipid-mediated DNA-transfection procedure. Proc Natl Acad Sci U S A 84:7413–7417
3. Leventis R, Silvius JR (1990) Interactions of mammalian cells with lipid dispersions containing novel metabolizable cationic amphiphiles. Biochim Biophys Acta Biomembr 1023:124–132
4. Gao X, Huang L (1991) A novel cationic liposome reagent for efficient transfection of mammalian cells. Biochem Biophys Res Commun 179:280–285
5. Felgner JH, Kumar R, Sridhar CN, Wheeler CJ, Tsai YJ, Border R, Ramsey P, Martin M, Felgner PL (1994) Enhanced gene delivery and mechanism studies with a novel series of cationic lipid formulations. J Biol Chem 269:2550–2561
6. Koltover I, Salditt T, Radler JO, Safinya CR (1998) An inverted hexagonal phase of cationic liposome-DNA complexes related to DNA release and delivery. Science 281:78–81
7. Caracciolo G, Caminiti R, Pozzi D, Friello M, Boffi F, Castellano AC (2002) Self-assembly of cationic liposomes–DNA complexes: a structural and thermodynamic study by EDXD. Chem Phys Lett 351:222–228
8. Kogure K, Moriguchi R, Sasaki K, Ueno M, Futaki S, Harashima H (2004) Development of a non-viral multifunctional envelope-type nano device by a novel lipid film hydration method. J Control Release 98:317–323
9. Yamauchi J, Hayashi Y, Kajimoto K, Akita H, Harashima H (2010) Comparison between a multifunctional envelope-type nano device and lipoplex for delivery to the liver. Biol Pharm Bull 33:926–929
10. Cedervall T, Lynch I, Lindman S, Berggard T, Thulin E, Nilsson H, Dawson KA, Linse S (2007) Understanding the nanoparticle–protein corona using methods to quantify exchange rates and affinities of proteins for nanoparticles. Proc Natl Acad Sci U S A 104:2050–2055
11. Sahoo B, Goswami M, Nag S, Maiti S (2007) Spontaneous formation of a protein corona prevents the loss of quantum dot fluorescence in physiological buffers. Chem Phys Lett 445:217–220
12. Lynch I, Dawson KA (2008) Protein–nanoparticle interactions. NanoToday 3:40–47
13. Lynch I, Cedervall T, Lundqvist M, Cabaleiro-Lago C, Linse S, Dawson KA (2007) The nanoparticle–protein complex as a biological entity; a complex fluids and surface science challenge for the 21st century. Adv Colloid Interface Sci 134(135):167–174
14. Owens DE III, Peppas NA (2006) Opsonization, biodistribution, and pharmacokinetics of polymeric nanoparticles. Int J Pharm 307:93–102
15. Caracciolo G, Callipo L, Candeloro De Sanctis S, Cavaliere C, Pozzi D, Laganà A (2010) Surface adsorption of protein corona controls the cell internalization mechanism of DC-Chol–DOPE/DNA lipoplexes in serum. Biochim Biophys Acta 1798:536–543
16. Motoyama A, Yates JR III (2008) Multidimensional LC separations in shotgun proteomics. Anal Chem 80:7187–7193
17. Liu H, Sadygov RG, Yates JR III (2004) A model for random sampling and estimation of relative protein abundance in shotgun proteomics. Anal Chem 76:4193–4201
18. Bondarenko PV, Chelius D, Shaler TA (2002) Identification and relative quantitation of protein mixtures by enzymatic digestion followed by capillary reversed-phase liquid chromatography-tandem mass spectrometry. Anal Chem 74:4741–4749
19. Chelius D, Bondarenko PV (2002) Quantitative profiling of proteins in complex mixtures using liquid chromatography and mass spectrometry. J Proteome Res 1:317–323
20. Wang G, Wu WW, Zeng W, Chou CL, Shen RF (2006) Label-free protein quantification using LC-coupled ion trap or FT mass spectrometry: reproducibility, linearity, and application with complex proteomes. J Proteome Res 5:1214–1223
21. Caracciolo G, Pozzi D, Capriotti AC, Marianecci C, Carafa M, Marchini C, Montani M, Amici A, Amenitsch H, Digman MA, Gratton E, Sanchez SS, Laganà A (2011) Factors determining the superior performance of Lipid–DNA/Protammine Nanoparticles over Lipoplexes. J Med Chem 54:4160–4171
22. Capriotti AL, Caracciolo G, Caruso G, Pozzi D, Samperi R, Laganà A (2010) Analysis of plasma protein adsorption onto DC-Chol-DOPE cationic liposomes by HPLC-CHIP coupled to a Q-TOF mass spectrometer. Anal Bioanal Chem 389:2777–2894
23. Zhang B, VerBerkmoes NC, Langston MA, Uberbacher E, Hettich RL, Samatova NF (2006) Detecting differential and correlated protein expression in label-free shotgun proteomics. J Proteome Res 5:2909–2918
24. Foss EJ, Radulovic D, Shaffer SA, Ruderfer DM, Bedalov A, Goodlett DR, Kruglyak L (2007) Genetic basis of proteome variation in yeast. Nat Genet 39:1369–1375
25. Gstaiger M, Aebersold R (2009) Applying mass spectrometry-based proteomics to genetics, genomics and network biology. Nat Rev Genet 10:617–627
26. Choudhary C, Mann M (2010) Decoding signalling networks by mass spectrometry-based proteomics. Nat Rev Mol Cell Biol 11:427–439
27. Caracciolo G, Pozzi D, Caminiti R (2005) Lipid mixing upon deoxyribonucleic acid-induced liposomes fusion investigated by synchrotron small-angle x-ray scattering. Appl Phys Lett 87:133901–133903
28. Searle BC (2010) Scaffold: a bioinformatic tool for validating MS–MS-based proteomic studies. Proteomics 10:1265–1269
29. Keller A, Nesvizhskii AI, Kolker E, Aebersold R (2002) Empirical statistical model to estimate the accuracy of peptide identifications made by MS–MS and database search. Anal Chem 74:5383–5392
30. Nesvizhskii AI, Keller A, Kolker E, Aebersold RA (2003) Statistical model for identifying proteins by tandem mass spectrometry. Anal Chem 75:4646–4658
31. Gene ontology project. http://www.geneontology.org
32. National Center for Biotechnology Information. http://www.ncbi.nlm.nih.gov
33. Capriotti AL, Caracciolo G, Caruso G, Foglia P, Pozzi D, Samperi R, Laganà A (2011) Differential analysis of "protein corona" profile adsorbed onto different nonviral gene delivery systems. Anal Biochem 419:180–189
34. Katz E, Fon M, Eigenheer RA, Phinney BS, Fass JN, Lin D, Sadka A, Blumwald EA (2010) Label-free differential quantitative mass spectrometry method for the characterization and identification of protein changes during citrus fruit development. Proteome Sci 8:68